Electrochemical Society

GLC Anodes Are CUSTOM MADE for

Frontier Chemical Company

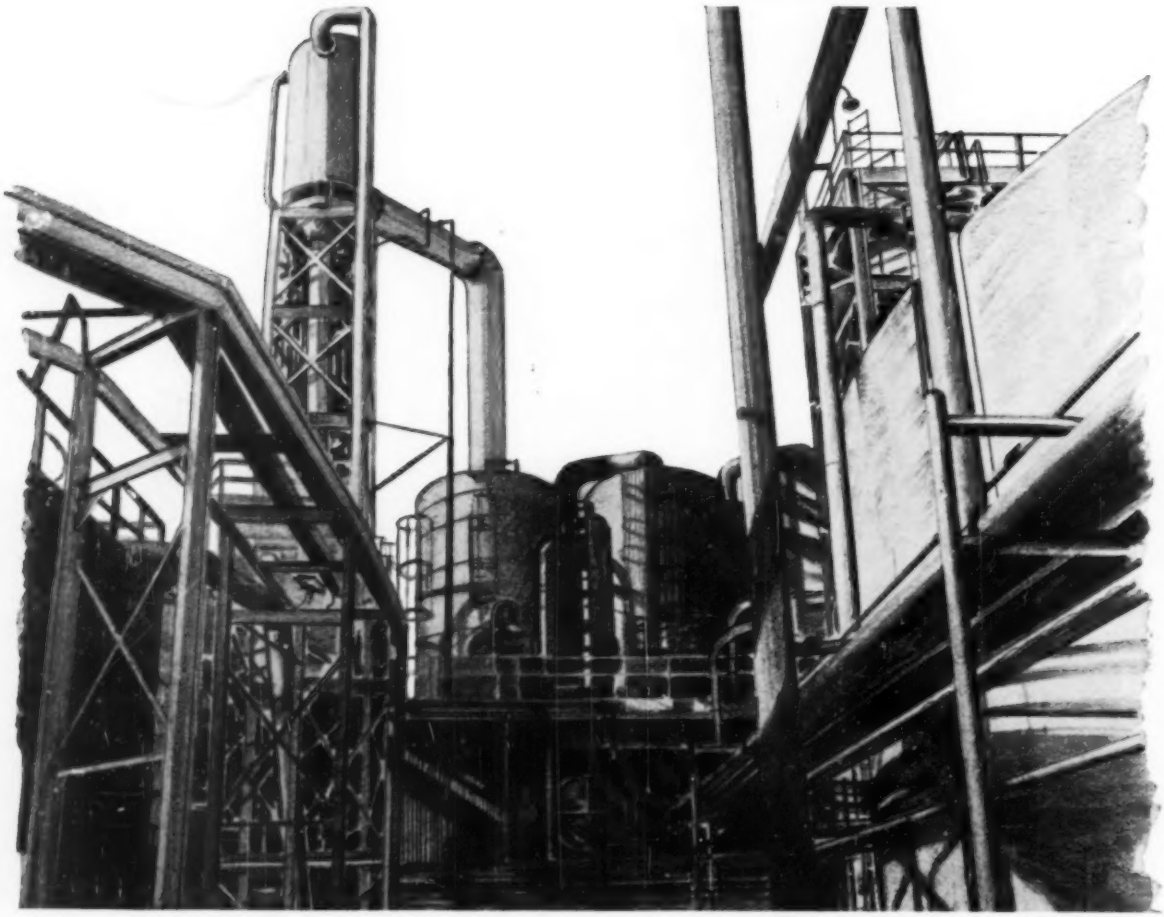

The Frontier Chlor-Alkali Plant at Wichita, Kansas

APPRECIABLE COST SAVINGS in their present electrolytic cell operations are being achieved by GLC anode customers through our past technical exchanges with them.

THIS GLC PROGRAM of technical progress is continuing so that still greater heights of anode performance will be reached in the future.

BY WORKING WITH YOU now, custom making anodes for your specific cell requirements, we can help bring greater economies to your chlor-alkali production in the years ahead.

PRODUCTS ELECTRODE GLC DIVISION YOU CAN TRUST

GREAT LAKES CARBON CORPORATION

18 EAST 48TH STREET, NEW YORK 17, N.Y. OFFICES IN PRINCIPAL CITIES

EDITORIAL STAFF

C. L. Faust, Chairman, Publication Committee
Cecil V. King, Editor
Norman Hackerman, Technical Editor
Ruth G. Sterns, Managing Editor
U. B. Thomas, News Editor
H. W. Salzberg, Book Review Editor
Natalie Michalski, Assistant Editor

DIVISIONAL EDITORS

W. C. Vosburgh, Battery
Milton Stern, Corrosion
R. T. Foley, Corrosion
Harry C. Gatos, Corrosion—Semiconductors
Louis J. Frisco, Electric Insulation
Seymour Senderoff, Electrodeposition
H. C. Froelich, Electronics
Ephraim Banks, Electronics
Ernest Paskell, Electronics—Semiconductors
D. R. Frankl, Electronics—Semiconductors
Sherlock Swann, Jr., Electro-Organic
Stanley Wawzonek, Electro-Organic
John M. Blocher, Jr., Electrothermics and Metallurgy
J. H. Westbrook, Electrothermics and Metallurgy
N. J. Johnson, Industrial Electrolytic
C. W. Tobias, Theoretical Electrochemistry
A. J. deBethune, Theoretical Electrochemistry
R. M. Hurd, Theoretical Electrochemistry

ADVERTISING OFFICE

ECS

1860 Broadway, New York 23, N. Y.

ECS OFFICERS

Henry B. Linford, President
Columbia University, New York, N. Y.

F. L. LaQue, Vice-President
International Nickel Co., Inc.,
New York, N. Y.

W. J. Hamer, Vice-President
National Bureau of Standards,
Washington, D. C.

Lyle I. Gilbertson, Vice-President
Air Reduction Co., Murray Hill, N. J.

Ernest G. Enck, Treasurer
Felicity Farm,
Gwynedd Valley, Pa.

Ivor E. Campbell, Secretary
National Steel Corp., Weirton, W. Va.

Robert K. Shannon, Executive Secretary
National Headquarters, The ECS,
1860 Broadway, New York 23, N. Y.

Manuscripts submitted to the Journal should be sent, in triplicate, to the Editorial Office at 1860 Broadway, New York 23, N. Y. They should conform to the revised Instructions to Authors, last published on pp. 145C-146C of the July 1961 issue. Manuscripts so submitted become the property of The Electrochemical Society and may not be published elsewhere, in whole or in part, unless permission is requested of and granted by the Editor.

The Electrochemical Society does not maintain a supply of reprints of papers appearing in its Journal. A photoprint copy of any particular paper, however, may be obtained by corresponding direct with the Engineering Societies Library, 345 E. 47 St., New York, N. Y.

Inquiries re positive microfilm copies of volumes should be addressed to University Microfilms, Inc., 313 N. First St., Ann Arbor, Mich.

Walter J. Johnson, Inc., 111 Fifth Ave., New York 3, N. Y., have reprint rights to out-of-print volumes of the Journal, and also have available for sale back volumes and single issues, with the exception of the current calendar year. Anyone interested in securing back copies should correspond direct with them.

Journal of the Electrochemical Society

DECEMBER 1961 **VOL. 108 • NO. 12**

CONTENTS

Editorial

Fallout Shelter 254C

Technical Papers

Valency of Ions Formed during Anodic Dissolution of Metals in Acids. *M. E. Straumanis* 1087
The Dissolution of Steel in the System NH_4NO_3-NH_3-H_2O. *J. D. Goodrich and N. Hackerman* 1092
Oxidation of Molten High-Purity Aluminum in Dry Oxygen. *W. C. Sleppy* 1097
Phase Equilibria and Tin-Activated Luminescence in Strontium Orthophosphate Systems. *J. F. Sarver, M. V. Hoffman, and F. A. Hummel* 1103
Magnesium Lithium Antimonate Phosphors. *R. W. Mooney* 1110
Preparation of High-Purity Silicon from Silane. *C. H. Lewis, H. C. Kelly, M. B. Giusto, and S. Johnson* 1114
An Explanation of the Superior Radiation Resistance of P-Type Base Si Solar Cells. *R. V. Babcock* 1119
High-Temperature Oxidation and Vacuum Dissociation Studies on the A{111} and B{111} Surfaces of Gallium Arsenide. *D. P. Miller, J. G. Garper, and T. R. Perry* 1123
Vapor Growth of Gallium Arsenide. *R. L. Newman and N. Goldsmith* 1127
The Contamination of Semiconductor Surfaces, I. Metal Ions from Acid Solution on the Intermetallics, GaAs and InSb. *G. B. Larrabee* 1130
Polarographic Studies in Acetonitrile and Dimethylformamide, VI. The Formation of Dihalocarbenes. *S. Wawzonek and R. C. Duty* 1135
The Formation of Elongated Iron and Iron-Cobalt Particles by Electrodeposition into Mercury. *F. E. Luborsky* 1138
Cation Diffusion in Cr_2O_3. *W. C. Hagel and A. U. Seybolt* 1146
A Microscopic Study of Oxide Films on Uranium. *L. Leibowitz, J. G. Schnizlein, L. W. Mishler, and R. C. Vogel* 1153
The Kinetics of Oxidation of Uranium between 125° and 250°C. *L. Leibowitz, J. G. Schnizlein, J. D. Bingle, and R. C. Vogel* 1155
Properties of the Electrical Double Layer in Solutions of Electrolytes in Some Organic Solvents. *S. Minc. J. Jastrzebska, and M. Brzostowska* 1160

Technical Notes

A-C Field Effect Measurements on Silicon. *N. G. Einspruch* 1164
The Effect of an Electric Discharge on the Oxidation Kinetics of Uranium. *J. G. Schnizlein, J. D. Bingle, and L. Leibowitz* 1166
The Influence of the Value of the Transference Number of the Univalent Ion on the Equivalent Conductance of Biunivalent Electrolytes. *N. Goldenberg and E. S. Amis* 1167

Brief Communication

Vapor Phase Growth of Gallium Arsenide Crystals. *W. J. McAleer, H. R. Barkemeyer, and P. I. Pollak* 1168

Discussion Section **1170-1173**

Current Affairs **259C-276C**

Published monthly by The Electrochemical Society, Inc., from Manchester, N. H., **Executive Offices, Editorial Office** and **Circulation Dept.,** and **Advertising Office** at 1860 Broadway, New York 23, N. Y., combining the JOURNAL and TRANSACTIONS OF THE ELECTROCHEMICAL SOCIETY. Statements and opinions given in articles and papers in the JOURNAL OF THE ELECTROCHEMICAL SOCIETY are those of the contributors, and The Electrochemical Society assumes no responsibility for them. Subscription to members as part of membership service; subscription to nonmembers $24.00. Single copies $1.70 to members, $2.25 to nonmembers.

Copyright 1961 by The Electrochemical Society, Inc.

Entered as second-class matter at the Post Office at Manchester, N. H., under the act of August 24, 1912.

Editorial

Fallout Shelter

THERE are fanatics at large, who are determined to subjugate the whole world. The people of the free countries most certainly will not continue indefinitely to talk big but yield ground, and, if the fanatics are madmen as well, like Hitler, grim and devastating nuclear war may be inevitable. Little can be done to protect anyone from direct nuclear-bomb hits; but many people could survive, around the perimeter of the blasts and in areas of intense fallout, by having quick access to adequate shelters.

It is estimated that to construct and stockpile shelters for everyone in the United States would cost at least $200,000,000,000, and the effort would have to be spread over 10 to 20 years. One view is that certain industries can thrive, and unemployment can disappear, if only people will start building shelters now. Another view is that many people are going to let themselves be "gypped," paying too much for badly built, poorly stocked shelters which will be useless if needed. We ought to be able to assume, if shelters are constructed at factories, or for the occupants of an apartment house, or by the American Chemical Society at its new Washington headquarters, that protection will be provided exactly to the extent that is announced by the sponsors, and that expert maintenance will be assured. The individual home owner should expect no less, but he will have to study the problem thoroughly, check and test every point personally, be his own maintenance man. A single flaw could ruin everything.

Under certain conditions, your own dwelling or apartment *could* serve as a shelter. You would just stay inside with everything closed up, crank the hand blower to bring in filtered air and the hand generator to charge the batteries, eat and drink your stockpile of food and liquids, listen for the Safe signal, and watch the radiation intensity meter. A basement shelter would be a little better, but external underground chambers with separate protected and baffled access are far to be preferred. They must be watertight or well drained, have adequate filtered air intake, and have air exit ports protected from back-drift of fallout dust. The do-it-yourself man will probably install a well, if at all possible, and provide drainage at least to a dry well.

Measurement of the radiation level is a serious problem. In case radio announcements were lacking or inadequate, you would be dependent on your own instruments. Unfortunately it is not easy to construct inexpensive (or even expensive) instruments which are rugged, durable, stable, and easy to read, interpret, and maintain by relatively untrained people. One type has been approved by the Office of Civil Defense Mobilization, and we hope that other types will become available.

In working with radioactive materials in the laboratory, one carefully watches radiation exposures of a few *milliroentgens* per *week*. It is a shock to discover that this radiation would not even be registered by the Survival Radiation instruments. One commercial ratemeter reads up to 120 *roentgens* per *hour*, roughly 400,000 times the average permissible laboratory level. The corresponding dosimeter reads up to 600 roentgens before it must be recharged.

We hope and trust that madmen will never get near the nuclear war push-buttons. But if, just in case, you build a fallout shelter—*do it well.*

—CVK

ANACONDA introduces PURE COPPER *Electranodes*®

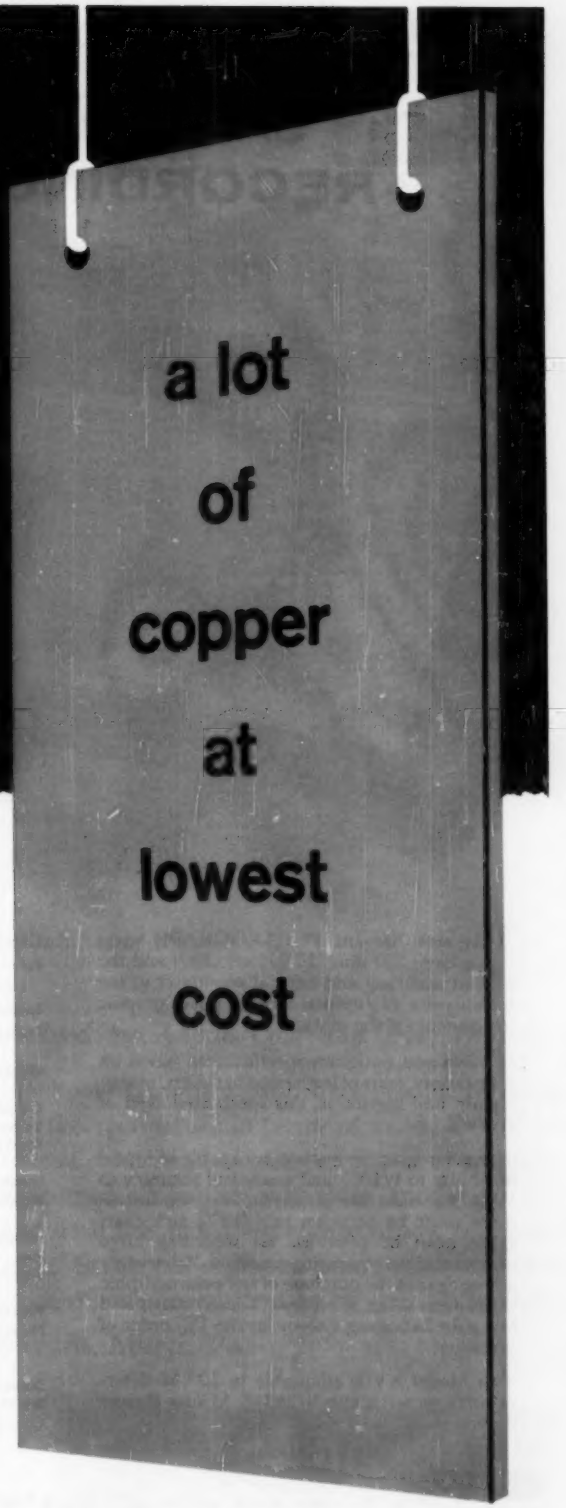

Now . . . pure copper anodes available in the lowest price range! Developed solely for the plating trade, Electranodes are produced from full 1" thick electro-deposited copper.

QUICK FACTS

Economical—in the lowest price range of any copper anodes of similar thickness.

Highest Commercial Purity—made from virgin metal of 99.925% minimum purity.

Ample Thickness—to drill and tap holes for insertion of suspension hooks.

Oxygen-Free—suitable for both acid and cyanide plating.

Dense Structure—no porosity.

Here, for the first time, is high-quality electrolytic copper available in full 1" thickness that cuts handling time, lowers costs. Electranodes can be used in any plating operation where a flat anode will fill requirements. If you want an economy type anode, Electranodes offer you the finest quality at the lowest possible cost.

Write for Electranode Specification Form. We'll follow up with prompt price and delivery information on Electranodes to meet your specific needs. Address: Anaconda American Brass Company, Waterbury 20, Conn. In Canada: Anaconda American Brass Ltd., New Toronto, Ontario. 61-812

ANACONDA®
AMERICAN BRASS COMPANY

The SARGENT Model XV
RECORDING POLAROGRAPH®

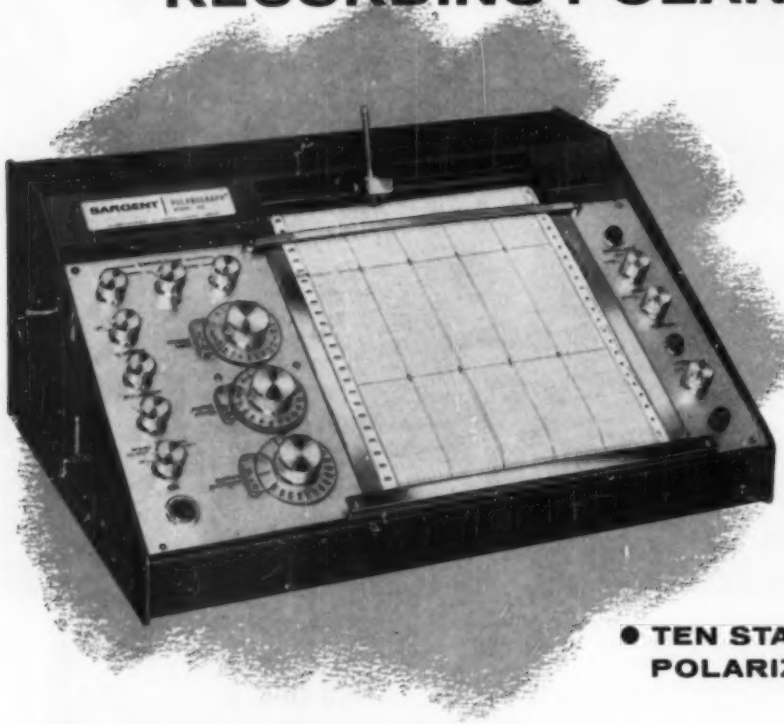

offers you—

- **FULL 10 INCH CHART**
- **1/10% ACCURACY OF MEASUREMENT**
- **TEN STANDARDIZED POLARIZING RANGES**

This new Sargent POLAROGRAPH gives you a large 250 mm (10 inches) chart and the highest accuracy and current sensitivity at the lowest price of any pen writing polarographic instrument on the market.

It offers you optimum specifications based on over twenty years of leadership in design, manufacture and service in this specialized field of analysis.

The polarographic method is capable of reproducibility to 1/10% and analytical accuracy to ½%. To make use of this facility, the instrument must be accurate to 1/10% and chart space must be provided for recording large steps to achieve measuring precision. We strongly advise against the purchase of any polarographic instrument using miniature (5 inch) charts and low gain balancing systems in the 1% order of precision.

This Model XV is adaptable to 10^{-4} M determinations with the S-29315 Micro Range Extender.

®Registered Trade Mark (Pat. No. 2,931,964)

Current Ranges:	19, from .003 to 1.0 μA/mm.
Polarizing Ranges, volts:	0 to −1; −1 to −2; −2 to −3; −3 to −4; +.5 to −5; 0 to −2; −2 to −4, +1 to −1; 0 to −3; +1.5 to −1.5.
Balancing Speed:	standard, 10 seconds; 1 second or 4 seconds optional.
Bridge Drive:	synchronous, continuous repeating, reversible; rotation time, 10 minutes.
Chart Scale:	current axis, 250 mm; voltage axis, 10 inches equals one bridge revolution.
Current Accuracy:	1/10%
Voltage Accuracy:	¼%
Chart Drive:	synchronous, 1 inch per minute standard; other speeds optional.
Writing Plate:	10½ x 12½ inches; angle of slope, 30°.
Standardization:	manual against internal cadmium sulfate standard cell for both current and voltage.
Damping:	RC, four stage.
Pen:	ball point; Leroy type optional.
Suppression:	zero displacement control, mercury cell powered, 6 times chart width, upscale or downscale.
Potentiometric Range:	2.5 millivolts, usable as general potentiometric recorder.
Finish:	case, enameled steel; panels, anodized aluminum; writing plate, polished stainless steel; knobs and dials, chromium plated and buffed.
Dimensions:	23 x 17 x 10.
Net Weight:	65 pounds.

Catalog number **S-29310** with accessories and supplies. . . . **$1585.00**

For complete information write for Sargent Bulletin P

SARGENT *SCIENTIFIC LABORATORY INSTRUMENTS • APPARATUS • SUPPLIES • CHEMICALS*

E. H. SARGENT & CO., 4647 WEST FOSTER AVE., CHICAGO 30, ILLINOIS

DETROIT 4, MICH. • DALLAS 35, TEXAS • BIRMINGHAM 4, ALA. • SPRINGFIELD, N. J. • ANAHEIM, CALIF.

how do you look at ANODES?

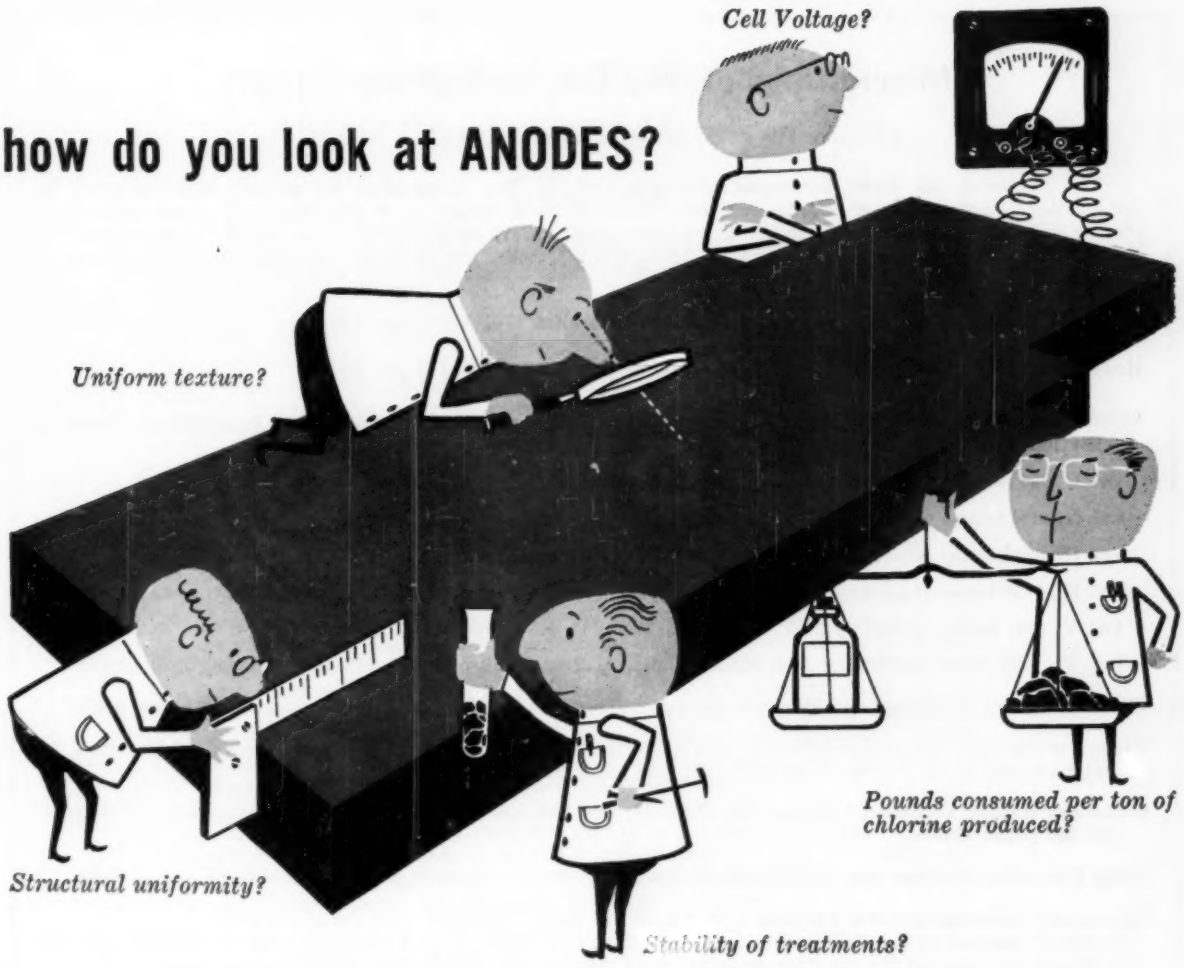

Judged by Cell Maintenance Costs Alone,

the highly stable impregnants used in Stackpole GraphAnode reduce diaphragm clogging to a bare minimum. The graphite is consumed slowly and evenly. Because GraphAnode anodes present uniform, low-porosity surfaces to the electrolyte, the graphite does not slough off to clog the diaphragm or to contaminate the cell.

Judged by Anode Cost and Performance,

Stackpole GraphAnode proves second to none whether you figure in terms of anode life, or in tons of chlorine produced per pound of graphite consumed. You get maximum anode life . . . and with the added advantage of low cell voltages. Stackpole engineers stand ready to offer a convincing demonstration on your equipment.

Stackpole Carbon Company, St. Marys, Pa.

CATHODIC PROTECTION ANODES • FLUXING & DE-GASSING TUBES • SALT BATH RECTIFICATION RODS • ROCKET NOZZLES • RISER RODS • GRAPHITE BEARINGS & SEAL RINGS • ELECTRODES & HEATING ELEMENTS • WELDING CARBONS • VOLTAGE REGULATOR DISCS • "CERAMAGNET"® CERAMIC MAGNETS • ELECTRICAL CONTACTS • BRUSHES for all rotating electrical equipment • and many other carbon, graphite and electronic components.

STACKPOLE
GraphAnode®

ELECTROCHEMICAL ANODES FOR DIAPHRAGM, MERCURY, MANGANESE DIOXIDE, & SODIUM CHLORATE CELLS. OTHER TYPES FOR CATHODIC PICKLING, ALUMINUM ANODIZING, AND OTHER USES.

Monographs of The Electrochemical Society

ECS Series

The following are books developed and sponsored by The Electrochemical Society and published by John Wiley & Sons, Inc., 440 Fourth Ave., New York 16, N. Y. Members of The Electrochemical Society can receive a 33 1/3% discount by ordering volumes from Society Headquarters, 1860 Broadway, New York 23, N. Y. Book and invoice will be mailed by John Wiley & Sons. Nonmembers (including subscribers) should order direct from Wiley.

Corrosion Handbook. Edited by Herbert H. Uhlig. Published 1948, 1188 pages, **$16.00**

Modern Electroplating. Edited by Allen G. Gray. Published 1953, 563 pages, **$8.50**

Abstracts of the Literature on Semiconducting and Luminescent Materials and Their Applications. Compiled by Battelle Memorial Institute.

Vol. I, 1953 Issue—published 1955, 169 pages, **$5.00** (soft cover)

Vol. II, 1954 Issue—published 1955, 200 pages, **$5.00** (soft cover)

Vol. III, 1955 Issue—Edited by E. Paskell; published 1957, 322 pages, **$10.00** (hard cover)

Vol. IV, 1956 Issue—Edited by E. Paskell; published 1959, 456 pages, **$12.00** (hard cover)

Vol. V, 1957 Issue—Edited by C. S. Peet; published 1960, 449 pages, **$12.00** (hard cover)

Vol. VI, 1958 Issue—Edited by J. J. Bulloff and C. S. Peet; published 1961, 528 pages, **$14.00** (hard cover)

Electrochemistry in Biology and Medicine. Edited by Theodore Shedlovsky. Published 1955, 369 pages, **$11.50**

Vapor Plating (The Formation of Metallic and Refractory Coatings by Vapor Deposition), by C. F. Powell, I. E. Campbell, and B. W. Gonser. Published 1955, 158 pages, **$5.50**

High-Temperature Technology (Materials, Methods, and Measurements). Edited by I. E. Campbell. Published 1956, 526 pages, **$15.00**

Stress Corrosion Cracking and Embrittlement. Edited by W. D. Robertson. Published 1956, 202 pages, **$7.50**

Arcs in Inert Atmospheres and Vacuum. Edited by W. E. Kuhn. Published 1956, 188 pages, **$7.50**
(Papers Presented at the Symposium on Arcs in Inert Atmospheres and Vacuum of the Electrothermics and Metallurgy Division of The Electrochemical Society, April 30 and May 1, 1956, San Francisco, Calif.)

Technology of Columbium (Niobium). Edited by B. W. Gonser and E. M. Sherwood. Published 1958, 120 pages, **$7.00**
(Papers Presented at the Symposium on Columbium—Niobium of the Electrothermics and Metallurgy Division of The Electrochemical Society, May 15 and 16, 1958, Washington, D. C.)

The Structure of Electrolytic Solutions. Edited by Walter J. Hamer. Published 1959, 441 pages, **$18.50**
(Based on a Symposium held in Washington, D. C., in May 1957, sponsored by The Electrochemical Society, New York, and The National Science Foundation, Washington, D. C.)

Mechanical Properties of Intermetallic Compounds. Edited by J. H. Westbrook. Published 1959, 435 pages, **$9.50**
(A Symposium, Sponsored by the Electrothermics and Metallurgy Division of The Electrochemical Society, May 4, 5, and 6, 1959, Philadelphia, Pa.)

The Surface Chemistry of Metals and Semicoductors. Edited by Harry C. Gatos, with the assistance of J. W. Faust, Jr., and W. J. La Fleur. Published 1960, 526 pages, **$12.50**
[Proceedings of an International Symposium Sponsored Jointly by the Office of Naval Research and The Electrochemical Society, Inc. (Corrosion and Electronics Divisions), October 19, 20, and 21, 1959, Columbus, Ohio]

Transactions of the Symposium on Electrode Processes. Edited by Ernest Yeager. Published 1961, 374 pages, **$20.00**
(The papers and discussions of the Symposium on Electrode Processes, sponsored jointly by the U. S. Air Force, Office of Scientific Research, and The Electrochemical Society, Inc., Philadelphia, Pa., May 1959)

Vacuum Metallurgy

Vacuum Metallurgy, third printing, 1958. Edited by J. M. Blocher, Jr.; 216 pages; **$5.00, less a 20% discount** to ECS members only. Available from Electrochemical Society Headquarters, 1860 Broadway, New York 23, N. Y.
(Papers Presented at the Vacuum Metallurgy Symposium of the Electrothermics and Metallurgy Division of The Electrochemical Society held in Boston, Mass., October 6 and 7, 1954)

Valency of Ions Formed during Anodic Dissolution of Metals in Acids

M. E. Straumanis

Department of Metallurgical Engineering,
University of Missouri School of Mines and Metallurgy, Rolla, Missouri

ABSTRACT

The charge of cations of active metals, going anodically into solution in acid or alkaline electrolytes, can be computed from the current applied and the total hydrogen evolution rate after the initial, self-dissolution rate has been subtracted. However, under such conditions an ionic charge, experimentally not provable, of much higher or lower value than the normal one is calculated. Evidently this charge is apparent and corresponds to the true one only then, if the self-dissolution rate does not change when the anodic current is applied.

It can be shown (by measuring the total hydrogen volume developed) that calculated abnormal valencies result when the change of self-dissolution rate (difference effect) due to the anodic current is disregarded. In the case of the positive effect, high charges and, in the case of the negative effect, low (apparent) cationic charges are computed. The impossibility of the calculated high cationic charges proves in turn that the positive effect cannot be explained by the expulsion of such cations by the anode. Since it was shown at least in the case of Be (which also might be true with Mg) that the metal partially disintegrated into tiny metal particles under the influence of the anodic current, the need for the assumption of Be^{+} formation is removed. The appearance of the negative Δ effect can be explained in a better way.

All the phenomena occurring in the anodic compartment in acidic as well as neutral solutions can be explained readily by the consequences of the altered self-dissolution rates, especially if the activation of the dissolving surface of the anodic metal, the breakdown of the protective films, and the formation of metal fragments by the anodic current are considered.

Indications that uncommon valency cations may be formed during anodic dissolution of metals can be found in the old as well as in the newest literature (1, 2). The authors of all these articles were mostly concerned with cations of a valency lower than the normal one. A brief survey of the question including the most important literature is given by Kleinberg *et al.* (2, 3).

The purpose of the present article is to check once more on an experimental basis the question of valency of cations expelled by a metallic electrode in acidic aqueous solutions while under an anodic current and to discuss the possible explanations of the effects observed in reference to the literature.

Experimental Arrangement and Calculation

The experimental arrangement was the same as described previously for the measurement of the difference effect (4). In order to eliminate completely the formation of gases other than hydrogen, an internal current was used. The metal itself acted as an anode while a platinized platinum electrode served as a cathode. The arrangement is shown schematically in Fig. 1A. The variable resistance *R* in the circuit permitted the control of the anodic current strength. The apparatus for collecting the hydrogen while the anode was undergoing self-dissolution and under an anodic current is sketched in

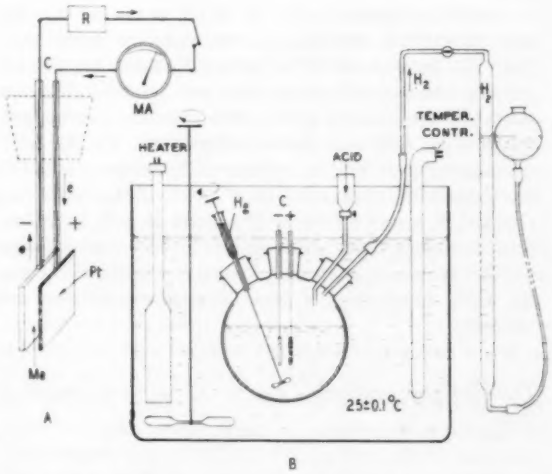

Fig. 1A. The cell consisting of an active anode and of a platinum cathode. Fig. 1B. The cell in the water thermostat (25° ± 0.1°C) connected with the gas buret for collection of hydrogen and for the determination of dissolution rates.

Fig. 1B. In the case of Ti the cell was flushed with hydrogen in order to prevent oxidation of Ti^{3+} to Ti^{4+} by the oxygen of the air leading to a decrease in the gas volume of the cell. In all other cases the

oxidation of hydrogen at the Pt-cathode by air in the flask was negligible.

The most interesting observation made with the arrangement (Fig. 1A) is that the rate of hydrogen evolution on the anodic metal dissolving in an acid (self-dissolution) changes as soon as the circuit is closed while some hydrogen evolution starts on the Pt cathode. The rate of H_2 evolution on the anode may increase or decrease under the influence of the flowing current or may not change at all, depending on various conditions. It was proposed that this change in hydrogen evolution rate could be explained by the change in valency of cations going anodically into solution (1-3) as discussed later. The rate measurements and the calculations of valencies were performed as follows.

At first with the circuit (Fig. 1A) open the rate of self-dissolution V (in mm^3/cm^2 min) of the soluble electrode was determined (after the rate became constant) from the volume of hydrogen developed; then the circuit was closed and the resistance R was set so that a certain current could pass the soluble electrode. The total amount of hydrogen produced by the dissolving plate and by the current was collected and the rate V_t was found. Then the current was stopped and the rate of self-dissolution, V, of the metal used in the combination, determined again. (The average, V_1, of both V self-dissolution rates was used later for the computations.) After that a higher density current was switched in, the total rate V_t determined, *etc.* This was continued in steps until the maximum current that could be drawn from the cell was reached. There was no necessity for weight loss determinations since the volume of hydrogen developed was a correct measure for this loss.

Assuming, tentatively, in order to show the improbability of the uncommon valency hypothesis, that the rate of self-dissolution V_1 does not change during the passage of the anodic current, the valency of the cations going into solution can be calculated as follows: Subtracting from V_t the self-dissolution rate V_1, the volume of hydrogen (at STP) developed in a certain time interval by only the current, I, can be found. The next step is to calculate the hydrogen equivalent f_1 for one faraday (96490 amp sec, chemical scale) from the difference $V_t - V_1$. Expressing I in milliampere minutes, one obtains

$$f_1 = 1608.2\ (V_t - V_1)/I\ \text{cm}^3 \qquad [1]$$

The average cationic charge C^+ of the metal is then

$$C^+ = n_M\ 11207/f_1 \qquad [2]$$

n_M being the normal valency of metal which goes into solution, *e.g.*, for Zn it is 2, for Al or Ti 3, and for Zr 4.

Results

With the assumption as indicated above, the average charge C^+ of cations going into solution under the anodic current was computed for several metals, using the data which were obtained in the rate measurements. The results for the metals Zn (5), Al (6), and Ti (4) are summarized in Table I. Table I clearly shows that the average charge of the cations of the three metals going anodically into solution appears to increase with their tendency to passivation (7). Still more interesting are the results obtained with Al in HCl (6). The calculated average cationic charge is plotted against the current density in Fig. 2 and shows that at low current densities the charge of the cations is high, decreases with current, becomes equal to 3 at about 13 ma/cm^2, and reaches a limiting value of 2.6 at still higher densities. Thus, the valency calculated appears to depend not only on the nature of the metal going into solution, but also on the electrolyte, current density, temperature, etc. (3). In addition, the valencies generally appear to be unusual, and only at one exceptional point (Fig. 2) are they normal (3-valent). This suggests that the calculated valencies might not be real at all, but only apparent, resulting as a consequence of an unusual approach to the problem, disregarding some important facts.

Table I. Average charge C^+ (valency) of cations going into solution at 25°C from Zn, Al, and Ti anodes

Anode	Electrolyte	$V_t - V_1$, mm^3/cm^2 min	I, ma min	f_1, cm^3	Apparent C^+ ion valency
Zn	2*N* H_2SO_4	53.3	9.6	8925	2.5
	2*N* H_2SO_4	90.0	20.8	6960	3.2
	2*N* H_2SO_4	150	40.0	6040	3.7
	2*N* H_2SO_4	360	73.7	6560	3.4
	2*N* H_2SO_4	732	127.0	9270	2.4
Al	2*N* HF	12.5	5.1	3940	8.5
	2*N* HF	115.7	36.5	5100	6.7
	2*N* HF	123.2	56.0	3450	9.5
	2*N* HF	90.3	58.0	2510	13.4
Ti	0.5*N* HF	6.5	5	2090	16.1
	0.5*N* HF	8	10	1286	26.2
	0.5*N* HF	17	14.8	1850	18.3
	0.5*N* HF	25.5	20.0	2050	16.4
	0.5*N* HF	36	24.3	2385	14.1
	0.5*N* HF	55	29.3	3010	11.4
	0.5*N* HF	76	35.8	3410	9.8

Discussion

Apparent valency cations.—According to the uncommon valency concept, a decrease or increase (2, 3) in rate of hydrogen evolution is explained as follows.

1. The anodic current (see Fig. 1A) produces ions of higher valency at the anode (Table I). The

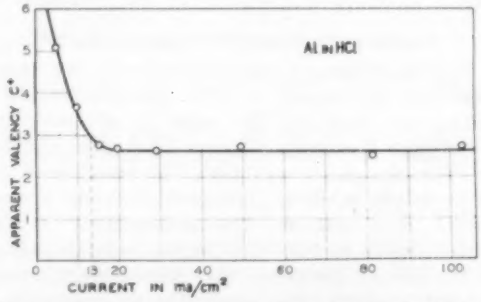

Fig. 2. Average charge of Al ions going anodically in 1N HCl (25°C) into solution in dependence of current density. The respective f_1 are: 6620, 9975, 12,520, 12,830, 12,350, 13,500, and 12,430 cm^3/faraday.

oxidizing power of these higher valency ions converts hydrogen gas into H^+ ions in the vicinity of the anode, *e.g.*

$$Al^{4+} + H = Al^{3+} + H^+ \qquad [3]$$

Since the hydrogen (in form of atoms or of small bubbles dispersed in the electrolyte) originates in the self-dissolution process, the result of this oxidation is an apparent decrease in rate of the process.

2. An increase in rate of hydrogen evolution results, according to the assumption of Kleinberg and other authors (2, 3, 8, 12, 14, 25), when ions of lower valency than normal are expelled by the anode (Fig. 2). Additional hydrogen is formed in the reaction of H^+ with these lower than normal valency ions, *e.g.*

$$Al^{2+} + H^+ = Al^{3+} + 0.5H_2 \qquad [4]$$

The result is an apparent increase in the rate of self-dissolution. However, the volume of hydrogen finally developed by one g equivalent of Al is the same (the theoretical) in both cases.

This theory explains the increase or decrease of hydrogen evolution caused by an anodic current on an electrode of an active metal; it explains the oxidation or reduction reactions in the anodic compartment and why the presence of uncommon valency ions cannot be proved. However, it does not explain why under certain conditions ions of various and unusual valencies are formed.

Furthermore, in case 1 not considered by Kleinberg *et al.*, it is very difficult to explain the existence of Al^{4+}, although short lived, in aqueous solutions. It is still more difficult to accept the formation of ions of a yet higher positive charge. Ions such as $Al^{13.4+}$ or Ti^{20+} (see Table I) are impossible for many reasons if only for the fact that there are not enough electrons within the atom. Therefore, for the explanation of the decrease in rate due to anodic current the hypothesis, as expressed by Eq. [3], has to be dropped.

The appearance of lower valency ions in the second base is also limited: ion charges lower than one cannot be expected. Nevertheless, $Mg^{0.27+}$ ions were calculated (8); Si dissolved anodically according to Schmidt and Blomgren with apparent current efficiencies of more than 400%, which rules out any explanation based on dissolution of Si as ions of lower valency (9) and makes explanation 2 for the increase in rate, based only on a reaction such as [4], quite impossible. Thus, doubt is also cast on the formation of uncommon valency ions with a charge between 1^+ and the normal valency (see experiments with Be).

Besides, concerning 1 and 2, in all our experiments the anodic metal itself was used as a source of current; hence, the emf of the cell Fig. 1A was never larger than the dissolution potential of the anode. Whether under such conditions the anode can expel highly unstable ions with very uncommon charges is at least doubtful if not impossible. Such a possibility may, however, exist if an external source with a much higher emf, *e.g.*, in electropolishing, is used for enforcement of anodic dissolution. In the present experiments the uncommon valency ions

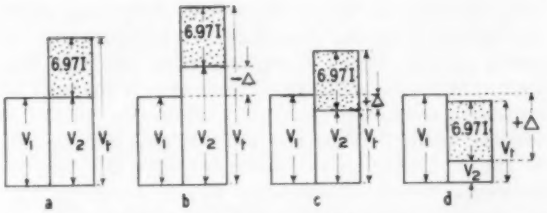

Fig. 3. Relationship between the difference effect Δ, the total rate of dissolution v_t, and the self-dissolution rates V_1 and V_2, the latter being the self-dissolution rate developed under the anodic current. a, $V_1 = V_2$, no Δ-effect, see Fig. 2 at I = 13 ma/cm²; b, $V_1 < V_2$, negative Δ-effect, Al in HCl (6); Mg(12), Fe(13), or Be(14) in NaCl; c, $V_1 > V_2$, positive Δ-effect, Al in NaOH(10), in HF(6); Zn in H_2SO_4(5); d, $V_1 >> V_2$, very strong positive Δ-effect, Zr in HF(7). 6.97I-H_2 in mm³ developed by I ma min.

can only be regarded as apparent, especially as there are other, simpler and better founded explanations for the phenomena of decrease or increase in hydrogen evolution rate due to the passage of an anodic current.

Difference effect.—This change in self-dissolution rate, the reasons for which will be discussed later, is known in the literature as the difference effect Δ (10, 11). The experience gained in dealing with this effect showed that it is not the self-dissolution rate V_1 (with the anodic current = 0) which has to be subtracted from the total rate V_t, but the self-dissolution rate V_2 which establishes itself during anodic polarization. This rate (V_2) may be larger, smaller, or equal to the self-dissolution rate V_1 (see Fig. 3), as established in various Δ effect measurements. Because of the reasons mentioned above the Δ effect cannot be explained by the change of charge of the cations going into solution anodically, but only by the alteration of the rate of self-dissolution from V_1 to V_2. The attempts of Kabanov et al. (15) to interpret the negative difference effect on Mg as a consequence of formation of Mg^+ ions must, therefore, be accepted with reservation, especially as it was shown by Robinson and King that the electrochemical behavior of Mg can be explained satisfactorily solely on the basis of divalent ion formation (16). The increased amount of Mg obtained during electrolysis ($6.97I + \Delta$, Fig. 3b) is not due to formation of Mg^+, but due to the increased rate of self-dissolution $V_1 \rightarrow V_2$. Of course, reasons have to be given why this change occurs when the anodic current is switched on.

Reasons for change in self-dissolution rates.—Every one of the active metals, such as Be, Mg, Al, Ti, Zr, Hf, and Zn under certain conditions, are covered with some kind of protective coatings or films consisting mostly of oxides or hydroxides (16). However, coatings consisting of hydrides (17) or of salts (18) are also possible. If now an anodic current is applied, the conditions in the interface change suddenly, which may cause according to Draley *et al.* (19) a change in composition, porosity, thickness (20), adherability, and even a breakdown of the protective layer followed by a change in the rate of self-dissolution of the metal underneath.

The decrease in hydrogen evolution rate of the dissolving metal (+ Δ effect) is explained by the polarization of the local elements: the anodic cur-

rent which flows to the Pt-cathode (Fig. 1A) shifts the potential of the dissolving metal toward more noble values. This can be measured directly. The emf of the local cells drops and with it the rate of hydrogen evolution ($V_1 > V_2$) while the current is flowing to the Pt electrode (5, 10). This explanation of the + Δ effect is in agreement with the electrochemical theory of corrosion and is accepted, *e.g.*, by Evans [(21), see also (22)]. No ions of a larger charge than normal (Table I, Eq. [3]) are necessary to understand the decrease in hydrogen evolution rate from V_1 to V_2.

There are two reasons for the increase in the rate of hydrogen evolution of the dissolving metal (— Δ effect), while the anodic current is flowing through the electrode: the breakdown of the protective layer, as already mentioned (11), and the chunk effect (22). Due to the impact of the anions suddenly leaving the anode, because of the anodic current, the oxide film on active metals partially breaks down and the acid comes in direct contact with the bare metal thus increasing the rate of self-dissolution from V_1 to V_2 (16). This increase augments with the current density (6). Evidently no film of the same composition is formed while the anodic current is flowing, but the film is regenerated as soon as the current stops (11). Usually oxide films are formed on electrodes while they are polarized anodically. However, under the conditions of the present experiments, where no external emf was used, the potential difference is much too small to enforce oxygen deposition and film formation. A "natural" film is formed only when the stream of cations expelled by the anode is stopped (turning off the current, Fig. 1A). It is interesting to note that the change in rate of self-dissolution (— Δ effect) is used by the defendants of the lower valency theory for the explanation of formation of Mg-ions with a charge less than one (8) without reference to the Δ effect. So, why not use this correct explanation throughout?

It is evident that an active metal with the protective film partially removed (while the anodic current is flowing) should act as a strong reducer ($Me \rightarrow Me^{n+} + 2e$), especially if an efficient oxidizer is present in the electrolyte. The amount reduced should be equivalent to the hydrogen lost, and the reduction should occur at the anode while the current is flowing. All this was confirmed by experiments (3, 8). Sometimes a reduction at some distance from the anode was observed. Again the explanation is simple: it could be directly observed, *e.g.*, in the case of dissolving Al (Fig. 1A), that very small metallic particles detached from the anode were floating in the electrolyte (11). These particles, as well as the hydrogen produced by them, could act as a reducer.

However, in the case of beryllium it was found that a black substance appeared throughout in the anolyte during the electrolysis (14, 23). It was shown that the dark portion of the suspension consisted of metallic Be particles, the formation of which was attributed to the disproportionation of Be^+ ions, initially expelled by the current:

$$2Be^+ = Be^{2+} + Be \qquad [5]$$

Thus, it was assumed that in aqueous solutions growth of Be particles occurred, which was and still is contrary to experience, since no one could deposit metallic Be on the cathode from aqueous solutions. The work done with Be in this laboratory disclosed another fact confirming the explanation for the increase in self-dissolution while under anodic current. The metal obtained from the Brush Beryllium Company dissolved in HCl with the formation of a black dispersion. The washed and dried dispersion was investigated by x-rays, and microscopically it was found to consist of various size Be particles, mostly in form of needles, about 0.0004 mm in diameter and up to 0.025 mm in length. The particles and needles had the same appearance and even diameter, like the formations which were observed on the deeply etched compact metal (24). Therefore, the metallic particles in the electrolyte or acid were not formed due to reaction [5], but simply originated from the metal itself which partially disintegrated while dissolving in HCl. Of course, when an anodic current passed the electrode, Be went into solution as Be^{2+}; at the same time fragments of the metal detached themselves from the anode [chunk effect according to Marsh and Schaschl (22)] and dissolved partially in the solution quite remote from the anode. From the current and weight loss an apparent charge lower than 2 was, therefore, calculated for the Be-ions. (To arrive at the correct valency, the weight of the dispersed particles had to be subtracted from the weight loss.) Because of the large surface of the dispersed metallic Be particles they act as reducers either directly or through the hydrogen (*in statu nascendi*) throughout the anolyte. Since a black product was also observed during anodic dissolution of Mg (25) the reason for the apparent formation of Mg^+ is the same. Thus, for the explanation of the — Δ effect and the reduction phenomena no ions of lower valency are necessary. The appearance of the bare metal and of chunks as a consequence of the applied anodic current explains both of them.

When the rate of self-dissolution V_1 of a metal in certain electrolytes is low or very low, activation of the metallic surface by the anodic current may occur (— Δ effect).

Activated surface.—A certain activation of the surface occurs when one part of the protective layer is broken off by the impact of cations forced into solution by the anodic current or by the changed conditions in the interface while the current is flowing. Already this increases the rate of self-dissolution. But that is not the only reason for surface activation.

According to the theory of crystal growth and dissolution, as developed by Kossel (26) and Stranski (27-29), it is most difficult to remove an atom from the middle of a crystallographic plane of a metal because it is held in position by all the nearest neighbors around, except the neighbors above the plane which are missing. However, one atom or groups of atoms can be forced into solution easily by an anodic current. Taking as an example a cubic metal, the situation on a (100)-plane is shown after

the application of an anodic shock (Fig. 4a). Arrows on Fig. 4 indicate the atoms which are bound by forces exhibited by only half of the closest neighbors or even by less (Fig. 4b). Groups of isolated atoms may remain on a crystallographic plane in the moment of interruption of current (Fig. 4c). There is enough electron microscope evidence that etching processes on metallic surfaces, *e.g.*, of Al, proceed in this way. The atoms on the edges or corners of rows and the single atoms and groups of them should exhibit a larger solution pressure, and therefore, a more negative potential or higher free energy. Thus, they will go into solution in addition to the anodic current increasing the rate of self-dissolution. The latter may increase proportionally to the current density. This increased rate will continue even after termination of the current (15) until all the activated atoms or clusters of them are gone and the previous conditions in the interface are restored. It is easily understood that the anodic current can even undermine fragments of the crystalline surface, as shown in Fig. 4, so that they will become completely separated from the anode and then will dissolve or react as separate entities with the electrolyte [chunk effect (22)]. There is enough experimental evidence for the separation of blocks, chunks, or fragments from the anodes of aluminum (30), magnesium (31), silver (32), etc., while the anodic current is flowing and, even with no such current, merely by the attack of the corrosive agent. These minute blocks, will react faster with more agressive agents, *e.g.*, in presence of strong oxidizers (3, 33), even if still in contact with the anode (Fig. 4), and will thus increase the rate of self-dissolution of the anode. Hence, the increased self-dissolution rate contributes only apparently to the efficiency of the faradic current. Subtracting this rate and the rate of fragmentation floating in the anolyte from the total rate (which is the sum of the increased self-dissolution rate on the anode, the rate produced by the fragments, and that contributed by the anodic current), in all probability no one would be able to calculate lower valency ions from the anodic current and the remainder of the reaction rate. *Vice versa*, this subtraction is absolutely necessary in order to prove formation of uncommon valency ions.

Conclusion

The experiments and the calculations made show distinctly that in all the cases of metals dissolving with hydrogen evolution in nonoxidizing acids, the decrease or increase in the rate of dissolution while an anodic current is superimposed, cannot be attributed to the formation of ions of uncommon valency because:

1. Only in exceptional cases would the metal then go into solution in the form of normal valency ions.
2. The calculated charge of the ions is in many cases physically and thermodynamically impossible, especially if one considers that the source of the anodic current is the dissolving metal itself.

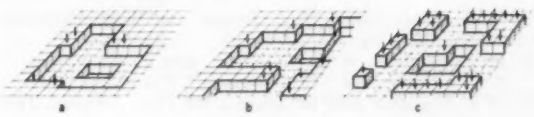

Fig. 4. Dissolution process on the (100)-plane of a metal grain. The cubes represent the unit cells.

3. The lower valency theory disregards any change in the self-dissolution rate, which undoubtedly occurs as a consequence of superimposition of an anodic current.
4. It disregards also the partial disintegration of the anodic metal into finest fragments or chunks (with the current on or without it), which have been proved experimentally, and which afterward react with the electrolyte.
5. The changes in rate, assuming formation of ions of normal valency, can be explained readily by electrochemical polarization (decrease in rate while the current is on, $+\ \Delta$ effect), or by breakdown of protective layers and activation of the metallic surface while the anodic current is flowing (increase in rate, $-\ \Delta$ effect), or by partial disintegration of the anodic metal into finest fragments experimentally proved (chunk effect).
6. All the observations and reducing properties of the anolyte found by the defendants of the lower valency theory can be better explained by the phenomena mentioned in point 5.
7. Authorities like Wöhler (1) or Lange (34) do not accept formation of uncommon valency ions in aqueous solutions under conditions of anodic dissolution.

Thus, the explanation of changes in self-dissolution rates of a metal due to the flow of an anodic current by the formation of uncommon valency cations and their subsequent reaction with the dispersed hydrogen or with the electrolyte is highly improbable. These changes can be explained more easily in another manner without introducing uncommon valency ions.

Acknowledgment

The author thanks the Atomic Energy Commission for the support of this work (At-11-1-73, Proj. 5, Suppl. 5) and Dr. W. J. James, Professor of Physical Chemistry at the School, for assistance with the manuscript.

Manuscript received July 21, 1960; revised manuscript received May 21, 1961. This paper was prepared for delivery before the Houston Meeting, Oct. 9-13, 1961.

Any discussion of this paper will appear in a Discussion Section to be published in the June 1962 JOURNAL.

REFERENCES

1. F. Wöhler and H. Buff, *Liebigs Ann.*, **103**, 218 (1857).
2. T. T. Tsai, W. E. McEven, and J. Kleinberg, *J. Am. Chem. Soc.*, **82**, 3326 (1960).
3. D. T. Sorensen, A. W. Davidson, and J. Kleinberg, *J. Inorg. Nucl. Chem.*, **13**, 64 (1959).
4. M. E. Straumanis and P. C. Chen, *This Journal*, **98**, 351 (1951).
5. M. Straumanis, *Z. physik. Chem.*, **A148**, 349 (1930); *Korros. Metallsch.*, **14**, 67 (1938).
6. M. E. Straumanis and Y. N. Wang, *This Journal*, **102**, 304 (1955).

7. M. E. Straumanis, W. J. James, and W. C. Custead, *ibid.*, **107**, 502, Fig. 1, (1960).
8. M. D. Rausch, W. E. McEwen, and J. Kleinberg, *J. Am. Chem. Soc.*, **77**, 2093, Fig. 1, Table I (1955).
9. P. F. Schmidt and M. Blomgren, *This Journal*, **106**, 694 (1959).
10. M. A. Streicher, *J. (and Trans.) Electrochem. Soc.*, **93**, 304 (1948).
11. M. E. Straumanis, *This Journal*, **105**, 284 (1958); **106**, 536 (1959).
12. J. H. Greenblatt, *ibid.*, **103**, 539 (1956).
13. T. P. May and F. L. LaQue, *Corrosion*, **10**, 91 (1954).
14. K. E. Heusler, Bunsen Tagung, Bonn, p. 93 (1960); *Z. Elektrochem.*, **65**, 192 (1961).
15. D. V. Kokoulina and B. N. Kabanov, *Dokl. Akad. Nauk SSSR*, **112**, 692 (1957).
16. J. L. Robinson and P. F. King, *This Journal*, **108**, 36, 41 (1961).
17. W. J. James and M. E. Straumanis, *ibid.*, **106**, 631 (1959).
18. M. E. Straumanis, W. J. James, and A. S. Neiman, *Corrosion*, **15**, 286t (1959).
19. J. E. Draley and W. E. Ruther, *This Journal*, **104**, 329 (1957).
20. J. S. L. Leach, *J. Inst. Metals*, **88**, 24 (1959).
21. U. R. Evans, "The Corrosion and Oxidation of Metals," p. 321, Edward Arnold, Ltd., London (1960).
22. G. A. Marsh and E. Schaschl, *This Journal*, **107**, 960 (1960).
23. B. D. Laughlin, J. Kleinberg, and A. W. Davidson, *J. Am. Chem. Soc.*, **78**, 559 (1956).
24. M. E. Straumanis and D. L. Mathis, to be submitted for publication.
25. R. L. Petty, A. W. Davidson, and J. Kleinberg, *J. Am. Chem. Soc.*, **76**, 363 (1953).
26. W. Kossel, *Nachr. Ges. Wiss. Göttingen, Math.-Phys. Kl.*, **1**, 135 (1927).
27. I. N. Stranski, *Z. phys. Chem.*, **136**, 259 (1928); **142**, 453 (1929).
28. I. N. Stranski, *Discussions Faraday Soc.*, **5**, 13 (1949).
29. I. N. Stranski, *Bull. Soc. franc. Miner. Crist.*, **79**, 360 (1956).
30. B. Roald and M. A. Streicher, *This Journal*, **97**, 283 (1950).
31. G. R. Hoey and M. Cohen, *ibid.*, **105**, 245 (1958).
32. D. A. Vermilyea, *ibid.*, **105**, 547 (1958).
33. I. Epelboin and M. Froment, *Comp. rend.*, **238**, 2416 (1954).
34. E. Lange, *Z. Elektrochem.*, **59**, 638 (1955).

The Dissolution of Steel in the System NH_4NO_3-NH_3-H_2O

J. D. Goodrich and Norman Hackerman

Department of Chemistry, The University of Texas, Austin, Texas

ABSTRACT

Rates ranged from near zero to almost 30,000 mdd at 30°C depending on the type of steel used. No cracking or pitting was observed. This variation did not correlate effectively with grain size or roughness factor, but may be related either to the amount or distribution of minor constituents in the steel. Both mechanical stress and quenching from 1000°C increased the dissolution rate. The reduction reaction was in part, if not wholly, nitrate to nitrite. The corrosion product was nonprotective and often nonadherent and appeared to be a hydrated or ammoniated iron (II) hydroxide.

It has been reported that intensive attack occurs on steel in the NH_4NO_3-NH_3-H_2O system (1) particularly near weld seams and other stressed areas. Many reports on the physical properties of this system, such as vapor pressure and specific gravity, are available [*e.g.*, (2, 3)]. The work on this problem until recently has been of a preventive nature, with chemical inhibitors being utilized as the sole form of protection for steel. Libinson *et al.* (4) reported that the effect of this system on steel, as well as on other metals, is influenced by the reduction of NO_3^- to NH_3. The present work indicates that the reduction is to NO_2^-. SAE 1020 steel dissolution rates as high as 3700 mdd at 30°C have been reported (5). Although this was verified here for this particular sample of steel, it was found that the rates were greatly dependent on the type of steel used. Values ranged from 200 mdd for zone refined iron to 29,000 mdd for a "killed" steel. These unusually high dissolution rates and the marked differences between steels prompted the present investigation.

Experimental

Reagent grade chemicals were used without further purification in all experiments. Large quantities of the solutions were prepared by weighing the reagents. These were used for numerous experiments so that the error involved in solution preparation was minimized.

All the steels were obtained from the U. S. Steel Company except for a sample of zone refined iron which was kindly provided by F. L. Wilkinson of Battelle Memorial Institute. The steels and their compositions are all listed in Table I. The sheet steel was cut into specimens of approximately 20 cm^2 total apparent surface area. The method of specimen preparation was found to be very important. Pickling in 6*N* HCl, followed by washing in H_2O prior to placing the specimens in the solution, gave high dissolution rates as previously observed (5). However, buffed specimens without acid pickling gave rates near zero for the same sample. Treatment of oxide-covered specimens with 750°C hydrogen, stress, cathodic polarization, pickling in acid, or galvanic coupling with a more active metal all gave high dissolution rates. The acid pickling procedure was used in all of the kinetic experiments reported here.

Wide mouth, 4-oz bottles with plastic screw caps were used as reaction vessels. The solutions were

Table I. Steel composition and other properties

Steel	% Constituents C	Mn	Si	S	ASTM grain size	Rate, mdd, 30°C	Å kcal/mole
E079	0.048	1.19	0.24	0.028	8	22,200	
E037	0.13	1.35	0.21	0.03		28,800	9.5
E126	0.59	1.30	0.23	0.035		23,200	
E127	1.00	1.19	0.19	0.034		25,000	11
E129	1.51	1.17	0.19	0.036		16,600	14
L67J	0.003				6	190 to 290	
D269B	0.048	0.32	0.006	0.028	6	650	22
F808B	0.077				6	135	
F811B	0.081				6	200 to 250	
F809B	0.069				6	135 to 550	
F810B	0.068				4.5	200 to 425	
SAE1010	0.08	0.42		0.03		1,500	
Zone refined iron	Negligible	0.0004	0.001			200	
K1876C	0.09	0.39	0.037	0.011		19,000	

maintained to ±0.1°C and were unstirred. The specimens were supported in the solution by means of glass trees.

The progress of the reaction was followed by removing the specimens from solution periodically, cleaning off the adhering corrosion product, and determining the weight loss. The corrosion product was removed easily by washing the specimens in dilute acid. The acid blank for this was between 1 and 2 mg per specimen. Specimens were removed periodically, cleaned, weighed, and placed back in solution after it had been shown that this type of experiment gave the same dissolution rate as did those using separate specimens for each point on the curve. This is illustrated in Fig. 1.

Dissolution rates, obtained from weight loss-time curves, were reproducible to within 2-10%. Since the rate is so dependent on the composition of the steel, it is probable that nonuniformity of specimens accounts for at least part of the error observed. "Rimmed" steels are particularly noted for their nonuniform composition. The best reproducibility was obtained with "killed" steels exhibiting very high rates (*e.g.*, > 15,000 mdd). No cracking or localized attack was observed in any experiments.

Rate curves.—All rate curves obtained were similar to those shown in Fig. 2. The solution used for determining the rates shown in column seven of Table I had the following composition:

NH_4NO_3 . . . 66.4, NH_3 . . . 14.3, H_2O . . . 19.3 w/o

The measured *p*H was 9.5 (all *p*H measurements were good to ±0.1 *p*H unit). This solution was used for all experiments unless otherwise noted.

The weight losses were found to be directly proportional to the apparent surface area of the steel. As dissolution progressed, slopes of the weight loss *vs.* time curves decreased with time (c.f., Fig. 2). The initial linear portion could be extended to longer periods by not opening the vessel as frequently for weight loss measurements. Thus the change of slope was due in part to loss of NH_3 on opening the containers, and all the reaction rates given were calculated from the initial slopes of the curves. Dissolution rates were found to be independent of solution volume (for constant specimen area) at least between 4 and 10 ml/cm².

Reaction products.—The corrosion product appeared in one of several forms, depending on the H_2O concentration. When the latter was high (> 30 w/o) the corrosion product was black, granular, and magnetic. At lower H_2O concentrations the whitish-green corrosion product was gelatinous and adhered only loosely to the metal surface. This material was not identified, but its green color on dissolution in

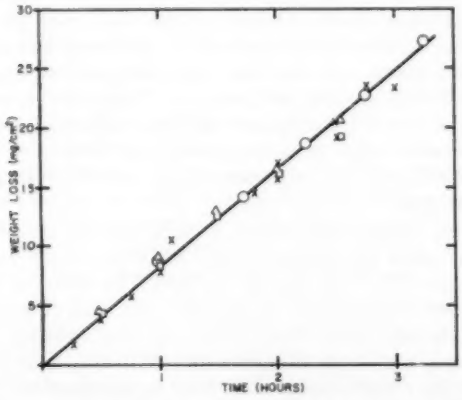

Fig. 1. Comparison of methods of weight loss determination; x, coupon weighed once; 0, △, □, coupon weighed periodically; 4M NH_4NO_3; 10M NH_3; Steel E127; 30°C.

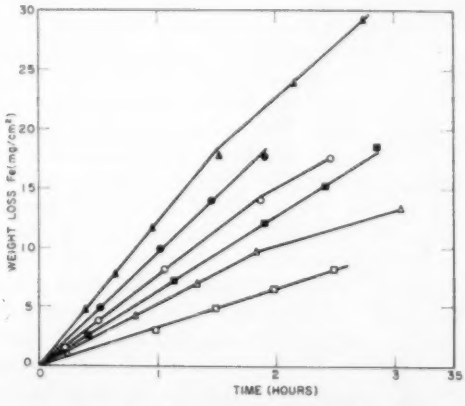

Fig. 2. Rate curves of Steel E127 at different temperatures, □, 20°C; △, 25°C; ■, 30°C; ○, 35°C; ●, 40°C; ▲, 45°C.

water and subsequent drying in vacuum indicated the presence of ferrous ion. On washing with air-free water it converted rapidly to a black, granular, magnetic compound indentified by x-ray diffraction as magnetite.

Filtered solutions in which steel had reacted gave a positive test for iron. After several hours this filtered, clear solution became turbid and a rust colored precipitate appeared in significant amounts. It is believed that iron exists in these solutions in the form of a soluble complex with NH_3. Voriskova (6) obtained a half wave-potential of −1.48 v *vs.* SCE for the system Fe^{++}-NH_4Cl-NH_3-H_2O. Due to the low solubility of ferrous hydroxide in this system the above reduction potential was interpreted (7) as being that of an iron-ammonia complex. Others (8, 9), using solubility and vapor pressure measurements, respectively, have suggested that a complex with coordination number of four exists in solution. In the NH_4NO_3-NH_3-H_2O-iron system the reduction of NO_3^- at a potential more positive than −1.48 v made it impossible to observe the reduction of the presumed iron-ammonia complex here.

Nitrite ion was detected in solution after the reaction got under way. Attempts to determine the NO_3^- concentration were not successful. Reaction between ferrous hydroxide and NO_2^- (10) may account for the difficulty in analysis. To pursue this viewpoint further an analogy may be drawn between the reaction of steel and of zinc in this system. The latter dissolves rapidly, and NO_2^- could be analyzed quantitatively since Zn^{++} does not interfere. It was found that sufficient NO_2^- formed to provide for the reduction reaction, $NO_3^- + H_2O + 2e^- \rightarrow NO_2^- + 2\ OH^-$. This reaction occurs in basic solution with a reduction potential of −0.01 v *vs.* NHE and is accelerated by ferrous hydroxide (11). It is suggested that the same cathodic reaction occurs on steel, except that ferrous hydroxide reacts further with NO_2^- formed. The marked dependence of dissolution rate on NO_3^- concentration (Fig. 5) supports this. Furthermore, oxygen did not affect the rate of reaction of steel in this solution while replacement of NO_3^- by Cl^- gave rates of only about 20 mdd.

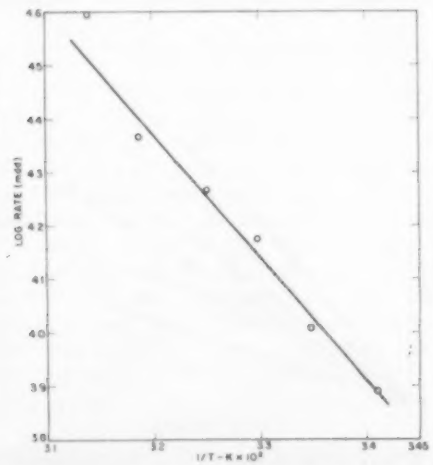

Fig. 3. Log rate vs. 1/T curve for Steel E127.

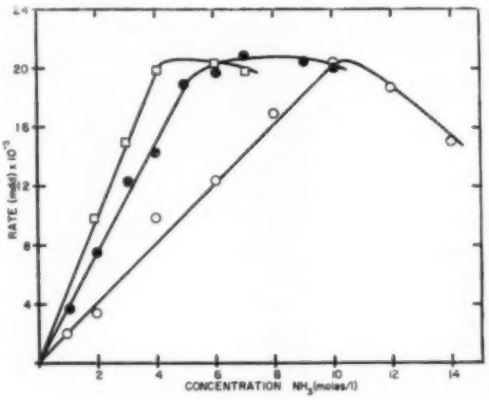

Fig. 4. Variation of dissolution rate with NH_3 concentration; o, 2M NH_4NO_3; •, 4M NH_4NO_3; □, 6.5M NH_4NO_3; Steel E127; 30°C.

Temperature dependence.—Plots of log rate *vs.* $1/T$ were linear over the temperature interval investigated, 20°-45°C. The slopes of these curves are related to an apparent activation energy, $\overset{*}{A}$ (Fig. 2 and 3). These values (Table I) vary inversely with the dissolution rate of the steel at 30°C and depend also on solution composition. The slopes are larger than are normally observed for purely diffusion controlled processes.

With a solution of composition, 10M NH_3, 2M NH_4^+, and 0.1M NO_3^-, $\overset{*}{A}$ for steels E127 and E129 decreased from 11 to 8 and 14 to 7 kcal/mole, respectively. With this solution the rate-controlling step for the reaction is believed to be NO_3^- diffusion to the surface.

Sample E127 was used for all experiments described below relating to the concentration dependence of NH_3, NO_3^-, and NH_4^+. The temperature dependence for this sample is given in Fig. 2 and 3.

NH_3 *effect.*—The reaction rate dependence on ammonia concentration was determined at constant NH_4NO_3 concentrations of 2, 4, and 6.5M, (Fig. 4). The curves exhibit apparent first order kinetics up to some critical concentration beyond which the rate decreases with increasing concentration, fairly rapidly in 2M NH_4NO_3 and much more slowly in the two more concentrated solutions. This decrease is believed to be related to the observed pH increase (Table III, rows 6 and 7) of the system. This effect, along with the fact that the slope of the initial linear portion of a rate *vs.* concentration curve is different at a different NH_4NO_3 concentration, is discussed later. Investigation of the effect of NO_3^- and NH_4^+ on rate was performed at 10M NH_3 concentration.

NO_3^- *effect.*—The effect of NO_3^- on rate could not be studied by changing the NH_4NO_3 concentration because NH_4^+ also affects the rate. The effect of NO_3^- on rate was studied at constant NH_3 and NH_4^+ concentrations using $NaNO_3$, NH_4Cl, and aqueous NH_3 solutions as the components. Figure 5 illustrates the rate dependence on NO_3^- concentration. The rapid increase in rate at low NO_3^- concentration supports the proposed reduction reaction. Attempts to obtain a kinetic reaction order over a reasonable

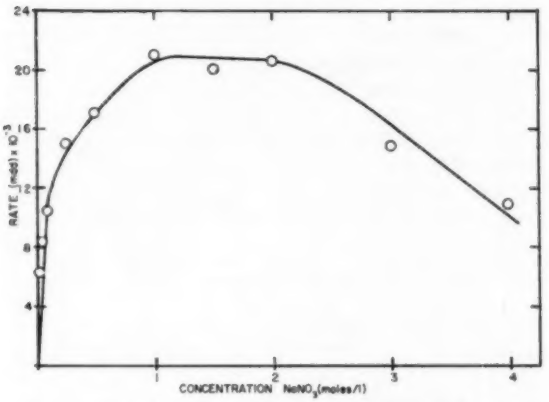

Fig. 5. Variation of dissolution rate with $NaNO_3$ concentration; 10M NH_3; 2.0M NH_4Cl; Steel E127; 30°C.

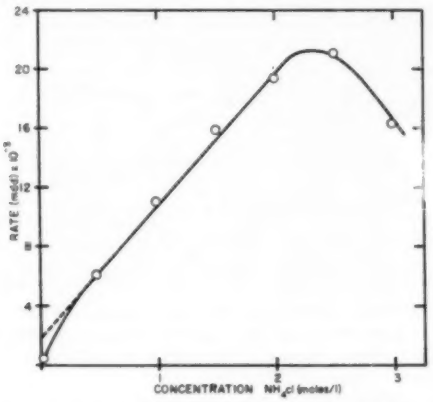

Fig. 6. Variation of dissolution rate with NH_4Cl concentration; 10M NH_3; 1.0M $NaNO_3$; Steel E127; 30°C.

range for NO_3^- below 1M $NaNO_3$ were not successful. Stirring did not alter the rate in this concentration region.

NH_4^+ *effect.*—In the absence of NH_4^+ the rates obtained were near zero. This fact alone warrants investigating the effect of NH_4^+ in addition to the different initial slopes for several NH_4NO_3 concentrations in Fig. 4. This effect was studied by using various NH_4Cl concentrations in solutions 1M in $NaNO_3$ and 10M in NH_3 (Fig. 6). The rate increased with NH_4^+ concentration up to 2M. Extrapolation of the linear portion of the curve to the ordinate gave an intercept of 2000 mdd. The figure shows that a suitable straight line could be drawn through most of the data points plus the origin. Others (12) working on a similar system observed independent reaction paths for both NH_3 and NH_4^+ giving a positive intercept for a rate *vs.* concentration curve involving NH_4^+. This effect may also be occurring in this system, but is not completely justified at this time by the data. Most important is the linear character of the curve below 2M NH_4^+ suggesting apparent first order kinetics with respect to NH_4^+.

Water effect.—The dissolution rate of steel in solutions of NH_3 plus NH_4NO_3 alone is negligible. Qualitative experiments showed an increase in rate with increase in water at low water concentrations.

Table II. Effect of NaOH on solutions of NH_4NO_3

No.	Concentration moles/l NaOH	Concentration moles/l NH_4NO_3	Rate, mdd, 30°C	pH
1	0.1	4.0	Negligible	8.3
2	1.0	4.0	3300	9.1
3	2.0	4.0	5000	9.5
4	4.0	4.0	1500	10.8
5	2.0	2.0	1200	10.6
6	2.0	3.0	2400	9.8

Table III. Rate and pH of NH_4NO_3-NH_3-H_2O solutions

No.	Concentration, moles/l NH_3	Concentration, moles/l NH_4NO_3	Rate, mdd, 30°C	pH
1	0	2.0	Near zero	5.0
2	2.0	2.0	3,600	9.5
3	4.0	2.0	9,800	9.7
4	6.0	2.0	12,500	10.1
5	8.0	2.0	17,000	10.3
6	10.0	2.0	20,000	10.4
7	14.0	2.0	15,000	10.8
8	10.0	0	Near zero	12.4
9	10.0	0.25	2,400	11.2
10	10.0	0.50	3,800	10.9
11	10.0	1.0	8,800	10.7
12	10.0	1.5	14,700	10.5
13	10.0	2.0	20,000	10.4
14	10.0	3.0	20,000	10.4
15	10.0	4.0	23,000	10.4

At higher water concentrations, *e.g.*, > 20 w/o, a decrease in rate occurs, suggesting simple dilution to decrease the concentration of other rate-controlling substances.

pH effects.—Tables II and III are presented to illustrate pH and dissolution rate changes for various solution compositions. Neither solutions concentrated in NH_4^+ and NO_3^- (NH_4NO_3—H_2O) nor those concentrated in OH^- and NO_3^- ($NaOH$—$NaNO_3$—H_2O) exhibit significant dissolution rates in the absence of free ammonia. Therefore, the ammonia liberated from NH_4^+ ion by the action of base is apparently necessary for the high dissolution rates observed for the solutions listed in Table II. At constant OH^- concentration the free NH_3 in solution increases with increasing NH_4^+ concentration and increases the rate. The increased concentration of free NH_3 produced by this effect of increased NH_4^+ concentration probably accounts for the variation of slope in Fig. 4.

Table III shows that dissolution rates are greatest at a pH near 10.4 and decrease above or below this value. The decrease of rate in Fig. 4, 5, and 6, giving rise to the maxima of these curves, is associated with a decrease or an increase of pH from 10.4. It should be noted that pH as well as rate is relatively constant (Table III, rows 13, 14, 15) for NH_4NO_3 concentrations between 2 and 4M. The observed maxima may be related to pH changes; however, activity coefficient changes of other components in such concentrated solutions must also be considered.

Microstructure effect.—In order to explain the different dissolution rates observed for different types of steel, the effects of surface area, grain size, and distribution of impurities were considered. Since the dissolution rates ranged from 200 mdd for zone

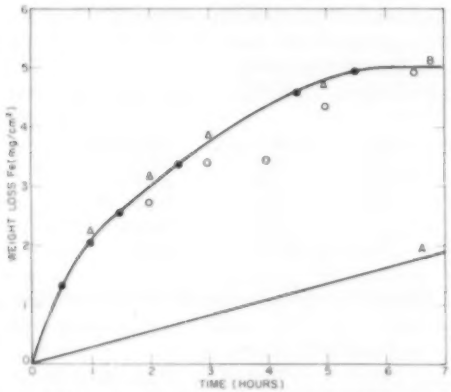

Fig. 7. Effect of heat treatment; Steel D269B; ○, 1000°C for 1 hr, quenched in cold H_2O, annealed for 3-5 hr at 750°C; ●, △, heat treated same way with no annealing; Curve A, no heat treatment.

refined iron to 28,800 mdd for steel E037, a roughness factor of the order of 140 would be necessary to account for the difference by surface area effect alone. Furthermore, the rates of many steels (E079, E037, etc., of Table I) were so great that new surfaces were being formed continuously, and it is unlikely that large surface area differences would be exhibited. Thus, this effect by itself is not sufficient to account for the observed differences.

Since zone refined iron (large grains) exhibited a much lower dissolution rate than those steels having extensive grain boundaries, consideration of grain size was necessary. ASTM grain sizes were available for some of the steels (Table I). The difference in average grain size for steels E079 and D269B is 2, whereas the dissolution rate differs by a factor as high as 35. On the other hand, no large rate factors exist between steels F809B and F810B even though the average grain size differs by 1.5. These last two steels are both "rimmed" steels and have almost the same percentage of carbon and other impurities. Thus, grain size does not appear to be a suitable basis for explaining the large dissolution rate differences.

Table I shows that high rates were observed for steels of high Mn and Si content. A commercial, aluminum-killed steel (K1876C) with 0.39 Mn and 0.037 Si gave a dissolution rate much like that of steel E127 which is much higher in Mn and Si. Also, there is no obvious relationship between carbon content and rate, as shown by the difference in rate between steels E079 and D269B.

The distribution of impurities (specifically carbon) in a steel was altered by heat treatment. Samples were heated near 1000°C and quenched in water. Figure 7 shows that an increase in rate occurs with this treatment. Annealing at 750°C for up to 5 hr failed to lower the rate again, thereby eliminating stress as a possible explanation for the increase. This type of heat treatment is known to alter the carbide structure although no conclusive difference was seen by microscopic examination. The difference in carbide distribution for two steels having widely different rates but the same carbon content is noticeable in Fig. 8A and B. Although

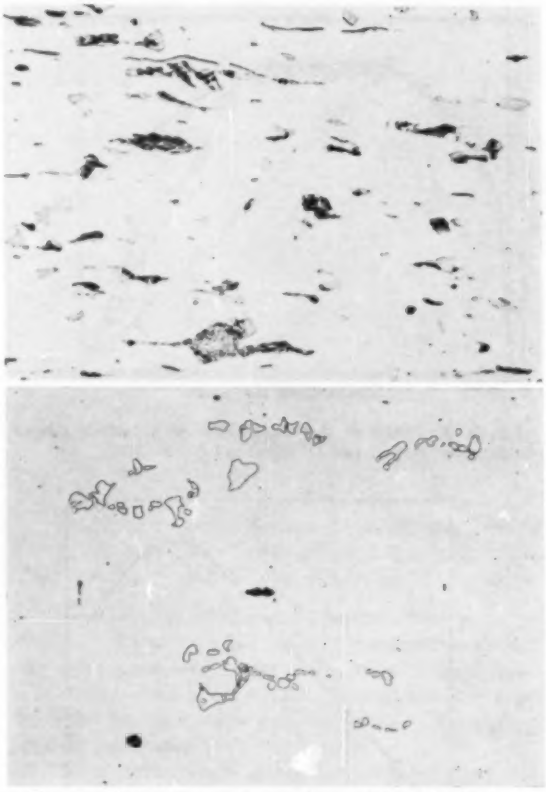

Fig. 8. Photomicrograph showing carbide distribution in steel; A, Steel E079; B, Steel D269B; picral etch. Magnification 500X before reduction for publication. (Courtesy of U. S. Steel Co.)

still speculative, the distribution of carbon and possibly other impurities appear to be responsible for some of the large differences observed in dissolution rates.

Conclusion

The first observable corrosion product is probably a hydrated or ammoniated form of ferrous hydroxide. The white to green to gray transition of the precipitate as oxidation occurs plus the change to magnetite agrees well with the known properties of ferrous hydroxide.

The presence of a stable iron-ammonia complex in solutions of this nature has been postulated before (8, 9) and is indicated here also. Formation of a transitory Fe . . . NH_3 complex on the surface, its subsequent coordination with more NH_3 molecules, and finally diffusion of the complex from the surface is considered the most likely mechanism of the oxidation reaction. This provides for the large rates since the corrosion products can be removed from the metal surface readily in the form of soluble species.

An oxide film on the metal surface is protective in this system. Leonard and Sellers (13) have shown that Fe_2O_3 is insoluble in solutions of NH_4NO_3 and NH_3. Steel is activated by stress, high-temperature hydrogen treatment, cathodic polarization, pickling in acid, or galvanic coupling with a more active metal, *e.g.*, zinc. All of these effects are best explained on the basis of an oxide covering.

The presence of NH_4^+, NH_3, H_2O, and NO_3^- in any proposed reaction mechanism is necessary since in the absence of any of these components the observed high dissolution rates are not obtained. In studying the specific effect on rate by any single component, the concentrations of the other components were held constant at sufficiently high values where their effect on rate was supposedly not limiting. The reaction appeared to show first order kinetics with respect to NH_3 and NH_4^+. The $\overset{*}{A}$ values (Table I) are indicative of an activation controlled process. The decrease of $\overset{*}{A}$ to lower and similar values for several steels in dilute NO_3^- solutions indicates a change from an activation to diffusion controlled process. This is in agreement with the proposal that activation control is dominant when the concentration of all species is above a limiting value and diffusion controlled with respect to any component below this value. The failure to see an increase of rate on stirring is attributed to a film on the surface.

It is interesting to note that Halpern (12) reached similar conclusions for the Cu-NH_3-H_2O system. Ammonia and NH_4^+ exhibited first order kinetics and a change of $\overset{*}{A}$ occurred with a change of oxygen concentration.

Reduction of NO_3^- may depend on steel composition (14) and thus be responsible for the different $\overset{*}{A}$ values (Table I). No detailed reaction mechanism is given at this time since it would be considered speculative.

Acknowledgment

The authors are pleased to acknowledge the financial support of this work by the Robert A. Welch Foundation of Houston and by the Office of Naval Research under Contract Number 375(02). They also with to take this opportunity to thank the U. S. Steel Company for the steel and photomicrographs and Battelle Memorial Institute for the iron which they kindly supplied for this study.

Manuscript received Nov. 21, 1960; revised manuscript June 6, 1961.

Any discussion of this paper will appear in a Discussion Section to be published in the June 1962 JOURNAL.

REFERENCES

1. R. O. E. Davis, L. B. Olmstead, and F. O. Lundstrum, *J. Am. Chem. Soc.*, **43**, 1580 (1921).
2. B. H. Sanders and D. A. Young, *Ind. Eng. Chem.*, **43**, 1430 (1951).
3. E. Herdegen and J. Nadolska, *Przemysl. Chem.*, **34**, 455 (1955).
4. I. Libinson, I. Kubushkin, and A. Morozova, *J. Chem. Ind. (Moscow)*, **12**, 590 (1935).
5. N. Hackerman, R. M. Hurd, and E. S. Snavely, *Corrosion*, **14**, 203t (1958).
6. M. Voriskova, *Collection Czechoslov. Chem. Communun.*, **11**, 588 (1939).
7. I. M. Kolthoff and J. J. Lingane, "Polarography," Vol. 2, Chap. 27, Interscience Publishers, New York (1952).
8. D. L. Leussing and I. M. Kolthoff, *J. Am. Chem. Soc.*, **75**, 2476 (1953).
9. E. Weitz and H. Muller, *Ber.* **58**, 363 (1925).
10. O. Baudisch and P. Mayer, *Biochem. Zeit.*, **107**, 1 (1920).
11. W. M. Latimer, "Oxidation Potentials," Chap. 7, 2nd ed., Prentice-Hall, Inc., New Jersey (1952).
12. J. Halpern, *This Journal*, **100**, 421 (1953).
13. G. W. Leonard, Jr. and D. E. Sellers, *ibid.*, **102**, 95 (1955).
14. E. N. Mirolyubov, M. M. Kurtepov, and N. D. Tomashov, *Proc. Acad. Sci.*, **125**, 363 (1959).

Oxidation of Molten High-purity Aluminum in Dry Oxygen

W. C. Sleppy

Alcoa Research Laboratories, Physical Chemistry Division, Aluminum Company of America, New Kensington, Pennsylvania

ABSTRACT

The rate of oxidation of high-purity aluminum, melted in vacuum at temperatures from 660° to 850°C and oxidized in dry oxygen, is strongly influenced by the initial surface conditions of the solid samples. The oxidation of aluminum in dry oxygen is characterized by a logarithmic oxide growth at temperatures ≤700°C, while at temperatures near 750°C, a modified parabolic oxidation law is obeyed. The disarray theory of Davies, Evans, and Agar is cited to account for the logarithmic oxide growth, while the parabolic controlled oxidation is attributed to the diffusion of aluminum ions through the eta-alumina oxide film to the oxide-gas interface. The activation energy for the diffusion controlled oxidation reaction is estimated to be 99 kcal/mole. A possible relationship between morphology and the kinetics of oxide growth on molten aluminum is presented in view of the correlation between data from the present work and that taken from the literature concerning the morphology of oxide growth on molten aluminum

The oxidation of liquid metals in various atmospheres is important in melting and casting operations. Many of the problems that arise in these operations originate from oxidation. From the standpoint of understanding and predicting the behavior of molten metal, a study of the oxidation mechanisms involved is helpful. Although extensive studies of the solid-state oxidation kinetics of aluminum and its alloys have been made by various workers, very little work has been reported con-

cerning the oxidation of these materials in the molten state.

In the work reported here, the oxidation of molten 99.99+% aluminum under specified conditions in a dry oxygen environment was investigated. This extends earlier work on the solid-state oxidation of aluminum and its alloys at elevated temperatures (1). In the earlier work, it was shown that the reaction between solid aluminum and dry oxygen could be followed manometrically in an essentially constant volume system by observing the drop in pressure caused by the consumption of dry oxygen by the metal specimens. The agreement found between the data derived from the manometric system and that obtained using an automatic recording vacuum microbalance led to the extension of the manometric technique to measuring the kinetics of oxidation of molten aluminum.

In the course of this investigation, a change in the mechanism of oxidation was observed as the temperature of the experiments increased. Although the oxidation curves did not conform to any one oxidation theory over the complete range of temperature studied, an excellent mathematical fit to established oxidation laws in definite temperature ranges was observed.

Experimental

The apparatus used in this work is shown in Fig. 1. It consists of two identical all-quartz cells mounted side by side inside a 4 in. diameter, Kanthal, wire-wound furnace core. One of the cells contained an aluminum sample while the other served as a reference cell. A differential oil manometer containing Octoil-S oil was connected between the tubes leading to the cells. The major modifications made on the system since its use in the solid oxidation studies (1) are contained in the manometer support section enclosed by dotted lines in Fig. 1. These entail the addition of stopcocks S-6 and S-7 and the attachment of 8.3 ml calibrated volumes via stopcocks S-8 and S-9.

In a typical experiment, the calibrated volumes were filled with an atmosphere of dried oxygen and the remainder of the system outgassed for several hours. A Wheelco Capacitrol Model 293 Temperature Controller was set for the desired temperature and power applied to the furnace while outgassing continued. When thermal equilibrium was achieved, stopcocks S-5 and S-7 were closed and stopcock S-6 checked to ensure free passage through all three sides of its T-bore. Stopcock S-8 was then opened allowing oxygen to expand into the reference cell and both sides of the differential oil manometer. Stopcock S-6 was then turned so that it was closed to the reaction cell side of the manometer, but open to the reference cell side. Stopcock S-9 was then opened, allowing a similar quantity of gas to expand into the reaction cell; this was taken as zero time or the start of the oxidation reaction. As quickly as possible, stopcock S-7 was opened so that differential pressure readings could be taken at suitable time intervals.

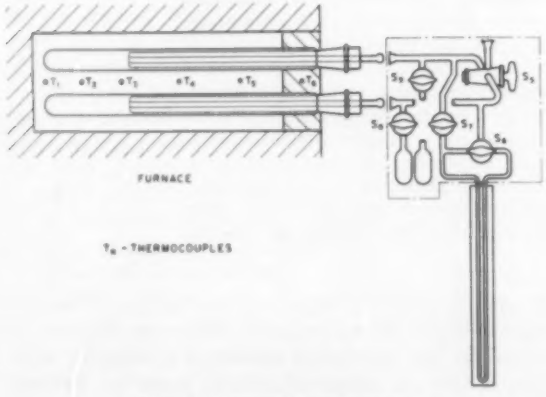

Fig. 1. Manometric apparatus

At the end of the experiment, usually 60 min long, the calibrated volumes were refilled with oxygen to the initial starting pressure, and the remainder of the system reevacuated. After outgassing for 30 min, a background determination was made following the same procedure as outlined above. The background reading was an instantaneous response on the manometer with no further change on standing.

After the background measurement, the pressure of gas in the reaction cell during the experiment was estimated by closing stopcocks S-8 and S-9 thus preserving a portion of the thermally equilibrated system under experiment conditions. The calibrated volumes were removed from the system and the pressure of oxygen trapped inside measured on an external mercury manometer. At most, the pressure drop due to reaction never exceeded 10% of the original pressure.

The use of the procedure described simplified calculation of the data and eliminated the possibility of missing some of the rapid initial oxidation which takes place at the beginning of an experiment.

Sample calculations.—The quantity of oxygen reacting with the aluminum, which is equivalent to the weight gain resulting from oxidation, is given in terms of experimentally measured quantities by Eq. [1] (1, 2).

$$\Delta W = K_1 h (1 + K_2) \qquad [1]$$

where

$$K_1 = 37.7 \left[\sum_i \frac{V_i}{T_i} \right] \rho \qquad [2]$$

$$K_2 = \frac{1.36 \pi r^2 P_o}{T_1 \left[\sum_i \frac{V_i}{T_i} \right] \rho} \qquad [3]$$

These equations are identical to the ones used in the study of oxidation of aluminum in the solid state (1) and each term is described in Ref. (1).

In the present work, the quantity $\left[\sum_i \frac{V_i}{T_i} \right]$ was evaluated in two ways: by measuring the volumes associated with temperature zones along the cells (1), and by measuring P_o as described in the experimental section, and solving Eq. [4].

$$RN_o = \frac{P_A V_c}{T_1} = P_o \sum_i \frac{V_i}{T_i} \qquad [4]$$

where N_o is the number of moles of oxygen initially in the calibrated volumes, V_c is the volume in ml

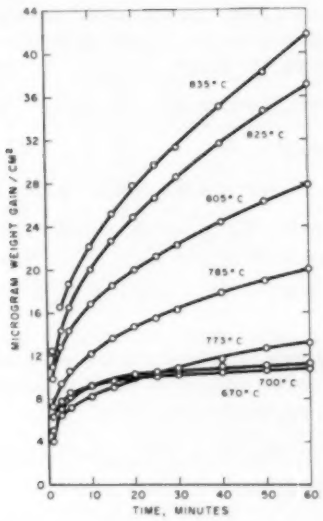

Fig. 2. Oxidation curves for as-rolled aluminum in 120 mm of dry oxygen.

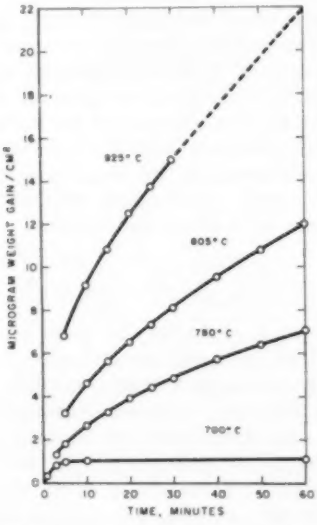

Fig. 3. Oxidation curves for preoxidized aluminum in 120 mm of dry oxygen.

of the calibrated volume attached to the reaction cell, and P_i in mm Hg is the initial pressure of the N_2 moles enclosed in the reaction cell calibrated volume before expansion.

The samples used in this work were all 99.99+% aluminum plates which were 1⅜ in. long, 1 in. wide, and ⅛ in. thick.

The oxygen used was Linde tank oxygen which was passed through a drying tube and cold trap to remove water vapor.

Results and Discussion

The experimental oxidation curves obtained in this work are presented in Fig. 2 and 3.

The oxidation curves shown in Fig. 2 are typical for degreased, as-rolled aluminum plates which were melted in vacuum at temperatures ranging from 660°-850°C. These oxidation experiments on surfaces relatively "oxide free" initially were all carried out in roughly 110-120 mm dry oxygen.

The oxidation curves shown in Fig. 3 represent the additional oxidation of molten samples which had previously been chemically polished (1) and then oxidized in dry oxygen at 600°C before being melted in vacuum and exposed to oxygen again. The additional oxidation of the molten samples was also carried out in dry oxygen at approximately 110-120 mm Hg.

As-rolled plate.—The experimentally determined oxidation curves for degreased, as-rolled aluminum plates melted in vacuum at temperatures of 660°-700°C were found to correspond to a logarithmic oxide growth. Obedience of the experimental data to the direct logarithmic law (3), Eq. [5].

$$W = K \log_e (at + 1) \qquad [5]$$

is verified by the straight line plot resulting when values of $e^{W/K}$ are plotted against time (see Fig. 4). In the construction of Fig. 4, the value of K used to calculate $e^{W/K}$ was obtained by assuming the quantity $(ta) >> 1$. Hence, Eq. [5] could be written:

$$W \cong K \log at \qquad [6]$$

and the slope of a line drawn through a plot of W in $\mu g/cm^2$, *vs.* log t, in minutes, gave the estimate of K.

As the temperature in these experiments was raised, a change in the oxidation character was observed. The oxidation curves at temperatures greater than 750°C conform to a modified parabolic rate law of the form:

$$W^2 + K_1 W = K_2 t + K_3 \qquad [7]$$

This modified parabolic expression has been derived by Evans (3) by combining the equations representing the physical diffusion of material across the oxide film and the chemical reaction of this material at the oxide gas interface, respectively.

In order to apply this equation to the experimental data, careful consideration must be given to the system under study.

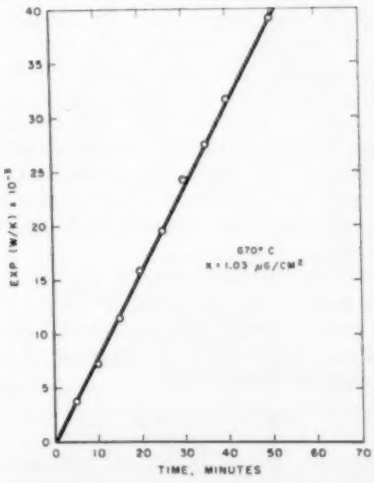

Fig. 4. Logarithmic plot of weight gain characteristic of molten aluminum oxidation in dry oxygen below 700°C.

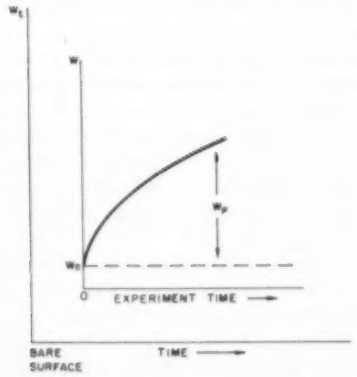

Fig. 5. Schematic representation of oxide growth

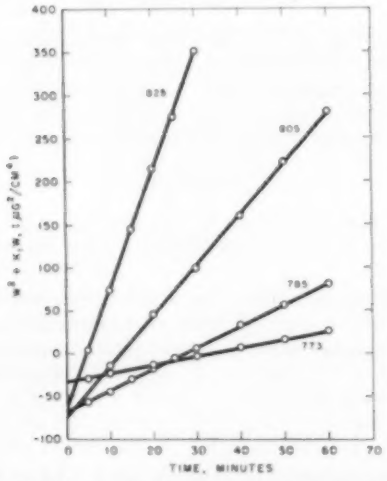

Fig. 6. Modified parabolic plots of oxidation data for as-rolled aluminum.

Assume that Fig. 5 represents the system with which we are concerned, where W_T represents the total oxide growth from the bare surface; W represents the experimentally measured oxide growth; W_P represents that part of W which occurs by diffusion controlled oxidation, and obeys a modified parabolic oxidation law which provides for partial control by an interface reaction; W_o represents that part of W which occurs very rapidly in the earliest stages of oxidation but by nonparabolic means. The quantity $(W_T - W)$ represents the oxide present on the sample before the experiment is started. This includes the natural oxide film present on as-rolled material and the oxide layer deliberately deposited on chemically polished surfaces at 600°C in some experiments.

The diffusion controlled contribution to the measured weight gain, W_P, by definition obeys the modified parabolic oxidation law represented by Eq. [7]. The equation for the rate of this type of oxidation is, as derived by Evans, (3)

$$\frac{dW_P}{dt} = \frac{K_P K_C C_0}{K_C W_P + K_P} \qquad [8]$$

where K_P is a physical constant related to the transport of matter across the oxide film, K_C is a chemical constant, and C_0 represents the concentration of the diffusing species at the metal-oxide interface. Integration of Eq. [8] gives

$$1/2K_C W_P^2 + K_P W_P = K_P K_C C_0 t + K'$$

or more simply

$$W_P^2 + k_1 W_P = K_2 t + k_0$$

Substitution for W_P in terms of the experimentally measured quantity W via $W_P = W - W_o$ gives

$$W^2 - 2WW_o^2 + W_o + k_1 W - k_1 W_o = K_2 t + k_0 \qquad [9]$$

For a given experiment W_o may be considered a constant in that it will not vary measurably with time. With this principle in mind, the terms in Eq. [9] may be regrouped as follows:

$$W^2 + (k_1 - 2W_o)W + (W_o^2 - k_1 W_o) = K_2 t + k_0$$

or more simply

$$W^2 + K_1 W = K_2 t + K_0 \qquad [10]$$

The numerical value of K_1 and K_0 will depend on the relative values of W_o and k_1.

The obedience of the experimental data to Eq. [10] is shown by the straight line plots resulting when values of $W^2 + K_1 W$ are plotted against time (see Fig. 6). In evaluating the quantity $W^2 + K_1 W$, the constant K_1 was determined by eliminating K_2 from the simultaneous equations (of the form of Eq. [11]) representing the instantaneous slope of the experimentally determined oxidation curve at various values of W along the curve.

$$m_1 = \left(\frac{dW}{dt}\right)_1 = \frac{K_2}{2W_1 + K_1} \qquad [11]$$

The derivation of Eq. [8] is based on an oxidation mechanism involving the diffusion of aluminum ions through the oxide film to the oxide-gas interface, where they react with adsorbed oxygen. If oxidation resulted from this mechanism, then from the temperature dependence of the slopes of the modified parabolic plots of Fig. 6, an experimental activation energy corresponding to a measure of the activation energy for diffusion of aluminum ions through crystalline eta-alumina is obtained.

Treatment of the experimental data in the manner just described results in the data plotted in Fig. 6 and 8 and tabulated in Table I. The diffusion activation energy was found to be 99 kcal/mole, a very reasonable figure for the process involved. Linder has reported similar activation energies for systems involving the diffusion of cations through their respective oxides in his self-diffusion studies using radiotracers (4).

Preoxidized plates.—In these experiments, a predominantly crystalline oxide layer, equivalent to roughly 4-5 $\mu g/cm^2$ weight gain (1), was deposited on the chemically polished surfaces of the solid plate sample during a 1-hr oxidation at 600°C in 120 mm dry oxygen before the additional oxidation of the molten metal was measured. At the conclusion of the 600°C oxidation, the system was outgassed for 1 hr at 600°C and then, while outgassing continued, the temperature was gradually raised

Table I. Tabulation of experimental data

Temp, °C	K_1, μg/cm²	K_2, μg²/cm⁴	K_3, μg²/cm⁴ min	ln K_3	E_a, kcal/mole
		Degreased, as-rolled surfaces			
773	−11.2	−32.5	0.97₅	0	
785	−15.85	−70.0	2.35	0.85	99
805	−17.72	−75.0	6.1	1.8	
825	−16.2	−65.0	14.1	2.65	
		Preoxidized surfaces			
766	−2.5	−1.5	0.6	−0.5	
780	+2.55	+2.0	1.15	0.14	99
805	+6.0	+10.0	3.5	1.25	

over a period of 1-3 hr to the temperature chosen for the additional oxidation of the molten metal.

Due to the presence of the crystalline oxide layer deposited at 600°C and the added epitaxial effect as the temperature of the sample was slowly raised in vacuum, the rapid, initial, nonparabolic oxidation ordinarily obtained on as-rolled samples was prohibited or at least reduced to a minimum. This is evidenced by the essentially negligible additional oxidation observed in the temperature range 660°-700°C on samples which had been previously oxidized in oxygen at 600°C, (see Fig. 3). At higher temperatures, >750°C, the additional oxidation of this type of sample was significant, but the effect of inhibition of nonparabolic oxide growth by the crystalline oxide layer deposited at 600°C was still evident. Treatment of these oxidation curves in a manner similar to that discussed before, yields the results shown in Fig. 7 and 8 and tabulated in Table I. Since the rate of this oxidation is believed to be governed by diffusion of aluminum ions, the obedience of the data to a parabolic rate law is not surprising. However, the values of K_1, K_2, and K_3 are quite different from those obtained from degreased, as-rolled samples indicating a closer approach to the simple parabolic rate law. This undoubtedly is an effect of the different surface conditions initially present on the two types of samples. The crystalline oxide layer formed on the sample before melting has reduced the nonparabolic contribution to oxidation of the molten metal to a minimum at the lower temperatures (note the small negative value of K_3, Table I) and apparently eliminated it entirely at the higher temperatures (note the positive values of K_3). Further, this crystalline oxide layer formed before melting apparently accounts for a portion of the parabolic oxidation which would have occurred in its absence.

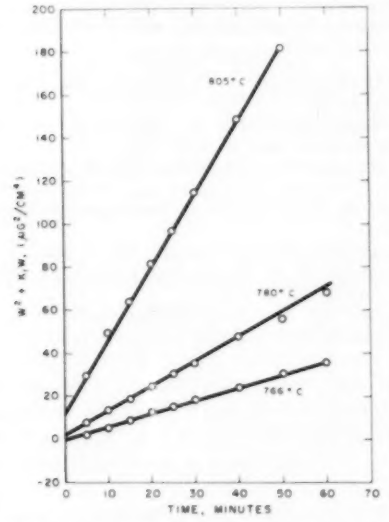

Fig. 7. Modified parabolic plots of oxidation data for preoxidized aluminum.

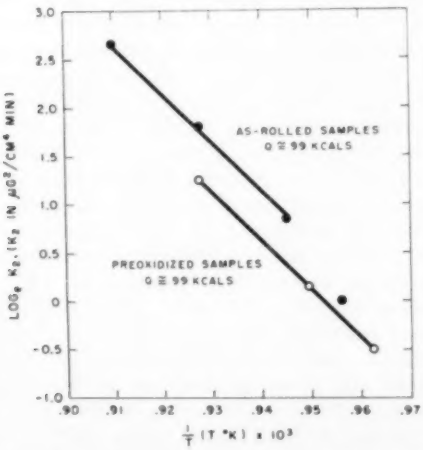

Fig. 8. Effect of temperature on the parabolic oxidation of molten aluminum.

It is of interest to note that the temperature dependence of the slopes of the modified parabolic plots for these experiments (see Fig. 7 and 8) give rise to the same estimate for the diffusion activation energy as that previously obtained for as-rolled surfaces, approximately 99 kcal/mole.

Several theories based on various hypothetical rate-determining mechanisms have been put forward to explain the fact that under certain conditions the oxidation of many metals obeys the direct logarithmic rate equation (3). Of the theories proposed, the disarray theory of Davies, Evans, and Agar (5) appears to account for the logarithmic oxide growth observed on molten aluminum at the lower temperatures. According to this theory, oxidation results from matter (usually oxygen) transported through continuous leakage paths penetrating the oxide film. The nature of the leakage paths need not be specified, but they are usually attributed to flaw paths, cracks, pores, or zones of loose structure inherent in the film or formed by the volume change associated with conversion of metal to oxide. As oxidation proceeds the rate of reaction, involving the temperature independent exponential closure of oxidation paths, is proportional to the amount of oxidation needed to reduce the number of paths by a given fraction. Thus the deposition of a crystalline oxide layer on the surfaces of the solid sample at 600°C before melting obviously must act to minimize logarithmic oxide growth on the metal when melted because of the very nature of the mechanism of such growth.

As mentioned previously, the mechanism of oxidation proposed to account for the parabolic oxide growth observed on molten aluminum at the higher

temperatures is one involving diffusion of aluminum ions through the oxide lattice. The high activation energy for this diffusion process accounts for the negligible contribution of this mode of oxidation at the lower temperatures while the logarithmic growth mechanism could account for the rapid, initial, non-parabolic oxidation occurring in the earliest stages of the higher temperature experiments (W_c), particularly when "as-rolled" samples melted in vacuum are used.

An interesting correlation is observed between data from the present work and that taken from an investigation carried out by Mal'tsev, Dhistyakov, and Tsypin (6) concerning the morphology of oxide growth on molten aluminum.

The Russian work consisted of electron diffraction investigations of oxide films that form on molten aluminum and its alloys. The films studied were skimmed directly off the melt by means of a nichrome wire loop. Samples were taken at temperatures ranging from 660°-1100°C. The investigation showed that at temperatures below 680°C the oxide film that formed on pure molten aluminum had an amorphous structure, but at about 690°C a transition from amorphous to crystalline eta-alumina formation occurred.

The formation of an amorphous oxide film on initially oxide free molten aluminum at the lower temperatures could easily explain the logarithmic oxide growth observed in the present work. Similarly the transition from amorphous to crystalline oxide formation at higher temperatures corresponds to the observed change to parabolic controlled oxidation.

However, only eta-alumina was detected by electron microscopic and diffraction examinations of similar oxide films formed at temperatures from 660°-690°C in these Laboratories. The amorphous character associated with these oxide films was not detected. The procedure followed was as near that of the Russians as possible, but it was concluded that all the films examined were basically comprised of eta-alumina. The only significant difference observed between films formed at high and low temperatures was the much smaller size, <100Å, of crystallites found on the films formed at 800°C as compared to the ≅250Å crystallites found on the films formed at 670°C. In addition, the films formed at 670°C appeared to consist of dual oxide layers.

One explanation for the differences observed in regard to the Russian work is that even on visual examination, our skimmed films appeared to be highly metallic. The possibility exists therefore that, on crystallization of the aluminum metal carried off in the skimming process, an epitaxical effect was exerted on the amorphous oxide thus converting it to crystalline material.

Manuscript received June 12, 1961; revised manuscript received Aug. 10, 1961.

Any discussion of this paper will appear in a Discussion Section to be published in the June 1962 JOURNAL.

REFERENCES

1. C. N. Cochran and W. C. Sleppy, *This Journal*, **108**, 322 (1961).
2. W. E. Campbell and U. B. Thomas, *J. (and Trans.) Electrochem. Soc.*, **91**, 623 (1947).
3. U. R. Evans, "The Corrosion and Oxidation of Metals," Scientific Principles and Practical Applications, St. Martin's Press Incorporated, New York (1960).
4. R. Lindner, *J. Chem. Phys.*, **23**, 410 (1955).
5. D. E. Davies, U. R. Evans, and J. N. Agar, *Proc. Roy. Soc.*, **A225**, 443 (1954).
6. M. V. Mal'sev, Yu. D. Dhistyakov, and M. I. Tsypin, *Bull. Acad. Sci. U.S.S.R. Phys. Sc.*, p. 747 (1956).

Phase Equilibria and Tin-Activated Luminescence in Strontium Orthophosphate Systems

J. F. Sarver, M. V. Hoffman, and F. A. Hummel

College of Mineral Industries, The Pennsylvania State University, University Park, Pennsylvania

ABSTRACT

Strontium orthophosphate undergoes a rapid, reversible transition at 1305°C. The high-temperature β form of pure $Sr_3(PO_4)_2$ cannot be quenched to room temperature, even with extremely rapid cooling. Determination of phase relationships on the orthophosphate joins between $Sr_3(PO_4)_2$ and each of the three orthophosphates, $Mg_3(PO_4)_2$, $Ca_3(PO_4)_2$, and $Zn_3(PO_4)_2$ showed that they form β-$Sr_3(PO_4)_2$ solid solutions which could be cooled to room temperature to form the basis for the so-called "modified strontium orthophosphate" phosphors. The ranges of composition and temperature over which the β-$Sr_3(PO_4)_2$ solid solutions exist were determined for each system, and the existence of two ternary compounds, $SrMg_2(PO_4)_2$ and $SrZn_2(PO_4)_2$, was confirmed. The latter compound has a transition at 1035°C, but the high-temperature form can be maintained at room temperature only by extremetly rapid quenching. Equilibrium diagrams of each of the systems are presented to show all stability relationships.

The behavior of tin-activated β-$Sr_3(PO_4)_2$ solid solution phosphors in each of the three systems was explored under 2537Å excitation, and the relation of phosphor composition to quantum efficiency, brightness, and temperature stability in the lamp-making range was determined. The tin-activated luminescence of the two ternary compositions was investigated using 2537Å, 3650Å, and cathode ray excitation.

Tin-activated alkaline earth orthophosphates which responded efficiently to 2537Å radiation have been described by Butler (1). He found that the α form of $Ca_3(PO_4)_2$ had an emission at 4900Å, but the part of his work which is of particular interest in the present investigation was the effect on luminescence emission produced by the progressive substitution of Sr^{2+} for Ca^{2+} in the low-temperature, whitlockite, or β form of $Ca_3(PO_4)_2$.

Butler found that the composition $(Ca_{2.96}^{2+}, Sn_{0.04}^{2+})(PO_4)_2$ has a broad emission band across the visible spectrum with two sub-bands at 4950 and 6300Å. A progressive increase of the strontium content to $(Ca_{2.96}^{2+}, Sr_{0.96}^{2+}, Sn_{0.04}^{2+})(PO_4)_2$ gradually creates a new band at 4000Å and suppresses the 4950Å band without appreciably changing the intensity of the 6300Å band, although it is shifted to 6150Å. Moreover, substitution of Mn^{2+}, *e.g.*, $(Ca_{2.90}^{2+}, Sr_{0.96}^{2+}, Sn_{0.04}^{2+}, Mn_{0.01-0.06}^{2+})(PO_4)_2$ gradually suppresses the tin emission at 4000 and 6150Å, with the development of a considerably sharper red band at 6350Å.

Koelmans and Cox (2) investigated the luminescence characteristics of tin-activated strontium orthophosphate containing various amounts of Ca^{2+}, Mg^{2+}, Zn^{2+}, Cd^{2+}, or Al^{3+}. Introduction of these ions into $Sr_3(PO_4)_2$ led to the formation of a material isotypic with β-$Ca_3(PO_4)_2$ and different from the usually observed $Sr_3(PO_4)_2$ structure. Excited by 2537Å radiation, the tin emission of this "modified" strontium orthophosphate consisted of a broad band at 6300-6500Å and a weak band at 4000Å which accounted for only about 5% of the total emission energy. In the case of calcium additions, it was necessary to substitute about 16 mole % of Ca^{2+} for Sr^{2+} to obtain the "modified" structure as a single phase with firings between 1000° and 1100°C. Smaller additions yielded a mixture of the normal $Sr_3(PO_4)_2$ and the new phase. The amounts of Ca^{2+}, Mg^{2+}, Zn^{2+}, and Cd^{2+} which had to be substituted for Sr^{2+} in order to obtain a predominant amount of the new structure were 11% Ca^{2+}, 3% Mg^{2+}, 7% Zn^{2+}, and 11% Cd^{2+}. Much larger additions of Mg^{2+}, Zn^{2+}, or Cd^{2+} led to the formation of a ternary compound having the composition $SrX_2(PO_4)_2$, where X is Mg, Zn, or Cd. The tin emission of these ternary compounds is a weak greenish-blue. The large Ba^{2+} ion was not effective in leading to the formation of the "modified" structure.

In the present investigation, the nature of the "modified" strontium orthophosphate phase was established by determining the phase equilibrium relationships in the systems $Sr_3(PO_4)_2$-$Ca_3(PO_4)_2$, $Sr_3(PO_4)_2$-$Mg_3(PO_4)_2$, and $Sr_3(PO_4)_2$-$Zn_3(PO_4)_2$. With an accurate knowledge of phase boundaries and stability fields, tin-activated phosphors subsequently were prepared and evaluated.

Experimental

Phase Equilibria Studies

Raw materials.—The following chemicals were used as starting materials for the preparation of all compositions in the three systems under consideration: (*a*) strontium carbonate, $SrCO_3$, C. P., Fisher Scientific; (*b*) calcium carbonate, $CaCO_3$,

phosphor grade, General Electric Company; (c) basic magnesium carbonate, $3MgCO_3 \cdot Mg(OH)_2 \cdot 3H_2O$, C. P., Fisher Scientific; (d) zinc oxide, ZnO, phosphor grade, New Jersey Zinc Company; (e) ammonium dihydrogen phosphate, $NH_4H_2PO_4$, Baker Analyzed Reagent.

Composition preparation.—All compositions were calculated on a mole percent basis, and the raw materials were weighed to an accuracy of 0.1 mg in batches ranging from 1-20 g. The batches were mixed initially for 20 min by hand in glass mortars. The blended material was reacted in platinum crucibles in a silicon carbide resistance furnace at temperatures between 400° and 700°C to drive off volatiles, CO_2, etc., and to initiate solid-state reactions. The calcined material was ground by hand for 15 min and reacted between 800° and 900°C for 24-48 hr. The reacted material was ground in acetone in an automatic agate mortar and pestle for 45-60 min. The final bulk firing was carried out at 900°-1000°C for 24-48 hr. The homogeneous reacted products were ground and reserved for subsequent quench experiments.

Differential thermal analysis.—Approximate temperatures of crystalline phase transformations and initial melting of pertinent compositions were determined by D.T.A. The furnace used was a platinum-wound resistance furnace, with power supplied by a motor-driven variable transformer which maintained a rate of temperature rise of about 8°-10°C/min. Differential emfs between the unknown and standard (calcined Al_2O_3) were recorded on a General Electric "XY" recorder.

Quench technique.—In order to establish phase equilibrium relationships at high temperatures, it is necessary to preserve the high-temperature phases for room temperature identification unless, of course, more elaborate experiments such as high-temperature x-ray work are carried out.

Milligram quantities of material are packed into small platinum envelopes and are suspended in a vertical platinum-wound resistance furnace in which the desired temperature is maintained constant (±2°C) for periods of several hours. In this work, at temperatures above 1000°C, compositions attained equilibrium very rapidly, i.e., in a few hours. After equilibration, the samples were dropped directly from the furnace into mercury. In most cases, mercury quenching or even air quenching was sufficient to preserve high-temperature phases.

X-ray diffraction.—The identities of all crystalline phases encountered in the phase equilibrium studies were established by standard x-ray diffraction procedures. The particular equipment used was a Norelco x-ray diffractometer with nickel-filtered CuK_α radiation, operating at 40 kv and 15 ma. For routine identification, a scanning rate of 1°-2θ/min was used. Very slow scanning at ⅛°-2θ/min was used for higher precision work.

In one series of experiments, a platinum-wound high-temperature x-ray furnace was used. Temperature could be controlled to ±3°C for periods up to several hours.

X-ray diffraction data for some of the compositions encountered in this investigation are given in the Appendix. For data which have been published, pertinent references are given. A scanning rate of ½°-2θ/min was used since these data are presented only for routine identification purposes. Relative intensities were estimated from peak heights.

Luminescence Studies

The raw materials used in the preparation of the phosphor samples were commercial reagent grades of ZnO and SnO, and phosphor grades of $SrHPO_4$, $SrCO_3$, $CaHPO_4 \cdot 2H_2O$, $CaCO_3$ and $3MgCO_3 \cdot Mg(OH)_2 \cdot 3H_2O$, produced by General Electric.

The samples were prepared by dry ball milling the raw materials. These were fired in air for 16 hr at temperatures dependent on the degree of sintering of the composition. They then were refired in an atmosphere of 1.5% H_2 in N_2 for 1.5 hr.

The phases present in the phosphor samples were identified by x-ray diffraction, using a General Electric XRD-5 unit, with Ni-filtered CuK_α radiation. For determination of d values, a scanning speed of 0.2°-2θ/min was used. The spectral distribution curves were run on a General Electric recording spectroradiometer, using 2537Å radiation and a Corning No. 9863 filter. The brightness measurements were made using a photocell corrected for eye response.

Phase Equilibrium Relationships

Strontium Orthophosphate Polymorphism

The findings of Butler (1) and Koelmans and Cox (2) strongly suggested the possibility of the existence of a second crystalline modification of $Sr_3(PO_4)_2$, different from the normally observed form which is rhombohedral. It was necessary, therefore, at the initial stages of this investigation to determine whether more than one polymorph of $Sr_3(PO_4)_2$ existed.

Stoichiometric samples quenched from temperatures between 1000° and 1600°C yielded the normal rhombohedral form. A differential thermal analysis run, however, indicated that the compound undergoes a rapid, reversible phase transformation at about 1300°C. An experiment then was carried out in which x-ray diffraction patterns of $Sr_3(PO_4)_2$ were recorded from room temperature to 1325°C. Between 1300° and 1315°C, the x-ray patterns indicated a definite change in crystal structure, the high-temperature form being isotypic with the low-temperature, hexagonal, or β form of $Ca_3(PO_4)_2$ known as whitlockite.

Solid solution of the orthophosphates of Mg, Ca, Zn, Cd, and Al in $Sr_3(PO_4)_2$ stabilize the high-temperature β form so that it can be retained to room temperature. The term "modified" strontium orthophosphate as used by Koelmans and Cox (2) should be replaced by "stabilized β-strontium orthophosphate" or β-$Sr_3(PO_4)_2$ solid solutions.

System $Sr_3(PO_4)_2$-$Ca_3(PO_4)_2$

Table I summarizes the quenching data used for the construction of the equilibrium diagram shown in Fig. 1. The figures in parentheses are the mole % $Ca_3(PO_4)_2$ in the β-$Sr_3(PO_4)_2$ solid solutions as determined by precision measurements of one of the

Table I. Compositions, heat treatments, and phases in the system $Sr_3(PO_4)_2$—$Ca_3(PO_4)_2$

No.	Mole % $Ca_3(PO_4)_2$	Temp, °C	Time, hr	Phases
1	1.0	1000	24	α-S_3Pss
2	2.0	1000	24	α-S_3Pss + β-S_3Pss
3	5.0	1204	7	α-S_3Pss + β-S_3Pss (10.0)
		1254	16	α-S_3Pss + β-S_3Pss (7.5)
4	10.0	1002	24	α-S_3Pss + β-S_3Pss (20.0)
		1040	16	α-S_3Pss + β-S_3Pss (17.5)
		1095	24	α-S_3Pss + β-S_3Pss (16.0)
		1156	17	α-S_3Pss + β-S_3Pss (13.5)
		1241	24	β-S_3Pss
5	20.0	1000	24	β-S_3Pss
		1300	24	β-S_3Pss
6	70.0	1300	24	β-C_3Pss (or β-S_3Pss)
7	80.0	1200	24	β-C_3Pss
		1260	21	β-C_3Pss
		1273	24	β-C_3Pss
		1290	23	β-C_3Pss
		1301	24	α-C_3Pss + β-C_3Pss
		1307	24	α-C_3Pss + β-C_3Pss
		1321	20	α-C_3Pss + β-C_3Pss
8	90.0	1000	24	β-C_3Pss
		1200	24	β-C_3Pss
		1210	26	β-C_3Pss
		1217	23	β-C_3Pss + α-C_3Pss
		1230	22	β-C_3Pss + α-C_3Pss
		1252	24	β-C_3Pss + α-C_3Pss
		1264	23	α-C_3Pss
9	100.0	1000	24	β-C_3P
		1093	20	β-C_3P
		1125	23	β-C_3P
		1135	22	α-C_3P
		1154	22	α-C_3P
		1177	21	α-C_3P
		1210	24	α-C_2P

higher angle x-ray diffraction peaks. A calibration was established by holding β-$Sr_3(PO_4)_2$ solid solutions containing 10, 15, and 20 mole % $Ca_3(PO_4)_2$ at 1300°C for 24 hr in platinum crucibles and quenching in air to room temperature. They were found to have CuK_α reflections at 50.23°, 50.34°, and 50.44°-2θ, respectively, using a scanning rate

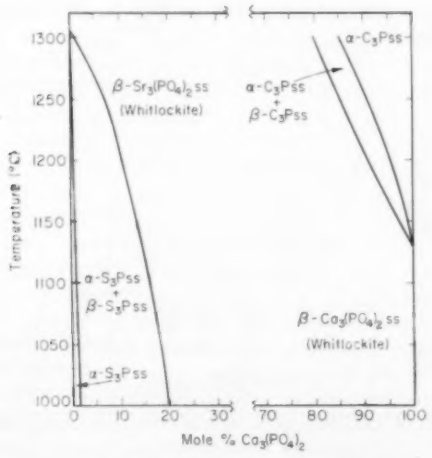

Fig. 1. System $Sr_3(PO_4)_2$ — $Ca_3(PO_4)_2$

Table II. Compositions, heat treatments, and phases in the system $Sr_3(PO_4)_2$—$Mg_3(PO_4)_2$

No.	Mole % $Mg_3(PO_4)_2$	Temp, °C	Time, hr	Phases
1	0.0	1000	24	α-S_3P
		1600	3	α-S_3P
2	1.0	960	29	α-S_3P + β-S_3Pss
3	2.0	961	18	α-S_3P + β-S_3Pss
4	3.0	1103	18	α-S_3P + β-S_3Pss
5	4.0	1300	24	β-S_3Pss
6	5.0	944	24	α-S_3P + β-S_3Pss
		1007	23	α-S_3P + β-S_3Pss
		1211	28	α-S_3P + β-S_3Pss
		1250	45	α-S_3P + β-S_3Pss
		1265	23	β-S_3Pss
		1300	24	β-S_3Pss
7	6.0	1059	24	α-S_3P + β-S_3Pss
		1195	25	α-S_3P + β-S_3Pss
		1259	26	β-S_3Pss
8	7.0	1057	19	α-S_3P + β-S_3Pss
		1103	20	α-S_3P + β-S_3Pss
		1159	24	β-S_3Pss
9	8.0	994	45	α-S_3P + β-S_3Pss
		1057	23	β-S_3Pss
10	9.0	955	27	α-S_3P + β-S_3Pss
		1001	21	β-S_3Pss
11	10.0	952	30	β-S_3Pss
		1000	24	β-S_3Pss
12	15.0	954	48	β-S_3Pss
13	20.0	959	25	β-S_3Pss
		1000	24	β-S_3Pss
		1300	1	β-S_3Pss
		1350	½	Fused
14	25.0	959	28	β-S_3Pss
		1200	1	β-S_3Pss
		1250	½	Fused
15	30.0	963	22	β-S_3Pss
		1000	24	β-S_3Pss
		1150	1	β-S_3Pss
		1200	½	Fused
16	35.0	945	48	β-S_3Pss
		1062	32	β-S_3Pss
		1100	16	β-S_3Pss
		1125	1	β-S_3Pss
		1180	½	Fused
17	40.0	954	21	β-S_3Pss + $SrMg_3(PO_4)_2$
		1000	24	β-S_3Pss + $SrMg_3(PO_4)_2$
		1057	26	β-S_3Pss + $SrMg_3(PO_4)_2$
		1107	32	β-S_3Pss
18	45.0	955	24	β-S_3Pss + $SrMg_3(PO_4)_2$
		1008	28	β-S_3Pss + $SrMg_3(PO_4)_2$
		1051	28	β-S_3Pss + $SrMg_3(PO_4)_2$
		1097	22	β-S_3Pss + $SrMg_3(PO_4)_2$
19	60.0	1040	—	Solidus (D.T.A.)
20	65.0	1100	20	β-S_3Pss + $SrMg_3(PO_4)_2$
21	66.6	947	24	$SrMg_3(PO_4)_2$
		1190	—	Fusion (D.T.A.)
22	70.0	1000	24	$SrMg_3(PO_4)_2$ + $Mg_3(PO_4)_2$
		1015	—	Solidus (D.T.A.)

of ⅛°-2θ/min. As shown in Table I, compositions 3 and 4 then were held between 1000° and 1250°C for various times and quenched. By observing the position of the high angle peak in these β-$Sr_3(PO_4)_2$

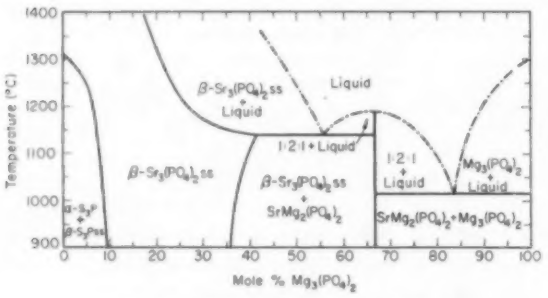

Fig. 2. System $Sr_3(PO_4)_2$ — $Mg_3(PO_4)_2$

solid solutions, their compositions could be determined, enabling the phase boundary to be constructed as shown in Fig. 1.

The two-phase region between β-$Ca_3(PO_4)_2$ solid solutions [low-temperature form isotypic with β-$Sr_3(PO_4)_2$] and α-$Ca_3(PO_4)_2$ solid solutions (high-temperature form) was constructed from data obtained by the quench technique supplemented by x-ray diffraction identification.

On the strontium side of the system, the solid solutions labeled β-$Sr_3(PO_4)_2$ss have the same crystal structure as β-$Ca_3(PO_4)_2$ solid solutions on the calcium side, indicating the great probability of a continuous, uninterrupted series between the orthophosphate compounds. There remains a possibility, however, that a two-phase region of unmixed solid solutions composed of β-$Sr_3(PO_4)_2$-rich and β-$Ca_3(PO_4)_2$-rich solid solutions exists in this area. Attempts to locate such a region by differentiation of x-ray diffraction patterns were unsuccessful. The two phases, if found, would have almost identical x-ray diffraction patterns. The region could exist below 1000°C where equilibrium is extremely difficult to obtain or it could be very narrow with respect to composition, making positive identification by means of x-ray diffraction virtually impossible.

System $Sr_3(PO_4)_2$-$Mg_3(PO_4)_2$

Quench D.T.A., and other data for construction of this system are given in Table II, and the phase equilibrium diagram is presented in Fig. 2, in which the solid lines represent experimentally determined phase boundaries. In the high strontium portion of the system it was necessary to prepare compositions for quench work at intervals of 1 mole %, since the temperature of the alpha to beta inversion of $Sr_3(PO_4)_2$ dropped so markedly with additions of $Mg_3(PO_4)_2$. Actually, it was shown later that the measurements of peak shifts in the β-$Sr_3(PO_4)_2$ solid solutions would have been satisfactory for the construction of the phase boundary, as was done for the calcium and zinc systems. From 10 to 65 mole % $Mg_3(PO_4)_2$, compositions were prepared at 5 mole % intervals in order to determine the boundary between the region of β-$Sr_3(PO_4)_2$ss and the same plus $SrMg_2(PO_4)_2$.

The existence of a high-temperature polymorph of $Mg_3(PO_4)_2$ has been claimed by Berak (3). A D.T.A. experiment revealed no heat effects up to the melting point at about 1300°C. Previous work with this compound ruled out the possibility of a sluggish inversion, so that in Fig. 2, $Mg_3(PO_4)_2$ is shown as a single crystalline modification.

Solidus temperatures for certain compositions were determined by D.T.A. and visual observation. No solid solution of $Sr_3(PO_4)_2$ in $Mg_3(PO_4)_2$ could be detected. Nor was there solid solution formation detected on either side of the ternary compound. $Mg_3(PO_4)_2$ is quite soluble in β-$Sr_3(PO_4)_2$, but the solubility in α-$Sr_3(PO_4)_2$ is less than 1 mole %, if any. Approximately 4 mole % $Mg_3(PO_4)_2$ in solid solution is required to prevent the β to α inversion on air quenching from 1300°C. About 3 mole % is sufficient for a mercury quench. For a slow cooling process, about 6 mole % is necessary to prevent exsolution in cooling a 5 g sample from 1300°C to room temperature over a period of 3-4 hr. Actually, there is no danger of exsolution for this composition until the temperature has fallen to about 1125°C, below which the cooling rate through the critical region to about 900°C must be sufficiently high to prevent exsolution. Below about 900°C diffusion processes become very slow in this system and prevent exsolution.

An interesting observation was made in connection with the intensities of x-ray reflections in the region of β-$Sr_3(PO_4)_2$ solid solutions. With increasing amounts of $Mg_3(PO_4)_2$ in solid solution, the intensities of the reflections dropped very markedly, causing at first considerable difficulty in the interpretation of x-ray patterns. These rather abrupt changes probably can be attributed to the large difference between the x-ray scattering factors of Mg^{2+} and Sr^{2+}, Sr^{2+} having twenty-six electrons in excess of the ten which the Mg^{2+} ion possesses.

System $Sr_3(PO_4)_2$-$Zn_3(PO_4)_2$

The phase equilibrium diagram of this system as shown in Fig. 3 somewhat resembles that of the $Sr_3(PO_4)_2$-$Mg_3(PO_4)_2$ system. Table III summarizes the quench and D.T.A. data for this system. The boundary between the region of β-$Sr_3(PO_4)_2$ solid solutions and the two phase region containing β-$Sr_3(PO_4)_2$ solid solutions and α-$Sr_3(PO_4)_2$ was determined by the measurement of shifts in x-ray diffraction peaks as was described for the calcium system. Solidus temperatures and a portion of the liquidus were determined by D.T.A. and visual observation.

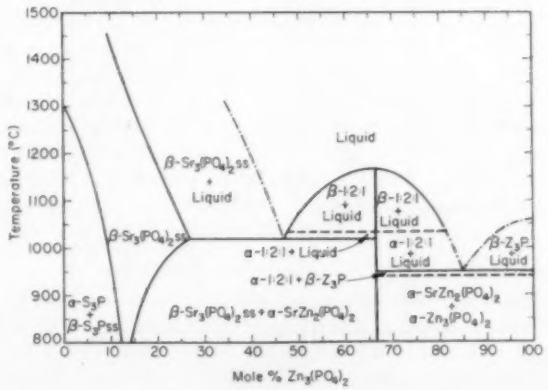

Fig. 3. System $Sr_3(PO_4)_2$ — $Zn_3(PO_4)_2$

Table III. Compositions, heat treatments, and phases in the system $Sr_3(PO_4)_2$ — $Zn_3(PO_4)_2$

No.	Mole % $Zn_3(PO_4)_2$	Temp, °C	Time, hr	Phases
1	1.0	950	24	α-S_3P + β-S_3Pss
2	5.0	1040	22	α-S_3P + β-S_3Pss (7.5)
		1116	21	α-S_3P + β-S_3Pss (6.5)
		1139	7	α-S_3P + β-S_3Pss (6.2)
		1192	22	α-S_3P + β-S_3Pss (5.2)
		1300	6	β-S_3Pss
3	10.0	850	24	α-S_3P + β-S_3Pss
		891	13	α-S_3P + β-S_3Pss (11.0)
		945	20	α-S_3P + β-S_3Pss (11.0)
		1200	24	β-S_3Pss
		1400	1	β-S_3Pss
		1450	½	Fusion
4	15.0	1040	6	β-S_3Pss
		1300	1	β-S_3Pss
		1350	½	Fusion
5	20.0	910	34	β-S_3Pss + α-$SrZn_2(PO_4)_2$
		950	26	β-S_3Pss + α-$SrZn_2(PO_4)_2$
		1050	17	β-S_3Pss
		1150	1	β-S_3Pss
		1200	½	Fusion
6	25.0	897	24	β-S_3Pss + α-$SrZn_2(PO_4)_2$
		950	16	β-S_3Pss + α-$SrZn_2(PO_4)_2$
		1004	4	β-S_3Pss
		1050	1	β-S_3Pss
		1100	½	Fusion
7	30.0	850	24	β-S_3Pss + α-$SrZn_2(PO_4)_2$
		899	36	β-S_3Pss + α-$SrZn_2(PO_4)_2$
		942	31	β-S_3Pss + α-$SrZn_2(PO_4)_2$
		1020	—	Solidus (D.T.A.)
8	60.0	1002	2	β-S_3Pss + α-$SrZn_2(PO_4)_2$
		1020	—	Solidus (D.T.A.)
		1150	—	Liquidus (D.T.A.)
9	66.6	850	24	α-$SrZn_2(PO_4)_2$
		960	16	α-$SrZn_2(PO_4)_2$
		1001	5	α-$SrZn_2(PO_4)_2$
		1021	5	α-$SrZn_2(PO_4)_2$
		1031	12	α-$SrZn_2(PO_4)_2$
		1038	5	β-$SrZn_2(PO_4)_2$
		1042	20	β-$SrZn_2(PO_4)_2$
		1086	27	β-$SrZn_2(PO_4)_2$
		1170	—	Fusion (D.T.A.)
10	80.0	850	24	α-$SrZn_2(PO_4)_2$ + α-$Zn_3(PO_4)_2$
		950	—	Solidus (D.T.A.)
		1060	—	Liquidus (D.T.A.)

In comparison with the magnesium system, the extent of β-$Sr_3(PO_4)_2$ solid solution in the zinc system is rather narrow, the maximum extent occurring at about 1025°C and extending from about 9 to 27 mole % $Zn_3(PO_4)_2$.

The ternary compound, $SrZn_2(PO_4)_2$, was found to have two crystalline modifications, the high-temperature form being stable between 1035°C and the melting point at about 1170°C. It can be retained to room temperature only by very rapid quenching. Small quantities such as a few milligrams can be quenched in mercury. Gram quantities can be quenched only by pouring a melted batch into water or over dry ice. Air quenching prohibits only a small fraction of the material from reverting to the stable low-temperature modification.

The phase transformation in $Zn_3(PO_4)_2$ at 942°C was determined previously by Katnack and Hummel (4).

Luminescence Studies

β-Strontium Orthophosphate Solid Solutions

General remarks.—Phosphor compositions were prepared in and near the β-$Sr_3(PO_4)_2$ solid solution regions with a calculated mole ratio of 2.97 base to 2.00 PO_4, with 0.02 mole SnO included in the base. Compositions made with an excess of base are nonluminescent, so that in order to insure maximum brightness, it is best to prepare phosphors with a ratio slightly less than the stoichiometric 3.00 to 2.00. The selection of 2.97 moles of base was made arbitrarily and was held constant in all compositions. Both the SrO and substituted bases, MgO, CaO, and ZnO, were reduced proportionally in order to incorporate the SnO and to obtain the 2.97 total moles of base. The presence of 0.02 mole SnO and the lower total base content combined to decrease exact correlation of phosphor composition with the phase equilibrium diagrams. For example, a composition containing 25 mole % $Mg_3(PO_4)_2$ with a ratio of 3.00 base to 2.00 PO_4 will consist entirely of the β-$Sr_3(PO_4)_2$ solid solution phase, but with 2.97 base to 2.00 PO_4, it will contain a small amount of $SrMg_2(PO_4)_2$.

Calcium-stabilized phosphors.—A range of compositions which included the entire solid solution region from pure β-$Ca_3(PO_4)_2$ to the point at which α-$Sr_3(PO_4)_2$ss appears were fired at 1100°C. Spectral distribution curves showed that a tin-activated β-$Sr_3(PO_4)_2$ solid solution with the minimum amount of $Ca_3(PO_4)_2$ required to stabilize the β form emits a major band at 6300Å and a minor band at 5800Å. As the calcium content is increased, the emission color is shifted due to an increase of the 5800Å band and the appearance of a band at 5200Å. The shift in color is not linear with increasing calcium content. This is effectively shown by color calculations made on the portion of the emission curves between 4500 and 7000Å. These limits were chosen to eliminate the effect of the blue emission (4000Å) which also increased with the calcium content, and to reduce any contribution from any blue $Sr_2P_2O_7$:Sn phosphor which might be present because of the nonstoichiometric composition used.

The plot of the calculated x coordinate against mole % $Ca_3(PO_4)_2$ is shown in Fig. 4. In the strontium-rich solid solutions, very little color change occurs. A major change occurs between 75 and 95 mole % $Ca_3(PO_4)_2$, but again very little change takes place between 95 and 100% β-$Ca_3(PO_4)_2$. This type of a color shift suggests that the strontium-rich β form exists to 75 mole % $Ca_3(PO_4)_2$, and that compositions between 75 and 95 mole % are merely physical mixtures of two phosphors. But measurements of *d*-spacing of the most intense low angle x-ray diffraction line of these phosphors, also plotted in Fig. 4, show a linear change up to 90 mole % $Ca_3(PO_4)_2$, indicating that one structure exists throughout this compositional range. No difference could be found in the width of any of the x-ray reflections measured, indicating that the shift did not result from two lines that almost superimpose. Above 95 mole % $Ca_3(PO_4)_2$, no consistent shift in *d* value could be found.

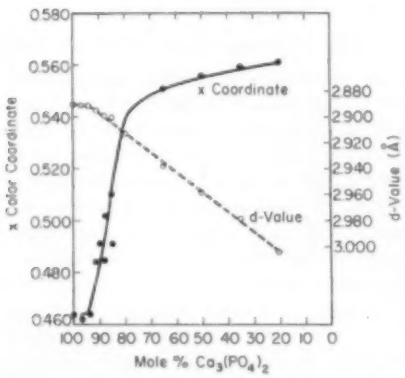

Fig. 4. Change in x color coordinate and d-value with calcium content of β-$(Sr,Ca)_3(PO_4)_2$: 0.02 Sn solid solutions.

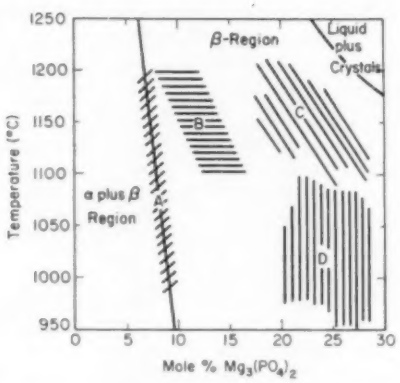

Fig. 5. A portion of the $Sr_3(PO_4)_2$-$Mg_3(PO_4)_2$ system showing results of firing phosphor compositions (Base/PO_4 ratio = 2.97/2.00).

From these data, it appears that if a two-phase region does exist, as discussed in the section on the phase relationships, it would not be found in the area of greatest color change, but would more likely be located around 90 to 95 mole % $Ca(PO_4)_2$. It must be remembered, however, that these measurements were made on nonstoichiometric phosphors in which the presence of Sn also will affect the d-spacings. The values obtained for β-$Ca_3(PO_4)_2$:Sn phosphor vary slightly from those of pure $Ca_3(PO_4)_2$. Therefore, the d-spacings on the low angle peak and the color data cannot be considered sufficiently reliable to furnish a basis for a conclusion about a two-phase region.

Magnesium-stabilized phosphors.—Phosphors were prepared at compositions ranging from 7.5 to 22.5 mole % $Mg_3(PO_4)_2$, with the ratio of 2.97 base to 2.00 PO_4, by firing in a reducing atmosphere for 1.5 hr at temperatures ranging from 1000° to 1200°C. Efficient phosphors cannot be made with higher magnesium contents. Color calculations made on the emission between 4500 and 7000Å show that there is a color change from $x = 0.522$ to $x = 0.558$ for the compositional change from 7.5 to 22.5 mole % $Mg_3(PO_4)_2$.

The brightness of the emission is determined both by the composition and the firing temperature. The presence of the nonluminescent α-phase is not highly objectionable, since this material has a low ultraviolet absorption. Phosphors containing approximately 20 to 30% of the α-phase are within 10% of the maximum obtainable brightness, and are soft and not sintered. The maximum brightness is obtained with compositions designed to contain only the β-phase, but close to the α-S_2P + β-S_2Pss boundary. Larger amounts of magnesium produce considerable sintering and lower the brightness but not the ultraviolet absorption. Compositions which are sufficiently high in magnesium to cause the reduced intensities of the x-ray reflections also will be lower in brightness even though severe sintering does not occur. The general areas of maximum brightness, sintering and reduced x-ray intensities are shown in Fig. 5. The letters A, B, C, and D represent, respectively, area of α-S_2P + β-S_2Pss, area of maximum brightness, area of maximum sintering, and area of diffuse x-ray lines.

Zinc-stabilized phosphors.—As shown in the phase diagram, the β region is considerably smaller than its counterpart in the magnesium system. This is reflected in a more limited compositional and temperature region in which optimum luminescence can be developed. The brightest phosphors lie in an area between about 8 and 12 mole % $Zn_3(PO_4)_2$, and below 1150°C. Again, the presence of the α-phase is not as harmful as high zinc contents and the resultant sintering.

The color shift across the β region in this system is from $x = 0.560$ to $x = 0.570$, calculated on the emission above 4500Å.

Efficiency measurements.—The relative efficiencies of the various β-$Sr_3(PO_4)_2$ solid solution phosphors can best be compared by measuring the quantum efficiency, since phosphors of the same color cannot be prepared with Mg^{2+}, Zn^{2+}, and Ca^{2+} substitutions. These measurements were made on the brightest phosphors in each system that were closest in color, and also on two of the brighter phosphors with high calcium contents. Calculations were made from spectral distribution curves, using the emission between 4000 and 7000Å. The National Bureau of Standards phosphor No. 1027 (magnesium tungstate) was used

Table IV. Relation of phosphor composition to quantum efficiency

Phosphor No.	Substitution in β-$Sr_3(PO_4)_2$:0.02Sn	Adjusted quantum efficiency, %	% 2537A Absorption
1	11 mole % $Mg_3(PO_4)_2$	98.0	93.0
2	10 mole % $Zn_3(PO_4)_2$	88.5	88.5
3	35 mole % $Ca_3(PO_4)_2$	81.5	89.5
4	85 mole % $Ca_3(PO_4)_2$	83.0	95.5
5	97 mole % $Ca_3(PO_4)_2$	88.0	93.5
6	NBS No. 1027	100.0	95.5

Table V. Relation of phosphor composition to brightness

Phosphor No.	Brightness, %	Calculated color	
		x	y
1	100	0.555	0.423
2	79	0.566	0.410
3	60	0.558	0.380
4	95	0.491	0.431
5	105	0.462	0.424

Table VI. Relation of phosphor composition to temperature stability

Sample No.	% of original brightness after heating at: 530°C	630°C	730°C
1	98.0	90.0	43.0
2	95.5	82.0	23.0
3	96.0	65.5	nil
4	93.5	81.5	7.0
5	97.0	85.5	14.0

as a standard, and taken as 100% quantum efficient. The values shown in Table IV, including that of the standard, were adjusted to give quantum efficiency at equal ultraviolet (2537Å) absorption.

The brightness differences between these phosphors are dependent on the quantum efficiency and the color. Brightness readings were made on these same phosphors under 2537Å excitation, using an eye-response corrected photocell. These are shown in Table V, compared to the β-$(Sr,Mg)_3(PO_4)_2$ phosphor which had the highest quantum efficiency.

The β-$(Sr,Mg)_3(PO_4)_2$:Sn phosphor gave 1820 lumens after 100 hr burning time in 40-w fluorescent lamps.

Another important feature of any phosphor prepared in a reducing atmosphere is its resistance to oxidation at temperatures approximating those found in lamp manufacturing. This was determined for the five phosphors by heating them in air for 30 min at various temperatures and measuring the remaining brightness as shown in Table VI.

Ternary Compounds

The ternary compounds, $SrMg_2(PO_4)_2$ and both forms of $SrZn_2(PO_4)_2$, can be activated with Sn^{2+}. The spectral distributions of the magnesium phosphor and the low-temperature form of the zinc phosphor are shown in Fig. 6.

The $SrMg_2(PO_4)_2$:0.05Sn phosphor is about 25% as bright as Zn_2SiO_4:Mn under 2537Å. It does not respond to 3650Å excitation and is blue under cathode ray excitation.

The high-temperature or β form of $SrZn_2(PO_4)_2$ is not readily quenched in amounts large enough to measure the phosphor characteristics. Since the phosphor must be cooled in a gaseous reducing atmosphere, the samples prepared always contain a mixture of the high and low forms. From visual observations, the β form with Sn^{2+} activation is a blue-white with a long afterglow under 2537Å excitation. Under 3650Å, the color is blue-white, considerably less bright, with no afterglow. It does not respond to cathode ray excitation.

The low-temperature or α form also has a blue emission with 2537Å radiation, but has no afterglow. Its emission is blue under cathode ray excitation, but it does not respond to 3650Å radiation.

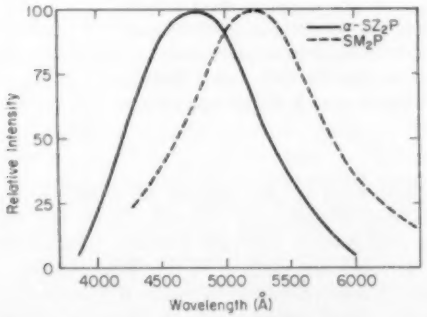

Fig. 6. Normalized spectral distribution curves of α-$SrZn_2(PO_4)_2$: 0.02 Sn and $SrMg_2(PO_4)_2$: 0.05 Sn.

Summary and Conclusions

1. A new high-temperature form of $Sr_3(PO_4)_2$, called β, has been found to exist above 1305°C. Below 1305°C, it reverts rapidly to the α form of $Sr_3(PO_4)_2$ usually observed and reported by many workers as the "normal" form. Consequently the β form must be detected either by D.T.A. or high-temperature x-ray diffraction.

2. $Ca_3(PO_4)_2$, $Mg_3(PO_4)_2$, and $Zn_3(PO_4)_2$ all form a range of solid solutions with β-$Sr_3(PO_4)_2$ and make possible their retention at room temperature, providing a matrix for "stabilized β-$Sr_3(PO_4)_2$ solid solution" phosphors activated with tin.

3. The composition and temperature limits in which the β-$Sr_3(PO_4)_2$ solid solutions exist have been determined for the three systems and in two of them ternary compounds have been found on the orthophosphate join. $SrMg_2(PO_4)_2$ is stable in one crystalline form to its melting point, but the analogous $SrZn_2(PO_4)_2$ inverts at 1035°C to a second form before melting at approximately 1175°C.

4. Examination of the tin-activated (0.02 mole Sn) phosphor compositions in the three solid solution series showed that the brightest phosphors in each system were obtained with the minimum amount of stabilizing agent (Ca^{++}, Zn^{++}, Mg^{++}) required to place the composition in the region of β-$Sr_3(PO_4)_2$ solid solutions. Larger amounts of stabilizer lowered the fluorescent brightness and led to objectionable sintering during firing.

5. The magnesium stabilized β-$Sr_3(PO_4)_2$ solid solution (11 mole % $Mg_3(PO_4)_2$:0.02 Sn) had the highest quantum efficiency, brightness, and temperature stability relative to the better phosphor compositions in the calcium and zinc stabilized systems.

6. Tin-activated $SrMg_2(PO_4)_2$ emits in the green region of the spectrum when excited by 2537Å u.v., but it is not responsive to 3650Å u.v. It is blue under cathode ray excitation. The tin-activated low temperature α form of $SrZn_2(PO_4)_2$ emits in the blue under 2537Å u.v. and cathode ray excitation, but does not respond to 3650Å u.v.

Manuscript received May 5, 1961. This paper is Contribution No. 60-71 from the College of Mineral Industries, The Pennsylvania State University.

Any discussion of this paper will appear in a Discussion Section to be published in the June 1962 JOURNAL.

REFERENCES

1. K. H. Butler, *This Journal*, **100**, 250 (1953).
2. H. Koelmans and A. P. M. Cox, *ibid.*, **104**, 442 (1957).
3. J. Berak, *Rocznik. Chem.*, **32**, 17 (1958).
4. F. L. Katnack and F. A. Hummel, *This Journal*, **105**, 125 (1958).
5. J. F. Sarver, F. L. Katnack, and F. A. Hummel, *ibid.*, **106**, 960 (1959).

APPENDIX

X-Ray Diffraction Data for Strontium Orthophosphate Systems

1. α-$Sr_3(PO_4)_2$

d (Å)	2θ	I/I_1
4.52	19.65	7
3.38	26.35	10
3.01	29.65	100
2.69	33.30	95
2.31	38.95	5
2.27	39.75	15
2.194	41.15	10
2.108	42.90	15
2.083	43.45	7
2.006	45.20	40
1.818	50.15	25
1.797	50.80	4
1.755	52.10	4
1.701	53.90	10
1.659	55.35	4
1.609	57.25	25
1.554	59.50	10

Other reflections

2. β-Strontium orthophosphate ($Sr_{0.66}$, $Mg_{0.33}$)$_3(PO_4)_2$

d (Å)	2θ	I/I_1
6.76	13.10	6
5.36	16.55	25
4.45	19.95	4
4.35	20.40	5
3.62	24.55	25
3.45	25.80	15
3.38	26.40	6
3.30	27.00	30
3.095	28.85	10
3.003	29.75	100
2.858	31.30	8
2.797	32.00	15
2.679	33.45	60
2.617	34.25	15
2.254	40.00	15
2.186	41.30	8
2.099	43.10	15
2.076	43.60	9
1.998	45.40	30
1.953	46.50	15

Other reflections

3. β-Strontium orthophosphate ($Sr_{0.85}$, $Ca_{0.15}$)$_3(PO_4)_2$

d (Å)	2θ	I/I_1
6.76	13.10	3
5.37	16.50	17
4.53	19.60	4
4.36	20.35	4
3.62	24.60	28
3.47	25.70	15
3.38	26.35	8
3.31	26.90	31
3.10	28.80	13
3.003	29.75	100
2.862	31.25	9
2.805	31.90	9
2.687	33.35	56
2.622	34.20	17
2.254	40.00	11
2.186	41.30	5
2.103	43.00	11
2.082	43.55	9
2.002	45.30	21
1.959	46.35	19

Other reflections

4. β-Strontium orthophosphate ($Sr_{0.85}$, $Zn_{0.15}$)$_3(PO_4)_2$

d (Å)	2θ	I/I_1
6.71	13.20	11
5.29	16.75	28
4.46	19.90	11
4.34	20.45	3
3.62	24.55	39
3.41	26.10	17
3.36	26.55	12
3.27	27.25	44
3.06	29.20	13
2.988	29.90	100
2.835	31.55	17
2.772	32.30	20
2.648	33.85	83
2.603	34.45	20
2.238	40.30	28
2.188	41.25	8
2.080	43.50	23
2.062	43.90	23
1.983	45.75	16
1.939	46.95	24

Other reflections

5. α-$Ca_3(PO_4)_2$ and β-$Ca_3(PO_4)_2$
See A.S.T.M. X-Ray Powder Data File

6. $Mg_3(PO_4)_2$
See ref. 5 (Sarver, Katnack, and Hummel)

7. α-$Zn_3(PO_4)_2$ and β-$Zn_3(PO_4)_2$
See ref. 4 (Katnack and Hummel)

8. $SrMg_2(PO_4)_2$

d (Å)	2θ	I/I_1
7.92	11.15	20
3.97	22.40	6
3.81	23.35	100
3.22	27.70	8
2.931	30.50	65
2.750	32.55	4
2.667	33.60	3
2.644	33.90	6
2.518	35.65	35
2.259	39.90	10
2.103	43.00	15
1.981	45.80	7
1.910	47.60	8
1.823	50.05	12
1.804	50.60	9

Other reflections

9. α-$SrZn_2(PO_4)_2$

d (Å)	2θ	I/I_1
6.26	14.15	10
4.15	21.40	47
4.03	22.05	100
3.90	22.80	37
3.78	23.55	41
3.72	23.90	69
3.60	24.70	24
3.55	25.05	33
3.47	25.70	60
3.27	27.30	84
3.125	28.55	29
2.993	29.95	82
2.959	30.20	76
2.858	31.30	41
2.739	32.70	7
2.679	33.45	41
2.607	34.40	30
2.578	34.80	36
2.539	35.35	53
2.459	36.55	13
2.442	36.80	10
2.404	37.40	13
2.380	37.90	14

Other reflections

10. β-$SrZn_2(PO_4)_2$

d (Å)	2θ	I/I_1
4.71	18.85	10
4.47	19.85	7
4.28	20.75	15
4.23	21.00	28
4.06	21.90	4
3.87	23.00	100
3.71	24.00	29
3.67	24.25	46
3.61	24.65	4
3.25	27.40	21
3.09	28.90	47
3.03	29.50	72
2.995	29.85	50
2.853	31.35	15
2.819	31.75	32
2.768	32.35	13
2.683	33.40	22
2.536	35.40	35
2.501	35.90	60
2.436	36.90	25
2.407	37.35	13
2.344	38.40	9
2.292	39.30	9

Other reflections

Magnesium Lithium Antimonate Phosphors

Richard W. Mooney

Chemical and Metallurgical Division, Sylvania Electric Products Inc., Towanda, Pennsylvania

ABSTRACT

The preparation and properties of phosphors of composition $Mg_3Li_6Sb_2O_{12}$ activated by Mn, U, Ti, Nb, and W are described. It is suggested that the transitions responsible for fluorescence in the Mn- and U-activated phosphors are associated with inner shell electrons while those in the Ti-, Nb-, and W-activated phosphors arise from transitions in the anionic group composed of the transition metal and its neighboring oxygen atoms.

While antimony is often used as an activator in oxide lattice phosphors, it is less common to find phosphors having an antimony oxide lattice activated by other elements. However, a few antimonate phosphors have been discovered and studied. Thus, antimony trioxide, Sb_2O_3, activated by manganese fluoresces in the green (1) while antimony tetroxide, Sb_2O_4, activated by manganese fluoresces in the red with a peak emission of 630 mμ (2) or 640 mμ (3). Kotera and Sekine (3) also mention that Sb_2O_4 activated by titanium gives a yellow fluorescence.

Bernard and co-workers extended their work on antimony oxide phosphors (1, 2) to the calcium metaantimonates, $CaSb_2O_6$, activated by manganese

(4), bismuth (5), and lead (6), and other workers (7, 8) prepared and studied the strontium and barium metaantimonates activated by the same three activators. Allsalu (8) also found that $SrSb_2O_6$:Ti gave a blue emission. Kotera and co-workers (9) prepared the pyroantimonates of the alkaline-earth metals, magnesium and zinc and found emissions which varied from blue to yellow with and without activation by Bi.

The patent literature contains references to a magnesium lithium antimonate activated by Mn and/or U (10) and the same compound activated by Ti or W (11). The Mn-activated phosphor also has been studied recently by Wilke (12). The object of the present paper is to discuss in some detail the preparation and properties of the magnesium lithium antimonate phosphors activated by Mn, U, Ti, Nb, and W.

Experimental Procedure

The phosphor composition was the same as that described in the original work (10), i.e., 35% MgO, 15% Li_2O, and 50% Sb_2O_5 by weight. Compositions deviating from the above were tried, but always resulted in less efficient phosphors. Similarly, replacement of MgO or Li_2O by fluorides or chlorides gave inferior products. Over 25 elements were tested as possible activators, but of these only Mn, U, Ti, Nb, and W gave phosphors of measurable efficiency. The compounds used to introduce the activators were manganous carbonate, uranyl acetate, titanium dioxide, niobium pentoxide, and tungsten oxide.

Originally, all of the ingredients were mixed in the dry state and fired to give the desired phosphor. However, a preferable method, used on all of the phosphors whose properties are reported herein, was as follows. The MgO and Sb_2O_5 were blended in the preferred ratio given above and fired for 1 hr at 1000°C, in fused silica crucibles. The resulting material was blended with the requisite amount of LiOH and activator and refired in silica boats. The final firing times and temperatures used were: 3 hr at 1100°C for Mn, 1.5 hr at 1125°C for U, and 1.5 hr at 1175°C for Ti, Nb, and W.

The methods used for the measurement of excitation and emission spectra (13), relative efficiency (14), and the effect of temperature on fluorescent efficiency (15) have been described previously. The x-ray diffraction data were obtained from Debye-Scherrer powder patterns taken with a 114.6-mm camera on a Philips Norelco unit using CuKα radiation.

Analyses.—The chemical analyses for matrix and activator components were conducted as follows:

Mg and Li: Samples were dissolved in HCl and gassed with H_2S to remove Sb. H_2SO_4 was added to the filtrate and the solution was evaporated to dryness, ignited, and weighed as mixed $MgSO_4$ and Li_2SO_4. Magnesium was then determined separately by precipitation as $MgNH_4PO_4 \cdot H_2O$ and ignition to $Mg_2P_2O_7$. Lithium was obtained by difference.

Sb: Samples were digested in HCl and gassed with H_2S to precipitate the antimony as the sulfide. The sulfide precipitate and filter paper were heated in Kjeldahl flasks with K_2SO_4 and H_2SO_4 to reduce the antimony to the antimonous condition. After cooling, the sample was titrated with $KMnO_4$ solution (16).

Mn: Samples were dissolved and gassed as above to remove Sb. The manganese was then oxidized to $HMnO_4$ which was determined colorimetrically on a Beckman Model B spectrophotometer (17).

U: HBr was added to the samples followed by heating to remove Sb. The samples were then fumed with H_2SO_4, dissolved in HCl and the uranium precipitated as $UO_2(OH)_2$ with NH_4OH. After ignition, the samples were again fumed with H_2SO_4 to convert to UO_2SO_4, which gave a yellow color on addition of H_2O_2 and NaOH. Uranium was then determined colorimetrically with a Beckman Model B spectrophotometer (18).

Ti: Samples were dissolved in HCl and gassed with H_2S as before to remove Sb. H_3PO_4, H_2SO_4, and H_2O_2 were added, and the resulting orange-yellow solution was analyzed colorimetrically with the Beckman Model B spectrophotometer (19).

Nb: Samples were fused with $KHSO_4$ in quartz crucibles and the melt leached with tartaric acid and H_2SO_4. The resulting solution was diluted and gassed with H_2S to remove Sb after which the Nb was precipitated with tannin solution and determined gravimetrically (20).

W: A Na_2CO_3 fusion was followed by leaching and acidification with HCl. KSCN, $SnCl_2$, and HCl were added and the resulting yellow color determined colorimetrically (21). Gravimetric determinations as tungstic acid were also made following the methods of Li (22).

Nature of the Matrix

Quantitative analyses for the three major constituents of the phosphor are given in Table I.

The ratios of Mg to Li to Sb are therefore 5:6:2 leading to the empirical formula $Mg_5Li_6Sb_2O_{13}$. Thirteen rather than fourteen oxygens are shown in the formula since $Mg_5Li_6Sb_2O_{13}$ is electrically neutral assuming antimony in a pentavalent state and also since the per cent oxygen values may be slightly high due to small amounts of adsorbed moisture or insoluble matter. If antimony were in the trivalent state, the electrically neutral formula would be $Mg_5Li_6Sb_2O_{11}$. However, the analytical data are not in agreement with this supposition, and, furthermore, the oxidizing nature of the firing process would favor the higher oxidation state. Surprisingly, very little Sb_2O_5 is lost during the firing process, and the ratios of Mg to Li to Sb are the same in the initial mixture and the fired phosphors.

If the empirically observed formula, $Mg_5Li_6Sb_2O_{13}$, is written as $5MgO \cdot 3Li_2O \cdot Sb_2O_5$, it bears a resemblance to Klasen's lithium-modified magnesium arsenate phosphor (23). In that work it was observed that one of the Mg atoms in $6MgO \cdot As_2O_5$:Mn could be

Table I. Quantitative analyses for Mg, Li, and Sb

	Sample A, %	Sample B, %	Average, %	Atoms/ 2 atoms Sb
Mg	19.0	19.6	19.3	5.0
Li	6.7	6.9	6.8	6.1
Sb	39.2	38.7	38.95	2.0
O (by difference	35.1	34.8	34.95	13.7

Table II. Lattice spacings and relative intensities of the x-ray reflections of $Mg_5Li_6Sb_2O_{12}$

d, A	I	d, A	I
4.70	VS	1.94	W
4.44	M	1.91	MW
3.88	M	1.83	MW
3.76	M	1.81	W
2.88	S	1.71	W
2.81	M	1.69	W
2.56	M	1.65	M
2.43	M	1.62	W
2.36	W	1.59	W
2.31	VW	1.57	W
2.24	M	1.55	VW
2.22	VW	1.54	M
2.15	S	1.52	VW
2.14	M	1.50	VS
2.09	VS	1.48	M

VS, very strong; S, strong; M, medium; MW, medium weak; W, weak; VW, very weak.

replaced by a Li atom giving $5MgO \cdot 0.5Li_2O \cdot As_2O_5$:Mn and resulting in a phosphor with improved chemical stability and increased efficiency at elevated temperatures.

The matrix used in this investigation contains considerably more Li atoms than Klasens's phosphor (23), yet has a much simpler x-ray powder diffraction pattern than $6MgO \cdot As_2O_5$ (24). The diffraction pattern also differs from that of magnesium metaantimonate, $MgSb_2O_6$, which is formed by the prefiring of MgO and Sb_2O_5 and ultimately converts to the final phosphor matrix, $Mg_5Li_6Sb_2O_{12}$, by reacting with the excess MgO and added LiOH during the final firing. The diffraction pattern of $Mg_5Li_6Sb_2O_{12}$ is given in Table II. In spite of the relative simplicity of the diffraction pattern, attempts to index the lines in terms of one of simpler crystal systems were unsuccessful.

Optical Spectra

The excitation and emission spectra of the Mn- and U-activated phosphors are shown in Fig. 1. Both exhibit broad excitation spectra and narrow emission bands. The positions of the emission bands are independent of the energy of excitation. The U-activated phosphor peaks at 523 mμ with excitation by either 267- and 332-mμ bands while the Mn-activated sample emits in the red at 660 mμ when excited by either 345- or 481-mμ wavelengths. The 660-mμ peak shown by $5MgO \cdot 3Li_2O \cdot Sb_2O_5$:Mn is very close to that of Klasen's $5MgO \cdot 0.5Li_2O \cdot As_2O_5$:Mn phosphor (23) and to Wilke's $6MgO \cdot 1.3Li_2O \cdot Sb_2O_5$:Mn phosphor (12).

Figure 2 gives the excitation and emission spectra of the Ti-, Nb-, and W-activated phosphors. In contrast to the narrow emission bands for Mn and U, the Ti, Nb, and W systems exhibit broad Gaussian emission bands with widths at half-maximum varying from 6600 cm^{-1} to 7200 cm^{-1}. The excitation curves do not extend into the visible as do those of Mn and U, but instead peak in the ultraviolet at or below 250 mμ.

Effect of Activator Concentration

The effect of activator concentration is shown in Fig. 3, where the normalized efficiency is plotted

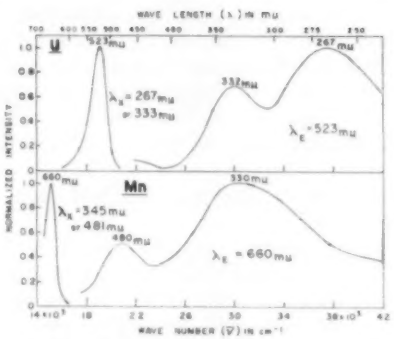

Fig. 1. Excitation and emission spectra of $Mg_5Li_6Sb_2O_{12}$: 0.020 U and 0.007 Mn.

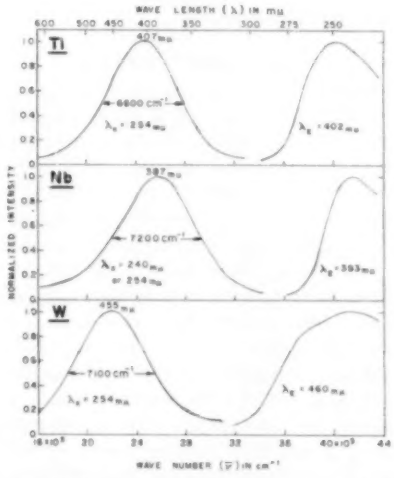

Fig. 2. Excitation and emission spectra of $Mg_5Li_6Sb_2O_{12}$: 0.035 Ti, 0.084 Nb, and 0.075 W.

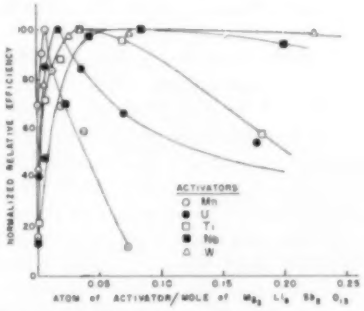

Fig. 3. Relative efficiency vs. activator concentration for $Mg_5Li_6Sb_2O_{12}$ activated by Mn, U, Ti, Nb, or W under 254-mμ excitation.

against the atoms of activator per mole of $Mg_5Li_6Sb_2O_{12}$. A similar although less definite grouping may be made of these results as was proposed for the optical spectra. Thus the phosphors activated by the transition metals Ti, Nb, and W have the broadest range of activator concentrations yielding efficient phosphors, whereas both the Mn- and U-activated phosphors are more easily concentration-quenched. The activator concentrations at which concentration quenching becomes appreciable vary in the order

$$Mn < U < Ti < Nb \approx W$$

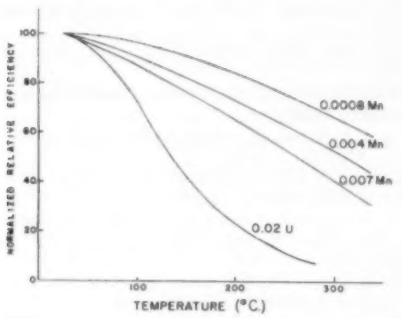

Fig. 4. Temperature dependence of fluorescence of $Mg_3Li_6Sb_2O_{12}$ activated by Mn or U under high-pressure mercury-vapor excitation.

No attempt was made to analyze these data quantitatively using existing theories since the results would have little meaning for a matrix of unknown structure.

Practical Applications

The Mn-activated phosphor is more responsive to long than to short wavelength ultraviolet, and therefore the possibility of use as a color-correcting phosphor in high-pressure mercury-vapor lamps arises. However, it is only 50-60% as efficient as magnesium fluorogermanate activated by manganese, and, furthermore, its efficiency drops off steadily with rising temperature (Fig. 4). In view of its poor temperature characteristics and mediocre efficiency it would find only limited application. The variation of efficiency with temperature exhibits the usual improvement at low activator concentrations.

The U-activated sample has an efficiency of about 70% of that of zinc orthosilicate activated by manganese. It is responsive to both short- and long-wavelength ultraviolet and exhibits a very saturated green color under either. The efficiency drops off sharply with increasing temperature (Fig. 4) although a detailed study of the effect of activator concentration was not made. The phosphor might be used for special applications with low-pressure mercury vapor discharges.

The efficiencies of the transition-metal activators to 254-mμ radiation vary in the order

$$Ti > W > Nb$$

The Ti-activated phosphor is equal in fluorescent output to the deep blue phosphor, calcium tungstate activated by lead. It has trichromatic coefficients of $x = 0.177$ and $y = 0.126$ which make it a slightly more saturated blue than the corresponding calcium tungstate. Hence, the Ti-activated phosphor might be used successfully as a deep blue lamp or in applications where its near ultraviolet emission could be used to activate other materials. The efficiencies of both the W- and the Nb-activated phosphors are low, and neither would be expected to have practical value.

Discussion

The ionic radii of the matrix cations are all approximately the same, i.e., $r_{Mg^{2+}} = 0.65$Å, $r_{Li^{+}} = 0.60$Å, and $r_{Sb^{5+}} = 0.62$Å. Since the ionic radii of the activator ions are also of the same general size, they may enter the lattice without greatly distorting the oxygen-dominated structure.

Manganese activation is the most common of those found and can be most easily explained. Excitation by tetravalent manganese rather than divalent manganese was first proposed by Kroeger (25) to explain the deep red emission composed of several sharp bands found for Mg_2TiO_4:Mn. The fine structure characteristic of Mn^{4+} having the d^3 configuration was observed in the emission spectra of several phosphors generically related to the antimonate under consideration, namely, $4MgO \cdot GeO_2$:Mn (26, 27); $3.5MgO \cdot 0.5MgF_2 \cdot GeO_2$:Mn (28); $6MgO \cdot As_2O_5$:Mn (24); and $5MgO \cdot 0.5Li_2O \cdot As_2O_5$:Mn (23). In all cases but one (27), the emission center was attributed to the Mn^{4+} ion, and it now seems likely that activation by Mn^{4+} is responsible for the emission in each of the above cases as well as for the narrow red band peaking at 660 mμ for $5MgO \cdot 3Li_2O \cdot Sb_2O_5$:Mn. However, because of instrumental limitations, it was not possible to resolve the emission band further. Spectra measured at lower temperatures might provide a separation. Wilke (12) was also unable to obtain narrow bands and as a consequence attributed the luminescence to a Mn^{3+} center.

Kroeger (29) has pointed out that the transitions responsible for the optical spectra of the Mn^{4+}-activated phosphors are associated with electrons in the incomplete inner shell of the Mn^{4+} ion. Therefore, the energy bands or levels responsible for the spectra are cencentrated near the cation, and the Mn^{4+} ion is isolated effectively from its surrounding oxygen network.

The narrow emission band exhibited by the U-activated phosphor would also lead to the assumption that the transitions responsible for the absorption and emission spectra occur in the inner shell of the U-ion and are shielded similarly from external perturbations. The exact nature of the transition is unknown.

For the phosphors activated by Ti, Nb, and W, it seems likely that the mode of activation is different. The emission spectra are broad rather than narrow, indicating a large degree of interaction of the activator ion with its surroundings, and therefore it is suggested that the activator center is composed of the transition metal and its surrounding oxygens. This is roughly equivalent to suggesting activation by anions since the transition metals would be most likely to substitute for antimony in the $Mg_3Li_6Sb_2O_{12}$ matrix. Activation by anions in oxy-acid phosphors has also been suggested by Kotera (30) who assumed that the electronic transitions responsible for luminescence originated in the anion in the cases of activation by pyrovanadate, tungstate, and molybdate groups.

Of the other possible 3d transition-metal activators, vanadium and chromium are somewhat smaller than the ions which make up the matrix ($r_{V^{5+}} = 0.59$Å and $r_{Cr^{6+}} = 0.52$Å) and hence might not substitute readily into the host lattice. Both proved to be ineffective as activators. Scandium was not tried, but would not be expected to substitute into the lattice due to its large size ($r_{Sc^{3+}} = 0.81$Å).

In the 4d transition series, activation by Y, Zr, and Mo was tried without success. Both Y and Zr would probably be too large for successful substitution, but Mo^{6+} with an ionic radius of 0.62Å would be expected to substitute easily. The lack of activation by Mo is difficult to explain.

None of the rare earths used (La, Ce, Sm, Nd, or Gd) produced luminescence and of the 5d transition metals tried (Ta and W), only W gave activation. The large ionic radius of Ta ($r_{Ta^{5+}} = 0.73$Å) would probably preclude its substitution into the lattice. Neither Hf nor Re were tried.

Finally, it is suggested that the anionic-type of activation postulated in this paper for $Mg_3Li_6Sb_2O_{12}$ activated by Ti, Nb, and W is also responsible for the fluorescent of other transition metal-oxide phosphors such as the self-activated tungstates and barium titanium phosphate, $Ba_2P_2O_7 \cdot TiO_2$.

Acknowledgment

The author is indebted to Dr. C. W. W. Hoffman for the x-ray diffraction measurements and to Mr. G. J. Meisenhelter for the analytical determinations. He would also like to express his thanks to Drs. K. H. Butler and J. S. Smith for their advice and encouragement during the progress of the work.

Manuscript received March 10, 1961; revision received Aug. 15, 1961. This paper was prepared for delivery before the Indianapolis Meeting, April 30-May 3, 1961.

Any discussion of this paper will appear in a Discussion Section to be published in the June 1962 JOURNAL.

REFERENCES

1. J. Janin and R. Bernard, *Compt. rend.*, **237**, 798 (1953).
2. R. Bernard and J. Janin, *ibid.*, **239**, 489 (1954).
3. Y. Kotera and T. Sekine, *This Journal*, **102**, 390 (1955).
4. J. Janin and R. Bernard, *Compt. rend.*, **240**, 614 (1955).
5. R. Bernard and J. Janin, *J. phys. radium*, **17**, 616 (1956).
6. R. Bernard, *Ann. univ. Lyon, Sci. Sect. B*, **10**, 49 (1957).
7. H. Witzmann and H. Kohler, *Naturwissenschaften*, **45**, 462 (1958).
8. M. L. Yu. Allsalu, *Izvest. Akad. Nauk. S.S.S.R. Ser. Fiz.*, **23**, 1360 (1959).
9. Y. Kotera, T. Sekine, and M. Yonemura, *Bull. Chem. Soc. Japan*, **29**, 743 (1956).
10. P. W. Ranby (to Thorn Electrical Industries Ltd.), British Pat. 707,101; U.S. Pat. 2,785,137, Mar. 12, 1957.
11. R. W. Mooney (to Sylvania Electric Products Inc.), U.S. Pat. 2,865,862, Dec. 23, 1958.
12. K.-Th. Wilke, *Z. physik. Chem. (Leipzig)*, **213**, 298 (1960).
13. W. Slavin, R. W. Mooney, and D. T. Palumbo, *J. Opt. Soc. Amer.*, **51**, 93 (1961).
14. K. H. Butler and R. W. Mooney, *Sylvania Technologist*, **9**, 121 (1956).
15. R. W. Mooney, *This Journal*, **105**, 456 (1958).
16. W. F. Scott, "Standard Methods of Chemical Analysis," 5th ed., Vol. I, pp. 76, 77, D. VanNostrand Co., Inc., New York (1939).
17. W. F. Scott, *ibid.*, p. 573.
18. W. F. Schoeller and A. R. Powell, "Analysis of Minerals and Ores of the Rarer Elements," 3rd ed., pp. 308, 309, Hafner Publishing Company, New York (1955).
19. W. F. Schoeller and A. R. Powell, *ibid.*, p. 124.
20. W. F. Schoeller and A. R. Powell, *ibid.*, p. 217.
21. W. F. Schoeller and A. R. Powell, *ibid.*, p. 285.
22. K. C. Li and C. Y. Wang, "Tungsten," Reinhold Publishing Corp., New York (1943).
23. H. A. Klasens, *Philips Res. Repts.*, **9**, 377 (1954).
24. M. Travnicek, F. A. Kroeger, Th. P. J. Botden, and P. Zahn, *Physica*, **18**, 33 (1952).
25. F. A. Kroeger, *Nature*, **159**, 706 (1947).
26. F. A. Kroeger and J. van den Boomgaard, *This Journal*, **97**, 377 (1950).
27. S. H. Patten and F. E. Williams, *J. Opt. Soc. Amer.*, **39**, 702 (1949).
28. L. Thorington, *ibid.*, **40**, 579 (1950).
29. F. A. Kroeger, "Same Aspects of the Luminescence of Solids," p. 64, Elsevier Publishing Co., Inc., New York (1948).
30. Y. Kotera, *J. Chem. Phys.*, **23**, 219 (1955).

Preparation of High-Purity Silicon from Silane

Charles H. Lewis, Henry C. Kelly, Mario B. Giusto, and Sidney Johnson

Research and Development Laboratories, Metal Hydrides Incorporated, Beverly, Massachusetts

ABSTRACT

The preparation, purification, and thermal decomposition of silane, SiH_4, were investigated for the purpose of preparing high-purity silicon. Quantitative yields of silane were obtained by the reduction of silicon tetrachloride with lithium aluminum hydride. Variables in the thermal decomposition of silane were evaluated with regard to purity of the elemental silicon produced and the efficiency of dissociation and deposition rate. Silane was dissociated on an inductively heated single crystal silicon substrate to yield high-purity silicon. Neutron activation analyses for microcrystalline high-purity silicon as deposited are given.

In the past five years, the electronics industry has developed a requirement for ultrapure silicon for semiconductor applications. To fulfill this need, a number of alternative processes for the preparation of high-purity silicon have been investigated by various laboratories throughout the world, and a number of these have progressed through research and development to production. The utilization of zone-refining as a physical method of purification represented a major technological breakthrough in ultrapurification procedures. The ineffectiveness of this method for removal of boron from a silicon sub-

strate pointed up the need for a process peculiarly adaptable to chemical methods of purification. Starting in 1956, Metal Hydrides conducted a research program to evaluate silane as an intermediate material for the preparation of ultrapure silicon (1, 2). The silane was generated by interaction of silicon tetrachloride with lithium aluminum hydride and then thermally decomposed in accordance with the equations

$$SiCl_4 + LiAlH_4 \xrightarrow{\text{tetraglyme}} SiH_4 + LiCl + AlCl_3$$

$$SiH_4 \xrightarrow{\Delta} Si + 2H_2$$

Since silane, SiH_4, is a highly volatile gas which forms spontaneously explosive mixtures with air and presents severe handling problems not common to other intermediates, the advantages to be gained by its use are summarized:

1. Silane is the least stable intermediate with respect to decomposition to the elements. Thermodynamically there is less energy to overcome to achieve decomposition, a factor which only can be beneficial for the preparation of silicon. The favorable comparison is readily seen from the standard heat of formation values in Table I.

2. The hydrides involved, SiH_4 and its contaminants, have greater differences in chemical and physical properties than other probable intermediates, *e.g.* chlorides. Therefore, sharper separations can be achieved (cf. items 6 and 7). This can be illustrated by comparing the simplest of physical properties, molecular weight, of silane with possible contaminating hydrides, and of silicon tetrachloride with possible contaminating chlorides. Table II shows that the ratio is large for hydrides, small for chlorides. The comparison is admittedly superficial, but is illustrative of the stated generality.

3. Silane contains a greater percentage of silicon than other intermediates. The quantity of various silicon compounds required to contain a unit weight of silicon is given in Table III.

4. The silicon tetrachloride-lithium aluminum hydride silane generator operates by mixing two solutions and is a homogeneous reaction. Silane is essentially instantaneously evolved. It is easy to start, stop, and regulate.

5. Use of the dimethyl ether of tetraethyleneglycol (bp 275°C) virtually eliminates solvent entrainment as a consideration.

6. The generation step is an exceedingly powerful purification procedure. It completely and quantitatively eliminates all elements which do not form volatile hydrides, or whose volatile hydrides are protonic in nature.

7. The silane gas stream is particularly susceptible to virtually complete quantitative removal of trace impurities by gas scrubbing techniques. Quality control of the product is relatively independent of starting materials.

8. Only hydrogen is evolved as a by-product. Hydrogen chloride and chlorine evolved in other processes may cause some corrosion, significant only to semiconductor applications.

9. No boron is evolved when excess lithium aluminum hydride is present. The relatively high acidity of the borane group, BH_3, compared to silane greatly enhances the separation of this element.

Where ultrapure silicon is the prime objective, these considerations indicate that the advantages of silane as an intermediate far outweigh its disadvantages. Indeed, its properties are so favorable, it is almost certain to be used where the ultimate in purity is sought.

Table I. Standard heats of formation at 25°C

Compound	ΔH_f	Reference
SiH_4 (*g*)	+7.8	(3)
SiI_4 (*c*)	−31.6	(4)
$SiBr_4$ (*l*)	−95.1	(4)
$SiCl_4$ (*l*)	−153.0	(4)
SiF_4 (*g*)	−370	(4)

Table II. Molecular weight ratios of selected hydrides and chlorides

Hydride	Mole wt	MH_x/SiH_4	Chloride	Mole wt	$MCl_x/SiCl_4$
CH_4	16.043	0.4999	CCl_4	153.839	0.9055
SiH_4	32.092	1.000	$SiCl_4$	169.888	1.000
GeH_4	76.632	2.388	$GeCl_4$	214.428	1.262
AsH_3	77.934	2.428	$AsCl_3$	181.281	1.067

Table III. Quantity of silicon compounds

Si Compound	Mole wt	Wt Si compound / Wt Si
Si	28.06	1.00
SiH_4	32.092	1.14
SiF_4	104.06	3.71
$SiHCl_3$	135.439	4.83
$SiCl_4$	169.888	6.05
$SiBr_4$	347.724	12.39
SiI_4	535.74	19.09

Generation of Silane

The investigation at Metal Hydrides started with a consideration of various methods of generating silane. A hydride reduction of a silicon halide in an ether solvent was most suitable. Lithium aluminum hydride and either silicon tetrachloride or trichlorosilane gave quantitative yields of silane. Any number of ethers are suitable, but its low volatility made the dimethyl ether of tetraethylene glycol (variously referred to as "tetraglyme," "E-181," or "M4M") the solvent of choice (5).

The reaction was carried out at room temperature by adding the glycol-ether solution of the chloride dropwise into a magnetically stirred glycol-ether solution or slurry containing an excess of lithium aluminum hydride. This afforded a ready and convenient means of controlling the reaction by adjusting the rate of addition. The reaction vessel was under evacuation and the evolved silane passed through a dry ice condenser, a purification train, and into the decomposition chamber. Here the purified silane was decomposed to yield a polycrystalline deposit of ultrapure silicon, and the by-product hydrogen expelled through vacuum pumps.

The reaction probably proceeds by the stepwise replacement of silicon-chlorine bonds with hydrogen. A donor solvent is necessary for the reaction (6).

This serves to assist in the transfer of a hydride ion to silicon with the displacement of chloride ion from the silicon atom. In subsequent steps, chloride displaces the hydride ion. Thus the sequential steps may be represented as shown below, where the postulated transitory reaction intermediates are indicated in brackets.

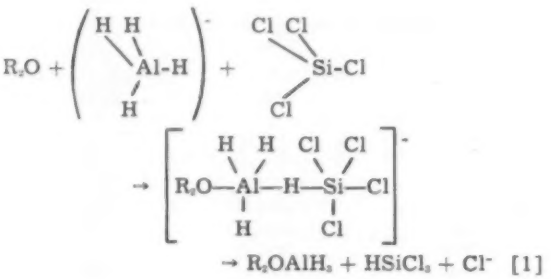

$$\rightarrow R_2OAlH_3 + HSiCl_3 + Cl^- \quad [1]$$

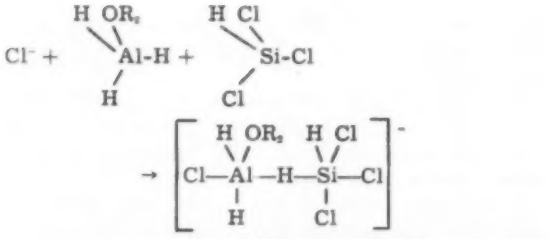

$$\rightarrow R_2OAlH_2Cl + H_2SiCl_2 + Cl^- \quad [2]$$

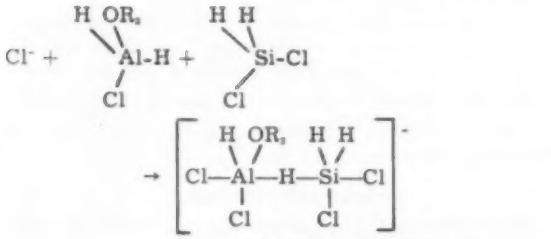

$$\rightarrow R_2OAlHCl_2 + H_3SiCl + Cl^- \quad [3]$$

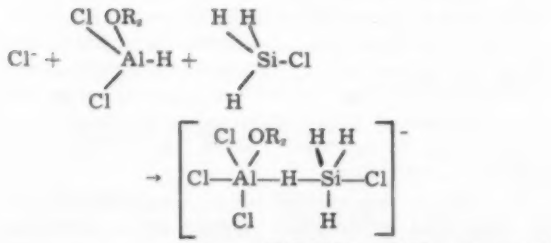

$$\rightarrow R_2OAlCl_3 + SiH_4 + Cl^- \quad [4]$$

The two essentially simultaneous nucleophilic displacements provide a reaction path of low activation energy, the energy required to break the reactant bonds being supplied principally by the concurrent formation of the product bonds.

The immediate formation of silane and the absence of partially reduced chlorosilanes suggest that the reaction rate for each succeeding step becomes increasingly more rapid. The four equations may be combined to give the over-all reaction

$$R_2O + LiAlH_4 + SiCl_4 \rightarrow R_2OAlCl_3 + SiH_4 + LiCl$$

Purification of Silane

The generation step is itself a powerful purification, quantitatively separating many inpurities. Contaminants in the effluent gas stream are limited to, (*a*) solvent vapor, (*b*) unreduced or partially reduced chlorosilanes, as $SiCl_4$ and SiH_xCl_{4-x}, and (*c*) those elements, originally present as impurities in the silicon tetrachloride, which form volatile hydrides and are liberated from the reaction mixture with silane.

Solvent vapor is removed from the gas stream by the use of dry ice (−78.5°) and isopentane slush (−160°) baths. The latter bath also is effective in controlling the flow rate of silane and the quantity of undecomposed silane present in the system. At that temperature, liquid silane exerts a vapor pressure of 9 mm Hg. Any silane gas surge from the generator which increases the pressure above this value causes condensation of liquid silane in the trap and is not transmitted to the decomposition chamber. Additionally, one can observe any accumulation of liquid silane in this bath. By keeping this accumulation small, one can readily assure that the hazard from accidental admixture of silane and air does not exceed the safety limits of the facilities being used.

No evidence for incomplete reduction of silicon tetrachloride was found. An excess of lithium aluminum hydride was always used. The silicon tetrachloride solution was introduced from the dropping funnel through capillary tubing which terminated in a hook at the very bottom of the reaction flask. This caused the evolved gas to pass up through the lithium aluminum hydride solution. The excess lithium aluminum hydride not only assured complete reduction of the silicon tetrachloride, but also reacted with any boron trichloride present to yield nonvolatile lithium borohydride, rather than gaseous diborane which is evolved in the presence of excess chloride (7,8). In some runs, a lithium aluminum hydride-glycol-ether solution gas scrubber was placed in the purification train to insure complete reduction, but this precautionary measure is not necessary.

Chemical absorption was considered to offer a most effective means of purifying silane. Differences in acid or base character were considered in selecting absorbents. Thus, on a relative basis, the silane molecule might be considered neutral; a Group III hydride (B_2H_6), acidic; and a Group V hydride (PH_3), basic. The silicon atom has more than four bonding orbitals, and certain of its tetravalent compounds are therefore susceptible to nucleophilic attack by a strong base. A given base, then, in order to function as an effective purifying agent (*e.g.*, absorption of diborane) must be selective, *i.e.*, inert to silane.

Amines are known to coordinate with boron compounds. An amine may be added directly to the silicon tetrachloride-glycol ether solution. Any boron trichloride present will coordinate with the amine, and the B-N bond will persist through the reaction, even though the substituents may undergo reaction. The evolution of any volatile boron compounds is thereby prevented. Alternatively, a liquid amine or amine solution gas scrubber can be inserted in the purification train, or a solid amine in a packed column. The latter methods preclude the possibility of

Table IV. Thermal stability of hydrides

Temperature (°C) necessary for rapid decomposition to elements		
$(BH_3)_2(g)$ 300°		
$(AlH_3)_x(s)$ 110°-160°	$SiH_4(g)$ >600°	
$(GaH_3)_2(l)$ 130°	$GeH_4(g)$ 340°-360°	$AsH_3(g)$ 300°
$(InH_3)_x(s)$ >80°	$SnH_4(g)$ 150°	$SbH_3(g)$ 200°
	$PbH_4(g)$ 25°	$BiH_3(g)$ 25°

the amines reacting with lithium aluminum hydride, although avoiding this is not essential since only small quantities of amine are required, and a substantial excess of lithium aluminum hydride is always used. Tertiary alkyl amines are unreactive in any event.

Activated carbon proved to be an excellent adsorbent. Tests indicated a strong affinity for both diborane and arsine. Arsine is not eluted at room temperature under vacuum. Diborane adsorbed at 0° is desorbed to the extent of 23-24% at room temperature (9). For maximum effectiveness, therefore, the activated carbon should be kept at 0° or below. It is undoubtedly also an excellent adsorbent for other polar molecules, as solvent vapor, chlorosilanes, amines, phosphine, etc.

A final property which may be utilized to purify silane is its relative thermal stability compared with that of possible contaminating hydrides. Although "decomposition temperature" is a rather imprecise term to apply to these compounds, the approximate temperature necessary to achieve rapid decomposition of various hydrides to their elements is shown in Table IV.

We found that passing silane through a quartz tube having a 12-in. zone heated to 600°-636° resulted in only 2-6% decomposition under normal operating conditions. This is a temperature far in excess of that required to completely decompose the other hydrides listed in Table IV. To purify silane, the gas stream was passed through a quartz-packed quartz tube heated to 350° before being introduced to the decomposition chamber.

Other volatile hydrides, as ammonia, water, other Group VI hydrides, and the hydrogen halides are not present in the silane gas stream because their protonic hydrogens react with the hydridic hydrogens of lithium aluminum hydride to give hydrogen and nonvolatile aluminum compounds. In fact, lithium aluminum hydride-ether solutions are perhaps the best protonic scavengers known, so that a more effective reagent for removal of these materials is unlikely.

Decomposition of Silane

Initially, the purified silane was decomposed by passing through a heated tube of fused transparent quartz. The decomposition efficiency was poor at 600°-636°, but quantitative at 777° and above. Due to the difference in thermal contraction of quartz and silicon, the tubes cracked on cooling. This led to the use of a quartz vacuum jacket over the decomposition tube. The silicon proved very difficult to remove from the quartz, and required prolonged leaching with hydrofluoric acid. Generally, the heavier the deposit of silicon, the better the purity. Thus, it became apparent that the impurities were coming primarily from the quartz and the leaching operation, and efforts were directed to depositing the silicon on inductively heated high-purity silicon with the apparatus illustrated in Fig. 1. Utilizing a four megacycle output frequency, induction heating of a silicon rod was accomplished by first coupling to a quartz-enclosed graphite rod adjacent to the silicon substrate. After the silicon had been heated by radi-

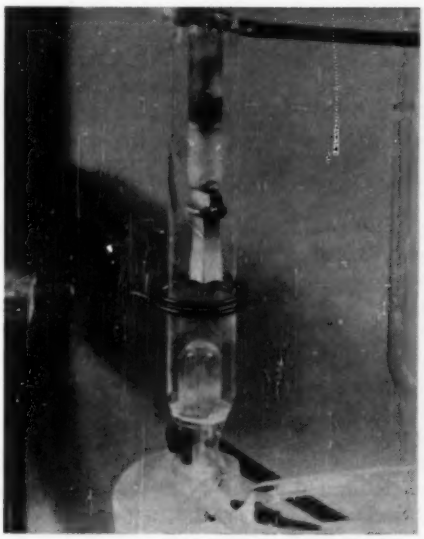

Fig. 1. A close-up view of the silane cracking chamber. At the bottom of the quartz chamber extending almost to the coil is the water-cooled orifice where the silane gas is jetted into the chamber. The R.F. coil, which may be hydraulically adjusted to any desired level, is on the outside of the chamber to reduce contamination. The silicon substrate is machined, leached, hung on a quartz holder, and leached again before inserting into the chamber. Although the silicon substrate is shown fixed, the apparatus was later modified so that it could be raised or lowered by a magnetic assembly. Directly above the silicon substrate is the carbon preheater enclosed in quartz under vacuum. This radiantly heats the silicon to a temperature where the R.F. unit will couple to it. At the top of the picture is the water-cooling tube which washes over the entire outer surface of the chamber.

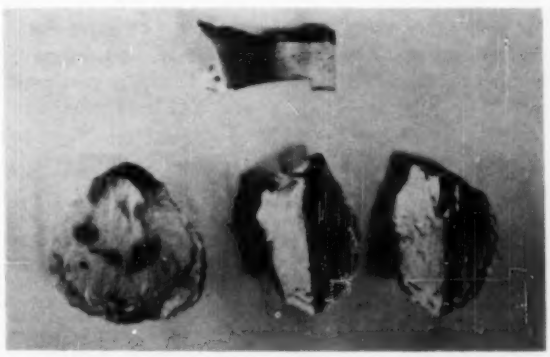

Fig. 2. Fragments of silicon deposit from thermal decomposition of silicon substrate showing cleavage angles.

Table V. Impurities in elemental silicon from thermal decomposition of silane

Fe	17.0*	As	1.0	Zn	0.41*	Ga	0.0062*
Cu	11.0	P	1.0*	Ni	0.27*	Sb	0.0037*
Bi	1.6*	Tl	0.91*	In	0.032*	Mn	0.00062*

* Not detected. Value shown is limit of detection in ppb.

ation, direct coupling to silicon was achieved. Silane, *in vacuo*, was directed at the base of the silicon substrate by means of a water-cooled jet. The quartz apparatus containing the substrate was cooled by running water down the outside jacket to prevent the deposition of metallic silicon on the inner wall of the cracking chamber. The substrate was raised and lowered by a magnetic device outside of the chamber.

The size of the silicon deposit obtained in this manner is limited by the dimensions of the cracking chamber. The deposits are easily fractured along definite angular boundaries, as shown in Fig. 2, which may be indicative of a preferred orientation in the crystal growth.

The temperature of the substrate, as measured by an optical pyrometer, ranged between 930°-1375°. The temperature was controlled to ±25°, the variation being due to the cooling effect of the silane gas stream directed at the base of the substrate. Operating at temperatures from 1250° to 1375°, it was noted that elongation of the substrate deposit was enhanced if the R.F. coil was 5-8 mm below the bottom of the substrate. At lower temperatures, the position of the coil did not influence elongation, provided it was positioned at the widest section of the substrate or below. The substrate was attached at the top by a quartz holder. Better decomposition efficiencies were obtained by adjustment of the distance between the base of the silicon substrate and the orifice of the silane jet. During the early stages of a run, the distance should be less than 20 mm. As the deposit grows, the distance between the substrate and orifice was increased to as much as 150 mm.

Progress was followed by spectrographic analyses in the early phases of the project. When the impurities were below the limits of spectrographic detection, neutron activation analyses were made. Values obtained are shown in Table V.

Acknowledgment

The sponsorship of the Electronics Research Directorate, Air Force Cambridge Research Laboratories, is gratefully acknowledged. Special thanks are due to Mr. J. Paul Cali of that organization for neutron activation analyses.

Manuscript received May 25, 1961; revised manuscript received Aug. 4, 1961. This paper was presented before the Conference on the Ultrapurification of Semiconductor Materials sponsored by the AFCRL in Boston, May 1961.

Any discussion of this paper will appear in a Discussion Section to be published in the June 1962 JOURNAL.

REFERENCES

1. H. C. Kelly, T. J. Flynn, C. W. Davis, and S. Johnson. AFCRC-TR-57-198; AD 133701. "The Preparation of Transistor Grade Silicon from Silane or Analogous Compounds," Final Report under Contract AF19(604)-1928, 31 August 1957.
2. C. H. Lewis, M. B. Giusto, and S. Johnson. AFCRC-TR-59-354; AD 228538. "The Preparation of Transistor Grade Silicon from Silane or Analogous Compounds," Final Report under Contract AF19(604)-3464, 30 October 1959.
3. E. O. Brimm and H. M. Humphreys, *J. Chem. Phys.*, **61**, 829 (1957).
4. F. D. Rossini, D. D. Wagman, W. H. Evans, S. Levine, and I. Jaffe, Natl. Bur. Standards Circ. 500, U. S. Government Printing Office, Washington, D. C. (1950).
5. H. C. Kelly, British Pat. 823,496, Nov. 11, 1959; *C.A.*, **54**, 11416 (1960).
6. N. L. Paddock, *Nature*, **167**, 1070 (1951).
7. J. M. Wilson, *Research*, **10**, 166 (1957).
8. J. M. Wilson, U. S. Pat. 2.888,328, May 26, 1959.
9. V. I. Mikheeva and T. N. Dymova, *Zhur. Neorg. Khim.*, **2**, 2539 (1957).

An Explanation of the Superior Radiation Resistance of P-Type Base Si Solar Cells

Richard V. Babcock

Radiation and Nucleonics Laboratory, Materials Laboratories, Central Laboratories, Westinghouse Electric Corporation, East Pittsburgh, Pennsylvania

ABSTRACT

Recent studies have shown p-type base Si solar cells to be considerably more resistant to 750 kev electron damage than similar n-type base cells. In this paper, the effects of electron flux on solar efficiency, current voltage characteristics, and spectral response are predicted on the assumption that the only significant damage mechanism is decrease in the minority carrier lifetime in the base region. The calculations agree well with the reported electron damage effects, except that a rapid initial loss in efficiency of about 1% observed in n-type base cells is not reproduced. The usual method of measuring solar cell efficiency, comparing the response to a 2800°K tungsten light with that of a calibrated solar cell, was found to overestimate the effect of electron damage on the actual solar efficiency by as much as 200%.

The growing use of solar cells for satellite power sources within the Van Allen radiation fields has generated interest in the charged particle damage rates of solar cells. Recently Mandelkorn *et al.* (1, 2) have developed high efficiency solar cells using p-type Si as a base material. Studies of electron damage rates by Berman (3) have shown these cells to be considerably more resistant to electron damage than a typical commercial n-type base Si solar cell. Proton and electron damage studies by Loferski *et al.* (4) have also shown considerably less radiation damage to the p-type base cells. This paper attempts to show that the observed electron damage effects are essentially the consequence of a single mechanism: decrease in the minority carrier lifetime in the base region. It also provides an estimate of the degree of error introduced by the use of relatively low-temperature (2800°K) light sources to simulate sunlight in testing radiation damage to solar cells. This possibility of error has been pointed out previously, notably by Wysocki, Loferski, and Rappaport (5, 6).

The important damaging effects of electrons with energies exceeding about 200 kev, in both n-type and p-type Si, are decrease in the minority carrier lifetime, decrease in the majority carrier conductivity, decrease in mobility, and possible increase in the surface recombination velocity. In Si solar cells the most serious of these effects will be the decrease in lifetime in the base region (τ_b). This will decrease the minority carrier diffusion length, $L (L^2 = D_b\tau_b$, where D_b is the minority carrier diffusion constant in the base region), which will in turn reduce the long wavelength response of the cell because much of the longer wavelength light is absorbed deep in the base region and the minority carriers produced must diffuse relatively long distances to be collected by the junction. Consequently, a p-type base solar cell (in which the minority carriers in the base are electrons) should be more resistant to electron damage for two reasons; (*a*) the diffusion constant for electrons in Si is approximately three times the diffusion constant for holes, (*b*) the lifetime of minority electrons decreases more slowly with electron irradiation than the lifetime of minority holes.

Damage Mechanism

If the effects of contact resistance[1] and the small electric fields outside the depletion region are neglected, the output of a solar cell is determined by the diffusion of minority carriers into the junction.[2] The diffusion equation can be written, for any region under constant monoenergetic illumination,

$$D\, d^2p/dx^2 - (p - p_o)/\tau = -aN \exp(-ax) \quad [1]$$

where p equals minority carrier concentration (cm^{-3}), $p_o = n_i^2/n_o$ is the equilibrium minority carrier concentration (cm^{-3}), n_i the intrinsic carrier concentration (cm^{-3}), n_o the equilibrium majority carrier concentration (cm^{-3}), D the diffusion constant of the minority carrier ($cm^2\ sec^{-1}$), τ the minority carrier lifetime (sec), a the absorption constant of Si (cm^{-1}), N the incident photon flux ($cm^{-2}\ sec^{-1}$), and x the distance from the surface of light incidence (cm).

Equation [1] is solved separately for the two regions of the cell. In the base region the appropriate boundary conditions, if the base thickness is assumed large compared to L, are

$$p_b \to p_o \quad \text{as} \quad x \to \infty$$

and

$$p_b = p_{jb} \quad \text{at} \quad x = x_j. \quad [2]$$

where $p_{jb} = n_i \exp(-[\Psi - eV]/kT)$ is the minority carrier concentration at the junction (cm^{-3}), Ψ the

[1] The contact resistances of n on p cells are reported by Mandelkorn to be in the range of 0.2 ohm, compared with load resistances, at maximum power, of 20-30 ohms.

[2] The model developed below to describe solar cell output follows a well-known theory originally formulated by Cummerow (7).

energy required to inject a minority carrier through a junction at equilibrium (ev), V the forward bias across the junction (volts), ϵ the electronic charge (ev/v); it is numerically equal to one and will subsequently be omitted, x_j the depth of junction (cm), k Boltzman's constant (ev/°K), T the temperature of Si (°K), and b and s refer to the base and surface regions, respectively.

When $V = 0$, p_{jb} is just the equilibrium carrier concentration p_{ob}, and therefore,

$$p_{ob} = n_i \exp(-\Psi/kT) \quad [3]$$

and

$$p_{jb} = p_{ob} \exp(V/kt) \quad [4]$$

Since $p_{ob} = n_i^2/n_b$, the second boundary condition can be written

$$p_{jb} = \frac{n_i^2}{n_b} \exp(V/kT) \quad [5]$$

In the surface region, since it can be shown that the effect of surface recombination is negligible,[a] the boundary conditions are

$$dp_s/dx = 0 \quad \text{at} \quad x = 0$$

and

$$p_{js} = \frac{n_i^2}{n_s} \exp(V/kT) \quad \text{at} \quad x = x_j. \quad [6]$$

Since the current into the junction from either side is proportional to the gradient of the minority carrier concentration at the junction,

$$I = | qD \, dp/dx |_{x=x_j} \text{ (amp cm}^{-2}\text{)} \quad [7]$$

where q is the electronic charge (coulombs), the spectral collection efficiency can now be calculated. The spectral collection efficiency (i_λ) is the probability that an incident photon of wavelength λ will contribute one electronic charge to the output current. Assuming that each photon absorbed ionizes one e-h pair, i_λ is equal to $I_\lambda/N_\lambda q$. Summing the contributions from both regions gives

$$i_\lambda = \frac{a \exp(-ax_j)}{1 + \exp(-2\alpha_s x_j)} \left[\frac{2a \exp(ax_j - \alpha_s x_j)}{a^2 - \alpha_s^2} - \frac{1}{a - \alpha_s} - \frac{\exp(-2\alpha_s x_j)}{a + \alpha_s} \right] + \frac{a \exp(-ax_j)}{a + \alpha_b} - \frac{n_i^2 [\exp(V/kT) - 1]}{N_\lambda} \left[\frac{D_b \alpha_b}{n_b} + \frac{D_s \alpha_s}{n_s} 2 \sinh(\alpha_s x_j) \right] \quad [8]$$

where $\alpha = (D\tau)^{-1/2}$. The first two terms of Eq. [8] depend on incident wavelength (thru a) and on the bombarding electron flux (thru τ and perhaps D). The last term depends on bombardment flux (thru τ and n) and on incident light intensity.

Quantitative examination of Eq. [8] indicates that the variation of τ_b with electron dosage (ϕ) will dominate the other effects completely. The effect of ϕ on n_b can be estimated from data reported by Wertheim (8). The term in Eq. [8] containing n_s can be neglected completely. Measurements of Hall mobility (μ_H) *vs.* electron bombardment reported by Wertheim (9) show that μ_{Hb} does not change noticeably under bombardment at 273°K to the dosage levels considered here. His measurements also provide an estimate of the change in μ_{Hs}. If only small changes in μ_H are considered, the per cent change in μ_H should equal the per cent change in conductivity mobility and, through the Einstein relation, the per cent change in D. Because of its extremely low initial value, τ_s will be constant under these levels of electron irradiation. Trial calculations based on the estimates described above showed no significant dependence on ϕ other than the contribution of τ_b.

Under short circuit conditions ($V = 0$) the last term in Eq. [8] becomes zero and the short circuit spectral collection efficiency ($i_{\lambda o}$) corresponding to a particular dosage (*i.e.*, a particular τ_b) is determined. In Fig. 1, $i_{\lambda o}$ for a p-type base solar cell similar to those made by Mandelkorn (2) is compared at several dosages with the spectral response observed by Berman. Figure 2 shows the same information for a similar cell formed from n-type Si. Figures 1 and 2 include the effect of reflection from a "clean" Si surface as given by Wolf and Prince (10). In the calculation of $i_{\lambda o}$,

τ_b was taken from a study by Wertheim (8) of the effect of 700 kev electrons on minority carrier lifetime in 5 ohm cm n- and p-type Si with initial minority carrier liftetimes of 12 μsec and 8 μsec, respectively. This data should approximate well the behavior of the base material used by Mandelkorn (≈1 ohm cm, τ_o approximately 10 μsec) in a 750 kev electron flux.

τ_s was assumed to be 10^{-10} sec for electrons and 3 x 10^{-10} sec for holes. These rather low values of τ_s were necessary to reproduce the observed short wave collection characteristics.

D was given by Knight (11) as 38 cm^2 sec^{-1} for electrons and 13 cm^2 sec^{-1} for holes.

a was given as a function of wavelength by Wolf and Prince (12).

x_j was taken as 10^{-4} cm.

Calculation of I-V Characteristics

If Eq. [8] is integrated over some incident photon intensity distribution, N_λ, the total current (I) is obtained as a function of the output voltage (V),

$$I = I_o - | q | n_i^2 [\exp(V/kT) - 1] \left[\frac{D_b \alpha_b}{n_b} + \frac{D_s \alpha_s}{n_s} 2 \sinh(\alpha_s x_j) \right] \text{ (amp cm}^{-2}\text{)} \quad [9]$$

where I_o, the total short circuit current, is obtained by numerical integration of $qN_\lambda i_{\lambda o}$ over all wavelengths. Quantitative examination of Eq. [9] indicates that the surface term can be neglected and that $[\exp(V/kT) - 1]$ can be taken as $\exp(V/kT)$. It is also apparent that only the I_o term depends on the incident photon intensity distribution. The integral I_o was obtained at several electron flux levels for two intensity distributions; vertical sunlight at sea level, as reported by Abbot (13), and a 2800°K black body source, both at a total intensity of 84 mw/cm^2. The short circuit currents under 2800°K light were normalized (at $\phi = 0$) to the value for sunlight, in order to simulate the usual testing procedure. In Fig. 3,

[a] The assumption of a surface recombination velocity of 3 × 10^4 cm/sec led to results which did not differ importantly from those given here for zero surface recombination.

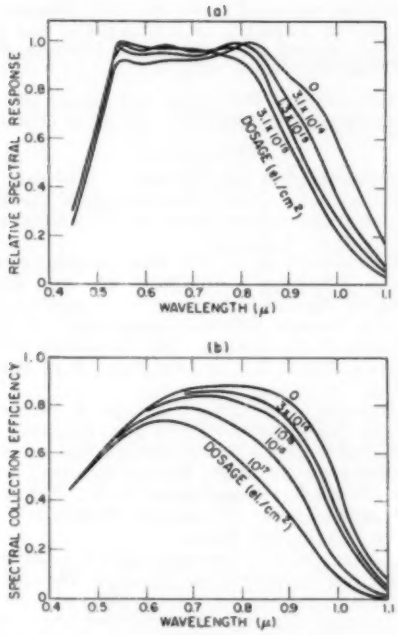

Fig. 1(a). Observed spectral response of a p-type base solar cell [reprinted from ref. (3)]. Fig. 1(b). Calculated spectral collection efficiency as a function of exciting wavelength for a p-type base Si solar cell.

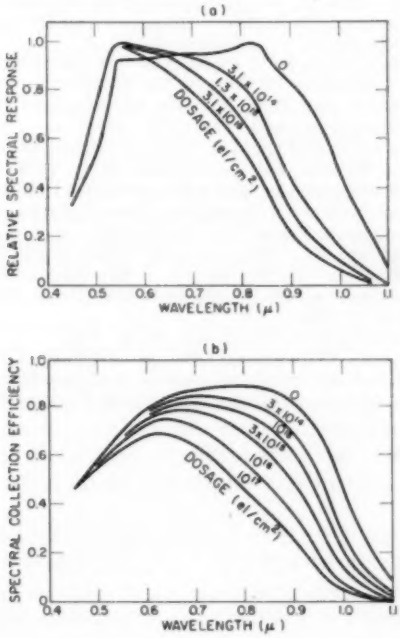

Fig. 2(a). Observed spectral response of a n-type base solar cell [reprinted from ref. (3)]. Fig. 2(b). Calculated spectral collection efficiency as a function of exciting wavelength for a n-type base Si solar cell.

the calculated I-V characteristics of a p on n solar cell, at several dosages, are compared to the I-V curves observed by Berman. In evaluating Eq. [9], n_b was inferred from the initial resistivity of 1 ohm cm to be 0.5 x 10^{16} cm^{-3} for electrons and 1.5 x 10^{16}

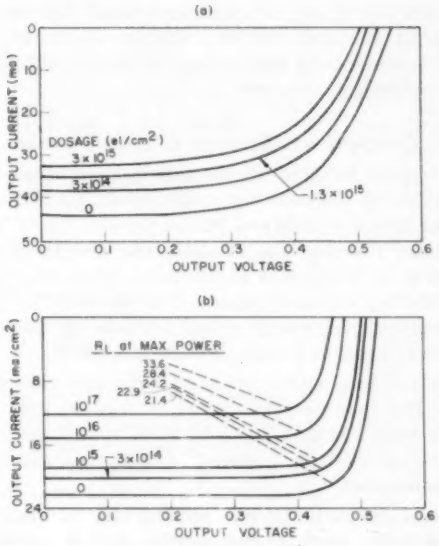

Fig. 3(a). Observed current voltage characteristics, at several electron dosages, of a p-type base Si solar cell [reprinted from ref. (3)]. Fig. 3(b). Calculated current voltage characteristics, at several electron dosages, of a p-type base Si solar cell. The load lines at maximum power are also shown.

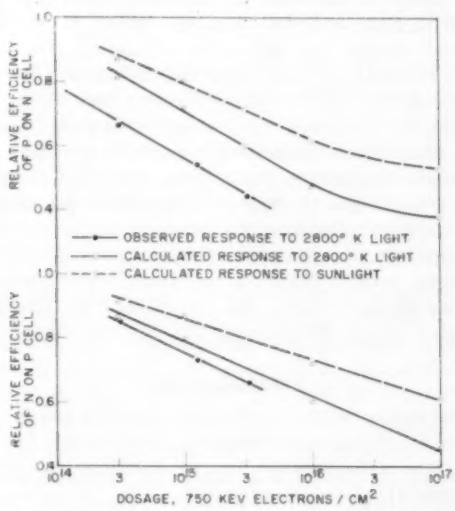
RELATIVE EFFICIENCY OF P ON N CELL
OBSERVED RESPONSE TO 2800° K LIGHT
CALCULATED RESPONSE TO 2800° K LIGHT
CALCULATED RESPONSE TO SUNLIGHT
RELATIVE EFFICIENCY OF N ON P CELL
DOSAGE, 750 KEV ELECTRONS / CM²

Fig. 4. Relative efficiencies of n- and p-type base Si solar cells as functions of electron dosage, for 2800°K light and for sea level, zenith sunlight. The values of observed response to 2800°K light are taken from ref. (3).

cm^{-3} for holes. n_i was assumed to be 10^{10} cm^{-3}. T was assumed to be 273°K.

Maximum Output Efficiency

The solar cell output power is given by the product

$$VI = VI_s - |q| n_i^2 \frac{D_b a_b}{n_b} V \exp(V/kT) \quad [10]$$

Since I_s is independent of V, the function $d(VI)/dV$ can be formed directly and equated to zero to give the output voltage corresponding to maximum power. Evaluating VI at this voltage and dividing by 100 x 84 mw/cm² gives the maximum efficiency. In Fig. 4 the efficiency, for each type of cell, is given

as a function of electron flux, as it would be measured in direct sunlight and in sunlight simulated by a 2800°K black body source. The maximum efficiencies reported by Berman are also shown.

Comparison to Observed Electron Damage

The gross behavior of the spectral response curves observed by Berman was reproduced by the model except that the observed initial (to $\phi = 3 \times 10^{14}$ electrons cm^{-2}) decrease in the long wavelength response of the p on n cell was about three times as great as indicated by the calculations. This discrepancy might be explained by a high initial lifetime (greater than 30 μsec), but such a high lifetime is unlikely.

The I-V characteristics are reproduced reasonably well. The decrease in output voltage at maximum power with electron flux which Berman appeared to observe is clearly demonstrated in the calculated characteristics.

The calculated rate of decrease in maximum efficiency with electron flux under 2800°K excitation agrees quite well with the observed data. However, the rapid initial drop in the observed efficiency of the p on n cell is not reproduced.

One interesting result indicated by Fig. 4 is that the rates of decrease in efficiency observed using 2800°K light are considerably higher than the expected change in true solar efficiency. For either type of cell, the flux required to reduce the solar efficiency by 25% is about three times as great as would be indicated by testing with 2800°K light. The use of low-temperature black body radiation to simulate sunlight in comparing solar cell responses is known to lead to error if the spectral responses are not identical. Because the primary electron damage mechanism is a decrease in charge carrier diffusion lengths, which destroys the long wavelength response preferentially, the use of 2800°K light gives a high estimate for the radiation damage rates.

Acknowledgment

The author wishes to thank R. Longini and H. John of the Westinghouse Research Laboratories for contributing substantially to the development of the hypothesis.

Manuscript received April 28, 1961; revised manuscript received August 7, 1961. This paper was prepared for delivery before the Indianapolis Meeting, April 30-May 3, 1961.

Any discussion of this paper will appear in a Discussion Section to be published in the June 1962 JOURNAL.

REFERENCES

1. J. Mandelkorn *et al.*, "Comparison of p-n and n-p Silicon Solar Cells," Proceedings of the 14th Annual Signal Corps Power Sources Conference, p. 42.
2. J. Mandelkorn *et al.*, "A New Radiation-Resistant High-Efficiency Solar Cell," delivered at a meeting on Radiation Damage to Semiconductors by High Energy Protons, sponsored by N.A.S.A., Wash., D. C., Oct. 20, 1960. Available from U. S. Army Signal Res. & Dev. Lab., Fort Monmouth, N. J.
3. P. Berman, "Radiation Damage in Silicon Solar Cells Using 750 kev and 2 Mev Electrons," delivered at a meeting on Radiation Damage to Semiconductors by High Energy Protons, sponsored by N.A.S.A., Washington, D. C., Oct. 20, 1960. Available from Transitron Electronic Co., Res. Dept., Wakefield, Mass.
4. J. Loferski *et al.*, "Observations of a Difference in Electron Bombardment Damage Thresholds in n and p Type Silicon," delivered at a meeting on Radiation Damage to Semiconductors by High Energy Protons, sponsored by N.A.S.A., Washington, D. C., Oct. 20, 1960. Available from RCA Laboratories, Princeton, N. J.
5. J. Wysocki, J. Loferski, and P. Rappaport, "Research on Photovoltaic Converters," Proceeding of the 14th Annual Power Sources Conference, May 17-19, 1960, p. 35. Available from Power Sources Division, U. S. Army Research and Development Laboratory, Fort Monmouth, N. J.
6. P. Rappaport, *RCA Review*, **20**, 373 (Sept. 1959).
7. R. Cummerow, *Phys. Rev.*, **95**, 16 (1954).
8. G. Wertheim, *ibid.*, **105**, 1730 (1957).
9. G. Wertheim, *ibid.*, **110**, 1272 (1958).
10. M. Wolf and M. Prince, "New Developments in Silicon Photovoltaic Devices and their Application to Electronics," in "Solid State Physics in Electronics and Telecommunications," Vol. 2, Part 2, p. 1186, Academic Press, New York (1960).
11. G. Knight, Jr., "Measurement of Semiconductor Parameters," in "Handbook of Semiconductor Electronics," p. 20-10, McGraw Hill Book Co., New York (1956).
12. M. Wolf and M. Prince, *op. cit.*, p. 1188.
13. C. Abbot, "The Sun as a Source of Continuous Radiation," in "Measurement of Radiant Energy," p. 76, McGraw Hill Book Co., New York (1937).

High-Temperature Oxidation and Vacuum Dissociation Studies on the A{111} and B{$\bar{1}\bar{1}\bar{1}$} Surfaces of Gallium Arsenide

Donald P. Miller, James G. Harper, and Thomas R. Perry

Texas Instruments Incorporated, Dallas, Texas

ABSTRACT

Gatos and Lavine (8) have proposed a model to explain the difference in etching behavior of the A {111} and B {$\bar{1}\bar{1}\bar{1}$} surfaces of gallium arsenide, indium antimonide, and related A^{III}-B^{V} compounds. The model associates unshared electrons to the B surface atoms and not to the A surface atoms. High-temperature oxidation of gallium arsenide has been undertaken to study directly the oxidation of both types of surfaces in order to test the proposed model. Experimental results verify the model. The B surface reacts with oxygen at a higher rate. Vacuum evaporation experiments on gallium arsenide A and B surfaces indicate that atoms from the B surface dissociate at a greater rate than from the A surface below 770°C. Above 800°C, the dissociation rates are equal, indicating a change of mechanism to "molecular" evaporation. The high-temperature (>800°C) heat of dissociation of gallium arsenide has been determined as 112 kcal/mole.

In recent years several investigators have reported on the polarity effects along the <111> direction in InSb and GaAs. These A^{III}-B^{V} compounds (in addition to GaSb, InAs, InP, and AlSb) are of interest for their semiconductor properties. During the study of these compounds it was noted that the parallel {111} and {$\bar{1}\bar{1}\bar{1}$} planes do not exhibit similar surface properties. It is the purpose of this paper to demonstrate further the polarity effect and to present evidence obtained in two new ways.

Of primary concern in the investigations to date has been the effect of various etching media on the {111} (to be designated A{111}) and the {$\bar{1}\bar{1}\bar{1}$} (to be designated B{$\bar{1}\bar{1}\bar{1}$}). It has been shown (1-5) that the surfaces behave differently in oxidizing etching media. These observations led to a group of investigations (6-9) concerning the nature of the surface. It was found, by x-ray methods (10), that the A{111} surface terminated predominantly in Group III atoms while the B{$\bar{1}\bar{1}\bar{1}$} surface terminated in Group V atoms.

Several significant features of the etching process were revealed by Gatos and Lavine (5, 8). They showed that the B{$\bar{1}\bar{1}\bar{1}$} surface is more reactive in oxidizing etch media, *i.e.*, dissolves at a faster rate. They also noted a significant electrode potential difference on InSb using an A{111} surface as one electrode and a B{$\bar{1}\bar{1}\bar{1}$} surface as the other. By properly adjusting the temperature and the etching solution, the A surface could be made to dissolve at a rate comparable to the B{$\bar{1}\bar{1}\bar{1}$} surface.

The effect of the polarity is not restricted to the etching behavior of the surfaces. Ellis (10) has noted that GaAs crystals tend to bound themselves with B(111) planes and Cronin of our laboratories has noted that the external morphology of GaAs crystals grown in the <111> or <$\bar{1}\bar{1}\bar{1}$> direction depends on in which surface the seed terminates.

Gatos and Lavine (8) have proposed a model to account for these polarity effects. The GaAs and InSb crystal lattices are cubic noncentrosymmetric and belong to the space group $F\bar{4}3m$ (T_d^2). Viewed along the [11$\bar{2}$] direction we see closely spaced double layers of gallium atoms and arsenic atoms. The atoms are tetrahedrally bonded, three bonds to atoms within the double layer and one bond to an atom in an adjacent double layer. A slice cut to expose both (111) and ($\bar{1}\bar{1}\bar{1}$) planes will occur between the double layers, leaving gallium or indium atoms on one surface and arsenic or antimony on the other. Gatos and Lavine argue that the surface atoms in both cases are triply bonded to the rest of the crystal, but the B{$\bar{1}\bar{1}\bar{1}$} surface atoms acquire both electrons used in forming the bond from one double layer to the next. Surface A{111} atoms are less reactive because they are normally trivalent, while the surface B{$\bar{1}\bar{1}\bar{1}$} atoms have a normal valency of five. This model has been used successfully to explain the effect of etchants on the two surfaces. It has been suggested that this polarity effect will lead to pronounced differences in surface electronic phenomena such as surface conductivity, photoconductivity, and surface recombination velocity.

The concept of directional polarity in these compounds leads to the expectation that other properties of these compounds which are surface sensitive will be different depending on the surface plane. Two of these properties of interest are the oxidation

Fig. 1. A{111} and B{$\overline{111}$} etched surfaces of gallium arsenide. Magnification 825X before reduction for publication.

of the A{111} and B{$\overline{111}$} for GaAs and the rate of weight loss of arsenic from GaAs heated in a vacuum. It was believed that these properties would be surface sensitive and would give further insight into the properties of these surfaces.

Experimental Equipment and Procedures

The study of the A{111} and B{$\overline{111}$} surface properties was conducted using two different instruments. The first was a differential thermal analysis (DTA) apparatus. The usual procedure of DTA is to record the endothermic or exothermic reaction of an unknown material against that of a nonreacting material. This is accomplished by measuring the temperature difference between thermocouples placed in contact with the sample material and the standard material, usually alumina. GaAs samples were cut into 4 mm diameter x 3 mm height cylinders with one face being the A{111} and the other the B{$\overline{111}$}. The type of the surface was determined by etching the faces of the cylinders (Fig. 1). The polarity of GaAs crystals has been related by x-ray diffraction techniques (11) to the surface etch condition.

Two cylinders were positioned so that only A or only B surfaces touch the sample thermocouple. The standard was Al_2O_3 powder.

The recording potentiometers which monitored the difference potential and the potential of the thermocouple in the alumina standard had a sensitivity of 0.03 μv and 50 μv, respectively.

In order to amplify the differences, other experiments were run with the A surfaces against the standard thermocouple and B surfaces against the sample thermocouple.

The second group of experiments employed a thermogravimetric vacuum balance. The system consists of a recording vacuum balance, an electric furnace with controls, and a vacuum unit. In order to determine the weight loss from the two surfaces as a function of time and temperature it was necessary to cut tetrahedra. That tetrahedra can be obtained with all A faces or all B faces can be easily shown. Figure 2 shows parts of two gallium arsenide unit cells in which are constructed two tetrahedra. One tetrahedron contains only type III atoms in {111} tetrahedral planes, the other only type V atoms in

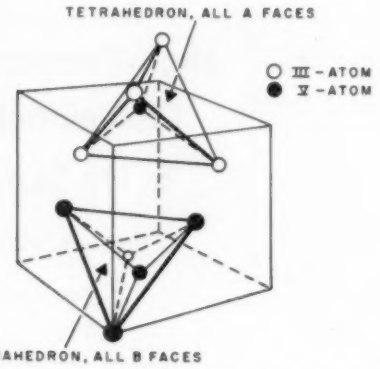

Fig. 2. A, Surfaced tetrahedron and B, surfaced tetrahedron

{$\overline{111}$} planes. Since a real crystal is the unit cell reproduced manifold in three dimensions, samples cut parallel to these surfaces will exhibit the same surface characteristics.

Several tetrahedra, either A or B type as desired, were placed in a tantalum weighing pan connected to the balance. The temperature and weight of the sample were recorded automatically. The sensitivity of the balance was 30 μg, and the recording potentiometer had a sensitivity of 1.5°C. The recorder chart displayed both the weight and the temperature. The temperature was raised until a weight loss rate could be established. Then a new and higher temperature was chosen. In this manner one sample could be used for several temperatures. One problem was the presence of free gallium on the evaporating surface after some arsenic loss had occurred. Visual observation indicated that some gallium remained as a thin layer on the faces. Further accumulation resulted in flow of the gallium toward the base of the tetrahedron. The base of the tetrahedron was soon surrounded by gallium and was not considered to be an active face in the weight loss calculations. The active surface area can be calculated from the weight of the sample by the following equations.

$$\text{Active area of sample} = \tfrac{3}{4}\,(1.732)\,l^2$$

$$\text{Volume of sample} = 0.118\,l^3 = W,$$

where l is the length of tetrahedron edge

$$\text{Active area of the sample} = 1.76\,(W)^{2/3}\ \text{cm}^2$$

Continuous monitoring of the tetrahedron weight yielded the arsenic weight loss, the gallium liquid weight, and the remaining tetrahedron weight. From the remaining tetrahedron weight the active area was determined at any time. The active area decreased by about 16% during the experiment in the extreme case.

Experimental Results

Oxidation of GaAs A and B surfaces (DTA).—Some of the data from the DTA is plotted in Fig. 3. This experiment is the A and the B faces run against Al_2O_3 powder. It should be noted here that no absolute rates may be obtained from these data. The recording thermocouple reads the temperature rise of the specified surface. The temperature rise of this system is a function of the oxidation of the particular face and the heat transfer away from the sample. If

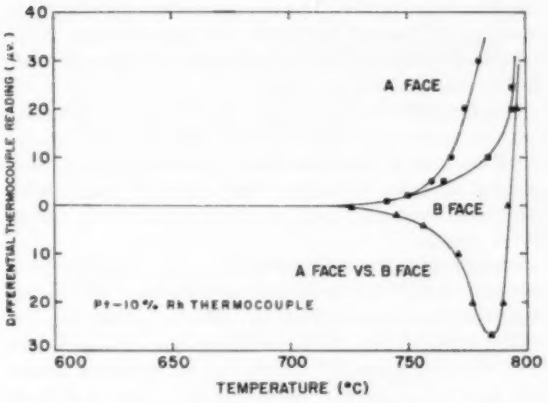

Fig. 3. Measurements of high-temperature oxidation of A and B faces of gallium arsenide.

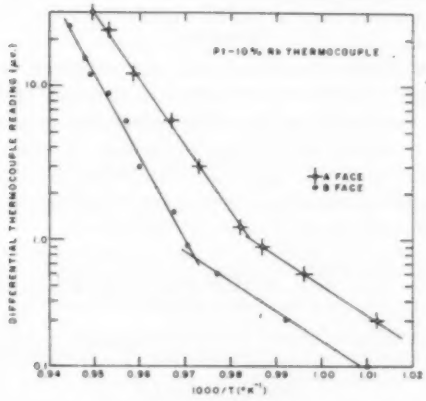

Fig. 4. High-temperature oxidation of gallium arsenide A and B surfaces.

the experiments are run carefully, however, it is possible to get an indication of the relative rates involved. Two things should be noted here. The first is that the A surface begins to react about 10°C below the B surface. The second is that the B surface starts to react later, but reacts at a faster rate after initiation.

Several assumptions must be made before the data can be interpreted as indicating relative reaction rates. First, the rate of heat leakage away from the thermocouple regions is very much smaller than the rate of heat generation. Second, oxygen is continuously available for reaction. And third, the rate of oxidation is a first order reaction. Under these assumptions the data may be displayed in the form shown in Fig. 3. The assumptions have governed the choice of ordinate and abscissa scales. The small scatter of the experimental data about the assumed exponential behavior shows the assumptions are correct. The oxidation rates of the A and B surfaces are directly related to the slopes of the curves of Fig. 4. The rates of the A and B surfaces are initially the same, but the A surface begins reacting before the B surface. The oxidation rates undergo abrupt changes after which the rate of the B surface is the larger.

Evaporation of arsenic from GaAs *A and B surfaces.*—Only these portions of the record of weight

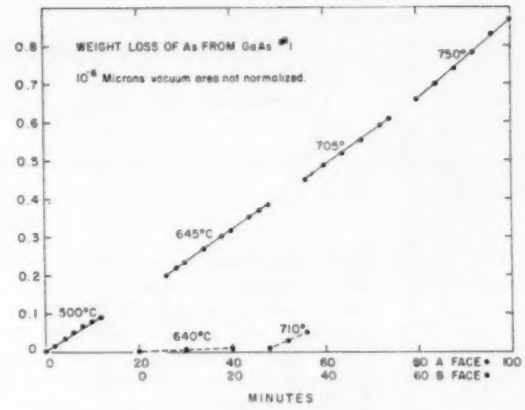

Fig. 5. Measurements of high-temperature vacuum evaporation of gallium arsenide.

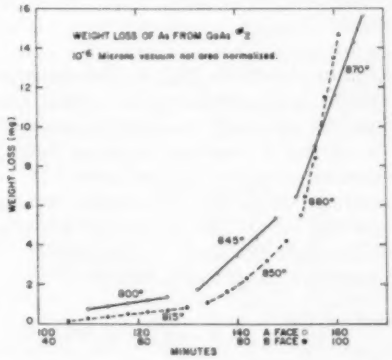

Fig. 6. Measurements of high-temperature vacuum evaporation of gallium arsenide.

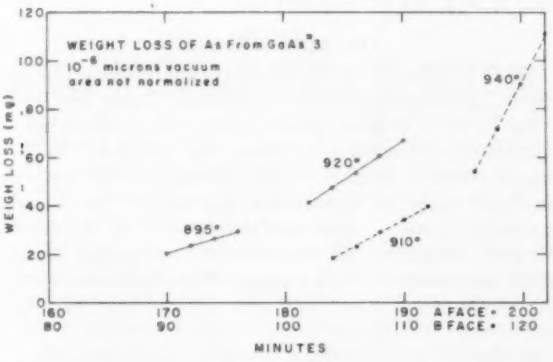

Fig. 7. Measurement of high-temperature vacuum evaporation of gallium arsenide.

vs. time were retained which were characteristic of constant temperature evaporation. The segments are shown in Fig. 5, 6, and 7. From these segments the rate of arsenic lost per unit time was determined for each sample at each temperature. The total weight loss up to each interval was used to determine the remaining surface area. The rate of arsenic weight loss was then normalized to unit area. Under the assumptions that the evaporation rate was directly proportional to the number of surface atoms and that a constant heat of dissociation was involved at any temperature, the normalized weight loss could

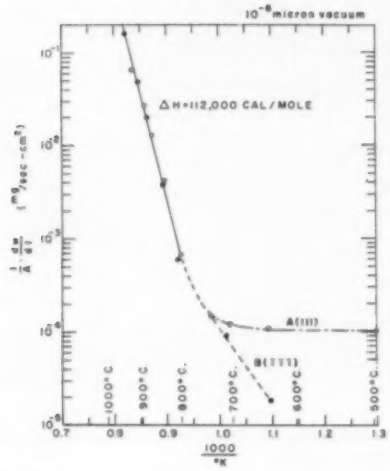

Fig. 8. Weight loss rate of GaAs vs. 1/T for A{111} and B{$\bar{1}\bar{1}\bar{1}$} surfaces.

be displayed as shown in Fig. 8. The experimental points exhibit very small scatter about the lines representing the assumed dissociation behavior. The dissociation of the A surface initiates first. The B surface dissociation rate is higher below 770°-800°C. Above this temperature the dissociation rates of both surfaces are the same. The Arrhenius equation can be used to calculate the heat of dissociation of GaAs in the temperature range above 800°C.

$$\frac{1}{A}\left(\frac{dW}{dt}\right) = K\exp(-\Delta H/RT)$$

At 920°C (1193°K), $W = 25.8$ mg for $t = 960$ sec and $A = 0.805$ cm^2, which yields $H = 112$ kcal mole and $K = 11.4 \times 10^{16}$ mg/cm^2 sec.

Discussion of Results

The results of the oxidation experiments are in close agreement with the findings of Gatos and Lavine in their etching experiments. The initial (low-temperature) oxidation rates are believed to be equal because an oxide layer already existed on the surfaces when the experiment was begun. The initial oxidation rate of both surfaces would be diffusion limited. However, on fracture of the surface oxide film, the reaction was no longer diffusion limited but reaction rate limited. The B atoms were clearly more reactive indicating they had, on the average, more unshared electrons and were more available for oxidation than did the A atoms.

The B and A surfaces also clearly exhibit different rate of dissociation below 770°-800°C. The rate of the B surface is high compared to the A surface, suggesting that the surface energy of the B atoms, with their unshared electrons, is much higher than that of the A atoms.

A striking feature of the evaporation experiment is that above 800°C, the evaporation rates of the A and B surfaces are equal. This strongly suggests that the entire mechanism of dissociation has changed and that at these temperatures double or multiple layers (or layered clusters) of atoms are removed from both surfaces. This is molecular dissociation and does not entail unshared electrons as does the low-temperature dissociation.

Summary

Experiments involving high-temperature oxidation and vacuum dissociation of gallium arsenide verify the model of unshared electrons on B{111} atoms proposed by Gatos and Lavine. At temperatures above 800°C, vacuum dissociation occurs by a molecular mechanism, and A{111} and B{$\bar{1}\bar{1}\bar{1}$} surface rates are equal.

Manuscript received June 12, 1961; revised manuscript received Aug. 18, 1961. This paper was prepared for delivery before the Houston Meeting, Oct. 9-13, 1960.

Any discussion of this paper will appear in a Discussion Section to be published in the June 1962 JOURNAL.

REFERENCES

1. H. A. Schell, *Z. Metallkunde*, **48**, 158 (1957).
2. J. W. Allen, *Phil. Mag.*, **2**, 1475 (1957).
3. J. D. Venables and R. M. Broudy, *J. Appl. Phy.*, **29**, 1025 (1958).
4. R. E. Maringer, *ibid.*, **29**, 1261 (1958).
5. H. C. Gatos and M. C. Lavine, *ibid.*, **31**, 743 (1961).
6. M. C. Lavine, A. J. Rosenberg, and H. C. Gatos, *ibid.*, **29**, 1131 (1958).
7. E. P. Warekois and P. H. Metzger, *ibid.*, **30**, 960 (1959).
8. H. C. Gatos and M. C. Lavine, *This Journal*, **107**, 427 (1960).
9. E. P. Warekois, M. C. Lavine, and H. C. Gatos, *J. Appl. Phy.*, **31**, 1302 (1960).
10. S. G. Ellis, *ibid.*, **30**, 947 (1959).
11. J. G. White and W. C. Roth, *ibid.*, **30**, 946 (1959).

Vapor Growth of Gallium Arsenide

R. L. Newman[1] and N. Goldsmith

Semiconductor and Materials Division, Radio Corporation of America, Somerville, New Jersey

ABSTRACT

Epitaxial layers of gallium arsenide, on a gallium arsenide substrate, have been grown from the vapor. An open system is used, with a chloride as the transporting agent. The gallium arsenide is transported from a hot region (*ca.* 1000°C) to a cooler region (*ca.* 900°C). Layers up to 6-7 mils in thickness have been grown. The interfaces between substrate and growth are quite good. Substrate orientation appears to be critical, controlling both amount of growth and crystalline perfection of the deposit. Some electrical properties of the junctions formed are discussed.

Recently, vapor growth of elemental semiconductors has become a useful technique for producing thin films of controlled electrical characteristics (1, 2). These systems usually have used disproportionation of a volatile halide in a sealed system

$$2\,GeI_{2(g)} = GeI_{4(g)} + Ge$$

These have produced both germanium and silicon layers of characteristics satisfactory for devices. Binary semiconductors can be grown from the vapor, if both elements can be placed in the vapor in some form, either in a volatile compound or as vaporized element. Prior (3) grew crystals of PbSe by this method in a sealed system.

Lee (4) reported vapor transport of metals by their volatile chlorides as

$$M + x\,Cl\ (\text{in some form}) = MCl_{x(g)}$$

Antell and Effer (5) have grown III-V compounds from the vapor by reactions of the type

$$3\,InCl_{(g)} + \tfrac{1}{2}\,As_{4(g)} = InCl_{3(g)} + 2\,InAs$$

It was decided to use the corresponding reaction for gallium arsenide modified to use an open system for convenience. Since preliminary experiments in a closed system showed that many sources of chloride would work, HCl seemed a satisfactory means of producing the sub-halide. Other systems also were tried using other forms of chlorides including $AsCl_3$, $GaCl_2$, and $GaCl_3$.

Materials and Apparatus

The reaction vessel is a quartz tube, placed in a gradient furnace. Hydrogen and helium are admitted to the tube through a liquid nitrogen trap and a flowmeter. Hydrogen chloride is admitted through a dry ice trap and a flowmeter. Except for stainless steel lines used to deliver the gases from the tanks, the system is all glass.

The reaction tube is loaded with arsenic, crushed gallium arsenide, used as feed material, and gallium arsenide seeds. The arsenic and feed material are packed in the tube with quartz wool. The arsenic is American Smelting and Refining arsenic, 99.999% pure, and used without further treatment. The feed material is crushed Bridgman crystals.

The seeds are oriented wafers of gallium arsenide, lapped and polished. Except for specific experiments involving surface treatment, they received no further preparation. The seeds are either laid flat or propped vertically.

Procedure

The materials are placed in the reaction tube and the system flushed, then brought to temperature, under helium. During the run, the furnace is held at temperature under hydrogen for a half hour before admitting the hydrogen chloride. This period serves to equilibrate the system. After the run, the HCl is turned off and the system cooled under hydrogen. Gas flows of a few cc/min for HCl and a few hundred cc/min for H_2 are used.

Results

Effect of surface preparation.—The physical appearance of the interface between the substrate and the regrowth is greatly dependent on the surface treatment used. The principal cause of poor interfaces seems to be the presence of an oxide film on the surface. Various surface treatments were tried with results listed in Table I.

The effect of orientation on the presence of oxide films in InSb was reported by Rosenberg and Lavine (6). This effect may explain in part the apparent difference between the (111) and (110) orientations, if the number of voids is dependent on the amount of oxide film present. The (111) wafers in the bottom line were etched briefly to undercut the supposed oxide film. Figures 1 and 2 show typical growths and interfaces.

Effect of substrate orientation.—The crystallinity of the deposit is slightly dependent on the substrate orientation. In general, the <111> appears to be the preferred direction, although heavy growth is noted along the higher index planes. In the case of (111) material deposited on (111) wafers, there is twinning corresponding to 180° rotation about the <111> direction at the interface. A substantial difference is observed in the growth on the (111) and ($\bar{1}\bar{1}\bar{1}$)

[1] Present address: Department of Chemistry, The Pennsylvania State University, University Park, Pennsylvania.

Table I. Surface treatments

Surface treatment	Interface	Voids at interface	Electrical junction
Lapped (Fig. 1a)	Very irregular	Considerable number present	Very leaky
Lapped and etched (reducing etch)	Irregular	Few present	Leaky
Lapped and etched (oxidizing etch)	Very irregular	Considerable number present	Very leaky
Lapped, rinsed in distilled water	Irregular	Large number present	Leaky-very leaky
Lapped and polished (111) orientation	Smooth	Few present	Sharp breakdown slightly leaky
Lapped and polished (110) orientation (Fig. 1b)	Smooth	None present	Good-very good
Lapped and polished (111) orientation vertical mount, etched in HCl gas (Fig. 1c)	Smooth	None present	Good-very good

Very sharp breakdown

planes. The growth is much heavier on surfaces terminating in gallium atoms, when both surfaces are exposed to the gas stream (Fig. 1c). The free growth direction is determined from the orientation of dendrites growing from nucleation sites on the quartz wall, and is along the <111> axis.

Other parameters.—The gallium arsenide has been deposited at temperatures as low as 600°C, but the crystallinity of the deposit seems to depend on temperatures and other factors, such as system geometry. Good growth has been obtained at temperatures between 750°-900°, using a feed temperature of about 1000° and an arsenic control temperature of 350°-450°. At larger gradients the deposit is quite polycrystalline and the growth quite rough. Dendrites also are noted under these conditions.

The hydrogen chloride concentration influences the deposition rate, and hence the crystallinity of the

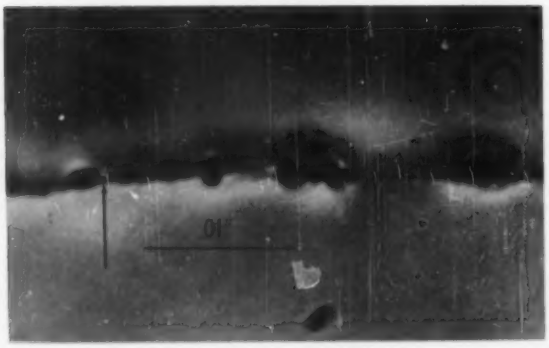

Fig. 1a. Interface, unpolished substrate. Arrows indicate interfaces.

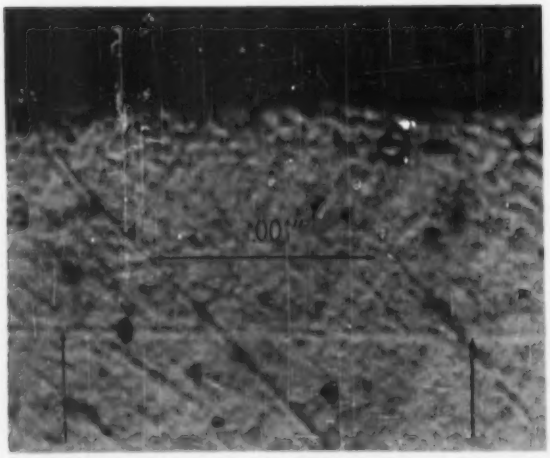

Fig. 1b. Interface, polished (110) substrate. Arrows indicate interfaces.

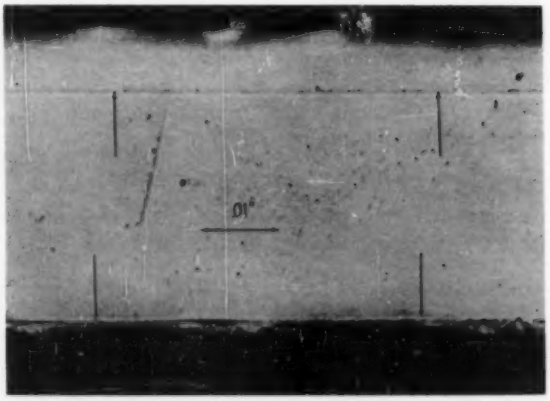

Fig. 1c. Interface, vertical (111) substrate. Note heavy growth on gallium face. Arrows indicate interfaces.

Fig. 2a. Surface, dendritic growth

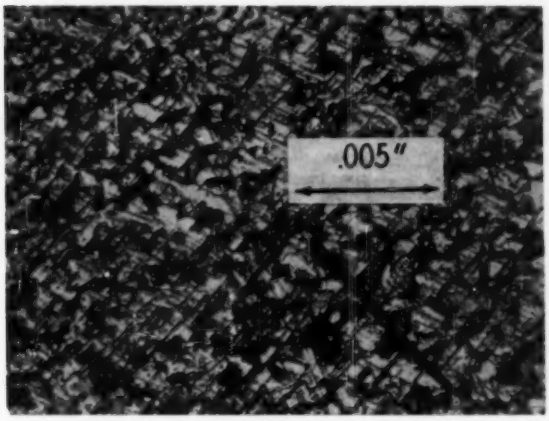

Fig. 2b. Surface, growth on (110) substrate

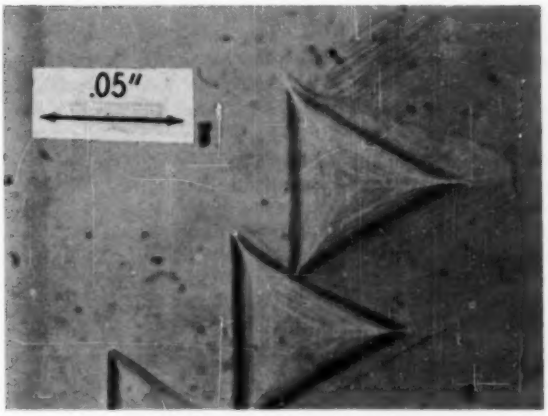

Fig. 2c. Surface, growth on (111) substrate

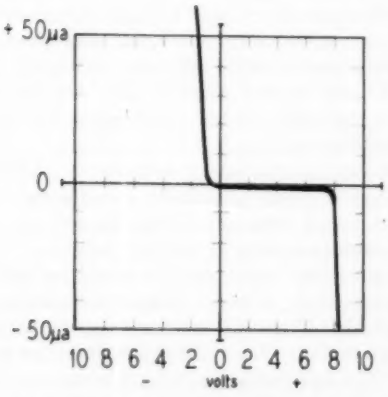

Fig. 3. Current-voltage trace of epitaxially grown diode

deposit. The lower this rate, the better the deposit becomes, although a compromise must be made in order to maintain reasonable running times. At high concentrations most of the gallium arsenide deposits on the tube walls. Even at best, only about half of the gallium arsenide transported deposits on the wafers. No attempt was made to vary the hydrogen concentration with an inert gas.

With a hydrogen chloride flow of 1 or 2 cc/min and a hydrogen flow of a few hundred cc/min, about 1.5 mils of regrowth is obtained on a (111) substrate

Table II. Properties of layers

Substrate type	Carrier conc.	Doping material	Breakdown, diode, v	Growth type	Carrier conc. (est.)	Resistivity of layer
n	8.66×10^{16}	None	10	p	$\sim10^{17}$	6Ω cm
n	1.48×10^{17}	None	—	p	$\sim10^{16}$	5Ω cm
p	4.6×10^{18}	Te	8*	n	$\sim5\times10^{18}$	0.0012Ω cm
p	1.6×10^{19}	Sn	12	n	$\sim5\times10^{17}$	0.0045Ω cm
p	3.51×10^{17}	None**	40	n	$\sim10^{17}$†	

* See Fig. 3.
** All quartz system.
† Estimated from point contact breakdown.

in 1 hr. Thicker deposits may be obtained by increasing the flow rate, time, or temperature gradient. The thickest growth noted was 7.2 mils at a deposition temperature of 810°C. This deposit was rather uneven.

Electrical properties.—Measurements have been made on only a small fraction of the wafers. Using low carrier concentration feed material, the electrical type of the regrown material cannot be predicted. Growth in a closed system, with particular care taken to insure cleanliness, usually results in p-type material (7).

Experiments using tellurium and tin doping have been carried out. N-type regrowths with carrier concentrations up to $\sim10^{18}$/cc have been produced using these dopes. The doping material is placed with the arsenic and is transported as either tellurium or tin chloride. Additional doping experiments are being performed at present.

These materials are evaluated by fabricating mesa diodes, using nickel contacts. Four-point probe measurements also are made on these layers, from which estimates of the resistivity (and the carrier concentration) can be made. On some layers, carrier concentrations are estimated from point contact breakdown. Thermal probe readings are made on all samples. Table II lists properties of some typical layers.

The diodes made from doped n-type layers on p-type substrates have electrical characteristics comparable with commercial silicon zener diodes (see Fig. 3). Several diodes (undoped growth, both n- and p-type) have been made with breakdowns in the 40-50 v range, but these cannot be duplicated at will. Work is continuing on the study of the electrical properties.

Conclusions

The gallium arsenide will deposit on a clean gallium arsenide substrate. Although the growth is not epitaxial on all orientations, the substrate orientation has some effect on the resultant layer. The effect of temperature and gas rates are still under study.

These layers can be made either n- or p-type, but further control is not yet possible. Although chlorine might be expected to be incorporated in the lattice (8), there is no evidence for its electrical activity.

Acknowledgment

The authors would like to express their appreciation to J. Gilbert and P. Hoss for orientation of the gallium arsenide, and to J. Mydosh and P. Kuz-

netzoff for their assistance with some of the electrical measurements. They also would like to thank L. J. Vieland and J. A. Amick for their helpful discussions.

This work was performed under the sponsorship of the Electronic Technology Laboratory, Wright Air Development Division, Air Research and Development Command, United States Air Force.

Manuscript received May 11, 1961; revised manuscript received Aug. 16, 1961. This paper was prepared for delivery before the Indianapolis Meeting, April 30-May 3, 1961.

Any discussion of this paper will appear in a Discussion Section to be published in the June 1962 JOURNAL.

REFERENCES

1. J. Marinace, *IBM J. Res.*, **4**, 248 (1960).
2. E. S. Wajda, B. N. Kippenham, and W. H. White, *ibid.*, **4**, 288 (1960).
3. A. C. Prior, *This Journal*, **108**, 82 (1961).
4. M. F. Lee, *J. Phys. Chem.*, **62**, 877 (1958).
5. G. Antell and D. Effer, *This Journal*, **107**, 252 (1960).
6. A. J. Rosenberg and M. C. Lavine, *J. Phys. Chem.*, **64**, 1135 (1960).
7. L. J. Vieland, Private communication (1960).
8. G. Antell, *J. Appl. Phys.*, **31**, 1686 (1960).

The Contamination of Semiconductor Surfaces

1. Metal Ions from Acid Solution on the Intermetallics, GaAs and InSb

Graydon B. Larrabee

Central Research Laboratories, Texas Instruments Incorporated, Dallas, Texas

ABSTRACT

A mechanism for the deposition of metallic ions from solution on the III-V intermetallics gallium arsenide and indium antimonide is presented. Those ions whose metal-metal ion couple lies below the electrochemical potential of the semiconductor will be physically adsorbed. This adsorption is a reversible process, following a Freundlich isotherm, and requires fairly high concentrations of impurity in solution to effect serious contamination. Those ions whose metal-metal ion couple lies above the electrochemical potential of the semiconductor will be electrochemically deposited on the surface. This deposition is irreversible and serious surface contamination results from fractional ppm concentrations of these metal ions in solution. The effect of both these types of impurity deposition on semiconductor devices is discussed.

Surface contamination of semiconductors sharply controls the electrical properties of both the surface and the bulk properties of the semiconductor. This surface contamination may take the form of oxides, water, adsorbed or chemisorbed gases, organic compounds, anions, cations, or a combination of any of these. The direct effect of most of these contaminants is not understood. Most of the research effort to the present time has been directed toward the physical (1, 2) and chemical (3) adsorption of gases in very high vacuum systems on "clean" silicon and germanium surfaces.

Synorov (4) in a study of the surface properties of A^{III} B^{V} intermetallic semiconductors confirmed the presence of surface acceptor levels and surface conduction in these compounds. Using fine films of AlSb, InSb, and GaSb, Synorov demonstrated a strong analogy with the surface properties of germanium. Many (5) feels that all the concepts and models related to the surface of silicon and germanium can be extended to other semiconductors with only minor modifications. If this is the case, one can discuss the effects of surface contamination on III-V intermetallics in terms of surface states. These surface states tend to bind electrons at the surface so these electrons cannot participate in lateral conduction. If the states are located at the semiconductor surface, with resultant good electrical contact, then they are referred to as fast states since any change in the state density will be rapidly reflected in the bulk (*ca.* 1 μsec). The slow states are thought to be on or in the oxide layer on the semiconductor, and any change in the slow states is reflected only slowly in the bulk (*ca.* 10^{-3} sec-several hours). The density of these states is believed to be $\sim 10^{13}$/cm^2 fast states and $> 10^{12}$/cm^2 slow states.

Atalla *et al.* (6) point out that 1/10,000th of a monolayer of ionic impurities is sufficient to invert the surface of 1 ohm-cm silicon. Therefore any study of the contamination of semiconductor surfaces involves impurity levels in the order of 10^{11}/cm^2. A microgram of most metal impurities contains in the order of 10^{15} atoms which means any surface studies will require that 10^{-4} μg/cm^2 impurities can be determined. The one technique which uniquely fills these requirements is radioactive tracer techniques.

Experimental

Procedures.—In this study of the contamination of intermetallic surfaces with metal ions from acid solutions, all radioactive tracers used were gamma emitters. The use of gamma emitters greatly facilitated the counting techniques and made it possible to use crushed samples to increase the surface area studied.

A Baird Atomic single channel spectrometer, Model 810, was used throughout these studies. The spectrometer was equipped with a 1½ x 2 in. sodium

iodide well crystal. The system had a counting efficiency of 35% for the 0.661 Mev gamma from Cs^{137}.

The two intermetallic semiconductors used were indium antimonide and gallium arsenide grown in the (111) plane and of the highest purity available at the time of the investigation. The intermetallics were crushed, carefully sieved, and the portion passing a fifty-mesh sieve but retained on a one hundred mesh sieve was used throughout these studies. The surface area was calculated (assuming a roughness factor of one) for this crushed size and found to be 63.4 cm^2/g for gallium arsenide and 58.7 cm^2/g for indium antimonide.

A known weight of the crushed intermetallic was equilibrated with the "tagged" metal ion contaminate for 10 min in 1N nitric acid. The solution was then decanted and the intermetallic washed once with 1N nitric acid, then counted. This washing and counting procedure was continued until the results were conclusive, which was usually after the third wash. In some cases, washing was continued for as many as eight times, but the conclusions after this wash were no more valid than after the third wash. As far as could be determined, the equilibration time, (from 1 min to 20 hr) had no effect on the amount of adsorption. This indicates that equilibration was set up very rapidly, certainly less than 1 min.

Experimental Results

Monovalent Ions

Sodium ion.—Using radioactive Na^{22}, the surface contamination of gallium arsenide was studied in 1*N* nitric acid. The results of this study are shown in Table I. The adsorption is a reversible process, and the sodium ion can be washed from the surface with 1*N* nitric acid. It is interesting to note that a new equilibrium appears to be set up each time and that a concentration dependence exists, that is, the more sodium ion presented to the surface, the more will be adsorbed.

This type of adsorption indicates a physical adsorption mechanism and is characterized by a Freundlich isotherm, where a log plot of equilibrium surface concentration *vs.* equilibrium solution concentration should be a straight line. As can be seen in Fig. 1, a straight line relationship is obtained. Since physical adsorption involves relatively weak Van der Waal forces, one would expect any two monovalent ions to contaminate the surface of the semiconductor to more or less the same extent.

Silver ion.—The contamination of gallium arsenide and indium antimonide surfaces by monovalent silver ion was studied using radioactive silver$^{110m-110}$. The equilibration was carried out from 1*N* nitric acid and the amount of surface contamination after each 1*N* nitric acid wash is shown in Tables II and III.

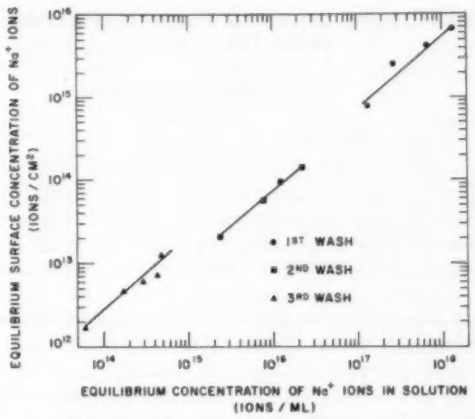
EQUILIBRIUM SURFACE CONCENTRATION OF Na+ IONS (IONS / CM²)
EQUILIBRIUM CONCENTRATION OF Na+ IONS IN SOLUTION (IONS / ML)
1ST WASH
2ND WASH
3RD WASH

Fig. 1. Washing of sodium ion contamination from gallium arsenide surfaces.

One of the more striking observations is the low level of silver impurity in solution that gives high surface contamination. As little as 0.48 ppm Ag in 1*N* nitric acid results in 2×10^{14} atoms/cm^2 on gallium arsenide. As can be seen in Tables II and III, the silver is irreversibly adsorbed which is in sharp contrast to the reversible adsorption of sodium ion.

This large irreversible adsorption of silver ion from nitric acid solution cannot be explained by a physical adsorption mechanism.

Divalent Ions

The mechanisms of deposition of divalent metallic ions on gallium arsenide and indium antimonide fall in two general classes just as with monovalent ions. First there is that class of metal ions that is weakly and reversibly adsorbed.

Zinc ion.—Zinc ion falls in this classification and the results of the adsorption of zinc by gallium ar-

Table I. Adsorption of sodium ion from 1N HNO_3 on gallium arsenide (1N HNO_3 washes)

Na^+ impurity, ppm	Surface contamination after 1st wash, ions/cm^2	2nd wash, ions/cm^2	3rd wash, ions/cm^2
100	$>10^{16}$	1.64×10^{14}	1.29×10^{13}
50	7.48×10^{15}	1.44×10^{14}	7.29×10^{12}
25	4.11×10^{15}	9.78×10^{13}	6.06×10^{12}
10	2.57×10^{15}	5.87×10^{13}	4.73×10^{12}
5	7.89×10^{14}	2.12×10^{13}	1.69×10^{12}

Table II. Deposition of silver ion from 1N HNO_3 on gallium arsenide (1N HNO_3 washes)

Ag^+ impurity, ppm	Surface contamination after 1st wash, atoms/cm^2	2nd wash, atoms/cm^2	3rd wash, atoms/cm^2
0.48	2.38×10^{14}	2.18×10^{14}	1.95×10^{14}
0.24	9.98×10^{13}	9.76×10^{13}	9.54×10^{13}
0.12	4.61×10^{13}	4.16×10^{13}	3.88×10^{13}
0.024	1.94×10^{13}	1.80×10^{13}	1.73×10^{13}
0.012	4.64×10^{13}	4.19×10^{13}	3.82×10^{13}

Table III. Deposition of silver ion from 1N HNO_3 on indium antimonide (1N HNO_3 washes)

Ag^+ impurity, ppm	Surface contamination after 1st wash, atoms/cm^2	2nd wash, atoms/cm^2	3rd wash, atoms/cm^2
1.20	4.18×10^{14}	3.54×10^{14}	3.31×10^{14}
0.60	1.65×10^{14}	1.43×10^{14}	1.35×10^{14}
0.24	6.73×10^{13}	5.65×10^{13}	5.24×10^{13}
0.12	3.26×10^{13}	2.69×10^{13}	2.50×10^{13}
0.048	1.55×10^{13}	1.25×10^{13}	1.16×10^{13}

Table IV. Surface contamination of gallium arsenide by zinc ion from 1N nitric acid

Zn^{++} impurity, ppm	Surface contamination after 1st wash, ions/cm²	2nd wash, ions/cm²	3rd wash, ions/cm²
84	1.15×10^{14}	6.21×10^{12}	2.04×10^{12}
42	5.24×10^{13}	5.11×10^{12}	5.65×10^{12}
21	3.10×10^{13}	3.41×10^{12}	5.08×10^{11}
8.4	8.27×10^{12}	1.14×10^{12}	1.50×10^{12}
1.7	3.05×10^{12}	8.90×10^{11}	8.90×10^{11}

senide are shown in Table IV. The adsorption and washings were caried out using 1*N* nitric acid as described above.

It should be pointed out that after the third wash the counting rate was very low and, as a result, the counting statistics were not good. This explains why there is a deviation from the concentration gradient observed after the first two washes. From these results it appears that the mechanism of deposition of zinc ion on the III-V intermetallics is the same as sodium ion.

The second class of metal ion deposition is the irreversible type where only very low levels of solution impurity are required to give serious levels of surface contamination. Two divalent iors were investigated which fell in this class, mercury(II) and copper(II).

Mercury(II).—The 65-hr radioactive mercury$^{197-197m}$ tracer was used in these studies to determine the manner in which the mercury is deposited on the two intermetallics. The results are shown in Tables V and VI and show how very low levels of mercury ion in solution will result in significant surface contamination. As is also apparent from the results, the deposition of the mercury is irreversible. This behavior is in sharp contrast to that of zinc ion.

It was found that the irreversibly adsorbed mercury contamination could be removed by placing the contaminated intermetallic semiconductor in a vacuum of *ca.* 1μ for an hour. It was not necessary to heat the system to effect this removal. This indicates the mercury is probably deposited on the surface as the metallic species.

Table V. Surface contamination of indium antimonide by mercury (II) ion from 1N nitric acid solution

Hg^{++} impurity, ppm	Surface contamination after 1st wash, atoms/cm²	2nd wash, atoms/cm²	3rd wash, atoms/cm²
0.93	6.63×10^{13}	5.82×10^{13}	5.71×10^{13}
0.46	3.81×10^{13}	3.38×10^{13}	3.33×10^{13}
0.19	1.53×10^{13}	1.32×10^{13}	1.32×10^{13}
0.09	6.87×10^{12}	5.58×10^{12}	5.31×10^{12}
0.04	2.02×10^{12}	1.75×10^{12}	1.62×10^{12}

Table VI. Surface contamination of gallium arsenide by mercury (II) ion from 1N nitric acid solution

Hg^{++} impurity, ppm	Surface contamination after 1st wash, atoms/cm²	2nd wash, atoms/cm²	3rd wash, atoms/cm²
0.93	1.35×10^{14}	1.26×10^{14}	1.23×10^{14}
0.46	6.41×10^{13}	5.81×10^{13}	5.62×10^{13}
0.19	2.03×10^{13}	1.88×10^{13}	1.78×10^{13}
0.09	8.23×10^{12}	7.67×10^{12}	7.13×10^{12}
0.04	2.42×10^{12}	2.16×10^{12}	1.90×10^{12}

Table VII. Surface contamination of gallium arsenide by copper (II) ion from 1N nitric acid

Cu^{++} impurity, ppm	Surface contamination after 1st wash, atoms/cm²	2nd wash, atoms/cm²	3rd wash, atoms/cm²
28	4.35×10^{14}	4.14×10^{14}	4.06×10^{14}
14	2.72×10^{14}	2.57×10^{14}	2.46×10^{14}
5.6	1.44×10^{14}	1.36×10^{14}	1.31×10^{14}
2.8	8.26×10^{13}	7.84×10^{13}	7.59×10^{13}
1.8	3.51×10^{13}	3.32×10^{13}	3.19×10^{13}

Table VIII. Surface contamination of indium antimonide by gold from 1N nitric acid solution

Au^{+++} impurity, ppm	Surface contamination after 1st wash, atoms/cm²	2nd wash, atoms/cm²	3rd wash, atoms/cm²
1.0	2.72×10^{14}	2.62×10^{14}	2.53×10^{14}
0.5	1.30×10^{14}	1.24×10^{14}	1.40×10^{14}
0.25	6.02×10^{13}	5.68×10^{13}	5.48×10^{13}
0.1	2.67×10^{13}	2.48×10^{13}	2.37×10^{13}
0.05	1.69×10^{13}	1.62×10^{13}	1.56×10^{13}
0.025	5.13×10^{12}	4.90×10^{12}	4.18×10^{12}

Copper.—The deposition of copper on gallium arsenide was studied using copper^{64}. From the results in Table VII it can be seen that the surface contamination is irreversible and large. The type of adsorption seen here is the same as observed for silver and mercury(II) and cannot be explained on the basis of a physical adsorption mechanism.

Trivalent Ions

Gold.—Using radioactive gold^{198}, the deposition on indium antimonide was investigated. The gold was found to deposit from solution in the same manner as did silver, copper, and mercury(II); that is, the gold was irreversibly deposited on the intermetallic surface. The results of the deposition from low levels of concentration in 1*N* nitric acid are shown in Table VIII.

Discussion

In the fabrication of any semiconductor device the III-V intermetallic must be cleaved in air. When the cleavage occurs, there will be immediate reaction with oxygen and water vapor to form some type of hydrous oxide at the surface. This is the first form of surface contamination. Whether this surface attack by the oxygen is chemisorption or oxidation is not clear. Rosenburg (7) studied the "chemisorption" and oxidation of vacuum crushed III-V intermetallics and observed the formation of metastable surface complexes prior to true oxide growth.

The second step in device fabrication is lapping and etching to remove surface damage. It is this latter step of etching and washing that presents metal ions in solution to the semiconductor surface to contaminate the surface.

The work reported here has been restricted to metal ion contamination from acid solutions because acid etches are used predominately in III-V intermetallic device fabrication. This restriction simplifies

the interpretation of the data by excluding surface effects such as hydrolysis. The work reported here shows that there are two mechanisms of metal ion impurity in operation. If the electrochemical potential of the metal-metal ion contaminate is lower than the electrochemical potential of the semiconductor surface, a physical adsorption will occur. Physical adsorption involves the establishment of an equilibrium between the amount adsorbed on the surface and the concentration of the contaminate in solution. The variation of the extent of adsorption with concentration of solute is usually represented by the Freundlich equation. In this work, this type of adsorption was observed for sodium and zinc ion on both indium antimonide and gallium arsenide. Similar results were obtained for other ions but were not reported here.

These physically adsorbed metal ions are adsorbed on or in the oxide structure and as such probably contribute to the slow state density. These ionic impurities would be detrimental to device characteristics such as reverse current in the case of diodes. It is this type of surface contamination which disturbs the electron-hole ratio in the bulk and results in the formation of inversion layers.

The second mechanism of metal ion impurity deposition observed was electrochemical deposition. This mechanism is observed for metal ion impurities when the metal-metal ion electrochemical potential lies above the semiconductor surface electrochemical potential. In these cases the metal ions are actually deposited as the metal on the surface and as a result cannot be washed off by normal washing techniques. The results in Tables II, V, VII, and VIII show silver(I), mercury(II), copper(II), and gold(III) are tenaciously held by an intermetallic semiconductor. As can be seen, even very low levels of these impurities in solution will seriously contaminate a semiconductor surface. The results also indicate a strong concentration dependence which indicates an equilibrium constant is being obeyed.

In the hypothetical reaction

$$aA + bB \rightleftharpoons cC + dD \qquad [1]$$

The electrochemical potential

$$E = E^\circ - \frac{RT}{n\mathbf{F}} \ln \frac{[C]^c\,[D]^d}{[A]^a\,[B]^b} \qquad [2]$$

when equilibrium is established $E = 0$ and

$$E^\circ = \frac{RT}{n\mathbf{F}} \ln k \qquad [3]$$

In Eq. [3], k is now the equilibrium constant for the reaction. Since this equilibrium constant must be obeyed, the more impurity there is initially, present in solution, the more impurity will be electrochemically deposited.

In the case where silver ion in contaminating gallium arsenide, the following equations hold,

$$Ga^\circ + 3Ag^+ \rightleftharpoons 3Ag^\circ + Ga^{+++} \qquad [4]$$

$$k = \frac{[Ag^\circ]^3\,[Ga^{+++}]}{[Ag^+]^3\,[Ga^\circ]} \qquad [5]$$

Since the activity of the metals = 1, the equilibrium constant simplifies to

$$k = \frac{[Ga^{+++}]}{[Ag^+]^3} \qquad [6]$$

In the radiochemical impurity deposition studies it was possible, using counting techniques, to determine the equilibrium concentration of silver ion in solution but not the equilibrium concentration of gallium ion because the gallium arsenide was not radioactive. Looking back to Eq. [4] it is apparent that the equilibrium concentration of gallium ion in solution is proportional by a mole ratio to the equilibrium concentration of silver metal deposited on the gallium arsenide. The equilibrium concentration can therefore be written

$$k = \frac{[Ag^\circ]}{[Ag^+]^3} \qquad [7]$$

Cross multiplying and taking the logarithm, a straight line relationship is obtained.

$$\log [Ag^\circ] = 3 \log [Ag^+] + \log k \qquad [8]$$

In practice (see Fig. 2) a slope of 3 is not obtained because we are dealing with gallium arsenide and not pure gallium. However, this in no way invalidates the electrochemical mechanism of impurity deposition.

The results after the third wash for the irreversible electrochemical deposition of silver, copper, mercury, and gold are shown in Fig. 2 for gallium arsenide and in Fig. 3 for indium antimonide. A straight line relationship was obtained in all cases. In all the results reported, a calculated surface area was used which assumed a surface roughness factor of one. Measurements of surface area using the B.E.T. technique confirmed the fact that the roughness factor was not unity but 3.1 for gallium arsenide and 3.9 for indium antimonide. Since these values were on the basis of a single determination on one batch of the intermetallics used, it was not felt reasonable to correct all the data using these factors. Since this paper is to present mechanisms of metal ion deposition on the intermetallics, it is not necessary to know the true surface area. In device fabrication the presence of 7×10^{14} atoms/cm^2 or 2×10^{14} atoms/cm^2 (roughness factor = 3.5) makes little difference

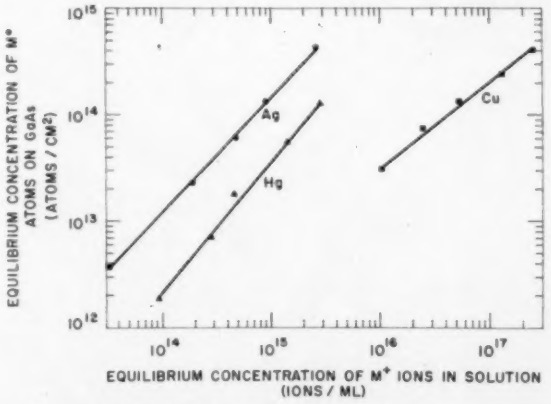

Fig. 2. Electrochemical deposition of silver, mercury, and copper on gallium arsenide.

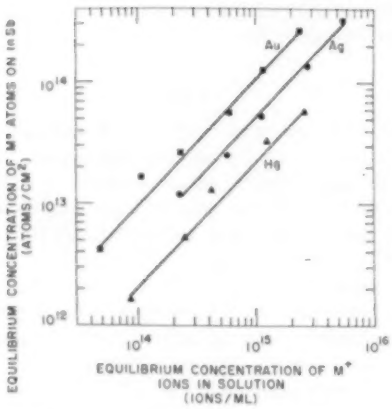

Fig. 3. Electrochemical deposition of gold, silver, and mercury on indium antimonide.

since the cleaning operation is striving to attain surface impurity concentrations approaching 10^{11} atoms/cm^2.

Inasmuch as the electrochemical deposition of the metal impurity occurs at the semiconductor surface, not at or in the oxide superstructure, the contaminate may contribute to the fast state density. If the work function of the deposited metal is smaller than that of the semiconductor, electrons will flow from the metal to the semiconductor to achieve equilibrium, causing an enriched boundary layer in the semiconductor. If the work function is larger, electrons will flow from the semiconductor to the metal forming a depletion layer in the semiconductor.

In the case of copper and other fast diffusers the thermal conversion problem is serious. This change in semiconductor type as a result of heating is generally acknowledged to be a surface effect (8). Many workers believe that copper is the contaminant causing this conversion (9, 10), and Wysocki (11) has been able to control thermal conversion by carefully removing copper contamination from the chemical reagents used to etch gallium arsenide. Our results show that copper metal is deposited on indium antimonide and gallium arsenide from nitric acid solution, and this copper would most certainly diffuse rapidly into the bulk of the semiconductor during any heat treatment.

The presence of electrochemically deposited metals on the surface of the semiconductor would have very detrimental effects on the properties of the p-n junction which is always extremely surface sensitive (12). The p-n junction may actually be electrically shorted when the surface contamination approaches a monolayer. A monolayer can be obtained from only fractional ppm levels of metal ion impurity in solution.

These mechanisms of metal ion impurity deposition undoubtedly hold for the other III-V intermetallic semiconductors and have been shown to be applicable on silicon and germanium (13).

Manuscript received May 15, 1961; revised manuscript received Aug. 10, 1961. This paper was prepared for delivery before the Houston Meeting, Oct. 9-13, 1960.

Any discussion of this paper will appear in a Discussion Section to be published in the June 1962 JOURNAL.

REFERENCES

1. J. T. Law, *J. Phys. Chem.*, **59**, 67, 543 (1955).
2. J. T. Law and E. E. Francois, *ibid.*, **60**, 353 (1956).
3. J. T. Law, "Semiconductors," N. B. Hannay, Editor, Reinhold Publishing Corp., New York (1959).
4. F. F. Synorov, *Isvestia, VUZ MVO, Phys. Ser.*, No. 4, 80 (1958).
5. A. Many, *J. Phys. Chem. Solids*, **8**, 87 (1959).
6. M. M. Atalla, E. Tannenbaum, and E. J. Scheibner, *Bell System Tech. J.*, **38**, 749 (1959).
7. A. J. Rosenburg, *J. Phys. Chem. Solids*, **14**, 175 (1960).
8. H. Rupprecht, *Z. Naturforsch*, **13a**, 1094 (1958).
9. F. D. Rosi, D. Meyerhaffer, and R. V. Jensen, *J. Appl. Phys.*, **31**, 1105 (1960).
10. F. A. Cunnel, J. T. Edmond, and W. R. Harding, *SERL Tech.*, **9**, 104 (1959).
11. J. J. Wysocki, *J. Appl. Phys.*, **31**, 1686 (1960).
12. G. deMars, *Semiconductor Products*, **2**, 24 (1959).
13. G. B. Larrabee, "The Study of Surface Contamination of Semiconductors by Radiochemical Techniques," Paper presented at the 1960 Houston, Texas meeting of The Electrochemical Society.

Polarographic Studies in Acetonitrile and Dimethylformamide

VI. The Formation of Dihalocarbenes

S. Wawzonek and R. C. Duty

Department of Chemistry, State University of Iowa, Iowa City, Iowa

ABSTRACT

Polarographic studies of methylene chloride, chloroform, carbon tetrachloride, carbon tetrabromide, dichlorodifluoromethane, chlorodifluoromethane, benzal chloride, benzotrichloride, and diphenyldichloromethane have been carried out in dimethylformamide and acetonitrile. The results with carbon tetrachloride and carbon tetrabromide point to the formation of dihalocarbenes as intermediates in the reduction of these compounds. This mechanism was verified by the large-scale electrolytic reduction of carbon tetrachloride in acetonitrile in the presence of tetramethylethylene and the isolation of 1,1-dichloro-2,2,3,3-tetramethylcyclopropane as one of the products.

Previous polarographic studies in acetonitrile and dimethylformamide have shown the polarographic method to be capable of furnishing evidence for the existence of stable anion-free radicals in the reduction of aromatic hydrocarbons (1-3), semiquinone anions in the reduction of quinones (4), and ketyl anions from aromatic ketones (5, 6).

In the present study, the polarographic behavior and electrolytic reduction of polyhalogenated methanes has been investigated to determine whether carbenes are formed as intermediates in these solvents.

Experimental

The solutions were studied in a cylindrically shaped cell with a mercury pool as previously described (5). All measurements were made in a water thermostat at 25° ± 0.1°C.

The current-voltage curves were obtained with a Sargent Model XII polarograph having a current-scale calibration of 0.005714 μa/mm at a sensitivity of one. The gas chromatograph was a Perkin-Elmer Model 154 with helium as a carrier gas. Perkin-Elmer columns A (didecyl phthalate) and C (silicon oil DC 200) were used as noted.

Two dropping-mercury electrodes were used in this study. Capillary one was operated at 48 cm pressure and had the drop time of 3.82 sec. Capillary two operated with a mercury head of 48 cm and the drop time of 4.12 sec. The $m^{2/3}\,t^{1/6}$ values were 1.91 $mg^{2/3}\,sec^{-1/2}$ and 1.88 $mg^{2/3}\,sec^{-1/2}$, respectively.

The dimethylformamide was purified in a manner described previously (4). Acetonitrile was purified by a variation of the directions of Wawzonek and Runner (7). The acetonitrile was shaken intermittently with a saturated solution of potassium hydroxide while cooling externally. The solvent was dried overnight with sodium carbonate and distilled from phosphorus pentoxide in a nitrogen atmosphere through a 100 cm Fenske column. The inside diameter of the column was 2 cm. A final distillation was made from either potassium carbonate or barium oxide. The fraction boiling between 81° and 81.5°C was used.

Tetra-*n*-butylammonium bromide (1), tetra-*n*-butylammonium iodide (8), diphenyldichloromethane (9), and tetramethylethylene (10) were prepared by methods reported in the literature. Methylene chloride, chloroform, carbon tetrachloride, benzal chloride, benzotrichloride were purified by distillation, and their purity was checked by vapor phase chromatography. Carbon tetrabromide was purified by recrystallization. Chlorodifluoromethane and dichlorodifluoromethane were obtained from the Matheson Company, Inc. and were used directly without purification.

Electrolytic reduction of carbon tetrachloride.—The electrolytic reduction of carbon tetrachloride was carried out with a platinum anode and mercury cathode as described previously (1). The area of the cathode was 40 cm^2, and the line voltage was 120 v. A solution of 300 ml of acetonitrile, 19.5 g of tetra-*n*-butylammonium bromide, and 26 ml of tetramethylethylene was degassed for 2 hr after which carbon tetrachloride (10 ml) was added to the cathode chamber. Direct current was allowed to pass through the solution for 37 hr during which no visible color change was observed. The direct current was controlled at 0.30 amp and fell to a final value of 0.15 amp. The reduction cell during the electrolysis was cooled in a dry ice-acetone bath to a temperature of −20°C.

The catholyte and anolyte were combined after the reduction was stopped. A sample removed for analysis on the gas chromatograph using column C at 79° indicated by comparison with samples of known concentration that approximately 2 ml of tetramethylene had disappeared and approximately 5 ml of carbon tetrachloride had been reduced.

Table I. Retention times for 1,1-dichloro-2,2,3,3-tetramethylcyclopropane on column A and column C at various temperatures

Column and temperatures, °C	1, 1-Dichloro-2, 2, 3, 3-tetramethylcyclopropane	Unknown peaks
C		
101	18 min and 14 sec	17 min and 40 sec
175	5 min	5 min and 10 sec
198	3 min and 26 sec	3 min and 36 sec
A		
125	27 min and 45 sec	28 min and 2 sec
165	11 min and 58 sec	12 min and 14 sec

The combined solutions were distilled and the fraction boiling below 80°C was collected. This fraction was analyzed on the gas chromatograph on the same column at 79°, and carbon tetrachloride, tetramethylethylene, acetonitrile, and chloroform were found. No peak for methylene chloride was observed. The retention times for carbon tetrachloride, tetramethylethylene, chloroform, methylene chloride, and acetonitrile were 4 min and 42 sec, 3 min and 54 sec, 3 min and 10 sec, 1 min and 56 sec, and 1 min and 35 sec, respectively.

The remainder of the solvent from the distillation upon removal at 100°C gave a residue (25 ml) of a viscous, dark-brown oil. The brown oil was distilled under diminished pressure (4 mm), and 1 ml of distillate was collected which boiled below 100°. The distillate, which was light yellow, was analyzed for 1,1-dichloro-2,2,3,3-tetramethylcyclopropane on the gas chromatograph. Column C was used at three different temperatures (101°, 175°, and 198°C), and column A was used at two different temperatures (125° and 165°). The retention times for the unknown compound are given in Table I.

A known sample of 1,1-dichloro-2,2,3,3-tetramethylcyclopropane, prepared according to the directions given by Doering and Henderson (9) was run in conjunction with the unknown sample. Satisfactory agreement in retention times was found on both columns at all temperatures. To establish further that the unknown peaks were for the cyclopropane derivative, a small crystal of 1,1-dichloro-2,2,3,3-tetramethylcyclopropane was added to the reduction sample which was run again on column C at 101°. A comparison of the two graphs showed that the original peak, that was believed to be the result of the cyclopropane derivative, was increased in height with no new peaks or shoulders occurring on the graph. A summary of retention times on column A and column C for the cyclopropane derivative and unknown peak appears in Table I.

Results

Most of the waves for the halogenated compounds were well defined. Small maxima occurred on the first wave for carbon tetrachloride and the wave for dichlorodifluoromethane in dimethylformamide. In acetonitrile the former compound gave two waves of equal height close together. The half-wave potentials were calculated by using one-fourth and three-fourths of the total diffusion current.

The first wave for carbon tetrabromide was unusual in that it started abruptly at −0.07 v.

Small rounded prewaves starting at approximately 0.0 v were obtained for benzotrichloride and diphenyldichloromethane. These waves appeared to increase with time and may be caused by mercurous or mercuric salts formed by a slow reaction of these compounds with mercury since mercuric nitrate forms a wave at the same point.

To help formulate the electrode reaction for carbon tetrachloride and to identify the intermediate species formed, a large-scale electrolytic reduction of carbon tetrachloride was carried out in the presence of tetramethylethylene in acetonitrile.

Discussion of Results

Examination of the results in Table II indicate that the reduction of methylene chloride and chloroform is normal in dimethylformamide and acetonitrile and parallels the behavior of the first two compounds in aqueous media (12, 13). Methylene chloride is reduced to methyl chloride in dimethylformamide and shows no reduction wave in acetonitrile. Chloroform

Table II. Polarographic behavior of halogenated methanes in 0.175M tetra-*n*-butyl ammonium bromide

Compounds[a]	Capillary	Solvent	1st Wave $E^{1/2}$	1st Wave I_d[c]	2nd Wave $E^{1/2}$	2nd Wave I_d[c]	3rd Wave $E^{1/2}$	3rd Wave I_d[c]
CH_2Cl_2	2	DMF[d]	−2.14	6.37				
$CHCl_3$	2	DMF	−1.45	3.18	−2.14	3.24		
CCl_4	2	DMF	−0.25	5.79	−1.49	1.42	−2.17	1.92
CCl_4	2	DMF-10% H_2O	−0.27	4.30	−1.61	4.35	−2.25	4.75
CH_2Cl_2	1	CH_3CN			No reduction wave			
$CHCl_3$	1	CH_3CN	−1.32	5.49				
CCl_4	1	CH_3CN	−0.25	4.40	−0.64	4.40		
CCl_4	1	CH_3CN-10% H_2O	−0.33	7.70	−1.64	5.22		
CBr_4[b]	2	DMF	−0.08	6.43	−1.36	2.20	−1.94	1.62
CCl_2F_2[c]	1	DMF	−1.45	14.2				
$CHClF_2$	1	DMF			No reduction wave			
$C_6H_5CHCl_2$	2	DMF	−1.43	3.22	−1.80	3.46		
$C_6H_5CCl_3$[f]	2	DMF	−0.53	2.38	−1.43	2.24	−1.75	2.52
$C_6H_5CHCl_2$	1	CH_3CN	−1.46	5.37	−1.88	4.33		
$C_6H_5CCl_3$[g]	1	CH_3CN	−0.54	3.13	−1.43	2.69	−1.87	3.73
$(C_6H_5)_2CCl_2$[h]	1	CH_3CN	−0.70	2.69	−1.44	4.48		

[a] Concentration 0.001M unless otherwise noted.
[b] Concentration 8.96×10^{-4}M.
[c] Concentration by v.p.c.
[d] Dimethylformamide.
[e] $I_d = \frac{i_d}{Cm^{2/3}t^{1/6}}$.
[f] Prewave $E^{1/2} = -0.14$; $I_d = 0.85$.
[g] Prewave $E^{1/2} = -0.11$; $I_d = 1.34$.
[h] Prewave $E^{1/2} = -0.11$; $I_d = 3.00$.

shows two waves in dimethylformamide of equal height and is reduced stepwise to methylene chloride and methyl chloride since the half-wave potential of the second wave is the same as that observed for methylene chloride. The reduction of chloroform in acetonitrile to methylene chloride is in agreement with the observation that methylene chloride does not show a wave in this solvent.

The diffusion current constant obtained for chloroform in acetonitrile is higher than that in dimethylformamide because of the lower viscosity in the former solvent. A similar behavior was found for stilbene in these media (1).

Carbon tetrachloride shows an abnormal behavior in dimethylformamide in that the first wave has a diffusion current which is much higher than those of the second and third waves. The abnormality in acetonitrile is even greater in that a wave corresponding to the formation of chloroform is not observed. The two early waves observed have diffusion current constants corresponding to reductions involving two electrons each.

After addition of water to dimethylformamide and acetonitrile three waves of equal height were found on examination of the former and two waves of unequal height of the latter, one of which corresponded to the reduction of chloroform. This behavior parallels that reported for carbon tetrachloride in aqueous media (12, 13). The addition of water must reduce the viscosity of the solutions since the diffusion current constants are higher.

The abnormal behavior observed in acetonitrile would indicate that the following reactions were occurring.

$$CCl_4 + 2e \rightarrow CCl_3^- + Cl^-$$

$$CCl_3^- \rightleftarrows CCl_2 + Cl^-$$

$$CCl_2 + 2e \rightarrow CCl_2^=$$

$$CCl_2^= + 2CH_3CN \rightarrow H_2CCl_2 + 2[CH_2CN]^-$$

The intermediate trichlorocarbanion formed at the electrode dissociates into dichlorocarbene and a chloride ion. The resulting dichlorocarbene undergoes further reduction to the dichlorocarbanion which on protonation yields methylene chloride. The reactions are rapid since the currents observed are diffusion controlled.

In dimethylformamide the reactions are accompanied by the protonation of the trichlorocarbanion and the formation of chloroform.

$$CCl_3^- + HCON(CH_3)_2 \rightarrow HCCl_3 + CON(CH_3)_2^-$$

The differences in the two solvents is caused no doubt by the lower viscosity of the acetonitrile. This property would permit a faster diffusion of the chloride ion from the cage of solvent surrounding the trichlorocarbanion. The wave for the reduction of dichlorocarbene in dimethylformamide was probably not observed because of the maximum present.

Addition of water furnishes a greater supply of protons and increases the rate of protonation of the trichlorocarbanion over that of the dissociation reaction and a normal stepwise reduction to chloroform, methylene chloride, and methyl chloride is observed in dimethylformamide.

In acetonitrile under the same conditions the wave for the reduction of dichlorocarbene disappears and a wave corresponding to the reduction of chloroform appears. The diffusion current constant of the first wave, however, is larger than that of the second wave and would suggest that a small amount of dichlorocarbene is still being formed as an intermediate and that the wave corresponding to this step has merged with the reduction wave for carbon tetrachloride.

Further proof of the formation of dichlorocarbene was obtained by electrolyzing carbon tetrachloride on a large scale in the presence of tetramethylethylene in acetonitrile at −20°C. Examination of the electrolytic products by gas chromatography indicated that 1,1-dichloro-2,2,3,3-tetramethylcyclopropane was formed as one of the products.

$$CCl_2 + (CH_3)_2C = C(CH_3)_2 \rightarrow (CH_3)_2C\text{—}C(CH_3)_2$$

$$\begin{array}{c} \backslash\ / \\ C \\ /\ \backslash \\ Cl\ \ Cl \end{array}$$

This compound has also been synthesized by generating dichlorocarbene from chloroform with potassium *t*-butoxide in the presence of tetramethylethylene (11).

The polarographic behavior of carbon tetrabromide in dimethylformamide is similar to that of carbon tetrachloride. The unusual shape of the first wave suggests that the reduction of this compound may be complicated by the formation of mercuric bromide. This example therefore was not studied any further.

The report (14) that difluorocarbene is more stable than dichlorocarbene suggested an investigation of the reduction of dichlorodifluoromethane. The polarographic behavior was not conclusive since the normal reduction product, chlorodifluoromethane, was not reducible at the dropping mercury electrode in dimethylformamide. No split was observed in the wave because of the maximum present. The high diffusion current obtained for dichlorodifluoromethane would suggest the formation of a carbene intermediate, but this could not be verified by a large-scale electrolytic reduction of dichlorodifluoromethane in the presence of tetramethylethylene. Evolution of the difluorodichloromethane occurred during the initial stages of the reduction while the electrolyte was held at −20°C.

Comparison of the polarographic behavior of benzotrichloride with that of benzal chloride indicates that the former is reduced stepwise to toluene. The lower diffusion currents obtained for benzotrichloride are no doubt caused by a decrease in its concentration through a reaction with mercury. This reaction is borne out by the formation of a prewave. The similarity in height of the first two waves indicates that the formation of a carbene is a minor reaction in dimethylformamide. The behavior in acetonitrile indicates that more of the carbene is formed since the second wave is smaller in height than the first wave. The difference was not considered large enough to warrant a large-scale electrolytic reduction study of this compound.

A prewave pointing to the formation of a mercuric salt was found with diphenyldichloromethane as mentioned earlier. The unequal diffusion currents obtained would point to the formation of a reducible organic product in this reaction. The nature of this reaction, however, was not studied any further.

Manuscript received April 20, 1961; revised manuscript received Sept. 1, 1961. This paper was prepared for presentation at the Columbus Meeting, October 18-22, 1959 and is based on the Ph.D thesis of R. C. Duty, February 1961. The research was supported by the Office of Ordnance Research under Contract DA-11-022-ORD-1868.

Any discussion of this paper will appear in a Discussion Section to be published in the June 1962 JOURNAL.

REFERENCES

1. S. Wawzonek, E. W. Blaha, R. Berkey, and M. E. Runner, *This Journal*, **102**, 235 (1955).
2. S. Wawzonek and D. Wearring, *J. Am. Chem. Soc.*, **81**, 2067 (1959).
3. P. H. Given, *J. Chem. Soc.*, **1958**, 2684.
4. S. Wawzonek, R. Berkey, E. W. Blaha, and M. E. Runner, *This Journal*, **103**, 456 (1956).
5. S. Wawzonek and A. Gundersen, *ibid.*, **107**, 537 (1960).
6. P. H. Given, M. E. Peover, and J. Schoen, *J. Chem. Soc.*, **1958**, 2674.
7. S. Wawzonek and M. E. Runner, *This Journal*, **99**, 457 (1952).
8. H. A. Laitinen and S. Wawzonek, *J. Am. Chem. Soc.*, **64**, 1765 (1942).
9. L. Gattermann and H. Schulze, *Ber.*, **29**, 2944 (1896).
10. I. Schurman and E. E. Boord, *J. Am. Chem. Soc.*, **55**, 4930 (1933).
11. W. von E. Doering and W. A. Henderson, Jr., *ibid.*, **80**, 5276 (1958).
12. M. von Stackelberg and W. Stracke, *Z. Elektrochem.*, **53**, 118 (1949).
13. I. M. Kolthoff, T. S. Lee, D. Stocesova, and E. P. Parry, *Anal. Chem.*, **22**, 521 (1950).
14. J. Hine and S. J. Ehrenson, *J. Am. Chem. Soc.*, **80**, 824 (1958).

The Formation of Elongated Iron and Iron-Cobalt Particles by Electrodeposition into Mercury

Fred E. Luborsky

Research Laboratory, General Electric Company, Schenectady, New York

ABSTRACT

The preparation of 100-300Å diameter highly elongated fibers of iron by electrodeposition into mercury is described. The mechanism of formation of these fibers is deduced from direct electron microscopic examination of the structures formed during electrolysis. The relations between the structure of these initial fibers. parameters of formation, and ultimate magnetic properties are discussed.

Rapid advances in modern technology have been due, in part, to a more fundamental understanding of the relation between structure and properties. In the field of permanent magnets we can point to the evolution of domain theory (1) as the stimulus which led to the development of fine particle permanent magnets. Conversely, practical advances in fine particle magnets stimulated theoretical advances. Fine particle theory, and in particular its extension to the elongated particle concepts (2), pointed out in some detail the specific particle size and shape needed to synthesize a microstructure having the best permanent magnet properties. The required particles had to be highly elongated rods of iron with a diameter of about 200Å. It was predicted that a perfectly oriented compact of such particles would attain a maximum energy product, $(BH)_{max}$, of 40 million gauss-oe, ten times as powerful a magnet as known at the time. This provided the initial incentive for experimental work, but theory could not describe how such particles were to be made.

The original method discovered for preparing particles approaching the desired shape comprised an electrodeposition of iron into mercury under carefully controlled conditions followed by a heat aging. Essentially the same process is now in use for the commercial production of permanent magnets composed of elongated particles of iron or iron-cobalt (3, 4). Other methods of preparation have been published (5-10) recently, but have not attained commercial development. In previous publications the preparation and properties of magnets composed of elongated particles made by electrodeposition into mercury have been described (2, 3). The magnetic behavior of these particles has been studied (2) intensively, but the mechanism of formation has not been discussed previously. This is the principal subject of the present paper.

General Preparation of Elongated Particle Magnets

A block diagram of the laboratory process for the preparation of elongated iron or iron-cobalt particle magnets is shown in Fig. 1. Rough sketches of the particle structures are included. The first step consists of an electrodeposition of iron or iron-cobalt into a mercury cathode, under conditions to be described in detail in this paper, so as to develop elongated iron structures. A relatively low-temperature aging, between about 100° and 300°C, transforms or grows the dendritic structure into the more rodlike particle shown in the second step. A further substantial improvement in the coercive force, rema-

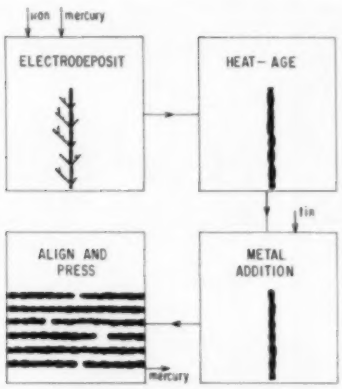

Fig. 1. Block diagram of the laboratory steps used to prepare magnets composed of elongated iron particles. A representative particle is depicted in each step.

nence, and packing characteristics is obtained in the third step by adding a reactive metal such as tin. In the final step the particles are aligned in a mold by a magnetic field and pressed to the desired packing fraction. The resulting bars are solid at room temperature with as little as 10–15 volume per cent iron.

Previous papers have described the relation between the structure and the magnetic properties of the particles in each of the four steps (3, 11, 12). The mechanism of heat treatment and the aligning and compacting of the particles have also been discussed in detail. In this paper the initial formation of these elongated particles in an unusual ordered structure is described. The structural variations of the particles are then related to their ultimate magnetic properties.

Electrodeposition

The electrodeposition was carried out in a cell with a circulating electrolyte system. The electrolyte was continuously filtered through activated charcoal and a filter cylinder and maintained at 25° ±2°C at a constant circulation rate, constant acidity, and free of excess vibration. The electrodeposition

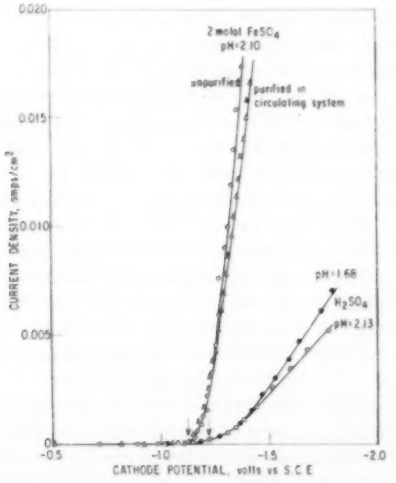

Fig. 2. Typical current-voltage curves for electrodeposition into a mercury cathode. Arrows indicate the potential at which H_2 was first observed.

cell consisted of a flat bottom glass jar with a close fitting iron anode supported by stainless steel posts. Contact to the mercury cathode in the bottom of the jar was made by a stainless steel rod through the center of the anode insulated with a glass tube. The bottom of the rod was welded to a coarse stainless steel screen submerged in the mercury. The screen provided good electrical contact and was used to remove the samples as will be described.

There are three possible simple cathode reactions on electrolyzing a ferrous sulfate solution.

$$Fe^{++} + 2e \rightarrow Fe \qquad [1]$$

$$2H^{+} + 2e \rightarrow H_2 \qquad [2]$$

and

$$Fe^{+++} + e \rightarrow Fe^{++} \qquad [3]$$

The standard potential for the reduction of ferric to ferrous ion, about +0.5 v *vs.* S.C.E., indicates that any Fe^{+++} present at the start of electrolysis is rapidly reduced. Thus only reactions [1] and [2] occur in practice. The reduction of ferrous ion to iron occurs at a potential 0.6–0.8 v more negative than the standard ferrous ion-iron potential, indicating a large overvoltage. The ferrous reduction is then virtually coincident with the usual reduction of the hydrogen ion making it difficult to deposit iron into mercury without the codeposition of hydrogen. Typical reduction characteristics are shown in Fig. 2 for H_2SO_4 solutions and for $FeSO_4$ acidified with H_2SO_4. The first visual appearance of H_2 on the mercury surface is pointed out. This "decomposition" potential was independent of acid or salt concentration, but the relative rates of deposition of iron and hydrogen did depend on concentration and on electrolyte treatment. On deposition of iron into mercury from electrolytes made from reagent grade ferrous sulfate and distilled water, hydrogen bubbles formed immediately over most of the surface at all acidities. Precipitation of iron occurred at a pH above 5. Vigorous evolution of H_2 occurred on continued electrolysis. The resulting dendritic iron particles in the mercury are described as a colloidal dispersion. On treatment of this same electrolyte with activated charcoal essentially the same i-V characteristic was obtained, as shown in Fig. 2, and the first visual appearance of H_2 occurred at the same potential. However, the hydrogen bubbles appeared only at widely separated spots. Very few new bubbles appeared in the course of time, and growth of the bubbles did not occur or at least was very slow even at normal operating currents of 0.001–0.1 amp/cm². Thus over the major portion of the mercury surface the overvoltage for the deposition of hydrogen was substantially increased and only iron was deposited. The product now obtained in the mercury had a remarkably different appearance, described best as a gel of iron particles in mercury with a pronounced texture. These gel structures were solid, readily handled at room temperature, and contained anywhere from 7 to about 15% iron by volume depending on the conditions of their formation.

This gel formation gave us a very convenient method for tracing the development of the iron fibers during the course of electrodeposition and thus pro-

Fig. 3. Electron micrograph of the iron fibers as formed in the gel at 0.017 amp/cm^2. The electrolyte interface was at the top. 1000Å scale marker.

Fig. 4. Electron micrograph of the iron fibers in the gel after aging for 15 min at 175°C. 1000Å scale marker.

vided a means of learning something about the mechanisms responsible for their formation.

Structure of the gel.—On a microscopic scale the structures were examined by splitting the gel to expose a fresh cross section, allowing the exposed surface to oxidize in moist air, casting a cellulose acetate film on this oxidized surface, and then carefully lifting it off when dry. Carbon was then deposited normal to the surface and the collodion dissolved away. The carbon film with the iron particles adhering to it was then used to obtain transmission micrographs. A typical example is shown in Fig. 3. The most striking feature of such microstructures is the highly oriented nature of the fibers. This orientation was maintained even after aging to develop optimum magnetic properties as shown in Fig. 4. There was no shrinkage in the thickness of the gel on aging while shrinkage in the transverse direction was only about 5%. The pronounced texture was also evident by the appearance of the cleavage surface shown in Fig. 5. The gel could be split perpendicular but not parallel to the original electrode surface.

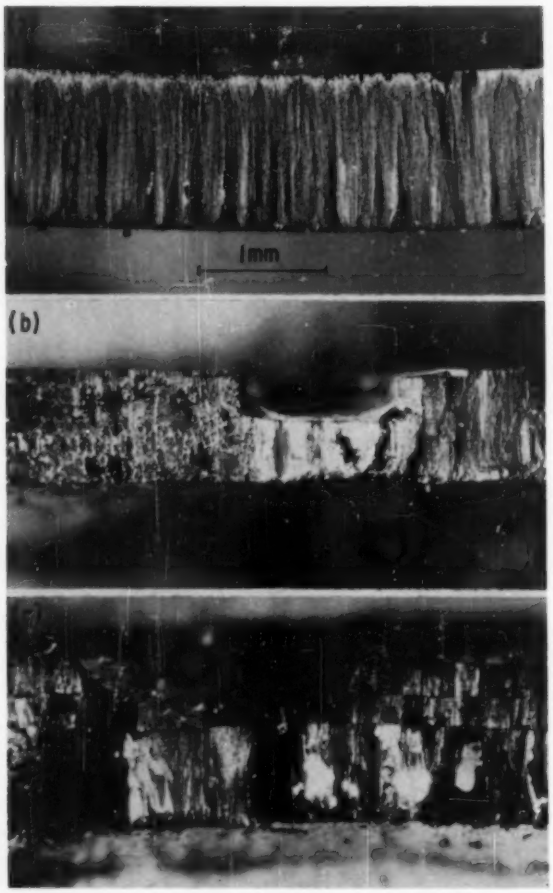

Fig. 5. Some cross sections of the gel structures: (a) well-formed gel; (b) cavity due to a bubble which did not increase in size; (c) cavity due to a bubble which increased in size with discontinuities in growth of the gel caused by mechanical disturbances.

The gel structure was completely unmagnetized as initially deposited. Freezing the gel structure without a magnetic field and measuring the properties along the direction, and transverse to the direction, of fiber alignment gave the properties reported in Table I. The high degree of magnetic anisotropy both before and after aging is apparent. Freezing the sample in a field in the direction of the fiber alignment did not improve the properties. Freezing in a transverse field was effective in rotating some of the particles, especially after the aging treatment.

Tests were also made to compare the properties of the particles obtained without disturbing the original particle orientation with the properties obtained by dispersing the original gel structure and then magnetically realigning the particles. Typical results are shown in Table II indicating that the same properties

Table I. Typical properties of the gel structure

	As deposited H_{ci}, oe	As deposited B_r/B'_{is}	Aged + tin H_{ci}, oe	Aged + tin B_r/B'_{is}
Frozen in no field				
measured parallel	600	0.78	1700	0.90
measured transverse	450	0.285	1025	0.28
Frozen in 7000 oe				
parallel	600	0.78	1700	0.90
transverse	450	0.290	1455	0.46

The saturation magnetization B'_{is} was measured in a field of 7000 oe. Properties all measured at 76°K.

Table II. Alignment of particles in the gel

	Cut from gel, mechanically oriented	Gel dispersed, magnetically oriented
As deposited[a]		
H_{ci}, oe	600	585
B_r/B'_{is}	0.78	0.79
Aged + tin[a]		
H_{ci}, oe	1700	1685
B_r/B'_{is}	0.90	0.90
Magnet pressed at 50,000 psi[b]		
H_{ci}, oe	700	720
B_r/B'_{is}	0.890	0.895
$(BH)_{max}$, gauss oe	3.5×10^6	3.8×10^6

The saturation magnetization B'_{is} was measured in a field of 7000 oe.
[a] Properties measured at 76°K.
[b] Properties measured at room temperature.

were obtained by either procedure provided some care was taken in the realignment.

On the basis of the above description of the gel we conclude that each fiber extends from the bottom surface to the top surface of the gel, and thus its length-to-diameter ratio is essentially infinite. Fibers are believed to stop growing and new ones to start because of local mechanical disturbances or local changes in the atom arrival rate at the surface.

Formation of the gel.—When electrodepositing iron into mercury the principal parameters affecting the gel formation were electrolyte purity, vibration, current density, time, and temperature. Electrolyte concentration, acidity, added inert salts, and magnetic fields had no direct effect.

The treatment of the electrolyte, for example with activated charcoal, removed certain organic contaminants and introduced others. If a piece of new plastic, for example, some polyvinylchlorides, Tygon or Dynel, were allowed to soak in the charcoal treated electrolyte or if a colloid like gelatin were added, vigorous evolution of hydrogen would occur soon after electrodeposition was started. The gel structure would no longer develop and the magnetic properties of the particles collected would be poor. Complete recovery of the electrolyte was accomplished simply by another treatment with the charcoal.

If the surface of the mercury was violently disturbed, for example by, rapidly stirring the mercury with a paddle or by depositing into a moving stream of mercury, predominately spherical particles resulted. This method of preparation and the properties of the resulting particles have been described previously (13). For very quiescent mercury surfaces a gel structure, as just described, could be removed after electrodeposition for a suitable time, but there was usually additional iron remaining in the mercury in a dispersed state. These iron particles in the dispersed state were almost spherical particles, of poor quality magnetically. They were observed to develop in the initial stages of deposition before the gel structure developed. The current density influenced the quality and quantity of these dispersed phase particles, but by far the major factor in their formation was the level of vibration. Only at a mercury interface completely quiescent during the initial stages of electrodeposition was the gel structure developed with negligible iron in the dispersed state. Under normal conditions on a solid bench top roughly 0.002 g of iron per cm² of Hg surface was found in the dispersed state. The effect of increasing the vibration level during deposition is shown in Table III. These "intermediate" levels of surface vibration were insufficient to disrupt the formation of the gel structure although there was a noticeable decrease in quality. The quantity of iron found in the dispersed phase, under the gel structure, increased with vibration although the properties remained the same.

Table III. Effect of vibration on properties

Vibration level	Dispersed phase % of total iron deposited	Dispersed phase H_{ci}, oe	Dispersed phase B_r/B'_{is}	Gel phase T, mm	Gel phase H_{ci}, oe	Gel phase B_r/B'_{is}
Minimum	4.5	1380	0.58	0.47	1660	0.91
Intermediate	6.8	1330	0.575	0.45	1650	0.895
High	12.2	1380	0.615	0.45	1635	0.875

The saturation magnetization B'_{is} was measured in a field of 7000 oe. Magnetic properties measured at 76°K.

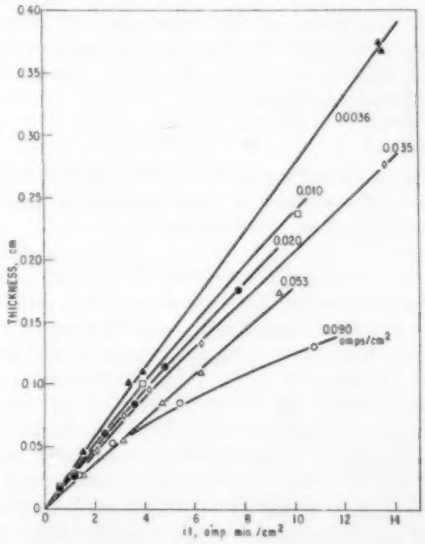

Fig. 6. Thickness of the gel structure as a function of the quantity of material deposited per cm² of mercury surface at different rates of deposition.

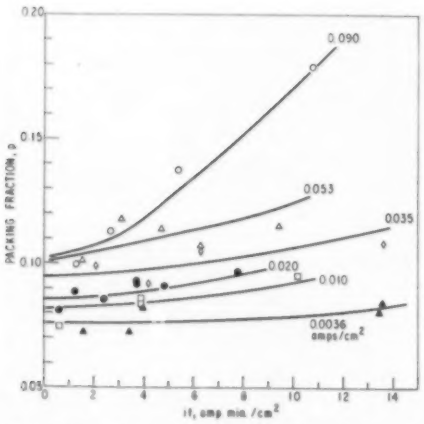

Fig. 7. Volume fraction of iron in the gel structure prepared at different rates and times of electrodeposition.

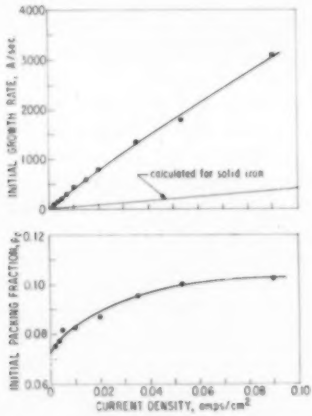

Fig. 8. Initial volume fraction and growth rate of the iron fibers in the gel.

The thickness of the gel structure depended on the quantity of iron deposited, the current density, and the time of deposition as indicated by the results in Fig. 6. The total iron deposited per cm² of mercury surface, assuming 100% cathode efficiency, is directly proportional to the current density i and the time of deposition t, and is given by

$$g = Eit/\mathbf{F} \qquad [4]$$

E is the equivalent weight of iron and $\mathbf{F}$ is Faraday's constant. The volume or packing fraction of iron can be calculated from the relation

$$p = (g - g_s)/\rho T \qquad [5]$$

where g_s is the grams of iron per cm² of mercury surface in the dispersed phase, ρ is the density of iron, and T the thickness of the gel structure. The value of g_s was determined directly by measurement of the magnetic saturation of an aliquot of the iron concentrated from the fluid mercury. The packing fractions calculated from the above relations are presented in Fig. 7 and the change in the initial packing in Fig. 8. This initial packing represents the state of the structure without the complications due to the effect of deposition time.

The growth rate of the iron fibers dl/dt is equal to the rate of increase in thickness of the gel dT/dt.

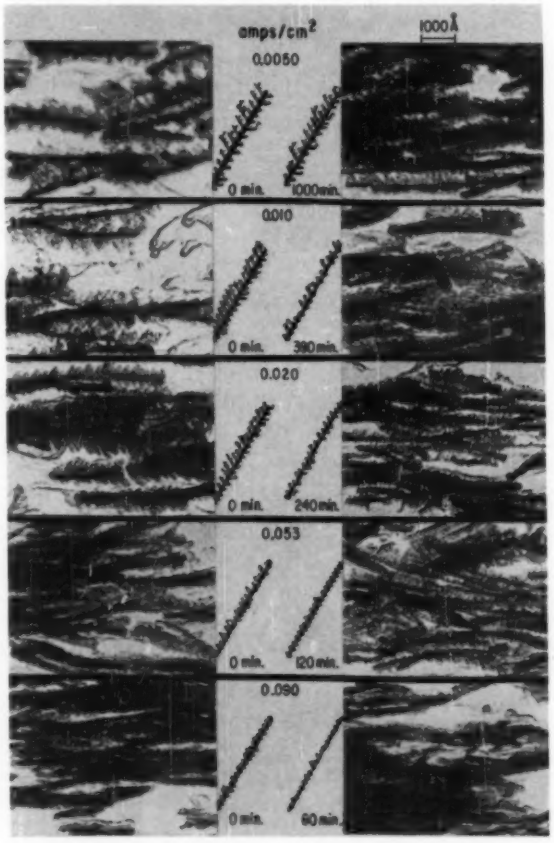

Fig. 9. Electron micrographs of particles in the gel structures formed at different current densities near the beginning of electrodeposition on the left, and after the times given on the right.

This growth rate in cm/sec depends on the number of growing fibers per cm² of surface n, and on the iron atom flux ϕ in cm³ of iron/cm² sec as given by the relation

$$dl/dt = \phi/nA = \phi/p \qquad [6]$$

where A is the average cross-sectional area of the growing fiber. The initial growth rates, from the initial slopes in Fig. 6, are also shown in Fig. 8 as a function of iron atom arrival rate. The rate of growth of the fibers decreased as the electrodeposition proceeded, especially at the higher currents as indicated in Fig. 6 by the departure from linearity. This change in dT/dt was accompanied by an increase in the packing fraction of iron in mercury and a decrease in the length of the side branches on the fibers with little or no change in the other dimensions of the fibers. Small sections of the microstructures of the gel obtained at different current densities are shown in Fig. 9 with a sketch of the appearance of a typical fiber. In the left column the micrographs were obtained from the bottom of the gel sheet near the beginning of deposition; on the right the micrographs were obtained from near the top of the gel sheet corresponding to the deposition times indicated. Measurement of the fiber dimensions from such micrographs are summarized in Fig. 10. The distance between branches s and the angle between the body

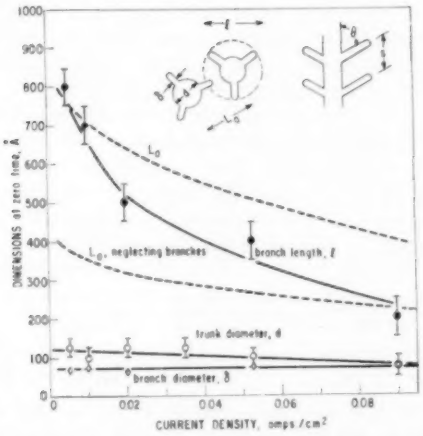

Fig. 10. Dimensions of the initial fiber structures. The distances between fibers given by the dashed curves were calculated using Eq. [7] and [8].

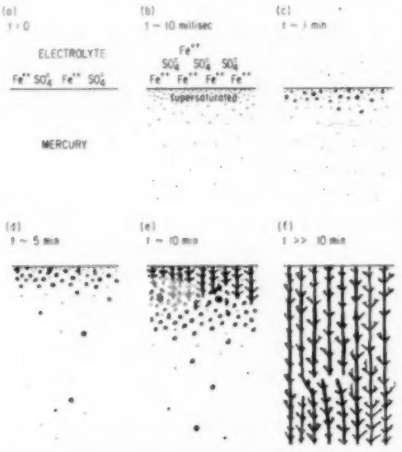

Fig. 11. Schematic representation of the sequence of steps in the formation of iron fibers in the gel structure at a current density of 0.01 amp/cm².

and branch θ were both constant over the range of current densities studied; $s = 150 \pm 25$Å and $\theta_{max} = 70 \pm 5°$. Many smaller angles were measured because of foreshortening of the image due to rotation of the fiber.

The effect of electrodeposition temperature on the formation of the gel has not been investigated. The effect of electrodeposition temperature on the structure of the particles in the gel has been reported previously (3).

The sequence of stages in the formation of the gel deduced from these observations are summarized schematically in Fig. 11. Electrodeposition at 0.01 amp/cm² was used as an example to indicate the approximate times required to attain the stages shown.

Particle properties.—The magnetic properties of particles are characterized most simply by their intrinsic coercive force at infinite dilution $H_{ci,o}$ and their remanence to saturation ratio B_r/B_{is}. The effect of current density and time of electrodeposition at room temperature on these properties of the gel are shown in the contour plots in Fig. 12 and 13. $H_{ci,o}$ was calculated from the measured $H_{ci,p}$ at a finite packing

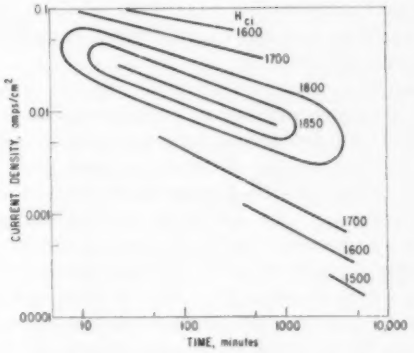

Fig. 12. Intrinsic coercive force of particles in the gel after an optimum aging, tin treatment, and alignment measured at 76°K and corrected to zero packing fraction.

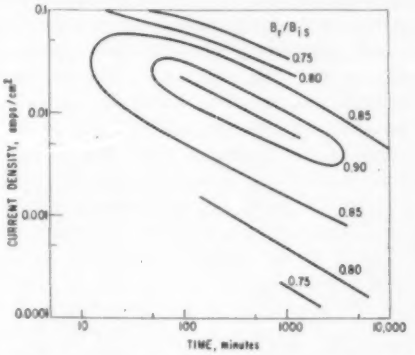

Fig. 13. Remanence to saturation ratio of particles in the gel after an optimum aging, tin treatment, and alignment measured at 76°K. Saturation magnetization was measured in a field of ~ 7000 oe.

from the relation $H_{ci,o} = H_{ci,p}/(1 - p)$. Similar elliptical contours were obtained for the particles before tin treatment and for the particles as deposited. The "as-deposited" fiber structures associated with these properties have been discussed and are shown in Fig. 9. The final particle sizes and shapes of samples along the ridge of maximum properties were of particular interest. The aging time-temperature exposure required to develop the optimum properties was found to vary systematically with electrodeposition current and particle composition. The relative particle shapes and diameter distributions were constant (2) while the average diameters varied from 130 to 305Å as the current was changed from 0.09 to 0.0025 amp/cm², respectively. Over this size range the $H_{ci,o}$ and B_r/B_{is} were also constant, in accord with a theoretical model for the behavior of particles with this irregular shape (2).

Particle Formation

Preliminary processes.—The initial process is the transport of hydrated iron ions through the electrolyte to the mercury-electrolyte interface under the influence of an electric field. A sequence of surface and electrical processes then occurs, resulting in the discharge of the iron ions to form iron atoms at the mercury surface. With proper electrode geometry and electrolyte purity this occurs uniformly over the entire mercury surface at a high rate; electro-

deposition currents between 0.001 and 0.1 amp/cm² correspond to iron atom arrival rates from 6×10^{15} to 10^{17} atoms/cm² sec.

Impurities, such as certain organic molecules, which absorb in patches on the mercury surface may alter the local ion arrival rate resulting in a nonuniform current density distribution over the mercury surface. Similarly, the formation of gas bubbles produced regions of low and high current density with the drastic results shown in Fig. 5. On the other hand the presence of inert electrolytes, for example K_2SO_4, which forms a $K^+ - SO_4^=$ double layer at the mercury interface, had no effect on the properties of the iron fibers even at concentrations up to 0.5M K_2SO_4; presumably the iron ions arrived at a uniform rate at all points on the mercury surface.

Particle nucleation.—In the initial stages of the electrodeposition the rapid influx of iron atoms could saturate the mercury cathode pool in a few hundred milliseconds. However, since the iron atoms diffuse relatively slowly, the surface of the mercury first becomes highly supersaturated as in Fig. 11(b). Iron atoms would require about 30,000 sec to diffuse to the bottom of the mercury pool. When the supersaturation reaches the critical nucleation concentration for iron in mercury, homogeneous nucleation occurs uniformly over the entire mercury interface region. These initial nuclei, containing only a few atoms, are vigorously kicked around by the kinetic energy of the surrounding mercury atoms or simply by gross motion of the mercury. Growth of these initial particles occurs uniformly, giving rise to the spherical particles observed in the "dispersed" phase as indicated in Fig. 11(c).

With continued electrodeposition the number of particles near the surface increases, increasing the "viscosity" of the medium and thus locking particles into a fixed position. When this condition is achieved no new nuclei form. Rather, the nuclei present continue to grow up toward the region of greatest supersaturation at the mercury-electrolyte interface as diagrammed in Fig. 11(e). Thus the number of fibers found in the final gel structure is equal to the number of initial nuclei held in a rigid position. The initial interparticle, or internucleus distance L_o, can be calculated as a function of current density from the packing fraction at zero time p_o and the particle dimensions. For example, if we consider the particles as rods all growing with a diameter d, and neglect the volume of the side branches it can be shown that for a hexagonal close packed array

$$L_o = \left(\frac{\pi}{4}\right)^{1/2} d/p_o^{1/2} \qquad [7]$$

Similarly if we consider the side branches

$$L_o = \left(\frac{\pi}{4}\right)^{1/2} [d^2 + (3\delta^2/2s)(l-d)]^{1/2}/p_o^{1/2} \qquad [8]$$

where s is the distance between branches, δ the diameter of branches, and $(l-d)/2$ the length of the side branches. The initial interparticle distances calculated from these relations, using smoothed values of the particle dimensions reported in Fig. 10, are shown in the same figure as a function of current density. It can be inferred from the correspondence between the total dendrite spread l and the interparticle distance that the length of the side branches is limited by the internucleus distances; the low volume fraction of iron represents a close packed array of dendritic particles.

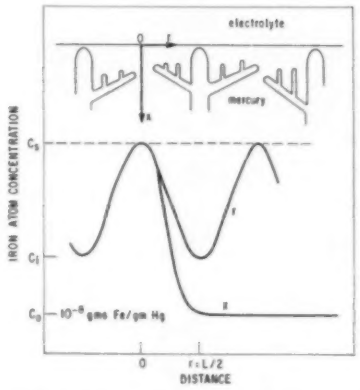

Fig. 14. Iron atom concentrations in the mercury during fiber growth where C_o is the equilibrium solubility of iron in mercury, c_i is the concentration maintained by the influx of atoms and depleted by condensation at the growing tip, and c_s is the critical supersaturation above which nucleation will occur. L is the distance between fiber centers.

After the initial nuclei deplete the mercury of supersaturated iron atoms in their vicinity, atoms subsequently arriving at the mercury interface diffuse the short distance to the growing particle surfaces before the concentration between nuclei reaches the critical concentration for homogeneous nucleation. Thus at each current density, or iron atom arrival rate, an equilibrium is established between the diffusion of iron atoms through the mercury to a growing particle and the buildup of supersaturation between particles. This equilibrium controls the interparticle distance. As deposition proceeds the continuing downward influx of iron atoms from the electrolyte promotes unidirectional growth of the existing fibers, resulting in the typical dendritic structure associated with the rapid growth of crystals into regions of high supersaturation. A possible model and boundary conditions for this diffusion and growth problem is shown in Fig. 14, but a quantitative solution has not been attempted.

At very high current densities even some of the initial particles found in the "dispersed" phase show some degree of elongation because of the very rapid growth; the disturbances giving rise to spherical particles become short in comparison to the growth rate of the fibers. As the current density approaches zero, the packing fraction of iron in the gel phase approaches a lower limit corresponding to the minimum packing for the formation of the solid gel. The supersaturation cannot reach the value needed for growth of dendrites because of the rapid diffusion of atoms away from the surface.

Growth during electrodeposition.—After the initial nucleation processes the remainder of the development of the gel phase is due entirely to growth of existing fibers. The particles are maintained within the mercury phase by the interfacial energy between

the iron and mercury. The iron particles are wet by the mercury. No new nuclei form unless the system is disturbed, for example by mechanical vibration, absorption of impurities at the mercury interface, or by development of gas bubbles on the mercury surface. In the case of absorption of impurities or bubble formation the iron fibers under these areas stop growing while the adjacent fibers receive an increase in the rate of arrival of iron atoms. New nuclei must then be generated with internuclear distances corresponding to equilibrium with the higher and lower arrival rates of iron atoms. As a result, a wide range of particle sizes and structures are produced.

Changes in the structure of fibers, and thus the ultimate magnetic properties, as the gel increases in thickness are accounted for in terms of the gradual change in the environment of the fiber at its growing tip. Two effects may influence this environment: the flow of mercury through the gel and the buoyancy of the gel.

We can consider the iron fibers already deposited as making up a network of very irregularly shaped capillaries. Thus the size of the capillaries, the number open, and their length are the major factors controlling the rate of flow of mercury to the growing tip at the surface. The static height to which mercury can be drawn up in these iron capillaries was estimated, assuming the contact angle is zero, from the relation

$$h = 2\gamma/Gr\rho_{Hg} \qquad [9]$$

to be in the order of 10,000 cm, assuming uniform 200Å radius capillaries r and using the interfacial tension γ between iron and mercury as 400 dynes/cm. Thus it is not likely that the limiting factor in the observed changes is the ability of the mercury to rise through the 0.2 cm long channels unless many of the capillary channels are closed off.

The flow of mercury through the channels can be estimated from the Poiseuille equation. The linear flow per sec through an assumed cylindrical capillary channel is

$$v = r\gamma/4T\eta \qquad [10]$$

where η is the viscosity of mercury. Again for a capillary length T of 0.2 cm the rate of flow is estimated to be 0.025 cm/sec or a factor of 10^4 faster than is required by the growth of the iron fibers. It is not likely that the tortuosity of the channels can reduce this estimate sufficiently to make the flow of mercury through the gel a limiting factor.

The buoyant force of the gel increases linearly with time and is given by $GV(\rho_{Hg} - \rho) \cong 3 \times 10^{-6}$ dynes for 200Å diameter particles 0.2 cm long. This is very small compared to the maximum force required to push an iron fiber through the mercury interface, $2\pi r\gamma \cong 3 \times 10^{-5}$ dynes, but sufficient to perturb the smoothness of the mercury surface. A rough estimate can be made of the angle ψ resulting from the surface tension γ of the mercury trying to straighten out the surface and the buoyancy of the iron fiber trying to poke through the surface. At equilibrium

$$2\pi r\gamma \sin\psi = GV(\rho_{Hg} - \rho) \qquad [11]$$

Assuming an effective channel radius $r = 200$Å and a particle volume V corresponding to a 200Å diameter rod 0.2 cm long where G is the gravitational acceleration, we find $\sin\psi \cong 10^{-6}$. This small value indicates an essentially smooth surface of mercury at this stage in the growth of the gel. This is confirmed experimentally by the still bright appearance of the surface. However the buoyant force increases linearly with time while the surface energy remains constant, thus $\sin\psi$ slowly increases. Experimentally the mercury surface is observed to take on a dry appearance gradually, indicative of increasing roughness. In the model shown in Fig. 14 this increasing bouyant force decreases the thickness of the mercury film at the growing tip making the already sharp concentration gradient from the mercury electrolyte interface to the iron-mercury interface even sharper as the gel increases in thickness. This appears to be the most likely explanation for the effect of electrodeposition time on the structure of the fibers and thus their ultimate magnetic properties.

Conclusions

The sequence of events leading to a gel of elongated iron or iron-cobalt fibers in mercury has been deduced from magnetic and microscopic examination as summarized schematically in Fig. 11. The initial nucleation step is followed by a growth process resulting in dendritic fibers of any desired length. It is inferred that the growth of the fibers is controlled by the iron atom concentration gradient between the mercury-electrolyte interface and the surface of the iron fibers. The gradient is primarily a function of the electrodeposition current density and, to a lesser degree, it is a function of the amount and structure of the previously deposited iron. The magnetic properties obtained after optimum aging, metal treatment, and alignment are a function of the conditions of formation of the gel which control the initial particle structure and distribution of structures.

Acknowledgments

The assistance of B. J. Drummond in carrying out the experimental work and E. F. Koch in obtaining the electron micrograph is greatly appreciated.

Manuscript received June 7, 1961. This paper was prepared for delivery before the Indianapolis Meeting, April 30-May 3, 1961.

Any discussion of this paper will appear in a Discussion Section to be published in the June 1962 JOURNAL.

REFERENCES

1. For a recent discussion see "Ferromagnetic Domain Theory," C. Kittel and J. K. Galt in "Solid State Physics," vol. 3, F. Seitz and D. Turnbull, Editors, Academic Press Inc., New York (1956).
2. F. E. Luborsky, *J. Appl. Phys.*, **32**, 171S (1961).
3. F. E. Luborsky, T. O. Paine, and L. I. Mendelsohn, *Powder Metallurgy*, No. 4, 57 (1959).
4. R. B. Falk, G. D. Hooper, and R. J. Studders, *J. Appl. Phys.*, **30**, 132S (1959).
5. A. L. Oppegard, F. J. Darnell, and H. C. Miller, *ibid.*, **32**, 184S (1961).
6. F. P. Levi, *Nature*, **183**, 1251 (1959); *J. Appl. Phys.*, **31**, 1469 (1960).

7. R. B. Campbell, U. S. Pat. 2,879,154, March 24, 1959.
8. J. H. L. Watson and M. W. Freeman, *Proc. Conf. on Magnetism and Magnetic Materials*, 1955 AIEE Spec. Publ. T-78, p. 150; 1956 Conf. T-91, *Kolloid Z.*, **148**, 3 (1956).
9. R. W. Fabian and J. L. Sienczyk, U. S. Pat. 2,884,-319, April 28, 1959.
10. C. D. Coxe, U. S. Pat. 2,967,794, Jan. 10, 1961.
11. W. Wright, *Powder Metallurgy*, No. 4, 79 (1959).
12. T. Kawaguchi, M. Nagakura, T. Yamaguchi, and I. Tanabe, *Nippon Kinzoku Gakkaishi*, **23**, 429 (1959); **24**, 585 (1960).
13. F. E. Luborsky and T. O. Paine, *J. Appl. Phys.*, **31**, 68S (1960).

Cation Diffusion in Cr_2O_3

W. C. Hagel and A. U. Seybolt

Research Laboratory, General Electric Company, Schenectady, New York

ABSTRACT

On employing a sectioning technique with Cr^{51} as the tracer, the diffusion of Cr ions in nitrogen-equilibrated Cr_2O_3 was determined from 1045° to 1550°C. Volume diffusion coefficients in hot-pressed compacts of three different impurity levels conform to the expression $D = 0.137 \exp(-61{,}100/RT)$ cm^2sec^{-1}. Additions of 2 w/o CeO_2 and 1 w/o Y_2O_3 do not cause a significant change. Use of lower density sintered compacts provides erroneous results. Conductivity measurements were performed in nitrogen, argon, and air over a wide temperature range; no dependence on oxygen partial pressure was observed. Calculated cation transference numbers vary from 10^{-3} to 10^{-4}. Postulating a simplified model for the defect structure of Cr_2O_3, the activation enthalpy for hole motion is 8.4 kcal $mole^{-1}$; the enthalpy of defect formation is 91 kcal $mole^{-1}$; the activation enthalpy for cation motion is about 31 kcal $mole^{-1}$.

Although studies of cation diffusion in spinels and in oxides with the NaCl structure are becoming more numerous, relatively little attention has been directed at oxides possessing the corundum structure, *e.g.*, V_2O_3, Ti_2O_3, α-Fe_2O_3, α-Al_2O_3, and Cr_2O_3. The latter effort is of twofold importance for an understanding of the role of lattice defects in asymmetric compounds and for establishing what is rate controlling during oxidation of the parent metal. The surface location of markers after oxidizing pure Fe and Al shows that α-Fe_2O_3 and α-Al_2O_3 grow primarily by the inward diffusion of anions; Kingery and co-workers (1, 2) have determined high self-diffusion rates for oxygen in these bulk oxides. Contrastingly, Seybolt (3) found platinum markers covered by Cr_2O_3 in Fe-20% Cr and Fe-30% Cr alloys to indicate that this oxide grows almost entirely by the outward diffusion of cations. Presumably, the same applies during the oxidation of pure Cr and Cr-base alloys, whenever only Cr_2O_3 is formed, with anion diffusion playing an insignificant part in the reaction.

Using sintered compacts of α-Fe_2O_3, Lindner (4) reported that Fe self-diffusion coefficients fit the Arrhenius expression $D = D_o \exp(-\Delta H^*/RT)$ where the frequency factor D_o equals 4×10^5 cm^2 sec^{-1} and the "activation energy" ΔH^* equals 112 kcal $mole^{-1}$. From six datum points, Lindner and Åkerström (5) have shown that D_o equals 4×10^3 cm^2 sec^{-1} and ΔH^* equals 100 kcal $mole^{-1}$ for Cr diffusion in sintered compacts of commercial-purity Cr_2O_3. Similar data were obtained at the same time for Ni diffusion in NiO, but further work (6, 7) has shown that the best relationship for this case is $D = 0.24 \exp(-62{,}000/RT)$ cm^2 sec^{-1}. The initial results for Cr in Cr_2O_3 remain uncorroborated, and the measurement is worth repeating with careful emphasis on controlling the variables of atmospheric equilibrium, minor oxide impurities, and compact density. Since scattered reports (8, 9) indicate that rare earth additions may inhibit the parabolic oxidation of Cr, another purpose of the study was to determine whether a substantial reduction in cation diffusion occurs on adding CeO_2 and Y_2O_3 to Cr_2O_3.

The crystal structure of Cr_2O_3 can best be visualized as a slightly distorted hexagonal close packing of fixed oxygen ions with chromium ions residing in the interstices; DiCerbo and Seybolt (10) found the hexagonal lattice parameters to be $a_o = 4.9591$Å and $c_o = 13.599$Å at 20°C. Chemical analyses of Cr_2O_3 usually disclose that the chromium content is somewhat less than the 68.4% expected for a pure stoichiometric compound; Michel and Bénard (11) have set the lower solubility limit at 67.6% Cr. From conductivity measurements up to 800°C, Hauffe and Block (12) noted Cr_2O_3 to possess a smaller dependence on oxygen partial pressure than would be expected for a metal-deficit p-type semiconductor. Fischer and Lorenz (13, 14) observed an abrupt change in slope at about 1250°C for curves of thermoelectric power and resistivity *vs.* temperature; they suggest that Cr_2O_3 is p-type below the change and intrinsic above. However, a wholly satisfactory description of the defect structure of Cr_2O_3 has not been established.

Experimental

Sample preparation.—The types of oxide powders used, sources of supply, and chemical analyses are listed in Table I. No trace elements in addition to

Table I. Composition of oxide powders

Type	Source of supply	Chemical analyses, weight %		
Cr_2O_3 (A)	Fisher Scientific Co.	99.0 Cr_2O_3 0.30 H_2O 0.22 S	0.04 Fe 0.01 Al 0.001 Cu 0.01 Si	0.005 Mg 0.002 Ca 0.003 Na
Cr_2O_3 (B)	C. K. Williams and Co.	99.3 Cr_2O_3 0.20 H_2O 0.14 S	0.06 Fe 0.01 Al 0.002 Cu 0.01 Si	0.005 Mg 0.003 Ca 0.001 Na
Cr_2O_3 (C)	C. K. Williams and Co.	99.7 Cr_2O_3 0.20 H_2O 0.05 S	Fe, Al, Cu, Si, Mg—trace Ca, Na—sl. trace	
CeO_2	American Potash and Chemical Corporation	99.9+ CeO_2		
Y_2O_3	American Potash and Chemical Corporation	99.9 Y_2O_3 <0.1 Dy_2O_3 Gd_2O_3 Tb_4O_7		

those mentioned were detected by qualitative emission spectroscopy. All pure powders, or mixtures thereof, were initially ball milled for 2 hr and dried with infrared heat for 12 hr. About 30 g of each mixture were prepressed in a ⅞-in. graphite die, using a pressure of 2000 psi. A few of these cold-pressed compacts were sintered in argon for 2 hr at 1700°C. Most of them were positioned in a 1-in. graphite die and surrounded by 100/150-mesh Al_2O_3 for an optimum hot-pressing treatment. After many test runs, a pressure on the compact of 5000 psi for 15 min at 1600°C was found to give maximum sample density. The surrounding layer of Al_2O_3 was used to minimize carbon absorption and chemical reduction from the graphite die during hot pressing in air; it was loose and could be removed by abrasion. To relieve hot-pressing stresses and prevent warpage during subsequent diffusion anneals, the rough compacts were heated for 24 hr at 1575°C in a pure, dry nitrogen atmosphere. The same atmosphere was also used during diffusion anneals, since Cr_2O_3 is known (15) to be volatile above about 1100°C, possibly owing to the formation of gaseous CrO_3.

The hard ⅞-in. diameter x ⅞-in. long compacts were reduced in size to cylindrical diffusion cylinders by centerless grinding to ¾-in. diameter and by grinding the faces flat and parallel at about ¾-in. apart. To conserve the number of acceptable compacts, one finely ground cylinder would be used for several diffusion anneals first at low and then at higher temperatures, after removing all traces of the previous run. Pycnometric densities of the hot-pressed cylinders varied from 5.12 to 5.21 g cm^{-3} for Cr_2O_3(A, B, and C). Addition of 2.0 w/o (1.8 mole %) CeO_2 caused little change in density, but addition of 0.5 and 1.0 w/o (0.34 and 0.67 mole %) Y_2O_3 decreased sample density to 5.10 and 5.03 g cm^{-3}, respectively. Sintered compact densities were less constant and varied from 4.50 to 4.90 g cm^{-3}. Applying the aforementioned hexagonal lattice parameters for Cr_2O_3, the calculated theoretical density is 5.23 g cm^{-3}, and so it can be seen that sintering and hot pressing provide compact densities approaching 93.7 and 99.5% of the theoretical limit. Typical microstructures comparing the two, as well as a hot-pressed sample containing 1.0 w/o Y_2O_3, are shown in Fig. 1. While some surface crumbling must have occurred during mechanical polishing, note the far less perfect bonding and higher porosity obtained by cold pressing and sintering. Owing to the slightly reducing atmosphere of hot pressing, some chromium metal was usually present in chemically determined amounts of 0.1-0.2 w/o. The Y_2O_3-containing compacts may still have some free Y_2O_3, although none was detected by x-ray phase identification. In the hot-pressed compacts, an average grain size of 0.05-0.10 mm was measured. While not extremely large, this is probably coarse enough to avoid the complications of grain-boundary diffusion in oxide compacts. Within the sensitivity of autoradiographs to the radioactivity of Cr^{51}, no increased darkening was observed at grain boundaries to give evidence of preferred tracer penetration. Shim and Moore's (7) comparison of cation diffusion coefficients in single crystal and polycrystalline NiO showed little or no grain-boundary diffusion. Similarly, the measurements of Himmel *et al.* (16) on single crystals of hexagonal α-Fe_2O_3 uncovered no dependence on crystal orientation, and it is believed that, within experimental error, the same may be said for Cr_2O_3.

Evaporation and annealing.—Radioactive Cr^{51}, a soft x-ray and gamma emitter with a half life of 27.8 days, was obtained from the Oak Ridge National Laboratory in the form of a 0.5 ml dilute HCl solution of $CrCl_3$ whose level of activity was about 13 millicuries. The tracer is best deposited on Cr_2O_3 compacts by vacuum evaporation from a tungsten coil plated with a 4300:1 metallic coating of $Cr:Cr^{51}$. Since the coil dimensions (20 mil wire, 0.4 cm diameter x 2.5 cm long) required a minimum plating solution of 10 ml, 1.25 g of nonradioactive CrO_3 were added, along with 13 mg H_2SO_4 and 10 ml H_2O, to the tracer made hexavalent by drying and oxidizing with perchloric acid. About 10 mg of chromium could be electroplated on each coil within 10 min by using dry-cell batteries and a current of 0.6 amp. On maintaining a vacuum of 10^{-4} to 10^{-5} mm Hg in the evaporation chamber, the plated coils were brought to

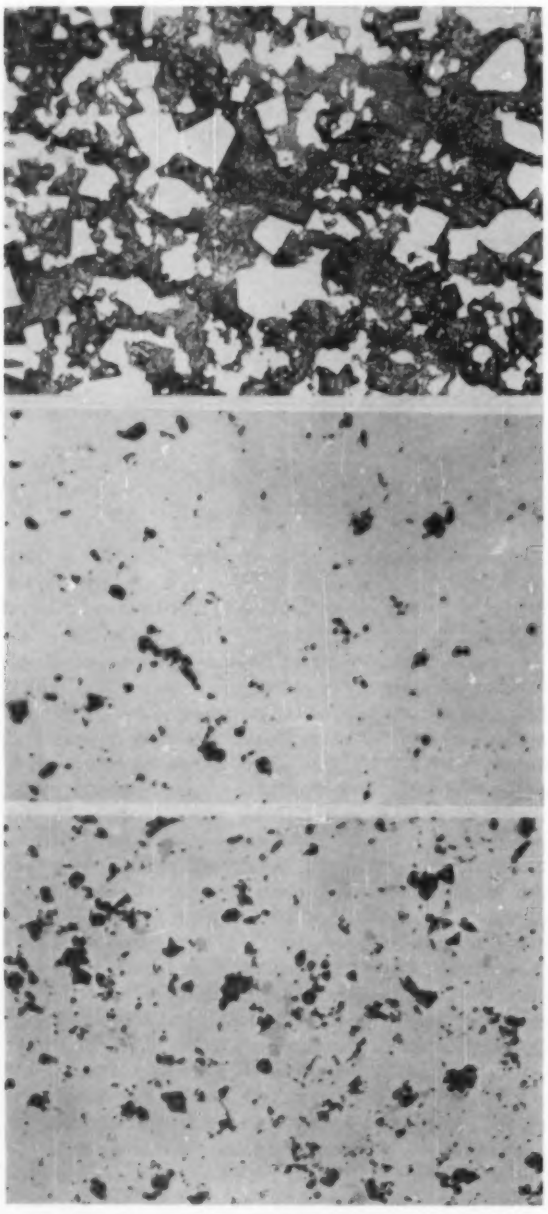

Fig. 1a. (top) Cr_2O_3 (A) compact sintered for 2 hr at 1700°C in argon; Fig. 1b. (center) Cr_2O_3 (A) compact held for 15 min at 1600°C under a pressure of 5000 psi; Fig. 1c. (bottom) Cr_2O_3 (A) + 1.0 w/o Y_2O_3 compact held for 15 min at 1600°C under a pressure of 5000 psi. As polished with diamond dust. Magnification 500X before reduction for publication.

about 1600°C by a surrounding conical heater for a time of 5-10 min. Possibly only a third of the chromium evaporated actually reached the sample face, but enough was deposited to give an initial unfiltered counting rate (after diffusion) of at least 6000 counts min^{-1}. After cooling, the sample was removed from the chamber, placed in alumina containers, and positioned in the 2-in. constant temperature zone of a Pt-40% Rh resistance furnace. To ensure complete oxidation of the few hundred angstroms thick evaporated film to chromium cations, the sample was first heated for 30 min at 1000°C in oxygen. This atmosphere was removed by evacuation; the furnace interior was filled with nitrogen, and the sample was quickly taken from 1000°C to the desired diffusion temperature. Here temperatures from 1045° to 1550°C, as measured by a calibrated Pt/Pt-10% Rh thermocouple located near the tracer interface, were maintained constant within ±5C° for times up to 168 hr. Annealing was ceased by turning off the furnace and slowly removing the samples out of hot zone while they were still under a nitrogen atmosphere. Slow withdrawal was necessary to avoid thermal-shock cracking of both the ceramic furnace tube and the oxide samples.

Sectioning.—Penetration curves were determined by measuring the radioactivity remaining in the sample after thin end sections had been removed. The hardness of hot-pressed cylinders required that surface grinding be done by a multi-diamond tool silver-soldered within a nickel tube. Each diffusion cylinder was mounted exactly 90° to the central axis of a precision lathe; then a rough diamond tool would remove a 0.07-in. layer from the cylindrical surface to eliminate any surface-diffusion effects. Chips and dust were captured by suction to prevent room contamination. A fixed-position dial gauge was used to measure the thickness of sections ground from the radioactive face. These were varied from 0.0002 to 0.0020 in., and measurements of total cylinder length before and after all sections had been removed showed close agreement with the sum of dial-gauge readings. A reproducible counting geometry was maintained by placing the counter on the tool mount so that it could be brought in line with the lathe axis after each section was removed. Plastic positioning cups, without and with an aluminum absorber for soft x-rays, kept the mica counter window a constant distance (⅛ in.) from the sample face. Counting rate was digitally recorded using a Nuclear-Instrument autoscaler with a dual timer.

Data reduction.—For a sectioning technique which measures residual activity I after removing a section of thickness x, Gruzin (17) has derived the appropriate Fick's law expression

$$I - \frac{1}{\mu}\frac{\partial I}{\partial x} = \frac{K}{\sqrt{\pi Dt}} \exp\left(-x^2/4Dt\right) \qquad [1]$$

where μ is the linear absorption coefficient, D is the diffusion coefficient, and t is the time of isothermal diffusion. The I used here is the difference in counts min^{-1} measured with and without a soft x-ray absorber, i.e., it is the soft x-ray residual activity which is wanted; no background correction is necessary. Equation [1] is independent of partial loss of the isotope through evaporation or spalling and only requires that the diffusion sample possesses a relatively high μ for a simple solution. The low energy (0.005 mev) of soft x-rays from Cr^{51} implies a high μ. Depending on initial sample activity and the accuracy required, I varied from 5000 to 10 counts min^{-1}. This low level of activity and a low tube dead time (~100 μsec) for the Anton mica-window counter used did not require correcting for coincidence at a plateau voltage of 1275 v. However, since

the half life of Cr^{51} is fairly short, decay corrections employing the relationship

$$N_o = \frac{N}{e^{-\lambda t'}} \qquad [2]$$

were applied whenever a series of counts extended over 8 hr. Here N is the actual experimental count, λ is 2.49 x 10^{-2} days $^{-1}$, t' is the decay time in days, and N_o is the corrected initial activity. With the source, counter tube, and geometry chosen, the counts through a series of 1.73 to 210 mg cm^{-2} Al absorbers, corrected for air-mica absorption and background radiation, showed that a 0.005-in. Al sheet would absorb all soft x-ray radiation effectively. For Cr^{51}, this should be the $K\alpha_0$ radiation of vanadium of wavelength 2.502Å. From Compton (18), the mass absorption coefficient μ/ρ for Al at this wavelength is 193 cm^2 g^{-1}; all absorption-data plots of I *vs.* ρd, where ρ is absorber density and d is its thickness, provided slopes (μ/ρ) ranging from 190 to 193.5 cm^2 g^{-1}.

The linear absorption coefficient for Cr_2O_3 was approximated from the relation

$$\mu = \rho(115\, f_{Cr} + 45.5\, f_o) \qquad [3]$$

where 115 and 45.5 are the x-ray values for the mass absorption coefficients for Cr and O at a wavelength of 2.502Å, and f_{Cr} and f_o are the weight fractions of Cr and O in Cr_2O_3. Values of μ varying from 418 to 484 cm^{-1} for the sintered and hot-pressed compacts, respectively, were used in solving for D from Eq. [1]. Although Eq. [3] provides only a fair determination of μ, D is rather insensitive to μ as long as the latter value is relatively large. To a first approximation, one can assume that I in Eq. [1] is

$$>> \frac{1}{\mu}\frac{\partial I}{\partial x}$$ and write

$$I = K' \exp(-x^2/4D't) \qquad [4]$$

Then, on plotting ln I *vs.* x^2, a straight line of slope $(-1/4D't)$ should result for volume diffusion. For all plotted penetration curves, this assumption was found to hold true; yet, a more exact determination of D comes from evaluating $1/\mu\ \partial I/\partial x$. This is achieved by differentiating Eq. [4] and substituting particular values of I and x into the relation

$$\frac{\partial I}{\partial x} = \frac{-x}{2D't} I \qquad [5]$$

One can now plot ln $(I - 1/\mu\ \partial I/\partial x)$ *vs.* x^2 to get a new corrected slope and a better value for D. The procedure can be repeated if necessary, although further reiteration was found to give a negligible change in D.

Other Measurements.—After powdering in air, chips from several compacts were checked before and after diffusion for changes in composition and lattice parameters. A few were given a variety of heat treatments in wet and dry hydrogen atmospheres to learn whether significant changes could occur.

While it was not the main purpose of this investigation to conduct conductivity studies, one of the hot-pressed high-purity Cr_2O_3(C) diffusion cylinders

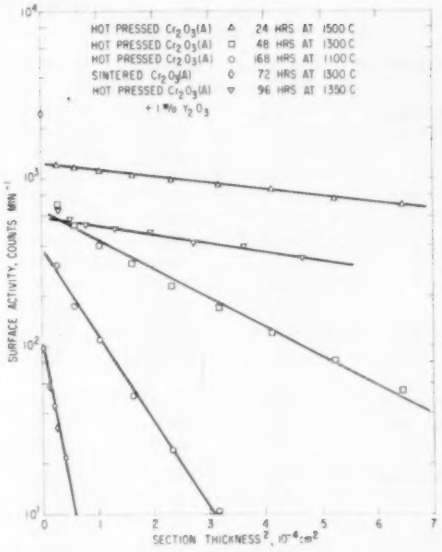
HOT PRESSED Cr2O3(A) △ 24 HRS AT 1500 C
HOT PRESSED Cr2O3(A) □ 48 HRS AT 1300 C
HOT PRESSED Cr2O3(A) ○ 168 HRS AT 1100 C
SINTERED Cr2O3(A) ◇ 72 HRS AT 1300 C
HOT PRESSED Cr2O3(A) ▽ 96 HRS AT 1350 C
+1 w/o Y2O3
SURFACE ACTIVITY, COUNTS MIN⁻¹
SECTION THICKNESS², 10⁻⁴ cm²

Fig. 2. Representative penetration curves for the diffusion of ionized Cr^{51} in various nitrogen-equilibrated Cr_2O_3 compacts.

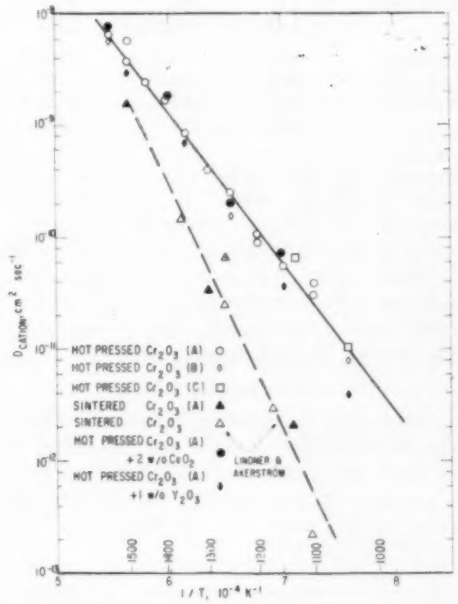

Fig. 3. Plot of D_{cation} vs. 1/T for various Cr_2O_3 compacts

was coated with platinum at both ends and given two circumferential grooves for the positioning of 4 electrodes. Use of the 4-electrode method for measuring sample resistance as a function of temperature was thought advisable for the elimination of any contact-resistance effects. These measurements sought to uncover how much confidence could be placed in previous 2-electrode conductivity studies where a significant oxygen partial pressure dependence was not observed. The sample was positioned in the hot zone of a vertical Pt-40% Rh furnace with a Pt/Pt-10% Rh thermocouple located at its midpoint. The surrounding atmospheres were flowing nitrogen, flowing argon, and static air. On passing a

Table II. Summary of diffusion data

Compact type	Sample No.	Time, hr	Temp, °C	D', $cm^2\ sec^{-1}$	D, $cm^2\ sec^{-1}$	ln D	$1/T \times 10^{-4} K^{-1}$
Hot-pressed Cr_2O_3 (A)	25	19.0	1550	6.21×10^{-9}	6.60×10^{-9}	−18.8362	5.48
	4	24.0	1500	3.30×10^{-9}	3.71×10^{-9}	−19.4123	5.64
	47	24.0	1500	4.94×10^{-9}	5.76×10^{-9}	−18.9724	5.64
	12	24.5	1450	2.22×10^{-9}	2.44×10^{-9}	−19.8313	5.81
	1177	24.0	1400	1.52×10^{-9}	1.70×10^{-9}	−20.1927	5.98
	37	72.0	1350	7.65×10^{-10}	8.64×10^{-10}	−20.8695	6.16
	2	48.0	1300	3.65×10^{-10}	4.02×10^{-10}	−21.6346	6.36
	31	96.0	1250	2.28×10^{-10}	2.50×10^{-10}	−22.1096	6.56
	48	96.0	1200	9.23×10^{-11}	1.07×10^{-10}	−22.9582	6.79
	1178	96.0	1200	7.80×10^{-11}	8.82×10^{-11}	−23.1515	6.79
	33	96.0	1150	4.73×10^{-11}	5.55×10^{-11}	−23.6147	7.03
	17	120.0	1100	2.71×10^{-11}	3.09×10^{-11}	−24.2003	7.29
	34	168.0	1100	3.48×10^{-11}	3.95×10^{-11}	−23.9548	7.29
Hot-pressed Cr_2O_3 (B)	70	20.0	1550	4.94×10^{-9}	5.69×10^{-9}	−18.9846	5.48
	59	96.0	1250	1.21×10^{-10}	1.55×10^{-10}	−22.5876	6.56
	96	168.0	1050	5.82×10^{-12}	7.84×10^{-12}	−25.5719	7.59
Hot-pressed Cr_2O_3 (C)	365	144.0	1150	4.96×10^{-11}	5.53×10^{-11}	−23.6183	7.03
	388	240.0	1045	9.02×10^{-12}	1.04×10^{-11}	−25.2893	7.59
Sintered Cr_2O_3 (A)	227	24.0	1500	7.94×10^{-10}	1.58×10^{-9}	−20.2659	5.64
	327	72.0	1300	2.33×10^{-11}	3.40×10^{-11}	−24.1047	6.36
	229	168.0	1135	1.46×10^{-12}	2.09×10^{-12}	−26.8939	7.10
Hot-pressed Cr_2O_3 (A) + 2 w/o CeO_2	76	20.0	1550	5.56×10^{-9}	7.73×10^{-9}	−18.6782	5.48
	172	24.0	1400	1.39×10^{-9}	1.78×10^{-9}	−20.1467	5.98
	115	84.0	1250	1.64×10^{-10}	2.00×10^{-10}	−22.3328	6.56
	194	168.0	1154	5.94×10^{-11}	7.08×10^{-11}	−23.3712	7.01
Hot-pressed Cr_2O_3 (A) + 1 w/o Y_2O_3	256	24.0	1500	2.58×10^{-9}	2.97×10^{-9}	−19.6347	5.64
	324	96.0	1350	6.05×10^{-10}	6.97×10^{-10}	−21.0843	6.16
	329	144.0	1150	3.21×10^{-11}	3.66×10^{-11}	−24.0320	7.03
	308	240.0	1045	2.83×10^{-12}	3.87×10^{-12}	−26.2778	7.59

known current between the two end electrodes, the potential drop between the two inner electrodes was determined by a high-resistance voltmeter. This provided a sample resistance value convertible to conductivity after measuring contact dimensions. Equilibrium temperatures were controlled by hand adjustments on a variac, and about 30 min of holding time were used for each datum point.

Results

Representative penetration curves of counts min^{-1} *vs.* section thickness squared are plotted in Fig. 2. These data are uncorrected for self absorption in Cr_2O_3 and, according to Eq. [4], permit only a determination of D'. One can see that they define a straight line whose slope gives a good approximation of D for each diffusion time and temperature. In all cases $1/\mu\ \partial I/\partial x$ was also evaluated and a final plot of ln $(I - 1/\mu\ \partial I/\partial x)$ *vs.* x^2 was used for a more exact D value. Table II gives the D' and D values determined in this manner for the various oxide samples; in addition, ln D and $1/T$ values are listed for a least-squares analysis. Figure 3 shows a plot of these experimental data in comparison with the data for cation diffusion in sintered Cr_2O_3 compacts obtained by Lindner and Åkerström (5). Diffusion results on sintered compacts of Cr_2O_3(A) fall about an order of magnitude lower, confirming to some extent the earlier work. Yet, it does not appear that sintered compacts provide a reliable determination, presumably owing to the more tortuous diffusion path available.

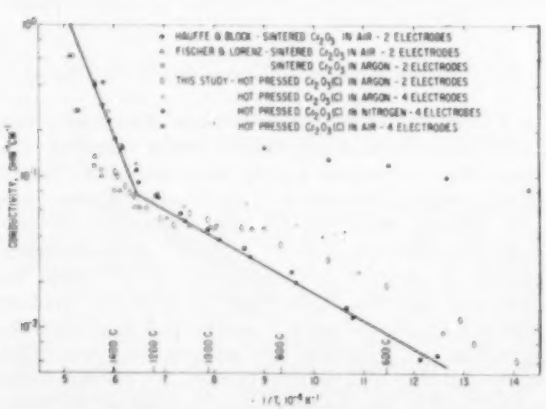

Fig. 4. Conductivity vs. 1/T of hot-pressed Cr_2O_3 as determined in this study and compared with previous measurements.

The sum of possible errors in measuring composition, radiation, section thickness, time, and temperature for each D value is estimated to be between 10 and 15%. This was confirmed by several repeat runs, although in a few cases greater deviations were observed for some unknown reason. The largest errors may result from small variations in compact density from outer edge to center and from the exact determination of absolute diffusion temperature. On occasion, there may have been unobserved large furnace-temperature variations over long diffusion intervals. Penetration curves for diffusion coefficients below 10^{-11} $cm^2\ sec^{-1}$ had to be drawn through only 5 or 6 points of 0.0002-in. section thickness. At high temperatures above about 1350°C, it was noted that some surface evaporation of the tracer and oxide oc-

curred to give initially erratic counts, but the subsequently deeper penetration permitted much better curve definition. Within experimental accuracy, there was no difference in the data for hot-pressed compacts of Cr_2O_3(A, B, and C) where minor impurities possessing 1+ and 2+ valence states could play a role. A least-squares line through this family of points can be expressed as

$$D = 0.137 \exp(-61{,}100/RT) \text{ cm}^2 \text{ sec}^{-1} \quad [6]$$

Although the diffusing cation is believed to possess the 3+ valence state, there was no way of detecting whether Cr cations with other valence states, *e.g.*, 2+, 4+ or 6+, were also diffusing. The maximum probable errors in D_o are ± 0.8 cm^2 sec^{-1}, and in ΔH^* they are ± 5.0 kcal mole^{-1}. Diffusion coefficients in hot-pressed compacts of Cr_2O_3(A) to which 2.0 w/o CeO_2 had been added show essentially no change from those for compacts containing only Cr_2O_3. Addition of 1.0 w/o Y_2O_3 caused a small decrease in D values, but, considering the lower density of these compacts, the decrease does not appear significant.

The composition of hot-pressed and sintered Cr_2O_3 compacts treated in a variety of atmospheres appeared to remain essentially constant at 67.5 ± 0.2% Cr. Their lattice parameters all were within $a_o = 4.957 \pm 0.002$Å and $c_o = 13.597 \pm 0.002$Å at 20°C. Whatever changes occur as a function of oxygen partial pressure must be very small, although some of this uniformity may have been caused by the unavoidably similar processing of sample powders for analysis. It seems likely that the hot-pressed compacts, which contained a small amount of reduced free chromium, would possess less of a chromium deficit than the porous sintered compacts, even though spectrometer traces taken of solid samples disclosed no detectable change in lattice parameters.

Figure 4 shows a plot of conductivity *vs.* $1/T$ for hot-pressed high-purity Cr_2O_3(C) in nitrogen, argon, and air up to 1500°C. A comparison can be made with the 2-electrode results of Hauffe and Block (12) and Fischer and Lorenz (13). The former investigators may have used low-purity Cr_2O_3 and not allowed sufficient time for atmospheric equilibration. There is fair agreement with the latter investigators, although they did not report measurements taken below 900°C. Two straight lines intersecting at about 1250°C can be drawn through data obtained in nitrogen, *i.e.*, the same atmosphere used for diffusion where $pO_2 \simeq 10^{-4}$ mm Hg. These data show no significant change from those obtained in air where $pO_2 \simeq 10^2$ mm Hg. Exposure to argon where $pO_2 \simeq 10^{-3}$ mm Hg causes some variation at lower temperatures, but this could result from an unknown source of sample contamination or a slight difference in heating rates rather than any atmospheric effect. As would be expected, use of 2 electrodes provides somewhat lower and less accurate conductivities since the contact resistances are also measured in series with the sample resistance.

Discussion

Assuming that Cr^{3+} is the primary diffusing cation, the diffusion and conductivity data can be combined to provide an approximate calculation of its transference number in Cr_2O_3 by using the Nernst-Einstein relation (19). This is generally expressed as

$$t_i = \frac{n_i z_i^2 e^2 D_i}{\sigma k T} \quad [7]$$

where t_i is the transference number, n_i is the number of cations cm^{-3} (which is of the order of 10^{22}), z is the cation valence, D_i is its self-diffusion coefficient, σ is conductivity, e is the electronic charge, k the Boltzmann constant, and T is absolute temperature. On making the appropriate substitutions for this specific case

$$t_{Cr^{3+}} = 1.65 \times 10^5 \frac{D_{Cr^{3+}}}{\sigma T} \quad [8]$$

and one can calculate the representative values listed in Table III. There are very few direct determinations of transference numbers in oxides, but these values are in fair accord with the experimental value of 5.2×10^{-4} obtained by Gundermann and Wagner (20) for Cu^{1+} in Cu_2O at 1000°C. Since the larger oxygen anions (1.32Å for O^{2-} *vs.* 0.65Å for Cr^{3+}) can be considered as being still less mobile, the low magnitude of $t_{Cr^{3+}}$ is strongly indicative that there is almost pure electronic conduction in Cr_2O_3 throughout the temperature range of this investigation. From Fischer and Lorenz's (13) thermoelectric power measurements, where they found that the negative pole of the solid cell $Pt/Cr_2O_3/Pt$ was always the hotter, there is good evidence that the electronic conduction is provided by the motion of excess positive holes.

Table III. Representative calculated cation transference numbers at various temperatures

T, °C	$1/T$, $\times 10^{-4}$K^{-1}	D, cm^2 sec^{-1}	σ, Ω^{-1} cm^{-1}	$t_{Cr^{3+}}$
1546	5.50	6.20×10^{-9}	4.90×10^{-1}	1.15×10^{-3}
1467	5.75	2.86×10^{-9}	3.04×10^{-1}	8.92×10^{-4}
1393	6.00	1.33×10^{-9}	1.85×10^{-1}	7.13×10^{-4}
1327	6.25	6.20×10^{-10}	1.15×10^{-1}	5.56×10^{-4}
1267	6.50	2.89×10^{-10}	7.50×10^{-2}	2.50×10^{-4}
1156	7.00	6.20×10^{-11}	6.08×10^{-2}	7.14×10^{-5}
1061	7.50	1.33×10^{-11}	4.92×10^{-2}	2.02×10^{-5}
977	8.00	2.86×10^{-12}	4.00×10^{-2}	5.72×10^{-6}

As discussed by Kröger and Vink (21), a large number of independent relations between various concentrations of cation vacancies $Cr\ \square'''$, interstitial cations $Cr\ \emptyset^{\cdot\cdot\cdot}$ and $Cr\ \emptyset^{\cdot\cdot\cdot\cdot}$, holes $\oplus$, and electrons θ could be devised to explain the pressure independence of nonstoichiometric Cr_2O_3. Rather than engaging in a speculative manipulation of many parameters, one can postulate the simplified defect structure first given by Hauffe and Block (12) and apply the scheme proposed by Birchenall (22) for treating enthalpies of defect formation and motion. If reasonable values result, the model should not be greatly in error. Here the premises are that Cr_2O_3 has Frenkel disorder, is of a constant composition not far from stoichiometry, and is independent of oxygen partial pressure. Then:

$$\text{ideal crystal} \rightleftharpoons Cr\ \square''' + Cr\ \emptyset^{\cdot\cdot\cdot} + \oplus \quad [9]$$

Referring to the Fig. 4 plot of ln σ *vs.* $1/T$ for hot-pressed Cr_2O_3(C) in nitrogen, one can accept (23)

that the negative slope (times R) at temperatures below 1250°C results principally from the activation enthalpy for hole motion ΔH_m^*, and this value is found to be 8.4 kcal mole^{-1}. The equilibrium slope of the line above 1250°C results from the sum of ΔH_m^* and the enthalpy ΔH_f for forming the lattice defects of Eq. [9] divided by 3. ΔH_f is associated with the formation of one mole of vacancies, one mole of interstitial cations, and one mole of holes. Hence, ΔH_m^* and $\Delta H_f/3$ equal the slope-determined quantity of 38.7 kcal mole^{-1}, and ΔH_f is found equal to 90.9 kcal mole^{-1}. Referring to Fig. 3, where the slope from 1550° to 1050°C results from a ΔH^* of 61.1 kcal mole^{-1} (which in turn is composed of an enthalpy for cation motion ΔH_m and the same $\Delta H_f/3$ for defect formation), one finds by subtraction that ΔH_m equals 30.8 kcal mole^{-1}. Although FeO possesses the simple NaCl structure, it is of interest to note that a direct measurement of ΔH_m at constant FeO composition by Himmel *et al.* (16) provided a value of 30.0 kcal mole^{-1}. Carter and Richardson (24) found that ΔH_m for Co in CoO is 35 kcal mole^{-1}. It may be that ΔH_m does not vary much among these oxides because the cation:anion size ratios are similar. Until other ΔH_m values are determined, further comparison would be impractical, but no inconsistency with the above model currently exists.

From another point of view, one can compare these cation diffusion data with those for the parabolic oxidation of Cr. Gulbransen and Andrew (25) have reported an "activation energy" of 59.4 kcal mole^{-1} for Cr oxidation between 1000°-1100°C; at lower temperatures some interference from linear oxidation caused a low apparent value of 37.5 kcal mole^{-1}. Further data on Cr oxidation have been obtained in this Laboratory, and the results (when the parabolic rate law is obeyed) are in fair agreement with the treatment of Mott and Gurney (26) using the cation diffusion coefficients gathered here. The growth of electronically conducting Cr_2O_3 must be controlled by the faster moving ionic species. Although anion diffusion in Cr_2O_3 has not been measured, the aforementioned marker-movement experiments and coherence of this study show that anions are far less mobile and that the rate-determining step for the high-temperature oxidation of Cr is the volume diffusion of cations through Cr_2O_3.

Acknowledgments

The authors are indebted to L. S. Butler for his assistance in preparing, sectioning, and counting the diffusion specimens; to E. L. Simons for developing a plating technique for Cr^{51}; to A. G. Pincus and J. W. Szymaszek for providing the hot-pressed and sintered compacts; to C. H. Rosner for the conductivity measurements. C. E. Birchenall, R. E. Hoffman, and S. P. Mitoff provided many helpful discussions.

Manuscript received June 14, 1961.

Any discussion of this paper will appear in a Discussion Section to be published in the June 1962 JOURNAL.

REFERENCES

1. W. D. Kingery, D. C. Hill, and R. P. Nelson, *J. Am. Ceram. Soc.*, **43**, [9], 473 (1960).
2. Y. Oishi and W. D. Kingery, *J. Chem. Phys.*, **33**, [2], 480 (1960).
3. A. U. Seybolt, *This Journal*, **107**, [3], 147 (1960).
4. R. Lindner, *Arkiv Kemi*, **4**, [4], 381 (1952).
5. R. Lindner and A. Åkerström, *Z. physik. chem. (Frankfurt)*, [N.F.] **6**, 162 (1956).
6. R. Lindner, Proc. of 10th Solvay Conference, Brussels, 459 (1956).
7. M. T. Shim and W. J. Moore, *J. Chem. Phys.*, **26**, 802 (1957).
8. J. E. Fox and J. A. McGurty, Chromium and Chromium-Base Alloys, Paper presented at Refractory Metals Symposium of AIME, Detroit, May 25, 1960; J. F. Collins, V. P. Calkins, and J. A. McGurty, Applications of Rare Earths to Ferrous and Non-Ferrous Alloys, paper presented to ASM-AEC Symposium, Chicago, Nov. 2, 1959.
9. T. Yukawa, R. Widmer, and N. J. Grant, Oxidation Behavior of Some Chromium-Base Alloys at 1800 to 2000°F, submitted to AIME (1961).
10. R. K. DiCerbo and A. U. Seybolt, *J. Am. Ceram. Soc.*, **42**, [9], 430 (1959).
11. A. Michel and J. Bénard, *Bull. Soc. Chem.*, **10**, 315 (1943).
12. K. Hauffe and J. Block, *Z. phys. chem.*, **198**, 232 (1951).
13. A. Fischer and G. Lorenz, *Archiv. f.d. Eisen.*, **28**, [8], 497 (1957).
14. W. A. Fischer and G. Lorenz, *Z. phys. chem.*, [N.F.], **18**, 308 (1958).
15. D. Caplan and M. Cohen, *This Journal*, **108** [5], 438 (1961).
16. L. Himmel, R. F. Mehl, and C. E. Birchenall, *Trans. AIME*, **197**, 827 (1953).
17. P. L. Gruzin, *Izvest. Akad. Nauk S.S.S.R., Otdel, tekh. Nauk*, 383 (1953).
18. A. H. Compton, "X-Rays in Theory and Experiment," pp. 802-805, D. Van Nostrand Co., New York (1935).
19. W. Jost, "Diffusion in Solids, Liquids, Gases," pp. 142-143, Academic Press Inc., New York (1960).
20. J. Gundermann and C. Wagner, *Z. physik. chem.*, **37B**, 155 (1937).
21. F. A. Kröger and H. J. Vink, "Relations between the Concentrations of Imperfections in Crystalline Solids," "Solid-State Physics," **3**, pp. 307-435, Academic Press Inc., New York (1956).
22. C. E. Birchenall, *Metallurgical Rev.*, **3**, [11], 235 (1958).
23. S. P. Mitoff, *J. Chem. Phys.*, **35** [3], 882 (1961).
24. R. E. Carter and F. D. Richardson, *Trans. AIME*, **203**, 336 (1955).
25. E. A. Gulbransen and K. F. Andrew, *This Journal*, **104** [4], 334 (1957).
26. N. F. Mott and R. W. Gurney, "Electronic Processes in Ionic Crystals," pp. 256-257, Clarendon Press, Oxford (1940).

A Microscopic Study of Oxide Films on Uranium

L. Leibowitz, J. G. Schnizlein, L. W. Mishler, and R. C. Vogel

Chemical Engineering Division, Argonne National Laboratory, Argonne, Illinois

ABSTRACT

Microscopic examination of the surface of uranium during the course of its oxidation has shown that the appearance and growth of oxide nodules coincide with the start of an increase in oxidation rate. Oxidation mechanisms are discussed, and the effects of oxide film cracking and surface area changes are considered.

It has been observed by several workers (1-4) that metal oxidations do not proceed uniformly over the surface but rather preferentially at certain sites. Moreover, differences in oxidation rates are often found for different crystal planes of metals (2). Work done with copper, nickel, iron, and other metals has been summarized by Gwathmey and Lawless (3). In almost all cases of theoretical treatment of metal oxidation rate data, it has been assumed that an oxide film of uniform thickness grows on the metal. It appears, however, that this is usually not the case. Evans (5) has treated the effect on metal oxidation rates of the appearance of gross flaws in the oxide film, while Cabrera (6) recently discussed the problem of oxide nucleation.

In connection with an extended study of the kinetics of oxidation of uranium, the oxidizing metal was examined microscopically to determine to what extent the oxidation is nonuniform and what relationships may exist between the superficial oxide appearance and the over-all oxidation rate. The kinetic measurements are reported elsewhere (7) and only the microscopic studies are discussed in detail here.

Experimental

The reaction cell used for the microscopic studies is shown in Fig. 1. This was mounted on the microscope stage and connected to a volumetric constant pressure apparatus by a Pyrex glass helix which allowed sufficient motion for focusing. A Leitz Panphot metallographic microscope was used, and in most of this work a 20X objective with a long working distance was employed.

For the time-lapse photography a motor-driven rotating brass disk, mounted below the microscope objective, was used as a combination heat shield, timer, and camera trip. Steel pins on the disk closed a microswitch controlling the camera drive when the metal sample was exposed to the optical system through slots cut in the disk. By suitable choice of speed of the motor rotating the disk, the desired exposure rate could be achieved. The camera used was a 16 mm Kodak Cine Special with a National Cine Equipment Company time-lapse control mechanism. The materials used and sample preparation techniques are described elsewhere (7).

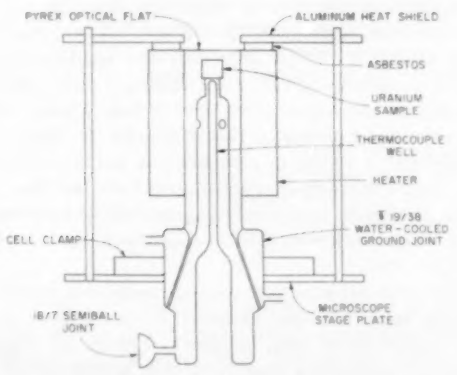

Fig. 1. Resistance-heated hot cell for microscopic examination.

Results and Discussion

For all metal samples examined a distinct heterogeneity was observed in the oxide films formed. Figure 2 is a graph of oxygen consumed as a function of time for a sample mechanically polished (through

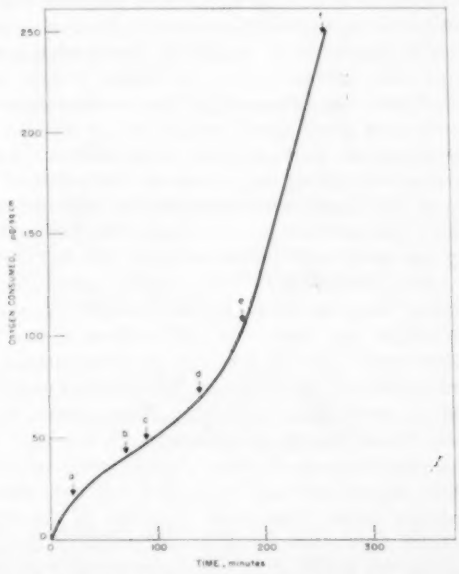

Fig. 2. Oxidation of uranium at 200°C in 200 mm oxygen. Arrows indicate extents of oxidation for each photograph shown in Fig. 3.

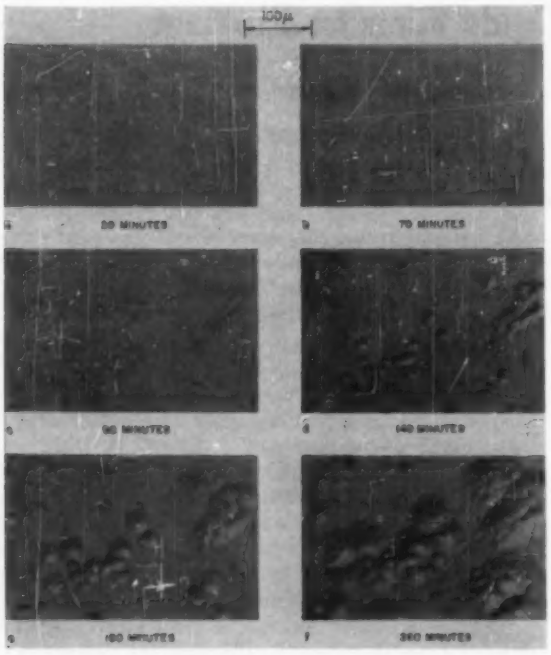

Fig. 3. Micrographs of surface oxidation of uranium at 200°C in 200 mm oxygen for designated times.

1μ diamond paste) and oxidized at 200°C and 200 mm oxygen pressure. Photomicrographs taken of the surface at various times during the course of the run are shown in Fig. 3. The oxide is clearly not uniform. At some point near c (Fig. 2) the slope of the kinetic curve begins to increase, *i.e.*, there is an increase in oxidation rate. This time (about c) coincides with the time at which nodules begin to grow rapidly on the oxide surface (Fig. 3c). Although not apparent in these photographs, most nodules begin at scratches or inclusions. Cubicciotti (8) in a uranium oxidation experiment at 120°C observed a similar abrupt rate increase. An oxidation which began parabolically was observed by him to increase markedly in rate after about 50 $\mu g/cm^2$ of oxygen had been consumed. In the present study additional work with electropolished and mechanically polished uranium at 200°C and with mechanically polished metal at 150°C using time-lapse methods yielded substantially the same relation between surface appearance and rate increase. While the initial portion of the oxidation was sensitive to the method of surface preparation the later rate and surface appearance changes were not. In general, electropolishing reduced the initial curvature of the kinetic curve compared to mechanical polishing. This aspect of the oxidation is discussed elsewhere (4, 7).

The examination of many photomicrographs such as those shown in Fig. 3 indicated that considerable variability exists from grain to grain in the extent of nodule formation. With electropolished samples, for which the initial grain structure is fairly distinct, some grains remain quite free of nodules while neighboring grains are almost completely covered. The relationship between oxide and the underlying metal has been discussed by several authors. Differences in oxidation rates on various crystal planes of metal seem to be related to the relative mismatch (3, 9) and to plastic flow properties of the oxide (10). Waber, O'Rourke, and Kleinberg (11), however, have shown that the first layers of uranium dioxide, produced by oxidation in moderate vacuum or in water vapor, are not epitaxially oriented with the underlying metal. Further study of this system is evidently necessary.

It has been proposed (12) that oxide formation occurs at the metal surface. In view of the appreciable volume increase involved in converting uranium to uranium dioxide, it is expected that substantial strain be developed in the oxide. It seems plausible, therefore, to ascribe to the nodule formation observed here a stress release function similar to that discussed for niobium and tantalum oxidation (13). As those authors point out, a three dimensional lattice expansion is required to bring the metal ions into their new positions in the oxide. It is, however, not at all clear with uranium that cracking of the oxide accompanies the formation of these nodules. The simple observation of a rate increase and an increased roughness of the outer oxide surface is not sufficient. If the reaction rate were controlled by a process occurring at the outer oxide surface, then the increased surface area resulting from mound formation would yield a rate increase as observed. For a reaction controlled by diffusion through a compact oxide layer, continuous cracking of the overlying oxide giving a diffusion barrier of constant thickness would be required. The applicability of these two interpretations to the present reaction is discussed elsewhere (7).

It has been reported (14) that uranium oxide formed after extensive linear oxidation is porous and of high specific area which is in contrast to nonporous and low specific area copper oxide formed during parabolic oxidation. The presumption is that the porosity of the oxide, and hence its lack of protective nature, determines the kinetic law followed. In the work of Aylmore, Gregg, and Jepson (14), however, only oxide formed after extensive reaction was examined. Those results are not necessarily representative of the situation in the work reported here. Those authors remark "at the end of the run, the weight gain was in excess of that required for complete conversion to uranium dioxide and yet some metal remained unoxidized." Their oxidation was at 240°C. Thus, although the oxide examined was not all uranium dioxide, their porosity estimates depend on the assumption that it was. Those authors are obviously aware of this difficulty. It would be of considerable value to measure the surface area of a uranium specimen at several points during the course of its oxidation to see what quantitative correlations may exist between rate and surface area and porosity.

The over-all kinetics to be expected for metal oxidations with a transformation from compact to porous oxide have been discussed briefly by Haycock (15). It is assumed that oxidation is controlled only by the thickness of the compact oxide. At some time t_c after the beginning of the oxidation (at time $t = 0$) a compact to porous transformation begins and continues to consume oxide at a linear rate until a steady

thickness of compact oxide is reached. The rate is thus $dx/dt = K_p/[x - K_l(t - t_o)]$, where x is the amount of metal consumed and K_p and K_l are the parabolic and linear rate constants, respectively. A two-stage rate curve is obtained, and this presents us with a reasonable picture for a diffusion-controlled oxidation process.

The presumption is made by Haycock (15) that the change in the oxide involves a recrystallization or a transformation of the oxide to a more stable form. If this were strictly true, it would be expected that once begun, the process would continue regardless of whether or not the oxidation continued. To test this, experiments were performed at 200°C in which the oxidation was interrupted at the onset of the rate increase by removing the oxygen without changing the sample temperature. During the interruption (about 90 min) the surface appearance of the sample did not change, and when oxygen was re-admitted the reaction resumed at an unchanged rate. This demonstrates that changes in the oxide occur only in response to the generation of new oxide.

From these observations alone, it is not possible to conclude that the rate increase results from oxide cracking with the rate-controlling step being diffusion through a compact oxide layer. If the rate-controlling step is one occurring on the exterior oxide surface, a rate increase resulting from increased surface area would be equally plausible.

Acknowledgment

The authors wish to express their appreciation to Dr. P. J. Pizzolato for his assistance in initiating this study. The assistance of Mr. D. Giroux and Mr. S. Andrews with the time-lapse photography is also gratefully acknowledged.

Manuscript received May 8, 1961; revised manuscript received July 25, 1961. Work performed under the auspices of the U.S.A.E.C.

Any discussion of this paper will appear in a Discussion Section to be published in the June 1962 JOURNAL.

REFERENCES

1. J. Bardolle and J. Bénard, *Rev. Met.*, **49**, 613 (1952).
2. W. W. Harris, F. L. Bell, and A. T. Gwathmey, *Acta. Met.*, **5**, 574 (1957).
3. A. T. Gwathmey and K. R. Lawless, "The Surface Chemistry of Metals and Semiconductors," H. C. Gatos Editor, p. 483, John Wiley & Sons, New York (1960).
4. C. Sella and J. J. Trillat, *Rev. Met.*, **56**, 105 (1959).
5. U. R. Evans, *Trans. Electrochem. Soc.*, **91**, 547 (1947).
6. N. Cabrera in "Semiconductor Surface Physics," R. H. Kingston, Editor, p. 327 University of Pennsylvania Press, Philadelphia (1957).
7. L. Leibowitz, J. G. Schnizlein, J. D. Bingle, and R. C. Vogel, *This Journal*, **108**, 1155 (1961).
8. D. Cubicciotti, *J. Am. Chem. Soc.*, **74**, 1079 (1952).
9. F. C. Frank and J. H. van der Merwe, *Proc. Roy. Soc. (London)*, **A198**, 205, 216 (1949).
10. W. Schottky, *Z. Elektrochem.*, **63**, 784 (1959).
11. J. T. Waber, J. A. O'Rourke, and R. Kleinberg, *This Journal*, **106**, 96 (1959).
12. J. G. Schnizlein, J. D. Woods, J. D. Bingle, and R. C. Vogel, *ibid.*, **107**, 783 (1960).
13. J. V. Cathcart, J. J. Campbell, and G. P. Smith, *ibid.*, **105**, 442 (1958).
    J. V. Cathcart, R. Bakish, and D. R. Norton, *ibid.*, **107**, 668 (1960).
14. D. W. Alymore, S. J. Gregg, and W. B. Jepson, *ibid.*, **106**, 1010 (1959).
15. E. W. Haycock, *ibid.*, **106**, 771 (1959).

The Kinetics of Oxidation of Uranium between 125° and 250°C

L. Leibowitz, J. G. Schnizlein, J. D. Bingle, and R. C. Vogel

Chemical Engineering Division, Argonne National Laboratory, Argonne, Illinois

ABSTRACT

Rates of oxidation of uranium have been measured volumetrically at constant pressure in the temperature range 125°-250°C and at oxygen pressures from 20 to 800 mm. The oxidation is best described by two linear rate laws, a marked increase in rate occurring after an average of 50 μg O_2/cm^2 has been consumed. The first stage rate in μg/cm^2-min is given by the expression

$$v_i = 1.48 \times 10^4 P^{1/n} e^{-E/RT}$$

where $E = 10{,}700$ cal, P is oxygen pressure in millimeters of mercury, and $1/n$ varies with temperature. The reaction is believed to be controlled by process occurring at the gas-oxide surface. The increase in rate leading to the second stage is not treated quantitatively, but is attributed to a net increase in surface area.

A review of the information available at present on the kinetics of the oxidation of metallic uranium shows a lack of agreement among the various authors (1) as well as an absence of detailed information on this important reaction despite numerous publications. The much-quoted finding of Wathen, (1-d) for example, that the product of uranium oxidation between 200° and 500°C is U_3O_8 while below 200°C it is UO_2, is based solely on measurements involving preferential dissolution of the oxide. When attempting to follow the same procedure, Greenwood (1-a) reports that for small amounts of oxidation appreciable quantities of metal dissolved, raising some question of the validity of Wathen's findings.

Further, Loriers (1-i) and Adda (1-l) have reported oxidation rates many times greater than those found by Cubicciotti (1-h). Because of these and similar uncertainties, it seemed advisable to carry out a systematic study of the kinetics of the reaction.

Experimental

Apparatus.—The rate of oxidation of uranium was measured volumetrically at constant pressure in an apparatus of conventional design which has already been described (2). The sample rested on top of a thermocouple well which contained the chromel-alumel thermocouple used to determine the reaction temperature. No self-heating was observed in the temperature range reported here although at 300°C and above self-heating did occur.

Materials.—All work reported was carried out using cubes of uranium 1 cm on an edge. The metal used, prepared by the Metallurgy Division, Argonne National Laboratory, was vacuum cast, heated to the beta-uranium temperature region and quenched to randomize the crystallite structure. Metallographic examination showed the bent twins and subgraining typical of uranium quenched from the beta phase. The principal impurities in parts per million are: O, 12; C, 21; H, 5; N, 56; Si, 40; Fe, 45; Ni, 15; Al, 7; Cr, 5; Mn, 2; Mg, 3; Cu, 3. Chemical analyses were carried out for O, C, H, and N while all other elements were determined by spectrographic means. Tank gases were used without further purification. Typical tank oxygen analyses show the following impurities (in volume percent): Ar, 0.1; CO_2, 0.06; N_2, 0.2; H_2O, 0.005.

Sample preparation.—In most of this work, electropolished uranium samples were used. This polishing was performed, after prior mechanical polishing through 1μ diamond paste, in approximately 7 min with a current density of 30 ma/cm^2 in an electrolyte consisting of 8 parts 95% ethanol, 5 parts ethylene glycol, and 5 parts 85% orthophosphoric acid. The cathode was stainless steel and the anode contact was made through a platinum touch wire. When mechanical polishing was employed samples were finished through 1μ diamond paste.

Results.—Oxidation rates have been measured in the temperature range 125° to 250°C and at oxygen pressures between 20 and 800 mm. The process occurs in two stages with the initial slow reaction followed by a transition to a more rapid second stage. This two stage process is evident in Fig. 1, 2, and 3. Figure 1 illustrates the linearity and duration of the first stage for typical oxidations at 150°, 200°, and 250°C. The point at which the major oxidation rate increase occurs is not highly reproducible. This occurs at about 40 μg O_2/cm^2 for the runs shown in Fig. 1. A somewhat better over-all average figure would be 50 μg/cm^2. In Fig. 2 is shown the oxidation of an electropolished uranium cube at 125°C and an oxygen pressure of 50 mm. The initial deviations from linearity at 125°C suggest that at low temperatures the first stage might indeed follow parabolic kinetics (1-h). Although the process is not initially linear at 125°C, it was decided that the entire collection of data could be best described by two linear rate laws. Values of these rates could readily be obtained graphically and these rates and standard deviations are listed in Table I.

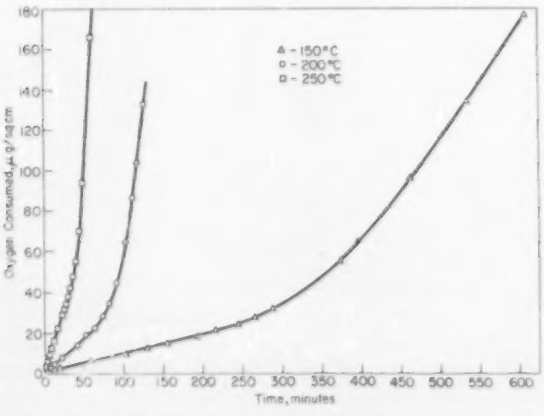

Fig. 1. Oxidation of electropolished uranium at 50 mm oxygen pressure.

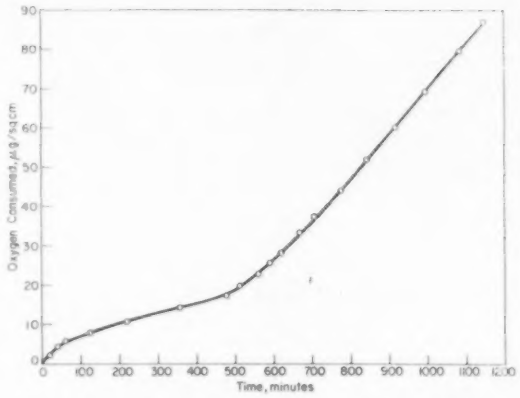

Fig. 2. Oxidation of electropolished uranium at 125°C and 50 mm oxygen pressure.

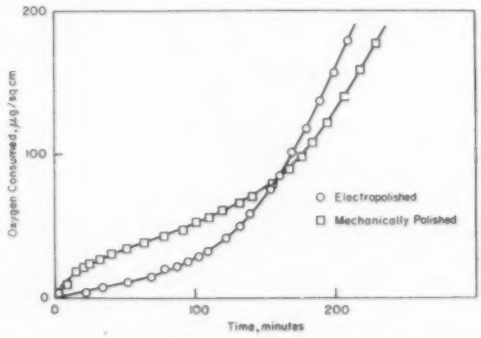

Fig. 3. Effect of polishing method on the oxidation of uranium (oxidation at 200°C and 200 mm oxygen pressure).

While most of the samples used were electropolished before use, differences in oxidation behavior have been observed between electropolished and mechanically polished uranium samples. This effect is illustrated in Fig. 3 with runs at 200°C and an oxygen pressure of 200 mm. It is noteworthy that even though the run with the mechanically polished specimen was not initially linear, the linear portion of that curve, beginning at about 20 min, has roughly

Table I. Oxidation rates of electropolished uranium

Oxygen pressure, mm	Temperature, °C							
	125		150		200		250	
	First stage rates (μg O_2/cm²-min)							
	Rate	Std. dev.	Rate	Std. dev.	Rate	Std. dev.	Rate	Std. dev.
20	0.026	0.010	0.073	0.028	0.31	0.09	1.1	0.1
50	0.029	0.002	0.086	0.028	0.39	0.12	1.4	0.1
200	0.032	0.011	0.11	0.02	0.49	0.05	3.2	1.7
800	[a]		[a]		0.66	0.31	5.8	1.5
	Second stage rates (μg O_2/cm²-min)							
20	0.11	0.02	0.47	0.05	3.5	0.7	10	2
50	0.13	0.01	0.59	0.04	5.1	0.2	18	2
200	0.13	0.03	0.60	0.07	6.6	0.8	32	6
800	[a]		0.56	0.09	7.4	1.2	40	1

[a] Under these conditions no reliable values could be obtained.

Table II. Phases detected by x-ray diffraction after oxidation of uranium in oxygen

Treatment	O_2 consumed, μg/cm²	Phases detected
In vacuum at room temperature overnight, then heated to 200°C in 10^{-5} mm	—	α-U preferentially oriented and UO_2 only barely detectible.
25-min oxidation at 200°C in 200 mm O_2	20	α-U preferentially oriented and UO_2 preferentially oriented (crystallite size less than 100 mμ).
334-min oxidation at 200°C in 200 mm O_2	1080	α-U random, barely detectible, and UO_2 preferentially oriented (crystallite size less than 100 mμ).
50-min oxidation at 295°C in 200 mm O_2	2270	UO_2 (crystallite size less than 100 mμ).

the same slope as the initial portion of the electropolished curve. Similar behavior has been observed at other temperatures. Since measured rates were converted to rates per unit area by using the geometric area of the metal cubes, an initial roughness factor (*i.e.*, the ratio of true to apparent surface area) of 3 to 4, accompanying mechanical polishing would account for the initially higher rate. If, as has been observed for copper (3), the roughness decreased during oxidation, the observed results would be quite reasonable. This effect is discussed further below.

Several experiments were carried out in which the oxidation was interrupted by removing the oxygen while maintaining constant temperature. In all cases, regardless of the kinetic region in which the interruption occurred, the process would resume at an unchanged rate on reintroduction of the oxygen. Cubicciotti (1-h) has reported slight increases in rate in a similar experiment.

In general, particularly at the highest temperatures, the second stage rate decreased markedly toward the end of the run. For this reason and others discussed below it is not possible at present to discuss this region from a fundamental standpoint.

Identification of reaction products.—The oxidized surface was examined[1] at room temperature by means of a Norelco x-ray diffractometer after oxidation to various extents at 200°C at an oxygen pressure of 200 mm. The samples used were oxidized in the usual manner for the desired time and cooled in vacuum before the x-ray examination. In all cases the only oxide found was uranium dioxide. Extreme broadening of the diffraction peaks indicated a crystallite size very much less than 100mμ. The crystal growth in these layers was oriented. Results of the examination after oxidation to three extents are summarized in Table II. After oxidation at 295°C in 200 mm until 2270 μg oxygen/cm² was consumed, x-ray diffraction study at room temperature showed that the product was uranium dioxide with crystallite size very much less than 100 mμ.

A few special oxidation kinetic studies were conducted on uranium foils to observe whether or not the uranium dioxide produced in the metal-gas reaction might have an unusual lack of reactivity. When a 30 μ foil was oxidized to completion at 200°C in 200 mm of oxygen, the characteristic first and second stages were observed. However, the second stage rate fell to a minimum followed by a second maximum just prior to the end of the oxygen consumption. The final O/U ratio was 2.43 based on both weight gain and oxygen consumption. This is slightly higher than the value 2.33 for U_3O_7 which would be expected on the basis of the work on the oxidation of UO_2. There is, however, some disagreement among the workers studying uranium dioxide oxidation. Backburn, Weissbart, and Gulbransen (4) find tetragonal U_3O_7 at compositions as low as $UO_{2.06}$ while both Anderson, Roberts, and Harper (5) and Aronson, Roof, and Belle (6) do not observe tetragonality until compositions in the neighborhood of $UO_{2.2}$ are reached.

Identification by x-ray diffraction was extremely difficult because of diffuse lines resulting from the very small crystallite size. The cell constant was closest to that of U_4O_9 ($UO_{2.25}$). No U_3O_8 was detected. A similar experiment at 295°C in 200 mm oxygen using a 270μ foil showed related behavior. The final O/U ratio was 2.73 and in this case was identified by x-ray diffraction as U_3O_8. These experiments demonstrate clearly that the uranium dioxide produced from the gas-metal reaction has similar reactivity to that of dioxide produced by aqueous precipitation procedures and is more reactive than sintered dioxide (7).

Because the extremely small crystallite size led to line broadening which might obscure indication of tetragonality in the x-ray identification of the oxide, oxidized uranium samples were examined by means of electron diffraction.[2] The smaller penetration of electrons offers an advantage in examining the outer surface where the higher oxide would be expected to occur.

The patterns obtained from both the first stage (45 μg/cm²) and the second stage (1760 μg/cm²) oxidations at 200°C in 200 mm oxygen were sharp and

[1] X-ray study and interpretation by D. S. Flikkema, Argonne National Laboratory.

[2] Electron diffraction studies by H. W. Knott, Metallurgy Division, Argonne National Laboratory. An RCA EMU-2 unit was used.

intense and were clearly identified as uranium dioxide. The rings were expanded in the case of the second stage oxidation so that all the face-centered cubic lines were resolved with no evidence of splitting as would be expected from any tetragonality. Since the penetration of electrons is only a few molecular layers, it is clear that no higher oxide was present when the sample was examined at room temperature after this oxidation into the second stage. The observation of only uranium dioxide on the surface of cubes after oxidation suggests that higher oxides are not produced until the uranium metal is consumed as was the case with the foils described above.

There exists the possibility of a change in the oxide, during cooling to room temperature which could be circumvented only by determination of the diffraction pattern during the oxidation. While this is possible with x-ray diffraction, the small crystallite size causes some uncertainty. For electron diffraction the oxidation would have to be interrupted and the equipment evacuated before a pattern could be obtained. Although such an experiment removes the problem of change of temperature, it does not avoid interruption of the oxidation process.

Based on the evidence available, however, we must conclude that until the reaction is near completion uranium dioxide is the only product. Loriers (1-b) using x-ray methods observed U_3O_8 formation above 240°C. He does not, however, report the extent of oxidation. If the oxidation is virtually complete we do indeed find higher uranium oxides. Wathen's early work, as mentioned above, was based on questionable experimental procedures.

Surface appearance of samples.—Microscopic examinations of oxidizing uranium samples (8) showed that at the onset of the rate increase leading to the second stage (about 80 min for the electropolished sample in Fig. 3), nodules begin to appear on the oxide surface. The nodule covered area increases rapidly as the second stage develops and, except for particular grains, the entire surface eventually becomes covered. This is similar to the behavior observed by Cathcart, Campbell, and Smith for niobium (9) and by Cathcart, Bakish, and Norton for tantalum (10). It has also been shown that formation of new oxide in the case of uranium oxidation (11) occurs at the metal-oxide interface as with niobium and tantalum.

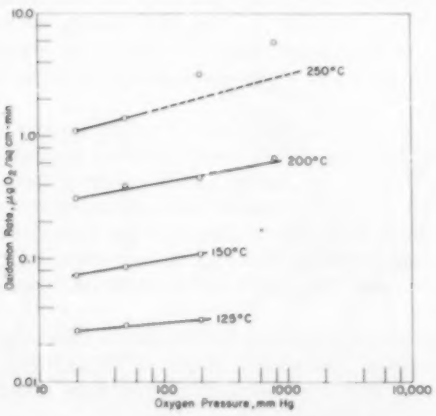

Fig. 4. Effect of pressure on the first stage oxidation rate of uranium.

Discussion

Linear oxidation kinetics generally are considered to indicate either continuous cracking of the oxide film yielding a diffusion barrier of constant thickness, or rate control at an oxide surface of constant area. In the first case (12) we expect initially parabolic oxidation kinetics followed by a linear rate law. In the second case a linear oxidation would be observed from the start provided the surface area remained constant.

The oxidation rate data (Table I) show a pressure effect, with the oxidation rate increasing with increasing pressure. As indicated in Fig. 4, the variation of first stage oxidation rate, v, with pressure, P, is well represented by the equation

$$v_1 = Z\,P^{1/n}$$

Z and $1/n$ are constants, values for which are listed below.

Temperature, °C	Z	1/n
125	0.0198	0.09
150	0.0412	0.18
200	0.159	0.21
250	0.508	0.26

It should be noted that, because of the brief duration of the first stage at high temperature and pressure, the first stage rates at 250°C and the two highest oxygen pressures do not represent true first stage conditions accurately. These values were not used in determining the above constants.

Consideration of the influence of oxygen pressure on the rate of metal oxidations for cases such as diffusion, in which a step dependent on vacancy concentration is rate controlling (13), has shown the pressure effect to be independent of temperature. It seems most reasonable to attribute an effect of the kind observed here to rate control by a process dependent solely on the concentration of adsorbed oxygen. The kinetics of such processes have been discussed by Fassel and co-workers for tantalum and other metals (14, 15).

Support for rate control by a surface process comes from the observation of only uranium dioxide on the outer oxide surface. If a diffusion process were the slow step as the length of the diffusion path increased, we would expect, eventually, to reach a point at which the rates of oxide and of metal oxidation were comparable. From this point on higher oxides should form. Since no such oxides are found, diffusion must be a fast step. The difference discussed above between electropolished and mechanically polished metal is thus attributable to changes in surface area during the early stages of the oxidation rather than to an effect of the electropolishing itself. The effect of surface preparation on the nature of the oxide film found on uranium has been discussed by Sella and Trillet (16).

The second stage results from an increased total surface area as indicated by the mound growth observed microscopically. While it is not possible to treat the second stage rate data quantitatively be-

cause of the lack of surface area information, it is noteworthy that the region of transition from the first to the second stages may be well represented by the Avrami equation $y = 1 - e^{-bt^n}$ (17) where y is the amount of transformed region at the time t, and b and n are constants, the latter related to the dimensionality of the process. This equation in general describes any nucleation and growth process, and microscopic examination of the oxidizing metal shows the mound development to proceed in this way (8).

If we now consider the rate of oxidation to be controlled by the rate of surface process (perhaps ionization, dissociation, or migration), we have

$$v_1 = k_1 C_s \qquad [1]$$

where v_1 is the first stage oxidation rate, C_s the surface concentration of adsorbed oxygen, and k_1 the rate constant. For adsorption on an energetically heterogeneous surface Halsey (18) has shown that the familiar Freundlich adsorption isotherm may be written

$$\theta = C x_m \left(\frac{P}{P^\circ}\right)^{kT/x_m(1-rT)} \qquad [2]$$

where θ is the fractional coverage, P pressure, T temperature, k Boltzmann's constant, and P°, x_m, C, and r are constants related to the energetics of the adsorption in the following ways: the entropy of adsorption ΔS_x on sites of adsorption energy x is presumed to vary linearly with x; $\Delta S_x = \Delta S_\circ + rx$ and

$$P^\circ = e^{\Delta S_\circ / k}$$

where $\Delta S_\circ$ and r are constants. The number of sites of energy x is given by $N_x = Ce^{-x/x_m}$ where C and x_m are also constants.

Using absolute reaction rate theory (19) we may write

$$k_1 = \frac{kT}{h}\frac{f\ddagger}{f_s} e^{-E/kT} \qquad [3]$$

where $f\ddagger$ and f_s are the partition functions for the activated and initial adsorbed states and we have assumed a unit transmission coefficient. The other symbols have their usual significance. Since only vibrational degrees of freedom are probably involved we may consider $f\ddagger \cong f_s \cong 1$ and combining [1], [2], and [3], we have

$$v_1 = \frac{kT}{h} C x_m \left(\frac{P}{P^\circ}\right)^{RT/x_m(1-rT)} e^{-E/RT} \qquad [4]$$

now using energies per mole.

To a good approximation we may determine the activation energy, E, from a graph of log $(v_1/p^{1/n})$ against $1/T$. This is shown in Fig. 5 from which a value of 10.7 kcal/mole may be estimated for E.

By introducing experimental numerical values into Eq. [4], we have the over-all equation

$$v_1 = 1.48 \times 10^4 \, P^{1/n} \, e^{-E/RT}$$

Written in this way $e^{-E/RT}$ is not the only temperature dependent factor. The variation of observed $1/n$ values with temperature is shown in the table above.

It thus appears that quite good agreement with all our experimental findings may be had by assuming the rate-controlling step to occur on the outer oxide surface. At low temperature (below 125°C), possibly, the rate of diffusion through the oxide is no longer fast enough for this to be the case. Careful surface area measurements and kinetic studies using oxide-free surfaces (20) would be necessary to clarify this area further.

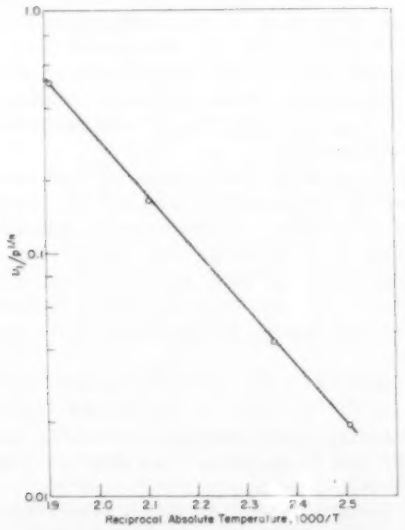

Fig. 5. Arrhenius plot of log $(v_1/p^{1/n})$ vs. reciprocal absolute temperature.

Acknowledgment

The assistance in the laboratory of D. Fischer and A. Porter is gratefully acknowledged. The authors are also indebted to D. S. Flikkema for x-ray diffraction analyses, and to H. Knott and M. Mueller for electron diffraction studies.

Manuscript received May 8, 1961; revised manuscript received July 25, 1961. Work performed under the auspices of the U.S.A.E.C.

Any discussion of this paper will appear in a Discussion Section to be published in the June 1962 JOURNAL.

REFERENCES

1-a. H. Greenwood, ME-24 (1943).
1-b. K. T. Perkins, CT-1008 (1943).
1-c. J. G. Thompson, CT-1006 (1943).
1-d. T. Wathen, BR-223 (1943).
1-e. A. S. Covert and M. Kolodney, LA-313 (1945).
1-f. W. E. Lindlief and V. C. F. Holm, CT-2733 (1945).
1-g. R. Hellyer, Poc-mem 16 (1948).
1-h. D. Cubicciotti, *J. Am. Chem. Soc.*, **74**, 1079 (1952).
1-i. J. Loriers, *Compt. rend.*, **234**, 91 (1952).
1-j. J. T. Waber, LA-1524 (1952).
1-k. K. Q. Bagley and D. S. Oliver, RDB(C)-TN-32 (1953).
1-l. Y. Adda, CEA-757 (1958).
2. H. A. Porte, J. G. Schnizlein, R. C. Vogel, and D. F. Fischer, *This Journal*, **107**, 506 (1960).
3. T. N. Rhodin, *J. Am. Chem. Soc.*, **72**, 4343 (1950).
4. P. E. Blackburn, J. Weissbart, and E. A. Gulbransen, *J. Phys. Chem.*, **62**, 902 (1958).
5. J. S. Anderson, L. E. J. Roberts, and E. A. Harper, *J. Chem. Soc.*, **1955**, 3946.
6. S. Aronson, R. B. Roof, and J. Belle, *J. Chem. Phys.*, **27**, 137 (1957).
7. Minutes of Uranium Dioxide Conference, January, 1956, TID-7514.
8. L. Leibowitz, J. G. Schnizlein, L. W. Mishler, and R. C. Vogel, *This Journal*, **108**, 1153 (1961).

9. J. V. Cathcart, J. J. Campbell, and G. P. Smith, *ibid.*, **105**, 442 (1958).
10. J. V. Cathcart, R. Bakish, and D. R. Norton, *ibid.*, **107**, 668 (1960).
11. J. G. Schnizlein, J. D. Woods, J. D. Bingle, and R. C. Vogel, *ibid.*, **107**, 783 (1960).
12. E. W. Haycock, *ibid.*, **106**, 771 (1959).
13. T. B. Grimley and B. M. W. Trapnel, *Proc. Roy. Soc. (London)*, **A234**, 405 (1956).
14. R. C. Peterson, M. W. Fassell, Jr., and M. E. Wadsworth, *J. Metals*, **6**, 1038 (1954).
15. J. P. Baur, D. W. Bridges, and M. W. Fassell, Jr., *This Journal*, **102**, 490 (1955).
16. C. Sella and J. J. Trillet, *Rev. Met.*, **56**, 105 (1959).
17. M. Avrami, *J. Chem. Phys.*, **7**, 1103 (1939); **8**, 212 (1940); **9**, 177 (1941).
18. G. D. Halsey, "Advances in Catalysis," Vol. IV, p. 259, Academic Press, Inc., New York (1952).
19. S. Glasstone, K. J. Laidler, and H. Eyring, "The Theory of Rate Processes," McGraw-Hill Book Co., Inc., New York (1941).
20. J. T. Waber, C. Olsen, and D. D. Whyte, AECU-4742 (1959).

Properties of the Electrical Double Layer in Solutions of Electrolytes in Some Organic Solvents

S. Minc, J. Jastrzebska, and M. Brzostowska

Department of Electrochemistry, University of Warsaw and Department of Electrochemistry, Polish Academy of Sciences, Warsaw, Poland

ABSTRACT

Differential capacities at the dropping mercury electrode in solutions of some inorganic halides in formamide, dimethylformamide, and acetonitrile have been measured. For cesium iodide in dimethylformamide and acetonitrile a rather large increase of the differential capacity, depending on the concentration of electrolyte in the region of high cathodic polarization, has been observed. For lithium chloride and bromide in the same solvents both effects were very small. It has been shown for a number of solvents that the minimum values of the differential capacity for 0.1M electrolyte solutions are roughly proportional to the dielectric constant of the solvent. The hump usually appearing on the curves of differential capacity for aqueous solutions of electrolytes has also been observed for formamide solutions, but was absent in the case of solutions in organic solvents of low dielectric constant.

Grahame has shown in one of his last papers that the differential capacity of the interface between mercury and electrolyte solution can be measured directly in water as well as in methanol, using in the latter case only slightly modified equipment and measuring technique (1).

It is well known that the differential capacity in solutions of some aliphatic alcohols, unless they do not have very low values of dielectric constant, can be measured by means of a similar method, as used by Grahame, and results are equally reproducible and easily obtained as in water (2-5).

In the course of interpretation of his results Grahame has accepted that for methanol also excellent agreement with the experiment is obtainable if the interface between mercury and electrolyte solutions can be taken as equivalent to two condensers connected in series. Their total capacity may be calculated from a simple and well-known equation (1).

From the above it follows that, in the absence of a specific adsorption of ions, for moderately concentrated solutions of the electrolyte and for a given range of potentials for nonaqueous solvents, the capacity of the inner region of the double layer at a given temperature is a unique function of charge density, but only in the sense that it does not depend on the electrolyte concentration in solution.

In our previous papers (2, 6) it was shown that the strong increase in the differential capacity observed by Grahame (1) in the region of sufficient cathodic polarization in methanol appears only for large cations of higher polarizability. We have suggested (2, 6) that this increase in the capacity observed for some cations in methanol, and to some extent for the ions of cesium in water, may be explained by Frumkin's hypothesis; the latter admits that there is some kind of specific adsorption of large cations on the inner Helmholtz plane (7 9). An assumption may therefore be made that the specific adsorption of some cations at the mercury surface is closely related to the dielectric nature of the solvent and particularly to the solvation energy.

It seems probable that a kind of electrostriction suggested by Grahame (1) and a high compressibility of the dipoles of some organic solvents in a strong electric field, as pointed out by Macdonald (10), may favor, at least partially, desolvation of large cations near the interface which undoubtedly facilitates their specific interaction with the mercury surface.

The influence of the dielectric properties of the solvent on the structure of the double layer is of great importance for interface phenomena and has been discussed many times from different points of view (11-14).

In the present paper some experimental data concerning certain properties of the electrical double layer are presented; the data were obtained from the

measurements of the differential capacity in several organic solvents of different dielectric behavior.

Experimental

Differential capacity was measured by means of an a-c symmetrical bridge using voltage amplitudes ranging between 2 and 6 mv and a frequency of 1000 cps. Some details concerning the circuit used were described previously (2). In the potential range between 0.1 and 1.8 v, the cathodic polarization of the dropping mercury electrode was achieved using the aqueous saturated calomel electrode as reference. The differential capacity values per 1 cm^2 of the mercury area are plotted against the potential and presented in Fig. 1-6. All experiments were carried out in an air-thermostat at 25° ± 0.5°C. The purification of mercury, preparation of LiCl, $SrCl_2$, and oxygen removal from the solutions were performed in the way previously described (2).

The formamide used, produced by "Prolabo", was not purified additionally because of its hygroscopy. The dimethylformamide used, produced by the "B.D.H.," was dried with anhydrous potassium carbonate and distilled on a laboratory column. The fraction used boiled between 153.0° and 153.3°C; its refractive index, n_D^{25}, was 1.4274; the water content, determined by Fischer's method, amounted to about 0.05%. The acetonitrile of " L.Light" production was shaken with sodium hydroxide, distilled on a 30 plate column, and then dried with phosphorus pentoxide. The fraction used boiled between 80.1° and 80.5°C; its specific conductivity was 3.0124×10^{-7} ohm^{-1} cm^{-1}; the water content was about 0.4%. Cesium iodide was

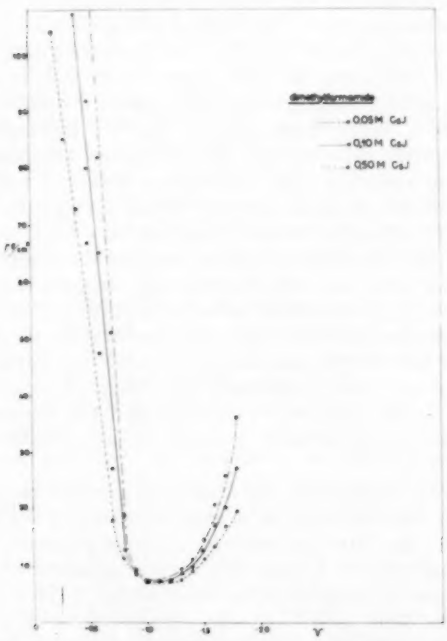

Fig. 1. Effect of concentration on differential capacity in solutions of CsJ in the concentration range 0.05-0.50M in dimethylformamide. (In all figures, the ordinate presents differential capacity of electrical double layer between dropping mercury electrode and solutions of electrolyte in $\mu F/cm^2$. Abscissa presents potential relative to saturated aqueous calomel electrode as reference in volts.

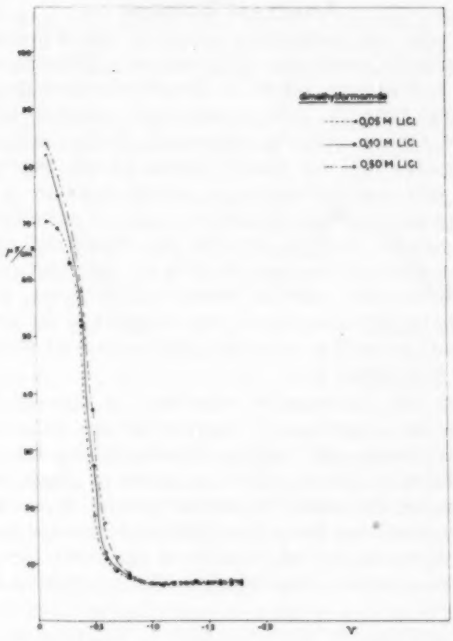

Fig. 2. Effect of concentration on the differential capacity in solutions of LiCl in the concentration range 0.05-0.50M in dimethylformamide.

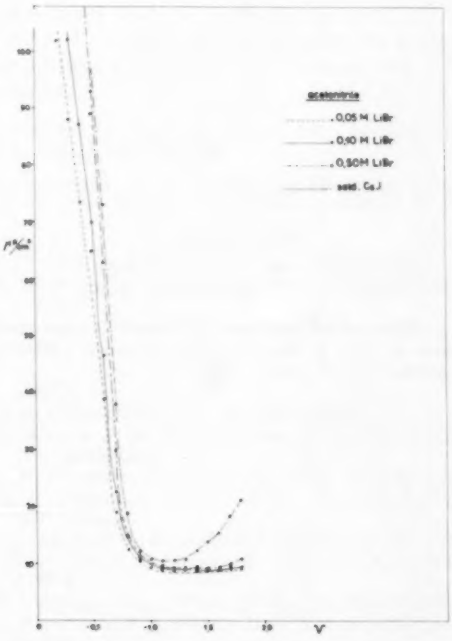

Fig. 3. Effect of concentration on the differential capacity in solutions of LiBr in the concentration range 0.05-0.50M and saturated CsJ in acetonitrile.

obtained from the product previously purified from an excess of J, HJ, and Cs_2CO_3. Unfortunately a complete removal of cesium carbonate by repeated crystallization was not achieved. However this fact had no influence on the measurements, because of insolubility of cesium carbonate in dimethylformamide or acetonitrile.

Results and Discussion

In Fig. 1-3 curves are given of the differential capacity for moderate concentrations of lithium chloride and cesium iodide in dimethylformamide and lithium bromide and a saturated, slightly below 0.05M, cesium iodide in acetonitrile. From the figures it appears that for cesium iodide in the region of high cathodic polarization a strong increase in the differential capacity in both solvents, as in methanol (6), can be observed, as well as a significant effect of the electrolyte concentration in the solution on the differential capacity measured. However, these effects for lithium chloride and bromide in the above solvents as well as in water, methanol, and ethanol were very small (2).

The great differences, observed in the capacity values in a number of solvents for the cations of various radii and various polarizability, may be attributed to the specific adsorption of some large cations on the inner Helmholtz's plane. It is to be emphasized that these great capacity changes occur very distinctly in the solvents of relatively low dielectric constant. This leads to the conclusion that

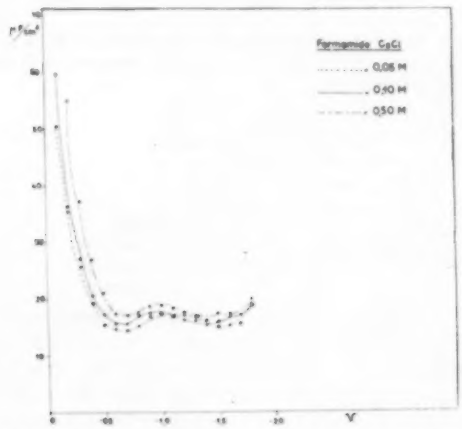

Fig. 4. Effect of concentration on the differential capacity in solution of CsCl in the concentration range 0.05-0.50M in formamide.

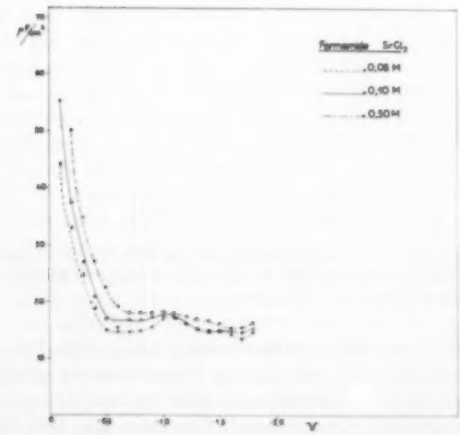

Fig. 5. Effect of concentration on the differential capacity solution of $SrCl_2$ in the concentration range 0.05-0.50M in formamide.

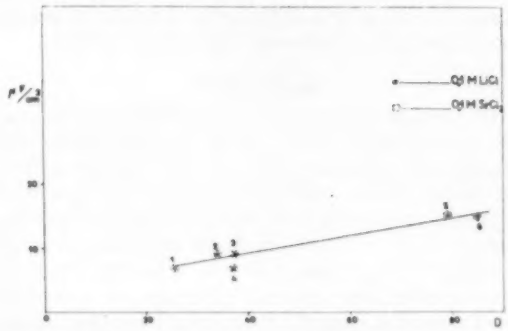

Fig. 6. Minimum values of differential capacity for 0.1M solutions of LiCl and $SrCl_2$ as a function of dielectric constant D of the solvents: 1, ethanol $D_{20°C}$ 24.3; methanol $D_{20°C}$ 31.5; 3, acetonitrile $D_{20°C}$ 36.7; 4, dimethylformamide $D_{20°C}$ 36.7; 5, water $D_{20°C}$ 78.5; 6, formamide $D_{20°C}$, about 84 (16).

solvation properties of the solvent play a significant role in the process of specific adsorption of cations at the mercury surface.

It seems partially justifiable to accept desolvation as one of the most important factors in the specific adsorption of large cations in the inner region of the double layer.

In agreement with Grahame's suggestions, partial desolvation of cations in the double layer, proceeding at least from the side of the metal surface, results from the reversibility of some electroreduction processes. It should be difficult to show that the electron transfer through the solvation layer could proceed without any activation energy (15).

Additional data which prove the above suggestion are presented in Fig. 4 and 5. A comparison of the differential capacities of cesium and strontium chlorides in formamide with the corresponding data obtained previously for water (6) shows that in solvents of high dielectric constant, where the solvation energy is large, both factors, i.e., the increase in differential capacity and the influence of concentration, are very small and almost identical for cations of various polarizability. Thus, the specific adsorption of such a cation as cesium may be difficult. Moreover, the capacity values measured for a number of organic solvents showed that, in some regions of cathodic polarization sufficiently shifted from the zero charge potential where for moderately concentrated electrolyte solutions a characteristic capacity minimum occurs, a relatively good linear dependence between the differential capacity and the dielectric constant of the solvent is observed, as is shown in Fig. 6.

In connection with the above, an assumption may be put forward that, in a certain region of the potentials, the interface mercury solution possesses the structure similar to that of a simple capacitor whose dielectric is probably a monomolecular layer of the solvent. This layer may be considered as a continuous medium with the dipoles polarized by a strong electric field.

The differential capacity of such a region of the electrical double layer for moderately concentrated electrolyte solutions, as it was discussed by Mott and Watts-Tobin (13, 14), may therefore be con-

Table I. Values of K°

Solvent	l_0, A	Differential capacity, $\mu F/cm^2$	K_0
Formamide	4.1	15.0	7.2
Water	3.4	15.3	5.9
Acetonitrile	5.2	9.2	5.5
Dimethylformamide	5.6	6.5	4.1
Methylalcohol	3.8	8.5	3.7
Ethyl alcohol	4.8	6.5	3.6

sidered as a fairly simple function of dielectric saturation and characteristic polarization of the dipoles of a given solvent. For water and methanol a relatively good proportionality between the lowest value of the differential capacity and the dielectric constant of 0.1M electrolyte solutions has already been found by Grahame (1). He explained this proportionality by a combined effect of dielectric saturation of the inner region and the electrostriction of solvent molecules.

A relatively good linear relationship, observed in a small range of potentials in moderately concentrated solutions of electrolytes between the lowest value of differential capacity and solvent dielectric constant, Fig. 6, permits one to evaluate very roughly at least the influence of the electric field of the double layer on the decrease of dielectric constant in this layer. The effective dielectric constant of the solvent between the ion at the outer Helmholtz plane and the mercury surface K° was calculated on the basis of a simple electrostatic formula, valid for a plane condenser of unit area.

It was applied under the assumption that only a monomolecular solvent layer takes part in the differential capacity of the inner region of the double layer, and no specific ion adsorption is observed in this potential range. Besides, it was assumed that the thickness of the inner layer, l_0, cannot be smaller than the molecule diameter plus the ion radius.

The constant K° was calculated for the Li^+ ion, using for the radius the value 0.6Å in agreement with Pauling. The effective molecule radius was estimated on the basis of known bond lengths and angles.

Values so obtained of K° for some solvents are given in Table I. From comparison of K° with squares of refraction indexes of solvents, changing from 1777 for water to 2088 for formamide, it follows that the decrease of dielectric constant in the inner region of the double layer is due not only to electron polarization, but also to orientation polarization caused by at least partial dielectric saturation of solvent molecules by the field of inner region of the double layer.

Finally, it is worthwhile to pay attention to a certain very characteristic property of the double layer, which has often been discussed. It is a well-known fact that on curves of the differential capacity, obtained in aqueous electrolyte solutions in the region of insignificant cathodic polarization, a kind of a hump appears which depends imperceptibly on the kind of an anion and varies with temperature.

It follows from all the data published until now that this hump does not appear in any organic solvents of relatively low dielectric constant.

This characteristic hump, only slightly shifted toward a more cathodic polarization, appears in all the plots of the differential capacity of strontium and cesium chlorides in formamide, as shown in Fig. 4 and 5.

Because no values of zero charge potential of mercury in formamide are given, it is impossible to predict on which side of zero charge potential the hump is observed. It is very likely that this hump exists on the cathodic side of zero charge potential. In this case it could be explained easily by the combined effects of increase of capacity of the diffusion layer and dielectric saturation in the inner region.

At the present time the explanation of the appearance of humps in the differential capacity curves cannot be given. It seems, however, that knowledge of oxidation potentials of halogenide ions in organic solvent solutions of low dielectric constants where the humps are not observed might be helpful in a discussion of this problem.

Acknowledgments

The authors wish to thank Professor N. F. Mott and Dr. R. J. Watts-Tobin for reading the paper before publication and Mr. Z. Koczorowski for helpful discussions.

Manuscript received March 27, 1961; revised manuscript received July 28, 1961.

Any discussion of this paper will appear in a Discussion Section to be published in the June 1962 JOURNAL.

REFERENCES

1. D. C. Grahame, *Z. Elektrochem.*, **59**, 740 (1955).
2. S. Minc and J. Jastrzebska, *This Journal*, **107**, 136 (1960).
3. A. Mousa, H. Sammour, and H. Ghaly, *J. Chem. Soc.*, **1958**, 1269.
4. P. A. Kirkow, *J. Phys. Chem. U.S.S.R.*, **34**, 2375 (1960).
5. G. A. Korczynski, *ibid.*, **34**, 2759 (1960).
6. S. Minc and M. Brzostowska, *Roczniki Chem.*, **34**, 1109 (1960).
7. A. N. Frumkin, *Trans. Faraday Soc.*, **55**, 156 (1959).
8. A. N. Frumkin, *Izvest. Akad. Nauk S.S.S.R.*, **12**, 1421 (1957).
9. B. Damaskin, N. Nikolajewa-Fedorovic, and A. Frumkin, *Doklady Akad. Nauk, S.S.S.R.*, **121**, 129 (1958).
10. R. J. Macdonald, *J. Chem. Phys.*, **25**, 364 (1956).
11. R. Parsons and M. Devanathan, *Trans. Faraday Soc.*, **49**, 673 (1953).
12. A. N. Frumkin, *Ergeb. exakt. Naturw.*, **7**, 235 (1928).
13. N. F. Mott and R. J. Watts-Tobin, *Electrochemica Acta*, To be published.
14. R. J. Watts-Tobin, *Phil. Mag.*, To be published.
15. D. C. Grahame, *This Journal*, **98**, 343 (1951).
16. F. Calton and R. Brooker, *J. Phys. Chem.*, **62**, 1595 (1958).

Technical Notes

A-C Field Effect Measurements on Silicon

Norman G. Einspruch

Central Research Laboratories, Texas Instruments Incorporated, Dallas, Texas

Evidence that a-c field effect measurements have proved to be a powerful tool in elucidating the electrical transport properties of semiconductor surfaces can be found in the recent review article by Watkins (1) and in the proceedings of the 1956 (2) and 1959 (3) semiconductor surface physics conferences. Because of the difficulty encountered in producing variations in the surface potential of silicon samples by application of transverse electric fields or by exposure to gaseous ambients, a preponderance of the reports in the literature deals with results of experiments on germanium surfaces. Much of the reported work on transport phenomena in silicon surfaces has been done on device structures. Measurements on single-conductivity silicon samples have been reported by Buck and McKim (4), who measured primarily surface conductance and surface recombination velocity of samples which had been subjected to various chemical treatments; Rupprecht (5) studied the behavior of a CP-4 etched surface on application of rectangular high voltage pulses between the sample and a field plate; Atalla *et al.* (6) and Millea and Hall (7) reported field effect experiments on surfaces on which a thermally grown oxide layer was formed; Peattie and Savage (8) used a-c field effect techniques to study the effects of the relative humidity of the ambient air in contact with the silicon surface. In the present report, results of a-c field effect measurements performed at 72°C on a CP-4 etched silicon surface are presented. The conductance minimum, necessary for interpretation of the data in terms of the analysis of Kingston and Neustadter (9), has been observed, the amount of charge in the surface states is evaluated as a function of surface potential, and an equilibrium surface potential is calculated.

Some Experimental Detail

The electrical circuit employed in this experiment is essentially the balanced bridge described by Sorrows (10) in his report of work on PbS photoconductors and used previously in this laboratory (8, 11). The output signal from the bridge is amplified and displayed along the y direction of an x-y oscilloscope; the sinusoidal voltage which is impressed on the capacitor formed by the field plate and the semiconductor sample is fed into the x drive of the oscilloscope. The trace displayed on the oscilloscope is thus a direct measure of the variation in sample conductance as a function of induced charge. Analysis of the circuit yields the following results:

$$\Delta G = \frac{\Delta V\, L}{I_s WR^2\left(\dfrac{R'}{R+R'}\right)}$$

where ΔG is the change in conductance, ΔV the unbalance voltage from bridge, L the field plate length, W the sample width, R the resistance of portion of sample subject to the applied field, R' the resistance in series with sample, and I_s the d-c drift current in sample. The field effect mobility, μ_{FE}, is defined as the derivative of the conductance change with respect to the density of induced charge.

The samples were cut from an ingot of floating zone refined 400 ohm-cm p-type (boron doped) silicon. The rough cut slabs measured 0.8 x 0.2 x 0.02 in. The major surfaces were then lapped with abrasives of increasingly fine grit; the finest abrasive used was 3200 mesh. Before mounting in the sample holder, a sample would be treated with a CP-4 etch and stored in room air. The holder is designed such that the field plate and the sample each act as one plate of a parallel plate capacitor. A polished slab of strontium titanate serves as a dielectric spacer yielding a capacitance of 40 $\mu\mu$f. The sample and holder are inserted into a container designed such that the temperature of the sample and the temperature of the room air exposed to the sample can be regulated by the circulation of heated water.

Results and Analysis

An unretouched photograph of a 70 c/sec field effect response at 72°C is included as Fig. 1. Note that the curve clearly manifests a minimum in conductance and resembles the responses obtained by numerous workers studying germanium. Note further that the oscilloscope trace is a closed curve rather than an open figure; this demonstrates that no hysteresis effect is being observed in the present measurement applicable in a narrow frequency range around 70 c/sec. A field effect response as obtained here lends itself to analysis on the basis of the numerical integration of Poisson's equation presented by Kingston and Neustadter (9). The analysis presented below follows that utilized by Brown (12) in his classic interpretation of field effect meas-

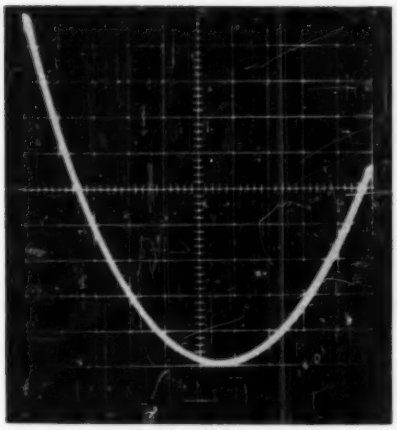

Fig. 1. Field effect response

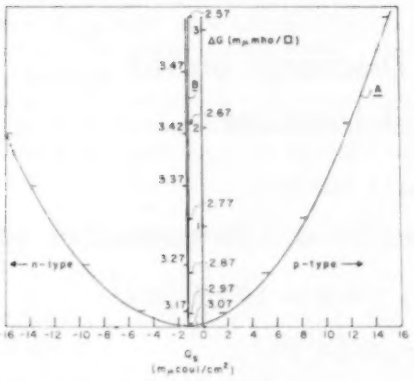

Fig. 2. Comparison of theoretical and experimental conductance curves.

urements on germanium. Curve A of Fig. 2 is a plot of the experimental data taken from Fig. 1; the data are presented as a curve illustrating the variation of surface conductance as a function of the total charge induced at the semiconductor surface, Q_s. Curve B results from the theoretical space charge calculation. Bulk mobilities, corrected for temperature variation using the results of Prince (13), were used throughout the calculations. The numbers indicated parametrically on the theoretical curve are values of the surface potential corresponding to the appropriate values of ΔG and Q_s. Since the minimum in sample conductance is a unique function of the material being studied, the experimental and theoretical curves are shifted along the ΔG axis such that the minima of the two curves lie on the $\Delta G = 0$ abscissa. The fact that the experimental curve is "broader" than the theoretical curve indicates that not all of the charge induced at the surface is available to contribute to the surface conductivity; it is concluded that this charge must be localized in surface states. In order to evaluate the magnitude of the charge immobilized in the surface states, Q_{ss}, as a function of surface potential, curves A and B are connected by horizontal segments drawn from each point on curve B at which the surface potential is known. The lengths of the segments are related to Q_{ss}. Figure 3 is a plot of the charge in the surface states as a function of surface potential. Sur-

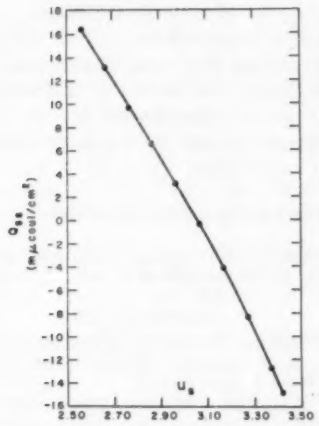

Fig. 3. Charge trapped in surface states as a function of surface potential.

face states with characteristic relaxation times longer than the inverse frequency of the signal applied between the sample and the field plate are not probed in this experiment.

Discussion

In the present paper, results are reported of a-c field effect measurements on silicon, analogous to those previously reported on germanium. The electric field has produced a variation in the density of charge trapped in the surface states over the range $+16.4$ to -14.8 mμ coulomb/cm^2 with a corresponding alteration in surface potential of less than one ($q\phi/kT$) unit.

The salient feature of this result is that, although substantial variations of the magnitude of the charge trapped in surface states can be produced by the transverse electric field, it is difficult to produce large variations in the surface potential [compare Fig. 3 with the results of Brown (12) or Margoninski (14) for germanium]. The problem of swinging the surface potential over a large range in order to observe the conductance minimum has been encountered in the past by workers in the field of semiconductor surface transport phenomena (15). Examination of Fig. 2 shows that at zero induced charge, $u_s = 3.0$; this corresponds to a surface potential of $+0.09$ v. The field effect mobility is taken from Fig. 2 as the slope of the experimental curve at zero induced charge and is found to be about 1/30 cm^2/v sec (p-type); one would expect an extremely low μ_{FE} in the present situation since the surface is almost intrinsic. Although the results reported here are of measurements made on one sample, similar effects have been observed on other samples prepared from the same ingot and from another ingot.

Information on the charge trapped in surface states combined with results of surface recombination velocity studies yields a complete physical description of the surface states. The success obtained in the course of work on field effect measurements at slightly elevated temperatures provides a basis for further experiments on silicon surfaces; a study of the effects of ambient gas cycles and the effects of illumination is presently in progress.

Acknowledgments

The author acknowledges with thanks the suggestion to pursue this line of research and helpful comments during the course of the work due to Dr. W. R. Savage. He also thanks Mr. D. J. Arnold for helpful discussions and for the numerical integration of Poisson's equation.

Manuscript received June 16, 1961.

Any discussion of this paper will appear in a Discussion Section to be published in the June 1962 JOURNAL.

REFERENCES

1. T. B. Watkins, "Progress in Semiconductors," **5**, pp. 1-52, A. F. Gibson, Editor, John Wiley & Sons, Inc., New York (1960).
2. R. H. Kingston, Editor, "Semiconductor Surface Physics," University of Pennsylvania Press, Philadelphia (1957).
3. J. N. Zemel, Editor, "Semiconductor Surfaces," Pergamon Press, New York (1960).
4. T. M. Buck and F. S. McKim, *This Journal*, **105**, 709 (1958).
5. G. Rupprecht, ref. (3), p. 208.
6. M. M. Atalla, E. Tannenbaum, and E. J. Scheibner, *Bell System Tech. J.*, **38**, 749 (1959).
7. M. F. Millea and T. C. Hall, *Phys. Rev. Letts.*, **1**, 276 (1958).
8. C. G. Peattie and W. R. Savage, *This Journal*, **106**, 61C (1959). Abstract.
9. R. H. Kingston and S. F. Neustadter, *J. Appl. Phys.*, **26**, 718 (1955).
10. H. E. Sorrows, Thesis-Catholic University of America, Washington, D. C. (1958). Navord Report 6164.
11. N. G. Einspruch, *Bull Amer. Phys. Soc. Ser.* II, **6**, 344 (1961).
12. W. L. Brown, *Phys. Rev.*, **100**, 590 (1955).
13. M. B. Prince, *ibid.*, **93**, 1204 (1954).
14. Y. Margoninski, *J. Chem. Phys.*, **32**, 1791 (1960).
15. Ref. (1), p. 42.

The Effect of an Electric Discharge on the Oxidation Kinetics of Uranium

J. G. Schnizlein, J. D. Bingle, and L. Leibowitz

Chemical Engineering Division, Argonne National Laboratory, Argonne, Illinois

It has been observed by several workers (1-6) that a variety of gas-solid reactions will proceed at an enhanced rate if the gas is activated by an electric discharge. In particular, Low (6) has clearly demonstrated the pronounced effect of a Tesla coil discharge in increasing the adsorption of oxygen on a variety of metals. In the course of work at this Laboratory on the kinetics of oxidation of uranium, an investigation was made of the effect of such an excitation and it is these exploratory measurements which are reported here.

Experimental

The apparatus used was an all Pyrex glass volumetric constant pressure system of conventional design. Details of construction and operation of the device are available elsewhere (7). For each experiment, the cm uranium cube used was mechanically polished to a 1μ diamond paste finish. The metal was of reasonably high purity with the major impurities in parts per million being N 56, Fe 45, Si 40, C 21, Ni 15, O 12. After the freshly polished metal cube was placed in the apparatus, the entire system was pumped down to a pressure below 10^{-5} mm Hg. Then, using a furnace operating in conjunction with a proportional controller, the reaction chamber was heated to 200°C. The sample temperature was maintained to within ± 1°C by this means. Tank gases were used without further purification. Typical oxygen analyses show the following impurities (in volume per cent), Ar, 0.1; CO_2, 0.06; N_2, 0.2; H_2O, 0.005. Oxygen was admitted at the desired time and its rate of uptake measured while an oxygen pressure of 20 mm was maintained. In the runs involving the Tesla coil, conditions were identical except that the spark discharge from a coil of the type used for leak testing was allowed to strike the glass apparatus just outside the furnace, some 20 cm from the metal. It was established that in the absence of a sample the discharge produced no detectable effect on the measuring system.

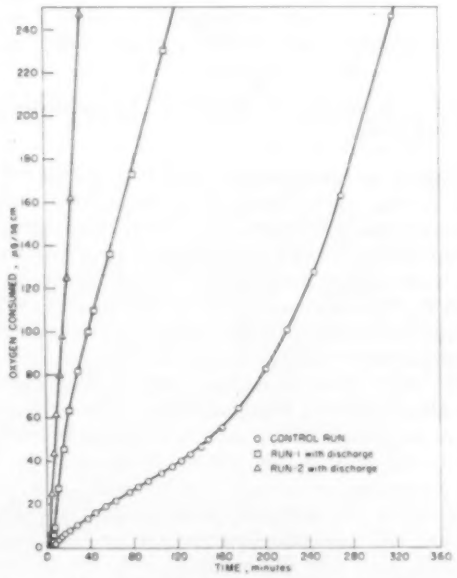

Fig. 1. Effect of Tesla coil discharge on the oxidation of uranium; oxidation at 200°C and 20 mm oxygen pressure.

Results and Discussion

Two experimental runs were carried out and these are shown, along with a control run, in Fig.

1. A marked increase in oxygen consumption resulted from the application of the discharge. The lack of control of the energy input was probably responsible for the poor reproducibility.

An interpretation of the kinetics of uranium oxidation has been suggested (8) in which the rate-controlling step occurs on the outer oxide surface. Any increase in the amount of gas adsorbed would be expected to increase the net rate of oxidation. As Low (6) has pointed out, although the amount of gas absorbed was increased by the Tesla discharge, the effects on the gas would be quite small, and the cause of the large effect on adsorption is to be sought in terms of a chain process involving the adsorbate. Taylor and Thon (9) have proposed that adsorption rates are determined by the rate of bimolecular site decay. Sites are presumed to be created on the surface by an initial branched chain reaction with the gas. The effect of the discharge would then be to create new adsorption sites on the solid surface. The active participation of the solid in the adsorption process has been discussed by many authors (10-13) and is to be contrasted with the Langmuir interpretation in which a fixed number of sites is always present on the solid surface.

Manuscript received May 8, 1961. Work performed under the auspices of the U.S.A.E.C.

Any discussion of this paper will appear in a Discussion Section to be published in the June 1962 JOURNAL.

REFERENCES

1. V. V. Tiapkina and P. D. Dankov, *Doklady Akad. Nauk. S.S.S.R.*, **57**, 1313 (1948).
2. A. V. Dravnieks, *J. Am. Chem. Soc.*, **72**, 3761 (1950).
3. H. J. Engell and K. Hauffe, *Z. Elektrochem.*, **57**, 762 (1953).
4. G. C. Fryburg, *J. Chem. Phys.*, **24**, 175 (1956).
5. R. I. Nazarova, *Zhur. Fiz. Khim.*, **36**, 79 (1958).
6. M. J. D. Low, *This Journal*, **104**, 439 (1957); **105**, 103 (1958).
7. H. A. Porte, J. G. Schnizlein, R. C. Vogel, and D. F. Fischer, *ibid.*, **107**, 506 (1960).
8. L. Leibowitz, J. G. Schnizlein, J. D. Bingle, and R. C. Vogel, *ibid.*, **108**, 1155 (1961).
9. H. A. Taylor and N. Thon, *J. Am. Chem. Soc.*, **74**, 4169 (1952).
10. F. F. Volkenshtein, *Zhur. Fiz. Khim.*, **23**, 912 (1949).
11. P. T. Landsberg, *J. Chem. Phys.*, **23**, 1079 (1955).
12. G. Parravano, H. G. Friedrick, and M. Boudart, *J. Phys. Chem.*, **63**, 1144 (1959).
13. A. Ciminio, E. Molinari, and E. Cipollini, *Gazz. chim. ital.*, **90**, 79 (1960); A. Cimino, E. Cipollini, E. Molinari, G. Liuti, and L. Manes, *ibid.*, **90**, 91 (1960); A. Cimino, E. Molinari, E. Cipollini, G. Liuti, and L. Manes, *ibid.*, **90**, 120 (1960).

The Influence of the Value of the Transference Number of the Univalent Ion on the Equivalent Conductance of Biunivalent Electrolytes

Neal Goldenberg and Edward S. Amis

Chemistry Department, University of Arkansas, Fayetteville, Arkansas

In our study (1) of the conductance of uranyl chloride in water, ethanol and water-ethanol solvents, it became necessary to know the transference number, $t^\circ_{Cl^-}$, at infinite dilution of the chloride ion in the various solvents in order to evaluate the equivalent conductance, Λ_o, of the uranyl chloride at infinite dilution and the dissociation constant, K, of the salt, which proved to be a weak electrolyte.

Much effort was expended in securing a good approximate value of the equivalent conductance at infinite dilution, Λ_o, in the various solvents. From these Λ_o values it is possible to obtain acceptable values of the transference numbers at infinite dilution of the chloride ion in pure water and pure ethanol from the equivalent ionic conductances at infinite dilution, recorded in the literature, of this ion in these solvents; namely, 76.34 mhos and 24.3 mhos, respectively, at 25°C. Since no data were available for $\lambda^\circ_{Cl^-}$ in the mixed solvents, it was assumed a linear relationship existed, and the transference number $t^\circ_{Cl^-}$ was calculated for the mixed solvents on the basis of this assumption. The transference numbers as calculated above showed little dependence on temperature and, since $\lambda^\circ_{Cl^-}$ was not known for pure ethanol, the transference numbers at these temperatures were taken to be the same as those at 25°C for a given solvent.

To justify our procedure with respect to the values of $t^\circ_{Cl^-}$ in the evaluation of Λ and K, calculations employing an I.B.M. 650 computer were carried out, based on the Shedlovsky (2) theory to test the sensitivity of values of Λ_o and K to the value of $t^\circ_{Cl^-}$ employed. The tests on Λ_o values were carried out using conductance data on strontium, barium, magnesium, calcium (3), and uranyl (1) chloride, and the tests on K values were made on conductance data for uranyl chloride.

In Table I are listed corresponding values of $t^\circ_{Cl^-}$, Λ_o, and K. The salts, other than uranyl chloride, were studied in water. Uranyl chloride data were calculated for the solvents indicated in the table.

It will be noted, first of all, that values of Λ_o are rather insensitive to small changes in $t^\circ_{Cl^-}$. Even a change of 0.1 of the magnitude of $t^\circ_{Cl^-}$ causes only a change in the fifth place of Λ_o values. Except for uranyl chloride in 20.2 w/o ethyl alcohol in water sovent, the Λ_o values increase slowly with decreasing values of $t^\circ_{Cl^-}$. The two sets of K values decrease somewhat more rapidly as $t^\circ_{Cl^-}$ is decreased.

Values of $t^\circ_{Cl^-}$ calculated from Shedlovsky's values of Λ_o are 0.562, 0.545, 0.590, and 0.562, respectively, for strontium, barium, magnesium, and calcium chlorides. These are reasonable and fairly consistent values of $t^\circ_{Cl^-}$. From the table, the values of $t^\circ_{Cl^-}$ cor-

Table I. Dependence of Λ_o and K on $t^\circ_{Cl^-}$

$t^\circ_{Cl^-}$	Λ_o						$K \times 10^4$	
	$SrCl_2$	$BaCl_2$	$MgCl_2$	$CaCl_2$	UO_2Cl_2		UO_2Cl_2	
					20.2 w/o EtOH	97.5 w/o EtOH	20.2 w/o EtOH	97.5 w/o EtOH
1.0	135.34	139.74	129.27	135.66	77.66	33.64	1.44	6.52
0.9	135.39	139.77	129.30	135.69	77.61	33.67	1.42	6.35
0.8	135.44	139.81	129.32	135.72	77.56	33.70	1.40	6.21
0.7	135.50	139.85	129.36	135.75	77.52	33.72	1.38	6.09
0.6	135.56	139.90	129.39	135.79	77.48	33.75	1.36	5.98
0.5	135.63	139.95	129.43	135.83	77.45	33.77	1.35	5.89
0.4	135.70	140.01	129.48	135.88	77.42	33.79	1.33	5.81
0.3	135.79	140.07	129.53	135.93	77.40	33.80	1.32	5.74
0.2	135.90	140.14	129.58	135.99	77.37	33.82	1.31	5.68
0.1	136.01	140.23	129.65	136.06	77.35	33.83	1.30	5.62
*	135.80	139.98	129.40	135.84	—	—	—	—

* Values determined by Shedlovsky and Brown, ref. (3).

responding to Shedlovsky's values are about 0.30, 0.45, 0.58, and 0.48, respectively, for strontium, barium, magnesium, and calcium chorides. These $t^\circ_{Cl^-}$ values are not so consistent, and the value for strontium is markedly small.

Acknowledgment

The authors wish to thank the Atomic Energy Commission for Contract No. AT-(40-1)-2069 which made this research possible financially.

Manuscript received May 31, 1961.

Any discussion of this paper will appear in a Discussion Section to be published in the June 1962 JOURNAL.

REFERENCES

1. Neal Goldenberg and E. S. Amis, *Z. physik. Chem.*, N.F., **22**, 63 (1959).
2. T. Shedlovsky, *J. Franklin Inst.*, **225**, 739 (1938).
3. T. Shedlovsky and A. S. Brown, *J. Am. Chem. Soc.*, **56**, 1066 (1934).

Brief Communication

Vapor Phase Growth of Gallium Arsenide Crystals

W. J. McAleer, H. R. Barkemeyer, and P. I. Pollak

Electronic Chemicals Research Department, Merck Sharp & Dohme Research Laboratories, Division of Merck & Co., Inc., Rahway, New Jersey

The formation of large bladelike crystals of gallium arsenide (Fig. 1) has been observed in the course of investigations directed in general toward the preparation of monocrystalline semiconductor compounds directly from the gas phase. The crystals can be prepared in a system containing the semiconductor compound components and some transfer agent in a dimensionally or time dependent temperature gradient. Previous work in the field of gas phase transport of solids has led to uncontrolled deposits (1). In contrast, the work described here permits the reproducible production of a specific crystal habit in the gallium arsenide system. The exact nature of the chemical reactions involved in the synthesis and the growth mechanism of these crystals is not known, but the reaction conditions existing in the reactor prior and during crystal growth suggest participation of a gallium subhalide which undergoes disproportionation and a specific combination of both a reactant supersaturation and a nucleation center, which control the formation of the specific crystal habit observed. Further studies of the detailed chemical and crystal growth mechanisms involved in this process are under way, and the results of this phase of the work will be reported at a later date.

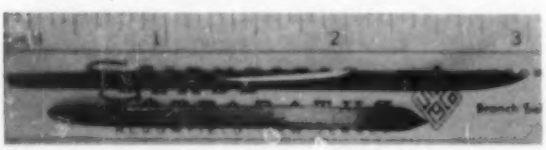

Fig. 1. Typical GaAs ribbon crystals

Using iodine as a transfer agent, crystals have been grown up to 10 cm long, 0.5 cm wide, and 0.01 cm thick; generally, however, the blades are approximately 5.0 cm long, 0.03 cm wide, and 0.0025 cm thick. Etching of the ribbons with a solution composed of 1 part HNO_3 (70%) in 2 parts H_2O (2, 3) revealed etch pits on one major face and none on the other (see Fig. 2 and 3). This behavior is character-

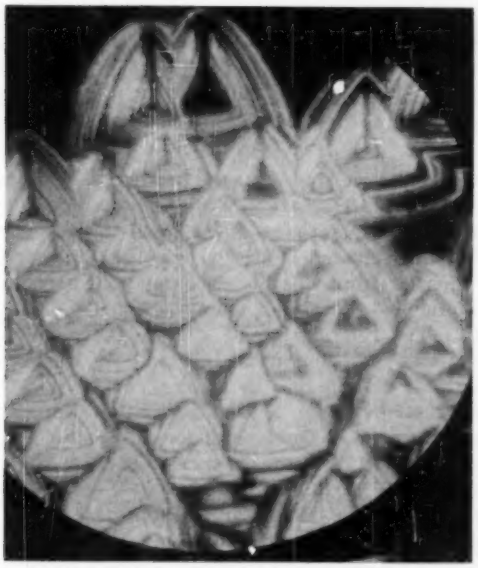

Fig. 2. One side of a GaAs ribbon after etching in HNO_3:H_2O (1:2). Magnification 500X before reduction for publication.

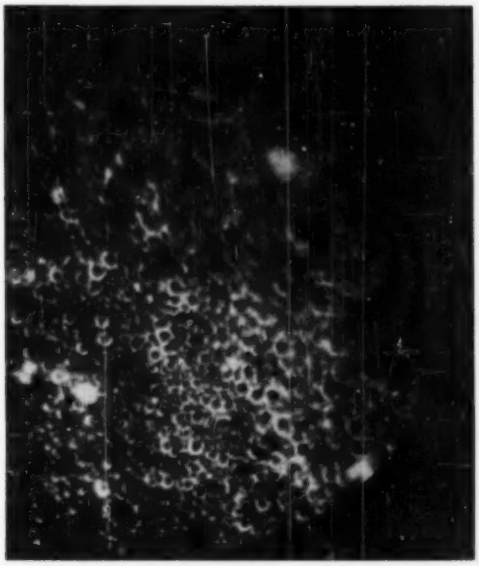

Fig. 3. Opposite side of the GaAs ribbon shown in Fig. 2 after etching in HNO_3:H_2O (1:2). Magnification 500X before reduction for publication.

istic of {111} and {$\bar{1}\bar{1}\bar{1}$} faces in III-V compounds (zinc blende structure) which exhibit polarity along the <111> directions (4).

Confirmation of the (111) orientation for the broad faces was also obtained from x-ray diffraction studies. X-ray diffraction photographs taken in oscillation about the ribbon axis indicated that growth takes place in a <112> direction.

The ribbons fracture readily at a 60° angle to the major growth direction revealing a {110} face, the preferred cleavage plane for gallium arsenide. The exposed {110} faces after cleavage are flat and mirrorlike; however, on etching in the Schell etchant some structure is revealed. Referring to Fig. 4, in which the etched {110} face is normal to the photograph, three distinct regions can be detected. Structures similar to the A-B region (Fig. 4) have been observed by Wagner (5) on cleaved surfaces of silicon ribbons grown in an iodide transport system. Wagner has shown that A and B (in the silicon case) are two {111} faces in twin relationship with the coherent twin plane parallel to the surface of the ribbon.

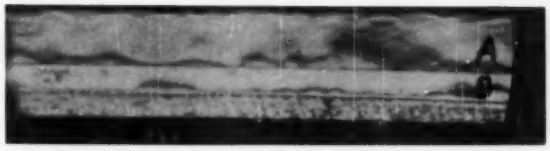

Fig. 4. A (110) face of a GaAs ribbon after etching in HNO_3:H_2O (1:2). Magnification 500X before reduction for publication.

Resistivity and Hall measurements show the crystals to be n-type with resistivities from 2×10^{-3} to 6×10^{-2} ohm-cm, and carrier concentrations from 5×10^{17} to 2×10^{18} electrons/cc. Mobilities calculated from the Hall coefficients and resistivities are between 1500 and 2000 cm^2 $volt^{-1}$ sec^{-1}, although in several instances mobilities of 3000 cm^2 $volt^{-1}$ sec^{-1} have been observed in crystals in the lower carrier concentration range.

Chemical analyses have shown that iodine in some form is incorporated in the ribbon at the rather high level of 0.07%. This observation has also been confirmed using radioactive iodine (I^{131}) as the transport agent and determining the iodine level by gamma counting. From the radioactive work it was found that the concentration of iodine at the surface was 0.11%, and that the interior, attained after etching away a layer of gallium arsenide, contained 0.024% iodine.

P-type ribbons doped to 6×10^{19} atoms/cc with zinc have been prepared by methods analogous to that already described for the n-type ribbons, and tunnel diodes have been prepared from this material.

Application of this technique of crystal growing from the gas phase to other compound and elemental semiconductors has yielded blade-like crystals of gallium phosphide, indium arsenide, silicon, and germanium.

Manuscript received Aug. 4, 1961.

Any discussion of this paper will appear in a Discussion Section to be published in the June 1962 JOURNAL.

REFERENCES

1. H. Schafer and B. Morcher, Z. *anorg. u. allgem. Chem.*, **290**, 279 (1957); R. F. Rolsten, *ibid.*, **305**, 25 (1960); G. R. Antell, and D. Effer, *This Journal*, **106**, 509 (1959).
2. H. Schell, Z. *Metallk.*, **48**, 158 (1957).
3. M. S. Abrahams and L. Ekstrom, "Properties of Elemental and Compound Semiconductors," p. 226, Interscience Publishers, New York City (1960).
4. H. C. Gatos and M. C. Lavine, *This Journal*, **107**, 427 (1960).
5. R. S. Wagner and R. G. Treuting, Submitted to *J. Appl. Phys.*

Discussion Section

This Discussion Section includes discussion of papers appearing in the JOURNAL of The Electrochemical Society, Vol. 108, No. 1, 3, 4, and 5 (January, March, April, and May, 1961). Discussion not available for this issue will appear in the Discussion Section of the June 1962 JOURNAL.

Thermodynamic Properties of Molten Mixtures of Cerium Chloride and Calcium Chloride

S. Senderoff, G. W. Mellors, and R. I. Bretz
(pp. 93-96, Vol. 108, No. 1)

M. A. Bredig[1]: The application by the authors of the principle that smaller size and higher charge of a solvent cation will result in less negative, or more positive, departures of the solute salt from ideality is, in general, well taken. However, a few details in the Discussion seem open to criticism.

If it is realized, as admitted by the authors, that the *positive* free energy values and, thus, also the activity coefficients for $CeCl_3$ in the second and third rows of Table I, at 90 and 80 mole % $CeCl_3$, are experimental errors, and if, consequently, the point at 60 mole % is considered the first correct point given for the mixtures, then the activity coefficient of $CeCl_3$ is still rising with the addition of $CaCl_2$ in the region even below 50 mole % $CeCl_3$ (Table I). Thus, "decomplexing" of $CeCl_3$ by $CaCl_2$ cannot be considered complete at 20 mole % $CaCl_2$ (80 mole % $CeCl_3$).

The word "activity" in parentheses in the middle of page 96, left column, should, of course, read "activity coefficients."

The correlation of the departure from ideality with the "charge density" of the ions does not seem reasonable as one is not concerned with a phenomenon inside the volume of this charged ionic sphere. The apparent correlation is obtained in the case of $CaCl_2$ at the cost of abandoning the well-established lanthanide contraction in accord with which Ce^{3+} is smaller than La^{3+}: If a radius of less than 1.15Å (La^{3+}) had been chosen for Ce^{3+}, for instance 1.12Å, the "charge density" for Ce^{3+} would come out to be equal to or slightly larger (2.13) than that for Ca^{2+} (2.06). Also, the more rational use of the ionic potential z/r, or of the force, z/r^2, would not show the correlation with the positive deviation in the case of $CaCl_2$, even with the radii used by the authors. It is believed that more subtle questions are involved, such as the problem as to which way cations of different charge distribute themselves together with possible cation vacancies in an ionic melt. Or, in other words, what really is the *ideal* entropy in mixing a 1:3 electrolyte such as molten $CeCl_3$ with 1:1 or with 1:2 electrolytes such as NaCl or $CaCl_2$?

S. Senderoff, G. W. Mellors, and R. I. Bretz: (*A*) We do not admit that the first two points in the table are experimental errors.

(*B*) Since we state that the departure from ideality of the $CaCl_2$ solution over its entire range (not only the first two points) is so small the we "cannot with full confidence ascribe physical meaning to it," then arguing whether decomplexing is complete at 80 or 60% $CeCl_3$ is sophistry.

(*C*) The relationship of Z/r^n to thermodynamic properties is an empirical one and we do not believe that a value of 1 or 2 for n can be said to be more "rational" than 3. We also see no rationality in the preference of Dr. Bredig for an r value of 1.12 rather than 1.18Å in the absence of any experimental confirmation, particularly in view of the approximation involved in using, for the ionic radius in the molten salt, the value determined for the crystal. We certainly would be interested in any correlation of the type suggested by Dr. Bredig, in which the entropy of mixing is related even approximately to the data of Fig. 2.

(*D*) We thank Dr. Bredig for noting the omission of the word "coefficients" on page 96.

[1] Chemistry Div., Oak Ridge National Lab. (Operated for the U.S. Atomic Energy Commission by the Union Carbide Nuclear Corp.), Oak Ridge, Tenn.
[2] Dept. of Chemistry, University of California, Berkeley 4, Calif.

The Formation of Chromium or Molybdenum Stabilized Tungsten Silicon Carbide

V. I. Matkovich and H. H. Rogers (pp. 261-262, Vol. 108, No. 3)

Leo Brewer[3]: The evidence presented by the authors for the composition triangle WC-W_5Si_3-WSi_2 allows the enthalpy of formation of W_5Si_3 to be fixed within a smaller range than given by Brewer and Krikorian.[3] If $\Delta H°_{298}$ for the formation of WSi_2 is taken as −22.4 kcal/mole, $\Delta H°_{298}$ for the formation of W_5Si_3 should be more positive than −44 kcal/mole and more negative than −34 kcal/mole. Thus, $\Delta H°_{298}$ of W_5Si_3 may now be given as −39±5 kcal/mole.

Oxidation and Equilibrium in Nonstoichiometric Zirconium Dioxide Powder

Seymour Aronson (pp. 312-316, Vol. 108, No. 4)

Leo Brewer[4]: The statement on pg. 314, "Since the results obtained using these variations in the experimental procedure were approximately the same, it seems reasonable to assume that equilibrium was attained . . .," is unacceptable in view of the data of Table I. The composition $ZrO_{1.9998}$ is reported to be in equilibrium at 1000°C with oxygen pressures in atm of 0.22, 1.7, and 18, all times 10^{-18}. Discrepancies in the data of 80-fold in pressure contradict any claim of equilibrium conditions. Thus, the claim that the partial pressure of oxygen in equilibrium with a fixed composition decreases with increasing temperature must be rejected in view of the contradictions among the data, as well as the impossibly large partial molal entropy of oxygen required by such a variation.

[3] L. Brewer and O. Krikorian, *This Journal*, 103, 702 (1956).
[4] Dept. of Chemistry, University of California, Berkeley 4, Calif.

Seymour Aronson: I agree with Dr. Brewer that the data in Table I are crude. In my opinion, their usefulness lies primarily in emphasizing the presence of significant nonstoichiometry in ZrO_2 and in indicating an approximate range of oxygen pressures and oxide compositions.

On the Mechanism of Cathodic Crystal Growth Processes

B. C. Banerjee and P. L. Walker, Jr. (pp. 449-454, Vol. 108, No. 5)

S. C. Barnes[5]: I have found the paper full of interest, and agree wholeheartedly with the authors that much has yet to be elucidated before we can fully understand the exact mechanism of cathodic crystal growth.

There are, however, one or two points which the authors fail to make clear in the paper, and also many about which further information would be appreciated.

Are we to believe that the 2.5 pH glycine bath produces a hexagonal form of copper?

It would appear so if the preferred orientation is $[10\bar{1}0] + [211]$. Do not the authors think the extra diffraction rings which they have observed, and obviously indexed as hexagonal copper, could possibly have originated from some codeposited impurity?

Shreir and Smith[6] quote an excess deposit weight, above the Faraday theoretical weight, of nearly 6% for a copper deposit obtained from a solution containing only 7.5 g/l glycine. Presumably, at least as much material would be codeposited from a bath containing 25 g/l glycine as used by the authors, probably more.

The authors say nothing about the number of times they used any one portion of electrolyte. Have they observed any difference between, for example, freshly made up glycine baths, and similar baths, after extended use?

Were the complex baths subjected to the low current density pre-electrolysis before, or after, addition of glycine? It is known that this addition agent is used up during electrolysis.[8]

The authors interpret the diffraction patterns originating from the specimens plated in baths [1] and [2] by suggesting that the deposit is of a larger grain size than the substrate. However, under the deposition conditions used (10 ma/cm^2, 25°C), it is known that deposits from uncontaminated acid-copper sulfate baths continue the substrate structure to thicknesses larger than those investigated by the authors. This has been shown for polycrystalline and single-crystal substrates.[7,8,9] It is difficult to see, therefore, how the deposit grain size could increase substantially after the comparatively short plating times used here. Deposits from glycine-containing solutions have likewise been observed to grow initially epitaxial,[10] although, at 25 g/l of addition agent, they would undoubtedly soon become polycrystalline, with their orientation completely unrelated to the substrate.

Epitaxial copper deposits, formed on the individual grains of polycrystalline strip, as well as on single-crystal cathodes, develop low index flat facets at varying angles to the mean substrate surface,[7,11] at times of the order of 30 min.[11,12] Even after plating times shorter than this, it is possible, by electron microscopy, to pick out the genesis of what ultimately become the well-defined crystallites.[11,12] Is it not possible that in their electron diffraction examination the authors have examined only the top few atom layers, and that they have observed these epitaxial crystallites?

In the Discussion section of their paper, the authors make use of the dislocation growth mechanism. This, it should be remembered, was originally proposed to account for the many experimental observations that crystal growth could occur at supersaturations below which, according to earlier theories, repeated nucleation at perfect surfaces was impossible.

In the present case, the supersaturation (as indicated by the overvoltage at the c.d. used, which was not measured) can be expected to be sufficient for repeated nucleation, particularly for those solutions containing large amounts of glycine.[8]

Furthermore, the preparatory treatment used for the copper strip in these experiments would also result in there being available numerous growth sites. The surface would, on an atomic scale, be far from smooth. In fact, it would probably be exceedingly rough. Thus growth could, under the experimental conditions used, continue without the necessity of invoking a dislocation mechanism, although sites at emergent dislocation steps would undoubtedly also contribute to the number of available sink positions. A mechanism suggested by Pick, *et al.*,[13] involving the "bunching" of growth layers, could be used to explain some of the authors' observations.

More information also would be appreciated on the actual metallurgical state of the substrate materials. Metal strip can have pronounced texture; after high deformations, face centered cubic metals can have, for example, a (110) [12] rolling texture or a (100) [001] annealing texture. In view of the small thickness dimensions of the materials used, it is difficult to visualize them having completely random orientations, unless special rolling and annealing schedules were employed.

Any initial texture would influence the first stages of deposition and, in the case of completely epitaxial deposits, be propogated completely. In fact, most of the early work on the crystal morphology of acid-copper deposits was carried out using base material with a cube texture.[13,14,15,16,17] This work has shown unambiguously that base-deposit continuity can occur over a wide range of deposition conditions.

[5] Joseph Lucas Group Research Centre, The Radleys, Birmingham 33, England.
[6] L. L. Shreir and J. W. Smith, *Trans. Faraday Soc.*, **50**, 393 (1954).
[7] G. G. Storey and S. C. Barnes, *Trans. Inst. Metal Finishing*, **37**, 11 (1960).
[8] G. Poli and L. P. Bicelli, *Metallurgia Ital.*, **51**, 548 (1959).
[9] S. C. Barnes, *Electrochim. Acta*, In Press.
[10] G. G. Storey and S. C. Barnes, *J. Inst. Metals*, In Press.
[11] H. J. Pick, G. G. Storey, and T. B. Vaughan, *Electrochim. Acta*, **2**, 165 (1960).
[12] V. R. Howes, *Proc. Phys. Soc. (London)*, **74**, 616 (1959).
[13] T. B. Vaughan, Ph.D. Thesis, University of Birmingham (1959).
[14] H. J. Pick and J. Wilcock, *Trans. Inst. Metal Finishing*, **35**, 298 (1958).
[15] R. Sroka and H. Fischer, *Z. Elektrochem.*, **60**, 109 (1956).
[16] H. Seiter and H. Fischer, *Z. Electrochem.*, **63**, 249 (1959).
[17] G. G. Storey, Ph.D. Thesis, University of Birmingham (1959).

When this occurs the deposit has, of necessity, the same texture as the base, and it is a two-degree preferred orientation, not a fiber texture.

Do the authors think this effect could be responsible for some of their observations on low c.d. nickel deposits which always seem to have a [110] orientation? The lattice parameters of copper and nickel are only 2.5% different, so thin deposits would probably be epitaxial. It is conceivable that any residual rolling texture in the copper strip cathode material could induce the observed texture in the nickel deposit.

In conclusion, I should like to congratulate the authors on their fine piece of work, but would recommend that as many of the now readily available experimental techniques, which can be used in studies such as these, be used simultaneously. It will be only by correlating chemical, electrochemical, metallurgical, and crystallographic information that a final solution to the complex problem of cathodic crystal growth will be possible.

P. V. K. Porgess[18]: I have found the paper a useful contribution to the complex field of electrodeposition and cathodic crystal growth. There is one point which the authors do not make clear. They state that the 2.5 pH glycine bath produces a copper deposit with a $(10\bar{1}0)$ + (211) preferred orientation. In other words, they have interpreted their electron diffraction patterns as being partly due to a new hexagonal copper. They do not, however, give any details as to its crystallography.

Fig. 1 and 2 of this discussion are theoretical electron diffraction patterns for f.c.c. copper having [211] and [111] preferred orientations, calculated using the methods given by Wilman.[19] Comparing these with the authors' electron diffraction photographs (Fig. 6 and 7) from the deposited copper, there seems to be little evidence of a [211] preferred orientation. Their photographs correspond well to a [111] orientation.

Electron diffraction photographs reproduced in journals lose a great deal of fine detail and are therefore difficult to examine properly. If the authors have found extra rings, corresponding to a hexagonal form of copper, which are not visible in the reproductions, then this undoubtedly would be a basis for a very useful paper.

B. C. Banerjee and P. L. Walker, Jr.: Drs. Barnes and Porgess have offered interesting comments on our report of the development of h.c.p. $(10\bar{1}0)$ + f.c.c. (211) orientations in electrolytic copper deposits. The following discussion may clarify some of the points raised.

The deposits under discussion were obtained by electrodepositing copper on polycrystalline Cu foils from a complex copper-glycine bath at 25°C and a pH of 2.5. Current density was 10 ma/cm^2. The diffraction patterns showing the mixed orientations obtained appear in Fig. 6 and 7 of our paper. Surface roughness of the copper deposits, resulting probably from adsorption of organic impurities from the bath even with comparatively small deposit thicknesses, caused losses in intensity, definition, and resolution in the reflection electron diffraction ring patterns. Further losses of definition in the final reproduction of the patterns, particularly the complete invisibility of (400) and (333) ring systems in Fig. 6 and 7, can easily lead to a mistaken interpretation of crystallite orientations in a visual examination of the figures. Hence, we can readily understand the temptation to attribute the characteristics of the published patterns to (111) preferred orientation, rather than a mixed $(10\bar{1}0)$ + (211), since the $(10\bar{1}0)$ and (111) ring systems are very close to each other. This point is emphasized by recent work on the development of h.c.p. $(10\bar{1}0)$ and f.c.c. (211) orientations by electrodeposited nickel, reported by Yang[20] and by Banerjee and Goswami.[21]

Examination of the theoretical patterns for f.c.c. structures furnished by Dr. Porgess shows the (311) and (222) ring systems lying very close to each other. The same is true for the (331) and (420) systems. Such close-lying systems will overlap each other in the absence of good resolution. However, examination of Fig. 6 and 7 shows that a faint (222) ring can, in fact, be detected, lying just beyond the much stronger (311). Careful study of the figures (or better, of the original plates) reveals no intensity maxima (arcing) at the intersection of the (111) normal (orientation axis) with the (222) and (333) ring systems, which should occur if (111) orientation is present. Thus, the evidence is strong that (111) orientation is absent. In drawing the opposite conclusion from our figures, Dr. Porgess may, we feel, have mistaken the (422) ring for the (333). The latter is not visible in the published figures.

[18] Joseph Lucas Group Research Centre, The Radleys, Birmingham 33, England.

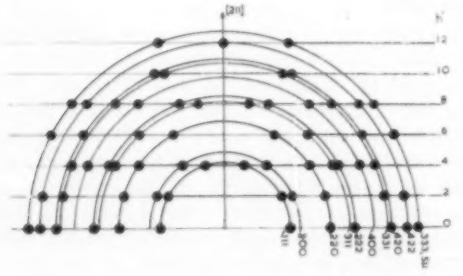

Fig. 1

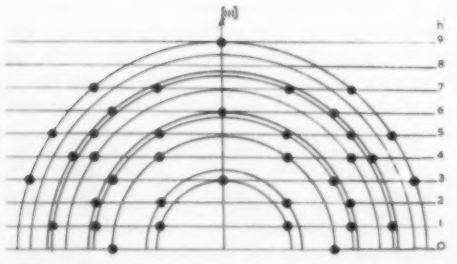

Fig. 2

[19] P. A. Wilman, *Acta Cryst.*, 5, 782 (1952).
[20] L. Yang, *This Journal*, 97, 241 (1950).
[21] B. C. Banerjee and A. Goswami, *J. Sci. Ind. Research (India)*, 14B, 322 (1955).

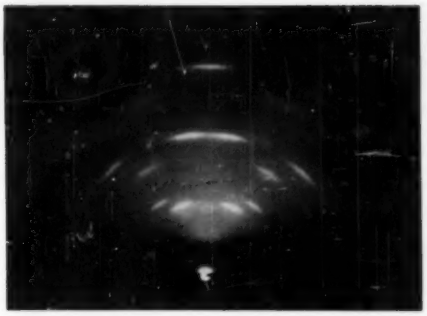

Fig. (A). A reflection electron diffraction pattern showing h.c.p. $(10\bar{1}0)$ + f.c.c. (211) orientations for electrodeposited nickel (sulfate chloride bath, pH 5.1, c.d. 10 ma/cm², bath temperature 25°C).

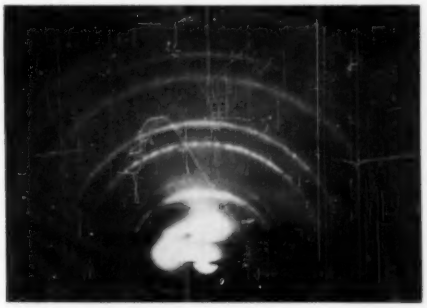

Fig. (B). A fresh reproduction of Fig. 7 in the original paper, showing $(10\bar{1}0)$ + (211) preferred orientation for electrolytic nickel.

Intensity maxima (arcing) can clearly be seen on the intersections of the (211) normal (orientation axis) with the (311) and (422) ring systems, in the figures. Therefore, the evidence for (211) orientation is very good. However, since the unit cell dimensions for hexagonal copper are not known, there remains the possibility that second order reflections from $(10\bar{1}0)$ planes could be falling approximately on the (311) ring. This possibility is strengthened considerably by the marked similarity of the patterns in Fig. 6 and 7 to those for electrodeposited nickel in which mixed structures have been established to be present. Fig. (*A*) published here shows a mixed structure of the electrolytic nickel for comparison with Fig. (*B*) which is a fresh reproduction of Fig. 7 in the original paper. More work remains to be done on the structure of the copper deposits, but the present evidence, in our opinion, definitely favors the presence of mixed structures.

The development of mixed structures in nickel has been attributed[20,21] to twinning introduced into the deposits during the growth process, caused by adsorption of impurities such as hydrogen or hydroxides. Similar considerations may hold in the case of copper. A second effect may arise from impurities such as those generated at the catholyte layer. These may hinder the mobility of atoms deposited on the cathode surface, which, in turn, may affect the manner in which they are incorporated into the crystal lattice.

Regarding purification of the plating solutions and the consumption of glycine resulting from repeated use, it can be stated that the acid-copper solutions were purified by prolonged low-current electrolysis using a dummy cathode, after which glycine was dissolved in the purified solution. This was followed by repeated filtration to remove suspended impurities. Fresh solutions from stock prepared in this way were used for electrodeposition, the used solutions being discarded after each experiment.

The current density used, 10 ma/cm², was not high enough to produce a large supersaturation of the ionic species at the catholyte layer. Hence, a dislocation growth mechanism must be considered to be important, although repeated nucleation may also have been occurring. However, we would like to point out that the dislocation growth mechanism may be important even at considerably higher current densities. The reason for this is that an impoverishment of metal ions will occur in the cathode-solution interfacial region, so that supersaturation of the metal ions may be comparatively low even though the current is large. Under these conditions, one finds that species other than the metal are also being deposited.

We completely agree with Dr. Barnes that a cathode surface can hardly be considered to be atomically smooth, and it may contain numerous imperfections or structural inhomogeneities that may be responsible for development of undulations of various sizes and shapes, at later stages of deposition. But the shapes of these undulations are not likely to be exact replicas of the microscopic inhomogeneities present in the original cathode surface.

Several factors besides the bath conditions and the structural imperfections in the original cathode surface are likely to influence the mechanisms of cathodic crystal growth. The following may be mentioned: (*a*) high porosity of the electrodeposits, especially in the early stages of deposition;[22] (*b*) the exothermic character of the electrodeposition process;[23] (*c*) influences of the considerable internal stresses developed in electrodeposits at various stages of deposition;[22,23] (*d*) influences of bath impurities;[24] and (*e*) the possibility of solid state reactions occurring at the surfaces of growing deposits. For a complete understanding of the complex processes involved in electrocrystallization, all of these factors must be explored. We hope that our work, though limited in scope, is a helpful contribution to the knowledge of electrodeposition phenomena.

Acknowledgment

Thanks are due to Professor Howard B. Palmer for helpful discussion during preparation of the manuscript.

[22] H. Wilman, *Proc. Phys. Soc. (London)*, **68B**, 474 (1955).
[23] I. L. Newell, *Metal Finishing*, pg. 56, Oct. 1960.
[24] B. C. Banerjee and A. Goswami, *J. Sci. Ind. Research (India)*, **16B**, 144 (1957).

FUTURE MEETINGS OF
The Electrochemical Society

Los Angeles, Calif., May 6, 7, 8, 9, and 10, 1962

Headquarters at the Statler Hilton Hotel

Sessions probably will be scheduled on

Electric Insulation (including sessions on Ceramics and Integrated Circuits, Thin Film Dielectrics and Electrolytic Capacitors, Reliability, and Paper), Electronics (including Luminescence, Semiconductors, Optical Masers, and Nonconventional Electron Emitters), Electrothermics and Metallurgy (including a Symposium on Thermodynamics and Kinetics of Gas-Condensed Phase Reactions at High Temperatures), Industrial Electrolytics, and Theoretical Electrochemistry

★ ★ ★

Boston, Mass., September 16, 17, 18, 19, and 20, 1962

Headquarters at the Statler Hilton Hotel

★ ★ ★

Pittsburgh, Pa., April 14, 15, 16, 17, and 18, 1963

Headquarters at the Penn Sheraton Hotel

★ ★ ★

New York, N. Y., September 29, 30, and October 1, 2, and 3, 1963

Headquarters at the New Yorker Hotel

★ ★ ★

Toronto, Ont., Canada, May 3, 4, 5, 6, and 7, 1964

Headquarters at the Royal York Hotel

Papers are now being solicited for the meeting to be held in Los Angeles, Calif., May 6-10, 1962. Triplicate copies of each abstract (*not exceeding 75 words in length*) are due at Society Headquarters, 1860 Broadway, New York 23, N. Y., *not later than December 15, 1961* in order to be included in the program. *Please indicate on abstract for which Division's symposium the paper is to be scheduled, and underline the name of the author who will present the paper.* No paper will be placed on the program unless one of the authors, or a qualified person designated by the authors, has agreed to present it in person. An author who wishes his paper considered for publication in the JOURNAL should send triplicate copies of the manuscript to the Managing Editor of the JOURNAL, 1860 Broadway, New York 23, N. Y.

Presentation of a paper at a technical meeting of the Society does not guarantee publication in the JOURNAL. However, all papers so presented become the property of The Electrochemical Society, and may not be published elsewhere, either in whole or in part, unless permission for release is requested of and granted by the Editor. Papers already published elsewhere, or submitted for publication elsewhere, are not acceptable for oral presentation except on invitation by a Divisional program Chairman.

Current Affairs

Norman Hackerman Appointed Vice-President and Provost of University of Texas

Dr. Norman Hackerman, former head of the Dept. of Chemistry and dean of research and sponsored projects, University of Texas, Austin, recently was chosen new vice-president and provost of the Main University. He succeeds Dr. Joseph Smiley who assumed the presidency of the Main University in June. In recommending Dr. Hackerman's appointment, president Smiley stated: "We are extremely fortunate in securing Dr. Hackerman's consent to serve the University in this important post. A scientist with a distinguished record of research and publication, Dr. Hackerman, who has been chairman of the Dept. of Chemistry since 1952, has had a wide and significant experience in administrative posts. His personal attributes as well as his long and successful service in the University make him ideally suited for his new position as the University's chief academic officer." He has been a member of the University faculty since 1945.

Dr. Hackerman has served as adviser to the University system on science development, and will continue as a member of the system committee for the planning of science programs.

Portrait by Walter Barnes Studio

Norman Hackerman

His research interests have dealt principally with the chemistry and physics of surfaces, especially as these phenomena apply to metal corrosion. He and his students have published numerous articles on adsorption on metal surfaces and its influence on electrochemical properties and reactivity, and on the passivity of metals.

Before joining the University of Texas, Dr. Hackerman taught chemistry at Loyola College, Baltimore, Md., and at Virginia Polytechnic Institute, Blacksburg, Va. He also was affiliated as research chemist with the Colloid Corp. and the Kellex Corp., and as assistant chemist with the Civil Service. In 1953, he was technical consultant to the Atomic Energy Commission, advising on hydrogen bomb production.

A member of The Electrochemical Society since 1943, Dr. Hackerman served as Chairman of the Corrosion Division in 1951, as President in 1957-1958, and has been Technical Editor of the JOURNAL since 1950.

He belongs to the American Association for the Advancement of Science, and was the 1950 Chairman of the Gordon Corrosion Research Conference. He also is a member of Phi Lambda Upsilon, Sigma XI, The Faraday Society, the American Chemical Society, and the National Association of Corrosion Engineers, having served on the Board of Directors for the latter. He also is a member of the Board of Editors of the Chemical Monograph Series of the American Chemical Society, and was Chairman of the Intersociety Corrosion Committee in 1956-1958.

Symposium on Multilayer Systems Scheduled for ECS Los Angeles Meeting, May 1962

A symposium on Multilayer Systems is scheduled for the Spring Meeting of The Electrochemical Society, to be held in Los Angeles, Calif., May 6-10, 1962.

The intended scope of the symposium is multilayer systems aimed at eliminating or restricting oxidation or chemical corrosion, or providing thermal protection.

It is hoped to cover the following topics in the program:

1. **Applications:** Environmental factors against which protection is required or which have to be controlled; nature and mechanism of damage to structural materials caused by aggressive environments; methods of protection and control.

2. **Composition and Structure of Multilayer Systems:** Criteria of choice of composition and structure of multilayer protective systems; physical and chemical compatibility of materials in composite multilayer structures; physical properties; microstructure.

3. **Fabrication:** Methods of preparation, application, and shaping of multilayer components; substrate's surface conditioning for coating application; scaling-up from a laboratory development to a practical application.

4. **Testing and Evaluation:** Testing in simulated environment; testing equipment; specifications and preparation of test samples; specifications for test conditions; mechanical strength and thermal stability of multilayer systems; environmental stability.

It is planned to introduce each of these topics with a paper discussing the general problem and the pre-

sent state of the art, and to follow with papers presenting the current investigations and developments.

Abstracts for the symposium were due by November 15, 1961. Program Chairman is Dr. E. C. Burke, Manager, Metallurgy and Ceramics (53-36), Lockheed Missiles and Space Co., Palo Alto, Calif.

Special Symposia Planned for Boston Meeting of Electrochemical Society, September 1962

Symposium on Phenomena at Interfaces

A joint symposium of the Corrosion and Electronics Divisions will be held at The Electrochemical Society's Boston Meeting, September 1962. The symposium will center about phenomena at interfaces. Metal and semiconductor materials will be included. Papers dealing with the following topics will be considered: **Solid-Gas Interfaces** adsorption and its role in surface behavior, oxidation, the role of imperfections, thermal etching, fundamentals of epitaxial growth, work function); **Solid-Electrolyte Interfaces** (electrochemical reactions of metals, semiconductors, and oxide-covered metals in aqueous electrolytes, including solute adsorption, and etching); **Solid-Melt Interfaces** (nucleation and growth, impurity effects, impurity distribution, crystal habit, etching).

Suitable papers are solicited for this symposium. Triplicate copies of abstracts (not exceeding 75 words in length) must be received at Society Headquarters, 1860 Broadway, New York 23, N. Y., by *May 15, 1962.* It should be indicated on the abstract that the paper is to be considered for the Phenomena at Interfaces Symposium.*

Inquiries and suggestions regarding the symposium should be addressed to the Program Chairman, Harry C. Gatos, Lincoln Lab., Massachusetts Institute of Technology, Lexington 73, Mass.

* No paper will be placed on the program unless one of the authors, or a qualified person designated by the authors, has agreed to present it in person.

Symposium on Electrochemical Processes for Semiconductor Devices

A special symposium on Electrochemical Processes for Semiconductor Devices will be held jointly by the Electrodeposition and Electronics Divisions of the Society at the Boston Meeting in September 1962. The primary object of the symposium is to integrate the widely scattered information regarding electrochemical processes used to make semiconductor devices. Emphasis will be placed on the science and technology of electrochemical processes for metal parts as well as the semiconductor material. The main topics of the symposium will be: 1. Cleaning and Treatment of Semiconductor Surfaces and Metal Parts; 2. Electrochemical Slicing and Shaping Semiconductors; 3. Electro- and Chemical-Polishing Metals and Semiconductors; and 4. Metal Deposition on Metal Parts and Semiconductors.

If you have a suitable paper and wish to have it considered for this symposium, triplicate copies of abstracts (not exceeding 75 words in length) must be received at Society Headquarters, 1860 Broadway, New York 23, N. Y., *not later than May 15, 1962.* Please indicate on the abstract that the paper is to be scheduled for the Electrochemical Processes for Semiconductor Devices Symposium.*

Inquiries and suggestions about the symposium should be sent to the Program Chairman, D. R. Turner, Bell Telephone Labs., Inc., Murray Hill, N. J.

Symposium on Semiconductor Phenomena

A symposium on Semiconductor Phenomena will be held as part of the meeting of The Electrochemical Society to be held in Boston, September 1962. Papers on all aspects of semiconductors will be welcomed. Papers on the following topics will be particularly welcome, since they will form the theme of the symposium: 1. Properties of Impure Semiconductors and Semimetals; 2. Properties of New and Exotic Semiconductors. In addition to contributed papers, it is expected that the program will include several invited papers on these topics.

Triplicate copies of abstracts (not exceeding 75 words in length) must be received at Society Headquarters, 1860 Broadway, New York 23, N. Y., *not later than May 15, 1962.* It should be indicated on the abstract that the paper is to be considered for the Semiconductor Symposium.*

Inquiries and suggestions regarding the symposium should be addressed to the Program Chairman, W. Crawford Dunlap, Raytheon Co., Research Div., Waltham 54, Mass.

Brief Communications

The JOURNAL accepts short technical reports having unusual importance or timely interest, where speed of publication is a consideration. The communication may summarize results of important research justifying announcement before such time as a more detailed manuscript can be published. Consideration also will be given to reports of significant unfinished research which the author cannot pursue further, but the results of which are of potential use to others. Comments on papers already published in the JOURNAL should be reserved for the Discussion Section published biannually.

Submit communications in triplicate, typewritten double-spaced, to the Editor, Journal of The Electrochemical Society, 1860 Broadway, New York 23, N. Y.

Abstracts of "Recent News" Papers

Presented at Electronics Division Semiconductor Symposia

Detroit Meeting October 2-4, 1961

Electrolytic Etching of Germanium and Other Semiconductors in Water

W. Rindner and R. Ellis, Jr., Research Div., Raytheon Co., Waltham, Mass.

The electrolytic etching of Ge, GaAs, and GaP in water is reported. The properties and mechanism of this new etching method have been studied with particular reference to Ge. It has been found that electrolytic etching with water can be employed usefully for the attainment of good resolution where localized etching is desired. The etching rate is considerably higher than that reported for Ge using water as a chemical etchant.

Localized Low Breakdown in Diffused Silicon Devices

P. S. Flint, Fairchild Semiconductor Corp., Mountain View, Calif.

This paper covers further studies on the "pipe" phenomenon, a principal cause of low breakdown in diffused silicon junctions. The electron probe x-ray microanalyzer is employed as a tool for determining the chemical composition of pipes. The roles of both bulk properties and surface cleanliness in pipe formation are discussed and some methods for the prevention of pipes are proposed.

The Masking of Phosphorus Pentoxide by Silicon Dioxide

P. S. Flint, Fairchild Semiconductor Corp., Mountain View, Calif.

It is already known that the diffusion profile of P_2O_5 through SiO_2 shows a very steep front, indicating that a second-phase glass of composition $P_xSi_yO_z$ probably is formed. This paper demonstrates that such a second phase does exist on the basis of (*a*) etching rates, and (*b*) visual means whereoy the glass thickness can be determined. Rate of formation of the glass is discussed. The possibility of different etching rates causing lifting problems associated with masking is discussed.

A Machine for Cleaning Semiconductor Slices

F. L. Gittler, Bell Telephone Labs., Inc., Allentown, Pa.

A machine for chemical cleaning of semiconductor slices is described. The materials of construction, method of slice transport, and handling of cleaning materials is such that highly corrosive agents can be used to accomplish the cleaning. Provision is made to clean at elevated temperatures. At present, 30 slices per hour are being produced.

Effects of Copper on Fast Surface States of Etched Germanium

D. R. Frankl, General Telephone & Electronics Labs., Inc., Bayside 60, N. Y.

Copper contamination is found to influence the fast surface states of Ge. The nature of the effect depends on the previous surface treatment: (*a*) on an etched surface, which is hydrophobic, the copper has little immediate effect but enhances the growth of recombination centers in oxidizing atmospheres; (*b*) on a KOH-treated surface, which is hydrophyllic, the copper immediately produces a large concentration of recombination centers. In general, there is no apparent correlation between surface recombination and charge trapping in fast states.

Surface Protection of Silicon Devices with Glass Films

H. S. Lehman, J. A. Perri, W. A. Pliskin, and J. Riseman, Development Labs., Data Systems Div., International Business Machines Corp., Poughkeepsie, N. Y.

A method and technology to protect silicon electronic devices from ambient effects is presented. The application of this method will increase their reliability, decrease their cost, and make them amenable for incorporation in miniaturized and integrated circuits. As compared to conventional methods of sealing, which consist of enclosing the device completely and using glass to metal seals, the present method protects only the sensitive areas; *e.g.*, where a p-n junction intersects the surface. The protective medium becomes an integral part of the device and is chemically bonded to it.

Flat, homogeneous, pin-hole-free layers of glass in the micron thickness range have been applied to planar silicon devices without affecting the device properties. These layers have manifested a protective capability well beyond that of a thick, thermally grown silicon-dioxide layer.

The Use of Infrared Spectroscopy for the Detection of Adsorbed Monolayers and Their Interaction with Semiconductor Surfaces

W. A. Pliskin and R. R. Dion, Development Labs., Data Systems Div., International Business Machines Corp., Poughkeepsie, N. Y.

Stearic acid was chosen for this study since it is a molecule containing an active functional group and it can be adsorbed as a monolayer by the Langmuir-Blodgett technique. Monolayers of the acid were adsorbed on single-crystal wafers of silicon and germanium. By transmission through four wafers in series and by use of a scale expander, absorption spectra of the adsorbed acid were obtained. The absorption bands due to the alkyl group showed little change from regular stearic acid, but the position of the carbonyl stretching absorption band indicated a stronger interaction with the germanium surface than with the silicon surface. Spectra are shown and precautions necessary to reduce interference effects are discussed.

Surface H_2O Retention of P-Type Germanium

S. S. Baird and Charley Dennis, Texas Instruments Inc., Dallas 22, Texas

The surface waterstoichiometry of crushed germanium treated with acid, base, oxidizing, and water reagents produced negligible changes in water retained by the surface particles, except for hot nitric acid treatment. The germanium surfaces were more hydrophobic than silicon surfaces treated under similar conditions with the exception of water-treated surfaces. A comparison is made of silicon and germanium surfaces similarly treated.

The Effect of Adsorbed Gases on Silicon Surfaces

R. P. Williams and S. S. Baird, Texas Instruments Inc., Dallas 22, Texas

The directions of surface-type shift of silicon surfaces caused by the adsorption of various inorganic gases are described. In most cases, the shift is believed not to be caused by ionic action but is believed due to the way the molecules are arranged on the surface. These results

may lead to the general statement that oxidizing atmospheres produce a P-type surface, and reducing atmospheres an N-type surface.

Oxidation-Induced Degradation of Reverse Characteristics of Silicon Diodes

C. R. Fuller and S. S. Baird, Texas Instruments Inc., Dallas 22, Texas

Oxidation of silicon diodes tends to degrade certain reverse characteristics. This paper shows that this degradation results in part from a surface rearrangement of the diffused dopant, and that the extent of the degradation can be controlled by controlling the surface concentration of the diffusant.

Electrical Properties of Thin TiO_2 Films

A. Feuersanger, General Telephone & Electronics Labs., Inc., Bayside 60, N. Y.

Thin insulating films of titanium dioxide have been formed on semiconductor and metal substrates at relatively low temperatures by a gas reaction process used previously for deposition on glass.

Films about 0.1μ thick have an effective dielectric constant of about 30 resulting in a specific capacitance of 0.3 $\mu f/cm^2$, with a dissipation factor of 0.028 at 1 kc and a d-c resistivity of 10^{12} ohm-cm.

This method is advantageous for formation of miniature capacitors, since one can fabricate them with various metals, whereas the anodizing technique is limited to titanium. By deposition of such films on germanium and silicon substrates, voltage-variable capacitors were obtained. The observed changes of capacitance with voltage are in good agreement with theory.

Epitaxial Silicon-Germanium Alloy Films on Silicon Substrates

K. J. Miller and M. J. Grieco, Bell Telephone Labs., Inc., Murray Hill, N. J.

Some properties of silicon-germanium alloy films grown epitaxially on (100), (110), and (111) silicon substrates have been studied over a composition range up to 30 atomic % germanium. The apparatus and method of preparation used to grow these films are described. The method provides a means of preparing semiconductor materials with properties which can be varied by changing the material composition.

Perfection of Epitaxial and Diffused Layers

G. H. Schwuttke, General Telephone & Electronics Labs., Inc., Bayside 60, N. Y.

X-ray diffraction microscopy is an excellent tool for the study of crystal perfection in thin layers. In investigating the perfection of epitaxial layers on silicon, it was found that the dislocation density in base material and layer can be quite different from each other. Defects present on the surface of the base material are shown to act as dislocation sources during growth of the epitaxial layer.

The method was also employed to study the perfection of shallow diffused surface layers. Here it was used to analyze the nature of regular arrays of lines as observed by Queisser and Prussin. It was established that these lines are dislocations lying in the diffusion plane and are introduced by the diffusion process.

The research reported in this paper was sponsored by the Electronics Research Directorate of the Air Force Cambridge Research Center, Air Research and Development Command under Contract No. AF-19(604)7313.

A Multislice Technique for Epitaxial Growth of Silicon Layers

V. Sils, J. Porter, N. Cerniglia, and P. Wang, Semiconductor Div., Sylvania Electric Products Inc., Woburn, Mass.

A multislice production-scale process for the epitaxial growth of silicon layers for mesa transistors in an induction-heated vertical furnace is described. Tight control of layer thickness, surface finish uniformity, and layer resistivity has been achieved. The collector breakdown voltage of transistors made from the epitaxial wafers can be controlled in tight limits. Techniques for checking layer resistivity and layer thickness are discussed.

Infrared Interference Measurements on Epitaxial Layers

P. H. Keck, General Telephone & Electronics Labs., Inc., Bayside 60, N. Y., and T. A. Longo, Sylvania Electric Products Inc., Woburn, Mass.

A nondestructive optical determination of the thickness of epitaxial layers for production control is described. The thin top layer of low free-carrier concentration usually is grown onto a heavily doped substrate. The dielectric constant in the infrared region depends on the free-carrier concentration; therefore, radiation impinging on an epitaxial wafer is reflected partially at the surface and partially at the interface between the epitaxial layer and the substrate. Consequently, an interference pattern can be produced under favorable circumstances, leading to an accurate measurement of the layer thickness.

We have studied the interference method for n-type silicon wafers and obtained good patterns in the wave-length range between 10 and 25μ for substrates with a resistivity smaller than 0.008 ohm-cm or an electron concentration larger than 6×10^{18} per cc; the carrier concentration of the epitaxial layer must be at least one order of magnitude smaller.

For routine measurements, a reflection attachment has been developed for the Perkin-Elmer Spectrometer Model 112. An image of the exit slit is formed on the sample surface, and the reflected light is picked up by the standard ellipsoidal mirror and thermocouple. Details of the instrument as well as measurements on epitaxial silicon wafers are discussed.

Correlation of Infrared and Staining Techniques for Epitaxial Film Thickness Measurements

E. G. Grochowski and W. A. Pliskin, Development Labs., Data Systems

Notice to Subscribers

Your subscription to the JOURNAL of The Electrochemical Society will expire on *December 31, 1961*. Avoid missing any issue. Send us your remittance now in the amount of $24.00 for your 1962 subscription. (Subscribers located outside the United States must add $1.50 to the subscription price for postage, and payment must be made by Money Order or New York draft, not local check.) An expiration notice has been mailed to all subscribers.

A bound volume of the 1962 JOURNALS can be obtained at the prepublication price of $8.00 by adding this amount to your remittance. However, no orders will be accepted at this rate after *January 1, 1962*, when the price will be increased to $24.00 subject to prior acceptance. Bound volumes are *not* offered independently of your JOURNAL subscription.

Div., International Business Machines Corp., Poughkeepsie, N. Y.

The measurement of infrared interference fringes has been found to be a useful nondestructive technique for determining the thickness of films grown epitaxially on heavily doped silicon substrates. By proper masking and reflection optics, this technique has been extended to give thickness measurements for areas as small as 1 mm². Infrared-determined thickness profiles of epitaxial films were checked against junction depths determined by staining techniques of N on N+ substrates. The investigation showed good correlation between the two techniques.

Thickness Measurement of Epitaxial Films by the Infrared Interference Method

M. P. Albert and J. F. Combs

Infrared interference measurement has proven to be an accurate nondestructive means for evaluating the thickness of epitaxially grown films on silicon. The measuring technique is discussed and the necessary relationships and constants are presented.

Also, a fringe wave length *vs.* film thickness chart is constructed, enabling rapid thickness measurement without calculation. The chart is for use with silicon films of low-carrier concentration deposited on substrate material of high-carrier concentration. The chart is most useful for low-order interference fringes.

Similar charts are applicable for other materials, and suggestions are given.

Vapor Phase Growth of Gallium Arsenide Crystals

W. J. McAleer, H. R. Barkemeyer, and P. I. Pollak, Merck Sharp & Dohme Research Labs., Rahway, N. J.

Large blade-like crystals of gallium arsenide up to 10 cm in length and 0.5 cm in width have been grown from the vapor, employing a halide transport system. Descriptions of the physical, crystallographic, and electrical properties of both N- and P-type crystals are presented.

Some possible chemical and crystal growth mechanisms involved in the synthesis are discussed.

Junction Diodes on Gallium Arsenide Dendrites

N. A. Jordan, Westinghouse Electric Corp., Pittsburgh, Pa.

The feasibility of making useful p-n junction diodes on dendritic gallium arsenide has been demonstrated.

Junction diodes have been made by alloying a p-type impurity on n-type gallium arsenide dendrites as the substrate. The dendrites are grown in the <211> direction and the junctions are formed on the (111) plane. Dendrites with a net impurity concentration varying from 5×10^{18} to 5×10^{15} atoms per cc have been used. The characteristics of these diodes (forward and reverse currents, capacitance, etc.) have been evaluated in a range of temperatures from 77°K to 350°K and under two different ambient conditions. Units were made with breakdown voltages above 70v.

Neutron Activation Study of Gallium Arsenide Contamination by Quartz

W. Kern, Radio Corp. of America, Somerville, N. J.

GaAs crystals were synthesized by the horizontal Bridgman method using neutron-activated boats of natural and synthetic fused quartz. Instrumental radiochemical techniques were applied to determine the Si concentrations and to identify other transferred trace elements. All crystals were found completely enveloped in an impurity-enriched surface layer with Si concentrations up to 0.2%. Bulk concentrations of Si ranged from 1×10^{17} to 3×10^{18} cm^{-3}. Evidence of several types of transfer mechanisms was obtained.

Other transferred impurities include Cu, Ga, Sb, and Au at concentrations below 10^{16} atoms cm^{-3}; these impurities were decreased effectively by use of high-purity synthetic quartz.

The work described in this paper was sponsored by the Electronic Technology Lab., Aeronautics Systems Div., Air Force Systems Command, United States Air Force.

The Traveling Solvent Method of Crystal Growth

A. I. Mlavsky, Materials Research Lab., Tyco Inc., Waltham, Mass.

A novel technique is described for the growth of single crystals of intermetallic compounds from solution. The technique involves the passage of a thin solvent zone through a material under the influence of a temperature gradient which may be produced by the Peltier effect. This technique is particularly applicable to high-melting-point compounds or compounds having a volatile component. It also can be adapted to the fabrication of junction structures. Some preliminary results are reported for the growth of GaAs on Ga.

Solid Solubility of Arsenic in Germanium at 865°C from a Saturation Diffusion Experiment

F. A. Trumbore, W. G. Spitzer, and R. A. Logan, Bell Telephone Labs., Inc., Murray Hill, N. J.

Arsenic was diffused into thin germanium slices (10–23 mils thick) at 865°C in a sealed-tube experiment lasting 97 days. The carrier concentration, n, in the as-diffused samples was 5×10^{19} cm^{-3} as determined from optical reflectivity measurements. After heat treatment and quenching of these samples, $n = 7.5 \times 10^{19}$ cm^{-3}. The arsenic concentration, determined chemically, agreed within experimental error with the quenched-in carrier concentration. These results indicate that the equilibrium solid solubility of arsenic in germanium is almost a factor of two lower than reported previously.

Fast and Slow Photoelectronic Effects in Single-Crystal Boron

J. T. Breslin and G. K. Gaule, U.S. Army Signal Research and Development Lab., Fort Monmouth, N. J.

Crystalline boron of the β-rhombohedral (high-temperature) form

Notice to Members
Re Voting Ballot

By now you have received your official voting ballot from Society Headquarters. If you have not already done so, please return the ballot *by December 15* so that your vote can be included in the final election count.

Notice to Members and Subscribers

(Re Changes of Address)

To insure receipt of each issue of the JOURNAL, please be sure to give us your old address, as well as your new one, when you move. Our records are filed by states and cities, not by individual names. The Post Office does not forward magazines.

We should have this information *by the 16th of the month* to avoid delays in receipt of the next issue.

is a material with a bandgap of 1.6 ev which has high resistivity (10^6 ohm-cm and more) even if relatively large amounts of impurities (up to 0.1%) are present. it is believed that many impurities create donor levels but also compensating vacancy-levels and that most carriers are locally bound in equilibrium. Properties of the "trap"-system were revealed by using light of varying wave length, combined with electric fields and also with changes of temperature. Recent experiments show that the very "slow" photoconductivity at low temperature is p-type and probably the indirect result of the excitation of surface states by visible light. The "fast" photoconductivity at room temperature, peaking in the near infrared, is apparently caused by the well-known "direct" mechanism. The "fast" photovoltage observed at both low and room temperature also is discussed.

A Simple Technique for Growing Seeded Single-Crystal Antimony Square-Sectioned Rods

Seymour Epstein, U. S. Army Signal Research and Development Lab., Fort Monmouth, N. J.

Numerous experimental arrangements differing in detail have been reported by which various-shaped unstrained monocrystalline rods of bismuth and higher-melting-point elements can be grown directly. Although in principal these are suitable for antimony, it was found desirable to make a modified apparatus and procedure by which have been obtained, at virtually 100% yield, nearly square (3 mm x 3 mm), long (6 cm or more), relatively unstrained, single-crystal rods whose axes are at either 0°, 45°, or 90° with the principal crystallographic axis. The direction of growth is the rod axis, and, by the use of both a fast crystallization rate and a crucible material of low thermal conductivity, growth normal to the preferred direction, which is the case for the 0° rods, is accomplished. Secondary axis orientation also is conveniently controlled by the apparatus and procedure to be described, and a measure of goodness of rods of the two principal orientations is indicated.

Section News

News from India

Seminar on Caustic Soda Industry in India.—The Development Council for Alkalis and Allied Industries, Government of India, held a Seminar on Caustic Soda Industry in India in Bombay during December 1960. Twenty-seven papers were presented under the following Sections: 1. brine purification in alkali industries; 2. power rectification techniques and equipment; 3. electrolytic cell design and operations; 4. caustic soda fusion and packaging; 5. caustic soda by chemical process; 6. preventive maintenance; 7. statistical quality control; 8. instrumentation; 9. material of construction and corrosion; 10. research and development: The list of papers can be found in *Chemical Age of India*, Vol. 12, No. 1 (1961); it is planned to publish the proceedings of the Seminar in *Chemical Age of India*.

Third Seminar on Electrochemistry.—The Central Electrochemical Research Institute is holding the third Seminar on Electrochemistry at Karaikudi during December 1961. The object of the Seminar is to provide an opportunity for scientists connected with different disciplines of electrochemistry to come together and discuss their contributions so as to be complementary to each other in the advancement of electrochemistry. Contributions are also invited related to personal experiences and data collected in the operation of electrochemical plants. Papers were due at the Institute by November 15.

Expansion of Steel Plants in India.—The Government of India is preparing project reports for the expansion of the Bhilai, Rourkela, and Durgapur Steel Works, tentatively estimated to cost Rupees 138,90 and 56 crores, respectively. The capacity of these plants would be expanded from 1 to 2.5, 1 to 1.8, and 1 to 1.6 million ingot tons, respectively. A proposal to set up a plant by the Madras State during the Third Plan period has been accepted. A project, estimated to cost Rs. 50 crores, is contemplated by a Madras firm for producing 50,000 tons per year of alloy and special steels, together with 20 tons per day of ferrosilicon and ferrochrome. The present annual demand of alloy steel —107,000 tons— is expected to rise to 275,900 tons by 1966. Alloy steel plants are proposed to be set up by Tata Iron and Steel Co. and Canara Workshops. The Canara plant is expected to go into production by the end of 1962, the initial production target of 800 tons per month being stepped up to 3000 tons per month.

Symposium on Chemical Process Design.—A Symposium on Chemical Process Design was held at the Indian Institute of Science, Bangalore, on July 24 and 25, 1961 under the auspices of the Chemical Research Committee, Council of Scientific and Industrial Research, India. There were 28 papers under the following sections: chemical process development; scaling-up of chemical processes; chemical process equipment design; and operating experiences of chemical production plants. The organizers have plans to publish the proceedings. The following papers were contributed by members of the India Section: 1. "Development of a Process and Plant for Manufacture of Potassium Chlorate," by S. Ramaswamy and N. Kalyanam; 2. "Scale-Up in the Design of Electrolytic Cells, Part II. Production of Salicylaldehyde by Reduction of Salicylic Acid," by S. Ganesan, K. S. Udupa, G. S. Subramanian, and H. V. K. Udupa; 4. "Design Problems in Corrosion Engineering," by J. Sundararajan and T. L. Rama Char.

Committee on Fundamentals of Corrosion Studies.—The Council of Scientific and Industrial Research, India, has constituted a Committee on Fundamentals of Corrosion Studies with representatives from the following organizations: 1. Ministry of Railways; 2. Naval Chemical and Metallurgical Laboratory, Bombay; 3. Indian Institute of Science, Bangalore; 4. Central Electrochemical Research Institute, Karaikudi; 5. National Metallurgical Laboratory, Jamshedpur; 6. National Chemical Laboratory, Poona. The object of

1962 Bound Volume

Members and subscribers who wish to receive bound copies of Vol. 109 (for 1962) of the JOURNAL can receive the volume for the low, prepublication price of $8.00 if their orders are received at Society Headquarters, 1860 Broadway, New York 23, N. Y., *by January 1, 1962*. After that date, members will be charged $12.00, and nonmembers, including subscribers, $24.00, subject to prior acceptance.

Bound volumes are *not* offered independently of JOURNAL subscription.

this Committee is to strengthen existing corrosion research centers, arrange symposia and refresher courses, and disseminate technical information.

San Francisco Section

The September meeting of the San Francisco Section was held at the Men's Faculty Club at the University of California in Berkeley. Following dinner, E. F. Duffek of Stanford Research Institute spoke on recent developments in electrodeposition.

Dr. Duffek discussed such developments as bright, duplex, and leveled platings, together with the baths, techniques, and problems involved. Alloy deposition was covered, including the properties and uses of such deposits. Dr. Duffek also described electroless plating, magnetic film plating, and electroforming. Mechanisms were discussed briefly, together with problems that have been encountered and areas in which research is needed.

New Members

In November 1961, the following were elected to membership in The Electrochemical Society by the Admissions Committee.

Active Members

M. M. Baizer, Monsanto Chemical Co., 800 N. Lindbergh Blvd., St. Louis 66, Mo. (Electro-Organic)

R. C. Barrett, Barrett Chemical Products Co., Inc., 5 Bridge St., Shelton, Conn. (Electrodeposition)

K. E. Bean, Eagle-Picher Research Labs.; Mail add: 2105 Rockdale Blvd., Miami, Okla. (Electronics—Semiconductors)

R. E. Biddick, Gould-National Batteries, Inc., 2630 University Ave., S.E., Minneapolis 14, Minn. (Battery, Electro-Organic, Theoretical Electrochemistry)

Louis Belove, Sonotone Corp.; Mail add: 29 Overlook Rd., Ardsley, N. Y. (Battery)

S. E. Blum, I.B.M. Corp., Box 218, Yorktown Heights, N. Y. (Electronics—Semiconductors)

R. W. Bohl, Dow Chemical Co., 3-261 Bldg., Midland, Mich. (Industrial Electrolytic)

J. S. Bone, General Electric Co.; Mail add: 3 Linden St., South Glens Falls, N. Y. (Battery)

M. H. Boyer, Aeronutronic, Div. Ford Motor Co., Ford Rd., Newport Beach, Calif. (Battery, Electronics—Semiconductors and Luminescence, Electro-Organic, Theoretical Electrochemistry)

J. M. Brown, National Carbon Co.; Mail add: 325 W. Rowan Court, Naperville, Ill. (Industrial Electrolytic)

J. E. Buskirk, Delco Remy Div., General Motors Corp.; Mail add: 309 Forest Ave., Muncie, Ind. (Battery)

J. G. E. Cohn, Engelhard Industries, Inc., 497 Delancy St., Newark 5, N. J. (Battery)

J. F. Demendi, Pure Carbon Co.; Mail add: R.D. 1, Kersey (Elk County), Pa. (Battery, Electrothermics & Metallurgy)

J. R. Duwve, Electric Autolite Co.; Mail add: 3326 Eastmoreland South, Oregon 16, Ohio (Battery)

A. P. Edson, International Nickel Co., Inc., 67 Wall St., New York 5, N. Y. (Battery)

H. R. Fellner, Hewlett-Packard Co.; Mail add: 691 Arastradero, Palo Alto, Calif. (Electronics—Semiconductors and Luminescence)

A. K. Foroud, Texas Instruments, Inc., Metals & Controls Div.; Mail add: 184 S. Main St., Attleboro, Mass. (Electrothermics & Metallurgy)

R. A. Foust, Jr., Philco Research Center; Mail add: Plymouth Rd., Gwynedd Valley, Pa. (Battery, Theoretical Electrochemistry)

H. M. Fox, Phillips Petroleum Co.; Mail add: 728 Winding Way, Bartlesville, Okla.

B. L. Gilbert, I.B.M. Corp.; Mail add: 2 California Rd., R.D. 1, Box S-28, Yorktown Heights, N. Y. (Electronics—Semiconductors)

Jose Giner, Pratt & Whitney Corp.; Mail add: 121 Shipman Dr., Glastonbury, Conn.

Irwin Gitin, Industro Transistor Corp.; Mail add: 53 Legregni St., Saddle Brook, N. J. (Electronics—Semiconductors)

J. W. Grenier, General Electric Co., ARO, Chemical Engineering, Bldg. 200, Evandale, Cincinnati 15, Ohio (Electrodeposition)

A. K. Hagenlocher, General Telephone & Electronics Labs., Bayside 60, N. Y. (Electronics—Semiconductors)

R. G. Haldeman, American Cyanamid Co., 1937 W. Main St., Stamford, Conn. (Battery)

E. D. Haller, Arthur H. Thomas Co., Third & Vine Sts., Philadelphia 5, Pa. (Theoretical Electrochemistry)

J. A. Henricks, Alcor Chemical Co.; Mail add: 742 N. Oak Park Ave., Oak Park, Ill. (Electrodeposition)

R. W. Hodgson, Western Electric Co., Inc.; Mail add: 2341 Eden Lane, Bethlehem, Pa. (Electronics—Semiconductors)

E. J. Jackson, Globe-Union Inc.; Mail add: 7132 Cliffside Dr., Racine, Wis. (Battery)

E. W. Jones, Remington Rand Univac; Mail add: 5301 Webster St., Philadelphia 43, Pa. (Corrosion, Electrodeposition)

F. J. Kaim, Superior Plating Inc., 315-1st Ave., N.E., Minneapolis 13, Minn. (Electrodeposition)

R. B. Kaplin, Pittsburgh Plate Glass Co., Chemicals Div.; Mail add: 760 Fifth St., New Martinsville, W. Va. (Industrial Electrolytic)

Ivan Kerzner, Seaway Nickel Corp., 101 East Ave., North Tonawanda, N. Y. (Electrodeposition)

J. E. Kettman, I.B.M. Corp.; Mail add: 920 Redbird Dr., San Jose, Calif. (Electrodeposition)

V. K. Kofron, Vactec Inc., 1209 Olive Way, St. Louis 30, Mo. (Electronics—Semiconductors)

A. F. Kravic, International Nickel Co., Inc., 67 Wall St., New York 5, N. Y. (Battery, Electrothermics & Metallurgy)

J. D. Little, Incar Inc., 2097 Columbus Rd., Cleveland 13, Ohio (Electrodeposition)

G. A. Louis, U. S. Semcor; Mail add: 1101 Mariposa Dr., Scottsdale, Ariz. (Electronics—Semiconductors)

D. V. Louzos, Union Carbide Consumer Products Co.; Mail add: 2746 Tonawanda Dr., Rocky River 16, Ohio (Battery)

F. T. Mansur, Avco Research & Adv. Development; Mail add: 658 Wilder St., Lowell, Mass. (Electrodeposition)

G. A. Marsh, Pure Oil Co.; Mail add: 155 Franklin Ave., Crystal Lake, Ill. (Corrosion)

Alfred Meyerhoff, Westinghouse Electric Corp.; Mail add: 605 De Gregory Dr., Greensburg, Pa. (Electric Insulation, Electrodeposition, Electronics—Semiconductors, Electrothermics & Metallurgy)

R. R. Moest, Bell Telephone Labs., Inc., Rm. 2A-235, Murray Hill, N. J. (Electronics—Semiconductors)

Yaqub Moradzadeh, I.B.M. Corp., Monterey & Cottle Rd., San Jose, Calif. (Electrodeposition, Electron-

---

By action of the Board of Directors of the Society, all prospective members must include first year's dues with their applications for membership.

Also, please note that, if sponsors sign the application form itself, processing can be expedited considerably.

ics—Semiconductors and Luminescence, Theoretical Electrochemistry)

R. H. Moss, Westinghouse Electric Corp.; Mail add: 206 Indian Dr., Pittsburgh 38, Pa. (Electronics—Semiconductors)

J. M. Nees, National Lead Co., Research Labs., 105 York St., Brooklyn 1, N. Y. (Battery)

T. E. Norby, A. O. Smith Corp.; Mail add: 1526 Alice St., Wauwatosa 13, Wis. (Battery)

R. A. Oriani, U. S. Steel Fundamental Research Lab., Monroeville, Pa. (Corrosion, Electrodeposition, Theoretical Electrochemistry)

H. G. Oswin, Leesona Moos Labs., Inc.; Mail add: P. O. Box 531, Ardsley, N. Y. (Battery, Corrosion, Theoretical Electrochemistry)

S. R. Ovshinsky, Energy Conversion Labs., Inc., 14121 W. McNichols Rd., Detroit 35, Mich. (Electronics—Semiconductors)

J. E. Oxley, Leesona Moos Labs., Inc.; Mail add: 18 Gay St., New York, N. Y. (Battery, Theoretical Electrochemistry)

G. C. Della Pergola, Westinghouse Research Labs., Beulah Rd., Pittsburgh 35, Pa. (Electronics—Semiconductors)

J. R. Piazza, Western Electric Engineering Research Lab.; Mail add: 206 Center, Princeton, N. J. (Electrothermics & Metallurgy)

D. M. C. Ramsey-Raisan, Western Asbestos Co., 675 Townsend St., San Francisco 3, Calif. (Electronics—Semiconductors and Luminescence)

J. D. Reynolds, Motorola Inc.; Mail add: 5421 Calle del Norte, Phoenix, Ariz. (Electronics—Semiconductors)

G. D. Rose, Westinghouse Research Corp.; Mail add: 521 South Braddock, Pittsburgh 21, Pa. (Electronics—Semiconductors)

A. S. Roy, Bell Telephone Labs., Inc., Murray Hill, N. J. (Battery, Corrosion, Electronics—Semiconductors, Electrothermics & Metallurgy, Theoretical Electrochemistry)

R. S. Gumucio, Yardney International Corp.; Mail add: Paseo de la Habana No. 105, Madrid 16, Spain (Battery, Electronics—Semiconductors and Luminescence, Electro-Organic, Electrothermics & Metallurgy, Theoretical Electrochemistry)

D. S. Scheufele, Shipley Co. Inc., Walnut St., Wellesley Hills 81, Mass. (Electro-Organic, Theoretical Electrochemistry)

D. J. Schinedhette, Chrysler Corp.; Mail add: 20170 Houghton Ave.,

ECS Membership Statistics

The following three tables give breakdown of membership as of Oct. 1, 1961. The Secretary's Office feels that a regular accounting of membership will be very stimulating to membership committee activities. In Table I it should be noted that the totals appearing in the right-hand column are *not* the sums of the figures in that line since members belong to more than one Division and, also, because Sustaining Members are not assigned to Divisions. But the totals listed are the total membership in each Section. In Table I, Sustaining Members have been credited to the various Sections.

Table I. *ECS Membership by Sections and Divisions*

Section	Division: Battery	Corrosion	Electric Insulation	Electrodeposition	Electronics	Electro-Organic	Electrothermics & Met.	Industrial Electrolytic	Theoretical Electrochem.	No Division	Total as of 1/1/61	Total as of 10/1/61	Net Change
Boston	19	37	16	34	93	5	23	9	28	5	177	189	+ 12
Chicago	25	33	11	36	36	18	19	15	38	6	148	152	+ 4
Cleveland	57	29	1	42	43	8	31	26	36	7	192	190	— 2
Columbus, Ohio	5	13	3	17	17	2	32	5	9	2	60	65	+ 5
Detroit	26	23	4	53	21	8	11	9	40	6	104	116	+ 12
India	9	10	2	22	7	6	6	8	16	3	42	39	— 3
Indianapolis	35	12	15	12	30	8	15	7	17	3	69	82	+ 13
Midland	10	15	2	5	6	3	9	16	10	0	43	46	+ 3
Mohawk-Hudson	17	29	19	9	25	2	12	4	27	4	76	89	+ 13
New York	121	112	34	177	199	41	107	78	134	36	618	657	+ 39
Niagara Falls	13	19	2	25	31	6	67	58	12	10	168	168	0
Ontario-Quebec	5	20	2	12	7	1	37	25	12	4	92	86	— 6
Pacific Northwest	5	9	0	9	4	0	6	8	13	3	38	36	— 2
Philadelphia	40	21	7	40	81	7	27	23	46	16	210	214	+ 4
Pittsburgh	6	46	5	29	47	6	34	19	38	1	133	139	+ 6
San Francisco	19	14	1	29	37	4	17	20	27	2	98	104	+ 6
S. Calif.-Nevada	28	26	4	42	75	7	32	22	48	6	150	168	+ 18
Texas	7	25	2	14	58	4	8	26	32	1	103	124	+ 21
Washington-Baltimore	39	35	8	36	27	4	14	6	23	3	144	141	— 3
U. S. Non-Section	60	68	11	81	76	34	62	48	88	27	349	352	+ 3
Foreign Non-Section	65	66	17	70	42	33	50	67	89	85	302	315	+ 13
Total as of Jan. 1, 1961	558	660	153	790	855	197	633	506	743	220	3316		
Total as of Oct. 1, 1961	611	662	166	794	961	207	619	498	784	230		3472	
Net Change	+53	+2	+13	+4	+106	+10	—14	—8	+41	+10			+156

Table II. *ECS Membership by Grade*

	Total as of 1/1/61	Total as of 10/1/61	Net Change
Active	2895	2912	+ 17
Faraday (Active)	33	37	+ 4
Deutsche Bunsen Gesellschaft (Active)	17	21	+ 4
Delinquent	84	184	+100
Active Representative Patron Members	10	10	0
Active Representative Sustaining Members	107	105	— 2
Total Active Members	3132	3245	+113
Life	16	16	0
Emeritus	65	87	+ 22
Associate	39	49	+ 10
Student	43	44	+ 1
Honorary	7	7	0
Total	3316	3472	+156

The figures pertaining to Patron and Sustaining Member Representatives, and Faraday and Deutsche Bunsen Gesellschaft members subscribing to the JOURNAL, have been added to reflect reclassifications and changes in membership status.

Table III. *ECS Patron and Sustaining Membership*

	Total as of 1/1/61	Total as of 10/1/61	Net Change
Patron Member Companies	5	5	0
Sustaining Member Companies	157	150	— 7

Detroit 19, Mich. (Battery, Electrodeposition)

I. M. Schulman, General Electric Co., Missile & Space Vehicle Dept.; Mail add: 118 Boulder Rd., Plymouth Meeting, Pa. (Battery)

A. K. M. Shamsul Huq, Tyco Inc.; Mail add: 18 Concord Ave., Cambridge, Mass. (Battery Corrosion, Electrodeposition, Theoretical Electrochemistry)

W. S. Strathdee, Union Carbide Canada Ltd., Metals & Carbons Div., Beauharnois, Que., Canada

Stanislaw Szpak, Stanford Research Institute, 820 Mission St., South Pasadena, Calif. (Corrosion, Electrodeposition, Industrial Electrolytic, Theoretical Electrochemistry)

Hideo Tamura, Osaka University; Mail add (after Jan. 1, 1962): 1042 Konoike, Kawachi-Shi, Osaka, Japan (Battery, Electrodeposition, Electronics—Luminescence, Electrothermics & Metallurgy, Industrial Electrolytic, Theoretical Electrochemistry)

R. F. Waters, American Oil Co., 2500 New York Ave., Whiting, Ind. (Theoretical Electrochemistry)

Louis Weaver, Tung Sol Electric Inc.; Mail add: 161 Munn Ave., East Orange, N. J. (Electronics—Semiconductors)

Joan T. Wiarda, Metals & Plastics Publishing Inc., 381 Broadway, Westwood, N. J. (Electrodeposition)

C. R. Wiese, General Motors Research Labs.; Mail add: 357 Manistique, Detroit 15, Mich. (Battery)

Martin Wolf, Heliotek Corp., 12500 Gladstone Ave., Sylmar, Calif. (Electronics— Semiconductors)

S. P. Wolsky, P. R. Mallory & Co., Inc.; Mail add: 1 Park St., Lexington 73, Mass. (Electronics—Semiconductors)

C. M. Wright, Hercules Powder Co., Research Center, Wilmington, Del. (Electro-Organic)

Associate Members

G. L. Baughman, Martin Co.; Mail add: 1018 Marlowe Ave., Orlando, Fla. (Corrosion)

B. T. Buzalski, Leesona Moos Research Corp.; Mail add: 8 Park Dr., Cranford, N. J. (Theoretical Electrochemistry)

T. J. Farrow, Owens-Illinois Glass Co.; Mail add: 4736 Overland Pkwy., Toledo 12, Ohio (Corrosion, Electrodeposition)

Gene Frick, Electric Auto-Lite Co.; Mail add: 3306 Middlesex, Toledo 6, Ohio (Battery, Theoretical Electrochemistry)

J. A. Nelson, Inland Steel Co., Research & Development Dept., 7035 Woodmar Ave., Hammond, Ind. (Corrosion, Theoretical Electrochemistry)

Lee Van Gorman, Texas Instruments, Inc.; Mail add: 320A Hilltop, Richardson, Texas (Electronics—Semiconductors, Electrothermics & Metallurgy)

N. E. Zetterquist, Shockley Transistor, Unit of Clevite Transistor; Mail add: 6363 Atherwood Ave., San Jose 9, Calif. (Electronics—Semiconductors)

Student Associate Members

L. M. Chambers, University of Illinois, 312B Noyes Lab., Urbana, Ill. (Theoretical Electrochemistry)

G. F. Uhlig, M.I.T. Graduate House, Cambridge 39, Mass. (Corrosion)

Reinstatements to Active Membership

Howard Lessoff, Radio Corp. of America, 64 "A" St., Needham Heights 94, Mass. (Electrodeposition, Electrothermics & Metallurgy)

Ferenc Schmidt, General Electric Co., 3198 Chesnut St., Philadelphia 1, Pa. (Electrodeposition, Electronics, Electrothermics & Metallurgy, Industrial Electrolytic, Theoretical Electrochemistry)

Transfer from Student to Active Membership

Ralf Koslow, Dept. of Chemistry, Louisiana State University, Lake Front, New Orleans 22, La. (Corrosion, Electro-Organic, Theoretical Electrochemistry)

Reinstatement and Transfer from Associate to Active Membership

L. C. Kenausis, Research & Technical Center, Anaconda American Brass Co., Waterbury 20, Conn. (Corrosion, Electrodeposition, Theoretical Electrochemistry)

Deceased Members

W. M. MacNevin, Columbus, Ohio
C. A. Knorr, Munchen, Germany
R. S. Dean, College Heights, Md.

Personals

Gerald M. Bestler has been appointed manager of the new film memory manufacturing department at Univac, Div. of Sperry Rand Corp., St. Paul, Minn. Mr. Bestler joined Univac a year ago as a production research engineer. In his new post, he is in charge of all

Manuscripts and Abstracts for Spring 1962 Meeting

Papers are now being solicited for the Spring Meeting of the Society, to be held at the Statler Hilton Hotel in Los Angeles, Calif., May 6, 7, 8, 9, and 10, 1962. Technical Sessions probably will be scheduled on Electric Insulation (including sessions on Ceramics and Integrated Circuits, Thin Film Dielectrics and Electrolytic Capacitors, Reliability, and Paper), Electronics (including Luminescence, Semiconductors, Optical Masers, and Nonconventional Electron Emitters), Electrothermics and Metallurgy (including a Symposium on Thermodynamics and Kinetics of Gas-Condensed Phase Reactions at High Temperatures), Industrial Electrolytics, and Theoretical Electrochemistry.

To be considered for this meeting, triplicate copies of abstracts (*not exceeding 75 words in length*) must be received at Society Headquarters, 1860 Broadway, New York 23, N. Y., *not later than December 15, 1961. Please indicate on abstract for which Division's symposium the paper is to be scheduled and underline the name of the author who will present the paper.* No paper will be placed on the program unless one of the authors, or a qualified person designated by the authors, has agreed to present it in person. An author who wishes his paper considered for publication in the JOURNAL should send triplicate copies of the manuscript to the Managing Editor of the JOURNAL, 1860 Broadway, New York 23, N. Y.

Presentation of a paper at a technical meeting of the Society does not guarantee publication in the JOURNAL. However, all papers so presented become the property of The Electrochemical Society, and may not be published elsewhere, either in whole or in part, unless permission for release is requested of and granted by the Editor. Papers already published elsewhere, or submitted for publication elsewhere, are not acceptable for oral presentation except on invitation by a Divisional program Chairman.

manufacturing activities connected with film memory production.

Claus Haake has been named research manager of the Giannini Controls Corp. Research Labs., Pasadena, Calif. Dr. Haake will be responsible for research efficiency, personnel supervision, staff development, and general project coordination.

Rolf R. Haberecht has joined the staff of P. R. Mallory & Co. Inc.'s new Lab. for Physical Science at Burlington, Mass. Dr. Haberecht will manage a research group concerned with the study of solid-state material properties. He joined Mallory, Indianapolis, Ind., in 1956 and has been a member of the Corporate Research and Development Labs.

Stanley Hills, research specialist in silver-zinc, silver-cadmium batteries, has joined The Electric Storage Battery Co., Philadelphia, Pa. He has been appointed to the staff of the Industrial Group consisting of ESB's Missile Battery, Exide Industrial, Nickel-Alkaline, and Jessall Plastics divisions. Dr. Hills will carry out research and development toward the attainment of a hermetically sealed-cell silver-cadmium battery for industrial and missile applications, and the continued rapid development of long-life silver-zinc storage batteries for use in propelling submarines.

The Board of Directors of Yardney Electric Corp. has announced the elevation of three officers of the company to higher posts and the election of additional officers: vice-president **Martin E. Kagan** and treasurer **Sandor Reich** have been appointed to the newly created positions of senior vice-presidents; **Paul Howard,** formerly assistant vice-president, has been elevated to a vice-presidency; **Aldo S. Berchielli,** formerly chief engineer, has been made assistant vice-president and chief engineer of the company's new Stonington, Conn., plant; **Frank Solomon,** formerly head of research and development, is now assistant vice-president.

T. L. Rama Char, Bangalore, has been elected a member of the Indian Institute of Chemical Engineers. He also has been nominated as a member of the C.S.I.R. Committee on Fundamentals of Corrosion Studies, on behalf of the Indian Institute of Science, Bangalore.

J. Sundararajan, Bangalore, has been appointed senior research assistant in the Dept. of Inorganic and Physical Chemistry, Indian Institute of Science.

M. S. Thacker, New Delhi, India, has been invited to become a member of the International Advisory Committee on Research in the Natural Sciences Program of UNESCO

Book Reviews

Zinc—The Science and Technology of the Metal, Its Alloys and Compounds. Edited by C. H. Mathewson. ACS Monograph No. 142. Published by Reinhold Publishing Corp., New York, N. Y., 1959. 721 pages; $1950.

This monograph constitutes a single source of information for anyone with a general or specific interest in zinc. It covers the metallurgy, chemistry, extraction, and uses of zinc in great detail, as well as the historical background, economics and statistics, and geology of zinc deposits. To cover such a broad field, it utilizes contributions from 45 specialists representing industrial, academic, and government experts from America, Canada, and England.

Some of the subjects covered include "Metallurgical Extraction," including ten subdivided, detailed reports prepared by 17 experts; "The Manufacturing of Zinc Oxide"; and "The Processing and Uses of Metallic Zinc and Zinc-Base Alloys." This broad chapter is divided into 22 separate subjects which cover 186 pages. The subjects of electrogalvanizing of sheet, general electroplating with zinc, and zinc anodes for cathodic protection are included in this chapter.

While uniformity of style is impossible in such a monograph, the arrangement of the material is logical and each contribution ends with appropriate appended references. The various chapters are written as complete technical papers and the net effect is a thorough coverage of the entire field of zinc. The monograph contains many fine photographs, illustrations, and diagrams. The paper used is a smooth, high grade.

George Stern
United Nuclear Corp.
White Plains, N. Y.

Soviet Electrochemistry. L. Nanis, Translation Editor; A. N. Frumkin, Supervisory Editor. Published by Consultants Bureau Enterprises, Inc., New York, N. Y., 1961. **Vol. I. Kinetics and Polarography,** 264 pages; $15.00. **Vol. II. Oxidation and Reduction,** 264 pages; $15.00.

Publication of symposia *in toto* has the merit of encouraging otherwise uncommunicative workers to publish. It also offers a medium for the publications of conjecture, digression, and argumentation, which would be ruthlessly deleted by the copy editors who manage to keep the periodic literature within reasonable bounds. Unfortunately, these ends are almost invariably accomplished at the cost of long delays in publication. The present work is no exception. It is the English translation (1961) of the Russian publication (1959) of the Proceedings of the Fourth Conference on Electrochemistry in Moscow (1956).

The first two volumes of the three-volume work deal with phenomena at solution-electrode interfaces. The third volume, on applied subjects, was not available to the reviewer. Each volume contains approximately 40 papers, largely by Soviet workers, but with others, *e.g.*, Bockris, Bonhoeffer, Grahame, Parsons, Piontelli, interspersed. Representative sectional headings are: (Vol. I) double layer adsorption, polarography, hydrogen discharge; (Vol. II) electrodeposition, passivity and corrosion, oxygen discharge. The papers are confined largely to review, with only occasional bits of new data and new ideas.

Since most of the important conclusions of the conference have long since been restated elsewhere, interest in the publications doubtless will stem largely from the broad collective picture it gives of the level and areas of emphasis of Soviet electrochemical research. Not surprisingly, it would appear that in Russia, as elsewhere, the leading research indicates the individual ingenuity of its authors rather than their national origins, and the vast bulk of research is concerned with filling in the gaps. Over half the papers in Vol. I give reference to work by Frumkin.

Two aspects of the present work particularly impressed the reviewer. The first was the extended and lively discussion (25 pages in Vol. I) which added immeasurably to the appreciation of the virtues and limitations of the formal papers. The second was the apparent awareness of Soviet workers of work in other countries. Translation problems may have inhibited reciprocal awareness of Soviet work in the past. For this

reason, if for no other, translations of this sort deserve support.

W. H. Reinmuth
Columbia University
New York, N. Y.

The Electrical Double Layer Around a Spherical Colloid Particle, by A. L. Loeb, J. Th. G. Overbeek, and P. H. Wiersema. Published by The M.I.T. Press, Cambridge, Mass., 1961. 375 pages; $10.00.

"According to the well-known model of Gouy and Chapman, the electrical potential in the electrolyte solution surrounding a colloid particle is governed by the so-called Poisson-Boltzmann equation. In the limiting case of a plane interface between particle and solution, this equation can be solved analytically. . . . In the case of a spherical particle, this equation has no tractable analytical solution, with the result that it must be solved by numerical integration."

The major portion of this book (325 pages) consists of tabulated values of the functions, obtained with the aid of an IBM-704 computer, from which the charge distribution and free energy can be calculated as a function of distance from the surface of a spherical charged particle. The tables cover the major electrolyte valence types, a considerable range of ionic strength, and surface values of $e\psi/kt$ up to 16 for 1-1 electrolytes, 8 for other types.

The first 17 pages suffice to introduce the problem and show the methods of mathematical attack; the next 26 pages give and discuss some of the results.

The Poisson-Boltzmann equation was set up by Debye and Hückel in 1923, as a means of calculating the charge distribution about each ion of an electrolyte. Their famous approximation is valid for ions which are not too small, whose charge is not too large, in solutions not too concentrated; or, specifically, when $ze\psi << kT$. Methods of obtaining exact solutions were outlined as early as 1927, and electronic computers have now made the calculations possible. E. A. Guggenheim has made the most recent applications to electrolytes (*Trans. Faraday Soc.*, 1959 and 1960); the present authors have made the most extensive computations, with the wide departure of highly charged colloid particles from the D-H approximation in mind.

C. V. King
New York University
New York, N. Y.

News Items

New ECS Sustaining Members

The following recently became Sustaining Members of The Electrochemical Society:

Minneapolis-Honeywell Regulator Co., Minneapolis, Minn.

Owens-Illinois Glass Co., Toledo, Ohio

The Pure Oil Co., Crystal Lake, Ill.

Remington Rand, Div. of Sperry Rand Corp., New York, N. Y.

United States Borax & Chemical Corp., Los Angeles, Calif.

1961 Annual Index of ECS Journal

The Annual Index for Vol. 108 (1961) of the JOURNAL will appear in the February 1962 issue. Reprints of the Index can be obtained about the middle of March 1962 by writing to The Electrochemical Society, Inc., 1860 Broadway, New York 23, N. Y.

Meetings of Other Organizations

Electric Furnace Conference, Dec. 6-8.—The Metallurgical Society of the American Institute of Mining, Metallurgical, and Petroleum Engineers has announced the preliminary program for the 19th Annual Electric Furnace Conference, to be held December 6-8, 1961 in the Penn-Sheraton Hotel, Pittsburgh, Pa. The event will be sponsored by the Electric Furnace Committee of the Iron and Steel Division. Subjects to be covered will include: "Use of Vacuum and Inert Gas Atmospheres in Steelmaking"; "Ingot Technical Session—Operating Metallurgy"; "Quality Improvements in Stainless Steel"; "Special Arc Technical Session—Refractories"; "Special Arc Session—Ferroalloys"; "Ingot Technical Session—International Developments"; "Castings Technical Session—Effect and Control of Metal Temperature." Plant trips will be made on December 8 to the Jessup Steel Co., Washington, Pa., and McConway and Torley, Pittsburgh.

Materials Research Conference, Dec. 18 and 19.—A Materials Research Conference will be held at Rensselaer Polytechnic Institute on December 18 and 19, 1961. Joint sponsors with the Institute are the Watervliet Arsenal with cooperation of the Advanced Research Projects Agency, the U. S. Atomic Energy Commission, the National Aeronautics and Space Administration, and the U. S. Army. Original research papers will be read on: mechanics of materials, solid-state physics, physical metallurgy, and the physicochemical properties of materials. Review will be made of progress in the materials research program supported by federal agencies. Rensselaer recently organized a broad interdisciplinary research materials program, with support of NASA.

Chemical Institute of Canada.—The following meetings of The Chemical Institute of Canada, 48 Rideau St., Ottawa, Ont., Canada, have been scheduled for 1962:

Feb. 22—Protective Coatings Division, Seaway Hotel, Toronto.

Feb. 23—Protective Coatings Division, Windsor Hotel, Montreal.

May 27-30—45th Canadian Chemical Conference and Exhibition, Macdonald Hotel, Edmonton, Alberta.

Sept. 6-7—Physical Chemistry Division, Quebec City.

Refractory Metal Symposium.—A Refractory Metal Symposium will be held in Chicago, Ill., on April 12 and 13, 1962. This symposium will be sponsored by the Refractory Metals Committee, Institute of Metals Division of A.I.M.E., in cooperation with the Chicago Section, A.I.M.E. Outstanding authorities have been selected to present up-to-

June 1962 Discussion Section

A Discussion Section, covering papers published in the July-December 1961 JOURNALS, is scheduled for publication in the June 1962 issue. Any discussion which did not reach the Editor in time for inclusion in the December 1961 Discussion Section will be included in the June 1962 issue.

Those who plan to contribute remarks for this Discussion Section should submit their comments or questions in triplicate to the Managing Editor of the JOURNAL, 1860 Broadway, New York 23, N. Y., *not later than March 1, 1962.* All discussion will be forwarded to the author(s) for reply before being printed in the JOURNAL.

date reviews of the current status of science and technology in the area of refractory metals.

Instrument Society of America.—The following are among Instrument Society of America and jointly sponsored national meetings during 1962:

April 30-May 2—8th National Symposium on Instrumental Methods of Analysis, Daniel Boone Hotel, Charleston, W. Va. Contact: M. D. Weiss, Section Head, Special Instrumentation Dept., Union Carbide Olefins Co., South Charleston, W. Va.

May 21-23—8th National Aero-Space Instrumentation Symposium, Marriott Motor Hotel, Twin Bridges, Washington, D. C. Contact: Cyrus Creveling, Goddard Space Flight Center, Greenbelt, Md.

Oct. 29-31—15th Conference on Electrical Techniques in Medicine and Biology, Edgewater Beach Hotel, Chicago, Ill. Sponsors: I.S.A. A.I.E.E. I.R.E. Contact: Dr. J. E. Jacobs, School of Medicine, Northwestern University, Chicago, Ill.

H. A. Liebhafsky Named Winner of ACS Fisher Award

Herman A. Liebhafsky, manager of the Physical Chemistry Section of the General Electric Research Lab., Schenectady, N. Y., recently was named winner of the Fisher Award in Analytical Chemistry at the 140th National Meeting of the American Chemical Society in Chicago.

This major award, consisting of $1000 and an etching, will be presented to Dr. Liebhafsky next spring at the National Meeting in Washington, D. C. It was established in 1947 to recognize and encourage outstanding contributions to the science of analytical chemistry, pure or applied, carried out in the United States and Canada, with special consideration given to the independence of thought and originality shown, and to the importance of the work when applied to public welfare, economics, or the needs and desires of humanity.

Dr. Liebhafsky joined the staff of the G.E. Research Lab. in 1934. A native of Zwittau, Austria-Hungary, he received his B.S. degree from the Agricultural and Mechanical College of Texas in 1926, his M.S. from the University of Nebraska in 1927, and his Ph.D. in 1929 from the University of California, where he served as an instructor from 1929 to 1934. During World War II, he served as a technical observer for the armed forces in the European Theater of Operations.

Dr. Liebhafsky is a member of the American Chemical Society, the National Association of Corrosion Engineers, The Electrochemical Society, Sigma Xi, and Phi Lambda Upsilon. He has published 116 papers in the fields of analytical and physical chemistry, and is coauthor of a book on "X-Ray Absorption and Emission in Analytical Chemistry."

ESB Co. and Sun Oil to Exchange Research Information

An agreement has been signed for the exchange of research information and for future cooperative development of fuel cells by the Electric Storage Battery Co. and Sun Oil Co.

The Electric Storage Battery Co., the country's oldest producer of packaged power devices, has been active in the development of electrodes for fuel cells, and Sun Oil Co. has conducted an independent research program in catalyst systems used in fuel cells.

Metal & Thermit and Udylite Announce Proposal to Merge

H. E. Martin, chairman of Metal & Thermit Corp., and L. K. Lindahl, chairman of The Udylite Corp., Detroit, Mich., have announced approval in principle by both Boards of Directors of a merger between the two companies. The action is subject to approval by the Directors of a formal Merger Agreement for submission to the stockholders of M & T and Udylite.

Udylite will continue under its present management as a division of Metal & Thermit Corp.

Under the proposed terms, each share of Udylite stock would be exchanged for 0.65 shares of M & T's stock. M & T's present common stock will continue, share for share, as common stock of the combined enterprise.

Holders of M & T outstanding $50 par value, 7% preferred stock may elect to receive 3½ shares of common stock or one share of new $50 par, 7% preferred stock for each share now held. The new $50 par preferred stock will carry a $3.50 annual dividend and be convertible through 1964 into common stock at current market value at the time of conversion, each converted share of preferred to be taken for this purpose at $75, but in no event more than 2½ shares of common stock. It is intended that the common stock be placed on an annual dividend basis of $1.50 for the year 1962. M & T's common stock at present is listed on the American Stock Exchange, and Udylite's on the New York Stock Exchange. Following the merger, application will be made to list the common stock of the combined enterprise on the New York Stock Exchange.

Metal & Thermit is a chemically orientated company whose diverse operations include chemicals, coatings, minerals, chromium plating processes and materials, welding equipment and detinning.

The Udylite Corporation manufactures a complete line of automatic plating machines, rectifiers, and plating accessories. Through a subsidiary, the Udylite Research Corp., the Detroit-based firm has been active in research and development of electroplating processes, particularly bright nickel plating processes.

Space Chambers Use Carbon Arcs to Simulate Solar Radiation

Solar radiation beyond the earth's atmosphere can be precisely simulated in environmental space chambers bathed in both visible and invisible light from a bank of carbon arcs, it was confirmed in a series of recent tests reported recently by the National Carbon Co., New York City. Such chambers should prove invaluable research tools in the earth-bound evaluation of space vehicles and equipment.

The visible light of the carbon arc has long been regarded as man's closest approximation of sunlight, and is widely used in motion picture projection and studio lighting, and in the graphic arts fields of photoengraving and photolithography. Technical data had previously been limited largely to the visible light wave lengths, from 4000 to 7000Å (0.4 to 0.7μ).

Scientists had assumed that the sun and the carbon arc had identical outputs over the entire range of the spectrum, and this significant correlation has just been confirmed in a series of measurements made in National Carbon's development laboratories.

Using a Perkin-Elmer recording spectrophotometer, National Carbon engineers measured the spectral energy distribution of radiation from the carbon arc all the way out to 150,000Å. Data then were plotted on a curve showing the spectral energy distribution of the sun outside the earth's atmosphere from 2500 to 60,000Å which includes from 98 to 99% of the sun's energy output, and the two curves were found to follow each other very closely over the entire range.

Armed with this scientific confirmation, space equipment designers can now use banks of carbon arcs

with no filters or added energy in test chambers to simulate conditions of solar radiation in outer space.

Solar cell evaluation will be conducted according to specifications developed by the American Institute of Electrical Engineers. The energy standards for such tests are based on Johnson's spectral energy distribution of the sun outside the earth's atmosphere, which is published in the "1960 Handbook of Geophysics."

According to National Carbon, special techniques have been developed for the continuous operation of the high-intensity arc carbons it manufactures, thus assuring uninterrupted performance in space chamber tests. The space chambers already in operation use carbon arcs, and large chambers now under consideration undoubtedly will also use this high-intensity energy source to simulate solar radiation.

B.M.I. Develops Zero-Gravity Electrolytic Cell

An electrolytic cell that operates under weightless conditions may provide a vital link in a workable chemical system that will convert an astronaut's breath into breathable oxygen during space voyages lasting up to two years. Battelle Memorial Institute, Columbus, Ohio, now is readying a prototype model of the rotating cell for evaluation by the Aerospace Medical Lab., a component of the Air Force Systems Command's Aeronautical Systems Division.

The unique feature of the cell is its ability to operate efficiently, independent of natural gravity. Conventional electrolytic cells depend upon the pull of this gravity on the electrolytic solution in separating gas bubbles as they are generated in the cell's liquid. The experimental cell operates in its own artificial gravity field, which is the centrifugal force produced as the cell rotates.

Development of the zero-gravity electrolytic cell dovetails with the recently announced completion, by Battelle scientists, of a device that chemically converts the carbon dioxide in an astronaut's breath into carbon and water. The device can use the hydrogen produced by the electrolytic cell, while the cell, in turn, can make use of the water to produce more breathing oxygen. Thus, the two devices complement one another in maintaining a livable atmosphere in a spacecraft for long periods without a supplemental supply of breathing oxygen.

John E. Clifford, who worked with James T. Gates in designing the cell, describes it as a drum-shaped unit about 3 ft high that rotates at up to 500 rpm. The cylindrical unit is comprised of 16 individual electrolytic cells stacked one on top of the other like pancakes. Alternate metal plates serve as anodes and cathodes. Interspersed between these plates are asbestos diaphragms—thin films that separate hydrogen from oxygen as these gases are generated on the electrodes. The gases are drawn from the chamber through separate collecting systems routed up through the center of the unit. A 500-w electrical input is required to electrolyze about 2 qt of water a day—sufficient to provide oxygen for two men.

Low-Energy Electron Diffraction Technique for Studying Surface Reactions

Some of the first experimental results from an important new technique for studying surface reactions were described at the International Conference on Magnetism and Crystallography held during September in Kyoto, Japan. Drs. L. H. Germer and A. U. MacRae of Bell Telephone Labs. reported on studies of adsorption of monolayers of gases on a crystal surface using a new experimental method perfected by Dr. Germer. In his technique, low-energy electrons are diffracted from a surface and accelerated to a fluorescent screen by a strong electric field. The diffraction pattern produced on the screen gives the arrangement of the first monolayer of atoms on the surface.

The technique is providing a powerful new tool for the study of surface reactions, since it gives a detailed picture of the arrangement of atoms entering into such reactions. It is opening the way to a far more detailed understanding of such surface phenomena as catalysis and corrosion. As a result of such understanding, according to Dr. Germer, "catalytic chemistry will be a different kind of science and very probably revolutionary advances will be made in it."

In their Kyoto paper, Drs. Germer and MacRae reported on studies of

New 10-Year Index of ECS Journal

The new 10-Year Index of the JOURNAL of The Electrochemical Society, covering Volumes 99-108 for the years 1952-1961, will be published in the spring of 1962.

This publication will include Subject Index and Author Index, the latter with title of paper following each author's name. This will be an invaluable addition to your library.

Price to ECS Members	$12.50
Price to Subscribers and Nonmembers	
prepublication (until April 1, 1962)	12.50
postpublication (after April 1, 1962)	15.00

If you have not yet ordered your copy of the new 10-Year Index, the order form below may be used. Remittance, made payable to The Electrochemical Society, Inc., should accompany your order.

Purchasers located overseas should remit by New York Bank Draft or United States International Money Order.

THE ELECTROCHEMICAL SOCIETY, INC.,
1860 Broadway, New York 23, N. Y.

Date .....

Please send me a copy of the 10-Year Index of the JOURNAL of The Electrochemical Society covering Vol. 99-108 (1952-1961).

Attached is remittance in the amount of $ ..... to cover cost of this publication, which I understand will be sent to me in the spring of 1962.

Name .....

Company .....

Street Address .....

City ..... State .....

Country .....

ECS Member ..... Subscriber or Nonmember .....

oxygen and hydrogen adsorption on a nickel crystal. They found that after a monolayer of oxygen had been adsorbed, nickel atoms diffused to the surface, producing an orderly arrangement containing either one or two oxygen atoms for each nickel atom. The arrangement containing equal numbers of oxygen and nickel atoms proves to be remarkably stable, persisting up to temperatures at which nickel evaporates rapidly. The Bell scientists found, however, that the oxygen can be removed easily by hydrogen at moderate temperatures, and that the hydrogen in turn is removed by slight heating, leaving a perfectly clean surface.

Major Advance in Tungsten Field Announced by Westinghouse

A major step forward in the tungsten field, which may have an important impact on America's space program, has been announced by Westinghouse Electric Corp., Bloomfield, N. J.

According to C. O. Young, manager of the Westinghouse lamp parts department, the company's engineers have developed a practical method to produce large single crystals of tungsten, of extremely high purity and density.

Tungsten rods 10 in. long and 0.2 in. in diameter are being produced as single crystals. Special refining techniques have been developed by Westinghouse engineers which even make it possible to grow these ultra-high-purity crystals in predetermined crystalline forms with a purity up to 99.9975%. The large crystals of tungsten are big enough to permit the commercial fabrication of small parts from them.

Tungsten is usually considered very difficult to machine or fabricate. However, Westinghouse engineers have shown that ultrapure single crystals are actually ductile, even at temperatures as low as —330°F, and have proven that ductility depends upon purity. This discovery points to the possibility of a major breakthrough in commercial fabrication.

High-purity single crystals are of particular value in studies of fundamental properties of high-temperature metals. Such knowledge is vital to the development of space materials. Tungsten, having the highest melting point and the greatest strength of all the metals, is a promising material for applications such as rocket motors. However, much remains to be discovered about its behavior.

The single-crystal tungsten is available commercially.

Cobalt Alloy Development

At a recent seminar of the Metallurgy Division of the Argonne National Lab., Lemont, Ill., F. R. Morral, director of Cobalt Information Center activities in the United States, suggested certain steps toward the achievement of better cobalt alloys.

Dr. Morral stated that the potential of cobalt-base alloys is far from exhausted. This is obvious from the high melting point of the metal, its work-hardening characteristics, and its ability to maintain properties at high temperatures. He reviewed recent research work and developments in cobalt (such as availability of high-purity material), cobalt binary and ternary alloys, dispersion hardening, and cobalt superalloys. Much of the work discussed and data presented have not yet been published; some have been sponsored by the Centre d'Information du Cobalt.

Better cobalt alloys (*e.g.*, those having improved reliability, greater ease of forming, machining, and joining, and increased high-temperature properties), Dr. Morral suggested, might be developed by: 1. Investigating the possibilities of less complex alloys (fewer alloying elements); 2. Further investigation of precipitation from cobalt solid solutions and dispersion hardening of cobalt solid solutions by means of oxides and intermetallics; 3. Determining the effects of alloying and tramp elements on commercial cobalt alloys. Dr. Morral further recommended that creep and stress-rupture testing of commercial and development cobalt-base alloys be carried out at higher temperatures (1900°-2150°F) than commonly is done.

G.E. Produces First Semiconducting Diamonds

Methods have been discovered at the General Electric Research Lab., Schenectady, N. Y., which make it possible for the first time to produce semiconducting diamonds, according to Dr. Guy Suits, vice-president and director of research. Such diamonds are extremely rare in nature, accounting for less than 1% of natural diamonds, but now can be grown at will in the laboratory using the high-temperature, ultrahigh-pressure process first developed at the G. E. Research Lab.

The method for making semiconducting diamonds was discovered by Dr. Robert H. Wentorf, Jr., of the Research Lab., and Harold P. Bovenkerk, of the Metallurgical Products Dept. Semiconducting borazon also was discovered by Dr. Wentorf, who developed the original process for making borazon.

Diamonds are made semiconducting by adding impurities such as boron, beryllium, or aluminum to the mixture of graphite and catalyst from which diamonds are made. The mixture is subjected to pressures of about 1,000,000 psi and temperatures above 2000°F. Under these conditions, diamonds form with concentrations of 1% or less of the desired impurity, and have electrical conductivities in the semiconducting range.

Drs. Wentorf and Peter Cannon of the Research Lab. also have prepared semiconducting diamonds by diffusing boron and aluminum into Man-Made or natural diamonds at high pressures and temperatures. All the semiconducting diamonds made so far have been p-type. A search for processes that will produce n-type diamonds is continuing.

In borazon, both p-type and n-type crystals can be produced, and one type can be grown onto a "seed" of the other type to form p-n junctions. Tests on such junctions have shown that they act as rectifiers. Beryllium as an impurity produces p-type borazon, and a number of substances including sulfur, silicon, many organic compounds, and potassium cyanide, when added to the synthesis mixture, result in n-type borazon.

The semiconducting diamonds prepared with boron are blue, in shades ranging from a pale blue-white to a deep blue-black, depending on how much boron is present in the crystal. Semiconducting diamonds found in nature, which have been studied for many years by a number of investigators, are also sometimes blue. One of the most famous blue-white diamonds is the Hope diamond and, although its conductivity has not been measured, its color suggests that it is probably a semiconductor.

Boston Area Research Lab. for Mallory

P. R. Mallory & Co. Inc. recently announced that its Lab. for Physical Science is located near Boston, Mass., in the vicinity of Route 128 and U.S. Highway 3. The new research facility, a 9600-sq.-ft building, will supplement existing corporate laboratories in Indianapolis.

Dr. Donald G. Wilson, Mallory vice-president for research and engineering, said that approximately 30 scientists and technical supporting personnel will staff the laboratory when recruiting has been com-

RESEARCH POSITIONS AVAILABLE

Professional staff positions have been created at Philco's new Research Center in suburban Philadelphia in such areas as Physics of Materials, Semiconductor Electrochemistry, Radiation Effects on Solids, Solid State Devices, Applied Radiochemistry, Thin Film and Tunneling Phenomena, and Fuel Cells. In general, the nature of these programs is such that the Ph.D. is required. Benefits of association with the Research Center include the opportunity for independent research, well-equipped laboratories, knowledgeable associates, and competitive salaries. Additional information may be obtained by writing Mr. R. K. Ruth, Philco Research Center, Blue Bell, Penna.

RESEARCH CENTER PHILCO
Famous for Quality the World Over
"An equal opportunity employer."

pleted. A substantial portion of the group will consist of scientific personnel having advanced backgrounds in the fields of the theoretical solid state, metallurgy, and chemistry. Dr. Sumner P. Wolsky is the director of the laboratory.

Laboratory activity will be directed toward achieving a basic scientific understanding of material and electronic phenomena to support Mallory product development activity. Dr. Wilson said that the laboratory will have responsibilities in the areas of thin films, electrochemistry, and molecular electronics. The facilities will include a crystal laboratory which has been designed for the preparation of epitaxial crystals for study of crystal growth behavior. A films laboratory will be used for the investigation of electrical, mechanical, optical, structural, and magnetic properties of films.

Relaxation Theory Applied to Electrode Reactions

The causes of deviations of electrochemical systems from thermodynamic reversibility are being sought at the National Bureau of Standards. The object of the study is the determination of the reaction mechanisms of various types of electrochemical processes.

The Bureau's representation of electrode reaction processes was developed from the point of view that the basis of earlier theories is unsatisfactory. This representation includes earlier theories in treating the electrode reactions as relaxation processes, with the controlling mechanism being a charge transfer reaction ($Ag = Ag^{+} + e$), a chemical reaction simultaneous with, preceding, or succeeding the charge transfer reaction, or a diffusional process of one or more of the participants in the reactions at the electrode-solution interface.

Present work is directed chiefly toward the application of relaxation theory and methods to impedance measurements of the electrode-solution interface.

References

1. R. J. Brodd, "The Electrode Properties and Kinetics of Electrode Reactions," *J. Research Nat. Bur. Standards*, **65A**, (Phys. & Chem.), No. 4, 275 (1961).
2. R. W. Gurney and R. H. Fowler, *Proc. Roy. Soc.* (*London*), **136A**, 378 (1932).
3. J. O'M. Bockris, "Modern Aspects of Electrochemistry,' Chapter IV, Academic Press, Inc., New York (1955).
4. E. Warburg, *Wied Ann.*, **67**, 493 (1899).

Growth of Metal Crystals from the Vapor Phase

The growth kinetics of zinc, potassium, and mercury crystals are being investigated in a basic research program of metal physics at the National Bureau of Standards. Thus far, experimental results obtained from growth measurements of zinc crystals support the screw dislocation theory rather than the surface nucleation theory of the crystallization process. The crystals, nucleated and grown in these experiments on a tungsten rod, formed in the shape of truncated hexagonal pyramids.

References

1. R. L. Parker and L. M. Kushner, "Growth Rates of Zinc Crystals from the Vapor Phase," *J. Chem. Phys.*, **35**, No. 4 (Oct. 1961).
2. W. K. Burton, N. Cabrera, and F. C. Frank, "The Growth of Crystals and the Equilibrium Structure of Their Surfaces," *Trans. Roy. Soc.* (*London*), **243**, 299 (1951).
3. R. Becker and W. Döring, "Kinetische Behandlung der Keimbildung in übersättigten

Scientists and engineers in research

CAREER OPPORTUNITIES IN A NEW FIELD

SEMICONDUCTOR VAPOR GROWTH

IBM THOMAS J. WATSON RESEARCH CENTER

The new IBM Thomas J. Watson Research Center in Yorktown, N.Y. is undertaking important new long-range projects requiring scientists and engineers with experience in, or relating to, various aspects of semiconductor vapor growth problems. Research projects under way are directed toward purely scientific goals as well as toward developing technology for engineering advanced information handling systems.

Applicants should be familiar with studies of vapor growth reactions in general as well as vapor grown junction technologies. This is a unique opportunity to work in advanced areas of semiconductor research, to open exciting new fields for research. An advanced degree in physical chemistry, metallurgy, or physics is desirable, but a B.S. with a strong background in relevant experience will be considered.

The Thomas J. Watson Research Center at Yorktown, N. Y. is located in pleasant, rural Westchester County countryside, just 35 miles from New York City. The Research Center was designed to provide the best possible working environment for scientists and engineers engaged in advanced research studies. The location provides excellent schools and housing. IBM offers a fully paid benefits program that is setting the pace for industry today. All qualified applicants will receive consideration for employment without regard to race, creed, color, or national origin.

Please write, outlining your education and experience, to:

Mr. J. B. Farrington, Dept. 613N
Thomas J. Watson Research Center
P. O. Box 218
Yorktown Heights, New York

IBM®

International Business Machines Corporation

Dämpfen," *Ann. Phys.*, **24**, 719 (1935).

4. *See* N. Cabrera and D. Vermilyea in "Growth and Perfection of Crystals," p. 393, edited by R. H. Doremus, B. W. Roberts, and D. Turnbull, John Wiley & Sons, Inc., New York (1958).
5. F. Hock and K. Neumann, "Die Verdampfungs - und Kondensationgeschwindigkeit des festen Kaliums," *Z. phys. Chem.*, **2**, 241 (1954).

Effect of Dodecyl Alcohol on Fatigue Crack Propagation

The National Bureau of Standards recently evaluated the effect of dodecyl alcohol on the rate of fatigue crack propagation in steel, stainless steel, aluminum, and a copper-beryllium alloy. It was found that the application of this liquid to the surface of the specimens increased the number of cycles required to propagate cracks by factors ranging from 1.4 in the stainless steel to 5.0 in the copper-beryllium alloy.

References

1. W. L. Holshouser and H. P. Utech, "Effect of Oleophobic Films on Fatigue Crack Propagation," *Trans. ASTM*, Preprint No. 72 (1961).
2. H. E. Frankel, J. A. Bennett, and W. L. Holshouser, "Effect of Oleophobic Films on Metal Fatigue," *J. Research Nat. Bur. Standards*, **64C**, 147 (1960); *also*, "Effect of Organic Compounds on Metal Fatigue," *Nat. Bur. Standards Tech. News Bull.*, **44**, 127 (1960).

Announcements from Publishers

"The Mechanism of Pressure Bonding," April 1961. AEC Report BMI-1512,* 115 pages; $2.25.

"Corrosion of Aluminum and Its Alloys in Superheated Steam," April 1961. AEC Report ANL-6207,* 31 pages; 75 cents.

"Metallurgy Division. Annual Report, 1960." AEC Report ANL-6330,* 274 pages; $3.50.

"Corrosion Behavior of Some Metal Borides," Oct. 1960. AEC Report GEAP-3548,* 18 pages; 50 cents.

"Effect of Surface Treatment on the Corrosion Resistance of Zircaloy-2," April 1961. AEC Report WAPD-TM-219,* 20 pages; 50 cents.

"Convergence of Transport Solutions for Thin Slab Cells," April 1961, AEC Report ANL-6345,* 24 pages; 50 cents.

"Electronuclear Research Division. Annual progress report ending January 16, 1961." AEC Report ORNL-3085,* 80 pages; $2.00.

"Corrosion of Alloys in Various ICCP Decontamination Solutions," April 1961. AEC Report IDO-14506,* 60 pages; $1.25.

"Electron Induced Radiation Damage in Pure Metals," R. M. Walker, General Electric Co., for Air Force Research Div., U. S. Air Force, Dec. 1960. Report PB 171 523,* 40 pages; $1.25.

"Physical Properties of High Temperature Materials, Part V. Thermal Diffusivity of Magnesia-Stabilized Zirconium Oxide at High Temperatures," H. F. Flieger, Jr., and others, National Bureau of Standards, for Wright Air Development Center, U. S. Air Force, Oct. 1960. Report PB 171 541,* 19 pages; 50 cents.

"Application of Ultrasonics to Solid Rocket Systems," R. E. Kleint and others, Automation Industries, Inc., for Wright Air Development Div., U. S. Air Force, Oct. 1960. Report PB 171 499,* 115 pages; $2.50.

"Field Ion Microscopy of Iron Whiskers," E. W. Miller, Pennsylvania State University, for Wright Air Development Div., U. S. Air Force, Oct. 1960. Report PB 171 598,* 26 pages; 75 cents.

"Radiation Tolerance of a Select Group of Semiconductor Diodes," C. I. Westmark, Sandia Corp., for U. S. Atomic Energy Commission, Nov. 1960. Report SCTM 404-60(14),* 15 pages; 50 cents.

"A Compendium of the Properties of Materials at Low Temperature (Phase 1)—Part 1—Properties of Fluids," V. J. Johnson, General Editor, National Bureau of Standards, for Wright Air Development Div., U. S. Air Force, July 1960. Report PB 171 618,* 446 pages; $6.00.

"A Compendium of the Properties of Materials at Low Temperature (Phase 1)—Part 2—Properties of Solids," V. J. Johnson, General Editor, National Bureau of Standards, for Wright Air Development Div., U. S. Air Force, Oct. 1960. Report PB 171 619,* 294 pages; $4.00.

* Order from Office of Technical Services, Business and Defense Services Administration, U.S. Dept. of Commerce, Washington 25, D. C.

"A Compendium of the Properties of Materials at Low Temperature (Phase 1)—Part 3—Bibliography of References (Cross-Indexed)," V. J. Johnson, General Editor, National Bureau of Standards, for Wright Air Development Div., U. S. Air Force, Oct. 1960. Report PB 171 620,* 166 pages; $3.00.

"Zinc Coatings for Protection of Columbium from Oxidation at Elevated Temperatures. (DMIC Memo 88)," W. D. Klopp and C. A. Krier, Defense Metals Information Center, Battelle Memorial Institute, March 1961. Report PB 161 238,* 20 pages; 50 cents.

"A New Electrochemical System for High-Voltage Low-Current Drain Applications," W. J. Pauli, Diamond Ordnance Fuze Labs., for Dept. of the Army, March 1961. Report PB 171 582,* 19 pages; 75 cents.

"A Study on Controlling High Temperature Oxidation of Vanadium Base Alloys," J. S. Klicker and H. B. Bomberger, Crucible Steel Co. of America, for Wright Air Development Div., U. S. Air Force, Feb. 1961. Report AD 258 378,* 88 pages; $2.25.

"Electropolishing and Chemical Polishing of High-Strength, High-Temperature Metals and Alloys. (DMIC Memo 98)," J. A. Gurklis and others, Defense Metals Information Center, Battelle Memorial Institute, April 1961. Report PB 161 248,* 15 pages; 50 cents.

"Review of Recent Developments in the Evaluation of Special Metal Properties. (DMIC Memo 94)," J. E. Campbell, Defense Metals Information Center, Battelle Memorial Institute, March 1961. Report PB 161 244,* 7 pages; 50 cents.

"Stereospecificity and Dielectric Properties of Polar Polymers," H. H. Zabusky and H. A. Pohl, Plastics Lab., for Office of Naval Research, Dept. of the Navy, Aug. 1960. Report PB 171 563,* 52 pages; $1.50.

Proceedings of the 15th Annual Power Sources Conference

"The Proceedings of the 15th Annual Power Sources Conference" was made available for distribution on October 10, 1961. This volume contains 37 papers presented at the 15th Annual Power Sources Conference held at Atlantic City, N. J., May 9-11, 1961, under the auspices of the Power Sources Div., U.S. Army Signal Research and Development Lab. (USASRDL), Fort Monmouth, N. J. The papers were presented in six sessions on Primary Fuel Cell Batteries, Regenerative Fuel Cell Batteries, Secondary Batteries, Primary Batteries, Solar Energy Conversion, and Thermal Energy Conversion.

Orders for copies of the Proceedings should be sent to the PSC Publications Committee, P. O. Box 891, Red Bank, N. J., accompanied by a remittance of $10.00 for a single copy, or $10.00 for the first copy and $5.00 for each additional copy when more than one copy is desired on a single order.

ISA Publishes Translated 1961 Russian Technical Journals

The 1961 issues of four leading Russian technical journals, translated cover-to-cover into English, are being published by the Instrument Society of America under a grant-in-aid from the National Science Foundation:

"Automation and Remote Control" ("Avtomatika i Telemekhanika"),

* Order from Office of Technical Services, Business and Defense Services Administration, U. S. Dept. of Commerce, Washington 25, D. C.

jpl needs

ELECTROCHEMISTS

To carry out feasibility studies on electrochemical energy systems with special emphasis on ENERGY STORAGE PROBLEMS and ENERGY CONVERSION DEVICES

FOR SPACE APPLICATION

With background in following areas

- BATTERY
- RADIOCHEMISTRY
- PHOTOCHEMISTRY

Knowledge of instrumentation and electronic equipment helpful.

Send complete resume to...
E. C. LOCKE
Placement Director

CALIFORNIA INSTITUTE OF TECHNOLOGY
JET PROPULSION LABORATORY
4800 OAK GROVE DRIVE, PASADENA, CALIF.

"An equal opportunity employer"

published monthly; approx. 150 pages per issue.

"Measurement Techniques" ("Izmeritel'naia Tekhnika"), published monthly; approx. 100 pages per issue.

"Instruments and Experimental Techniques" ("Pribory i Tekhnika Eksperimenta"), published bimonthly; more than 175 pages per issue.

"Industrial Laboratory" ("Zavodskaya Laboratoriya"), published monthly; approx. 125 pages per issue.

The 1961 translations, as well as translations of previous years published under ISA's program, are available at low subscription rates ranging from $25.00 to $35.00 per annual subscription. On a combined order for all four journals, special rates apply. Libraries of nonprofit academic institutions also are offered subscriptions at special rates.

For subscriptions or additional information, write to: Foreign Translations Dept., Instrument Society of America, Penn-Sheraton Hotel, 530 Wm. Penn Place, Pittsburgh 19, Pa.

Employment Situation

Please address replies to box shown, c/o The Electrochemical Society, 1860 Broadway, New York 23, N. Y.

Position Available

Engineer: background in rolling of silver brazing alloys, clad metals in gold, silver, copper, kovar, nickel, etc., wire drawing experience helpful; to establish and supervise new department including set-up and quality control; send resumé; all replies confidential; *address Box No. A-290.*

Advertiser's Index

Anaconda American Brass Co. 255C
Great Lakes Carbon Corp., Electrode Div. ..... Cover 2
International Business Machines Corp. 274C
Jet Propulsion Laboratory 275C
Philco Research Center 273C
E. H. Sargent & Co. 256C
Solvay Process Div., Allied Chemical Corp. 276C
Speer Carbon Co., Inc. 276C
Stackpole Carbon Co. 257C

RESEARCH AND DEVELOPMENT

Staff positions available immediately in research and development laboratories of major producer of carbon and graphite products.

Excellent opportunities for technical advancement and growth with a small progressive organization. Openings in Niagara Falls, New York, and St. Mary's, Pennsylvania.

1. Carbon and graphite nuclear and high temperature materials technologies. A broad spectrum of materials research. B.S., M.S., or Ph.D. with 2-5 years' research experience. Training and background in chemistry, physics, and/or ceramics.

2. Electrochemical studies, reactions and kinetics of fuel cell electrodes and their relations to electrode structure. B.S., M.S., or Ph.D. with 0-5 years' experience.

3. Development engineer or scientist for applied work in carbon and graphite technology. B.S. or M.S. with 0-5 years' research and/or development experience.

For an immediate response with full details, send resume' in complete confidence to

Dr. William E. Parker
Manager Carbon and Graphite Research
SPEER CARBON COMPANY, INC.
Packard Road
Niagara Falls, New York

Allied Chemical

RESEARCH ELECTROCHEMIST

Challenging opportunity in expanding research laboratory investigating electroplating and metal finishing.

Require aggressive scientist, having M.S. or B.S. degree and 2 to 4 years' experience, to conduct applied research projects with minimum of supervision. Applicant should have sound background in inorganic and physical chemistry and a real interest in research. Modern research facilities located near Finger Lakes and Adirondack recreational areas of New York State. Liberal employee benefits.

Please send detailed resumé including salary requirements to

Personnel Supervisor
SOLVAY PROCESS DIVISION
Allied Chemical Corporation
Syracuse 1, New York

The Electrochemical Society

Patron Members

Aluminum Co. of Canada, Ltd.,
Montreal, Que., Canada
International Nickel Co., Inc.,
New York, N. Y.
Olin Mathieson Chemical Corp.,
Chemicals Div., Industrial Chemicals
Development Dept., Niagara Falls, N. Y.
Union Carbide Corp.
Divisions:
Union Carbide Metals Co.,
New York, N. Y.
National Carbon Co., New York, N. Y.
Westinghouse Electric Corp., Pittsburgh, Pa.

Sustaining Members

Air Reduction Co., Inc.,
New York, N. Y.
Ajax Electro Metallurgical Corp.,
Philadelphia, Pa.
Allen-Bradley Co., Milwaukee, Wis.
Allied Chemical Corp.
Solvay Process Div., Syracuse, N. Y.
General Chemical Div., Morristown, N. J.
Alloy Steel Products Co., Inc., Linden, N. J.
Aluminum Co. of America,
New Kensington, Pa.
American Metal Climax, Inc.,
New York, N. Y.
American Potash & Chemical Corp.,
Los Angeles, Calif. (2 memberships)
American Smelting and Refining Co.,
South Plainfield, N. J.
American Zinc Co. of Illinois,
East St. Louis, Ill.
American Zinc, Lead & Smelting Co.,
St. Louis, Mo.
American Zinc Oxide Co., Columbus, Ohio
M. Ames Chemical Works, Inc.,
Glens Falls, N. Y.
Armco Steel Corp., Middletown, Ohio
Basic Inc., Maple Grove, Ohio
Bell Telephone Laboratories, Inc.,
New York, N. Y. (2 memberships)
Bethlehem Steel Co., Bethlehem, Pa.
(2 memberships)
Boeing Airplane Co., Seattle, Wash.
Burgess Battery Co., Freeport, Ill.
(4 memberships)
Canadian Industries Ltd., Montreal,
Que., Canada
Carborundum Co., Niagara Falls, N. Y.
Catalyst Research Corp., Baltimore, Md.
Consolidated Mining & Smelting Co. of
Canada, Ltd., Trail, B. C., Canada
(2 memberships)
Continental Can Co., Inc., Chicago, Ill.
Cooper Metallurgical Associates, Cleveland,
Ohio
Corning Glass Works, Corning, N. Y.
Diamond Alkali Co., Painesville, Ohio
Dow Chemical Co., Midland, Mich.
Wilbur B. Driver Co., Newark, N. J.
(2 memberships)
E. I. du Pont de Nemours & Co., Inc.,
Wilmington, Del.
Eagle-Picher Co., Chemical and Metals Div.,
Joplin, Mo.
Eastman Kodak Co., Rochester, N. Y.
Thomas A. Edison Research Laboratory, Div.
of McGraw-Edison Co., West Orange, N. J.
Electric Auto-Lite Co., Toledo, Ohio
C & D Division, Conshohocken, Pa.
Electric Storage Battery Co., Yardley, Pa.
Engelhard Industries, Inc., Newark, N. J.
(2 memberships)
The Eppley Laboratory, Inc., Newport, R. I.
(2 memberships)
Exmet Corp., Tuckahoe, N. Y.
Fairchild Semiconductor Corp., Palo Alto,
Calif.
Food Machinery & Chemical Corp.
Becco Chemical Div., Buffalo, N. Y.
Westvaco Chlor-Alkali Div., South
Charleston, W. Va.
Foote Mineral Co., Paoli, Pa.
Ford Motor Co., Dearborn, Mich.
General Electric Co., Schenectady, N. Y.
Chemistry & Chemical Engineering
Component, General Engineering
Laboratory
Chemistry Research Dept.
General Physics Research Dept.
Metallurgy & Ceramics Research Dept.
Aircraft Accessory Turbine Dept.,
West Lynn, Mass.
General Instrument Corp., Newark, N. J.
General Motors Corp.
Allison Div., Indianapolis, Ind.
Delco-Remy Div., Anderson, Ind.
Guide Lamp Div., Anderson, Ind.
Research Laboratories Div., Warren, Mich.
General Telephone & Electronics
Laboratories Inc., Bayside, N. Y.
(2 memberships)
Gillette Safety Razor Co., Boston, Mass.

(Sustaining Members cont'd)

Globe-Union, Inc., Milwaukee, Wis.
Gould-National Batteries, Inc., Minneapolis, Minn.
Grace Electronic Chemicals, Inc., Baltimore, Md.
Great Lakes Carbon Corp., New York, N. Y.
Hanson-Van Winkle-Munning Co., Matawan, N. J. (2 memberships)
Harshaw Chemical Co., Cleveland, Ohio (2 memberships)
Hercules Powder Co., Wilmington, Del.
Hewlett-Packard Co., Palo Alto, Calif.
Hill Cross Co., Inc., West New York, N. J.
Hoffman Electronics Corp., Semiconductor Div., El Monte, Calif. (2 memberships)
Hooker Chemical Corp., Niagara Falls, N. Y. (3 memberships)
Hughes Aircraft Co., Culver City, Calif.
International Business Machines Corp., Yorktown Heights, N. Y.
International Minerals & Chemical Corp., Skokie, Ill.
ITT Federal Laboratories, Div. of International Telephone & Telegraph Corp., Nutley, N. J.
Jones & Laughlin Steel Corp., Pittsburgh, Pa.
K. W. Battery Co., Skokie, Ill.
Kaiser Aluminum & Chemical Corp.
Div. of Chemical Research, Permanente, Calif.
Div. of Metallurgical Research, Spokane, Wash.
Kawecki Chemical Co., Boyertown, Pa.
Kennecott Copper Corp., New York, N. Y.
Leesona Moos Laboratories, Div. of Leesona Corp., Jamaica, N. Y.
Libbey-Owens-Ford Glass Co., Toledo, Ohio
Lockheed Aircraft Corp., Missiles & Space Div., Sunnyvale, Calif.
Mallinckrodt Chemical Works, St. Louis, Mo.
P. R. Mallory & Co., Indianapolis, Ind.
Merck & Co., Inc., Rahway, N. J.
Metal & Thermit Corp., Detroit, Mich.
Miles Chemical Co., Div. of Miles Laboratories, Inc., Elkhart, Ind.
Minneapolis-Honeywell Regulator Co., Minneapolis, Minn.
Minnesota Mining & Manufacturing Co., St. Paul, Minn.
Monsanto Chemical Co., St. Louis, Mo.
Motorola, Inc., Chicago, Ill.
National Cash Register Co., Dayton, Ohio
National Lead Co., New York, N. Y.
National Research Corp., Cambridge, Mass.
National Steel Corp., Weirton, W. Va.
North American Aviation, Inc., Rocketdyne Div., Canoga Park, Calif.
Northern Electric Co., Montreal, Que., Canada
Norton Co., Worcester, Mass.
Ovitron Corp., Long Island City, N. Y.
Owens-Illinois Glass Co., Toledo, Ohio
Peerless Roll Leaf Co., Inc., Union City, N. J.
Pennsalt Chemicals Corp., Philadelphia, Pa.
Phelps Dodge Refining Corp., Maspeth, N. Y.
Philco Corp., Research Div., Blue Bell, Pa.
Philips Laboratories, Inc., Irvington-on-Hudson, N. Y.
Pittsburgh Plate Glass Co., Chemical Div., Pittsburgh, Pa.
Potash Co. of America, Carlsbad, N. Mex.
The Pure Oil Co., Research Center, Crystal Lake, Ill.
Radio Corp. of America
Tube Div., Harrison, N. J.
RCA Victor Record Div., Indianapolis, Ind.
Ray-O-Vac Co., Madison, Wis.
Raytheon Co., Waltham, Mass.
Remington Rand, Div. of Sperry Rand Corp., New York, N. Y.
Reynolds Metals Co., Richmond, Va.
Rheem Semiconductor Corp., Mountain View, Calif.
Schering Corporation, Bloomfield, N. J.
Shawinigan Chemicals Ltd., Montreal, Que., Canada
Speer Carbon Co.
International Graphite & Electrode Div., St. Marys, Pa.
Sprague Electric Co., North Adams, Mass.
Stackpole Carbon Co., St. Marys, Pa.
Stauffer Chemical Co., New York, N. Y.
Tennessee Products & Chemical Corp., Nashville, Tenn.
Texas Instruments, Inc., Dallas, Texas
Metals and Controls Corp., Attleboro, Mass.
Three Point One Four Corp., Yonkers, N. Y.
Titanium Metals Corp. of America, Henderson, Nev.
Tung-Sol Electric Inc., Newark, N. J.
Udylite Corp., Detroit, Mich. (4 memberships)
United States Borax & Chemical Corp., Los Angeles, Calif.
Universal-Cyclops Steel Corp., Bridgeville, Pa.
Upjohn Co., Kalamazoo, Mich.
U. S. Steel Corp., Pittsburgh, Pa.
Victor Chemical Works, Chicago, Ill.
Western Electric Co., Inc., Chicago, Ill.
Wyandotte Chemicals Corp., Wyandotte, Mich.
Yardney Electric Corp., New York, N. Y.